Universitat Politècnica de València
Departamento de Máquinas y Motores Térmicos

An experimental study of the effects of fuel properties on diesel spray processes using blends of single-component fuels

Doctoral Thesis

Presented by:
Ing. Walter Martín Vera-Tudela Fajardo
Directed by:
Dr. José María García Oliver
Prof. José María Desantes Fernández

Valencia, November 2015

Doctoral Thesis

An experimental study of the effects of fuel properties on diesel spray processes using blends of single-component fuels

Presented by: Ing. Walter Martín Vera-Tudela Fajardo
Directed by: Dr. José María García Oliver
Prof. José María Desantes Fernández

Examining Board:

President: Prof. Raúl Payri Marín
Secretary: Prof. Francisco Vicente Tinaut Fluixá
Examiner: Dr. Ezio Mancaruso

Reviewing Board:

Dr. Carlo Beatrice
Dr. Blanca Giménez Olavarria
Dr. Ezio Mancaruso

Valencia, November 2015

Resumen.

Estos últimos años, la tendencia en motores diesel ha sido la de emplear distintos tipos de combustibles para identificar su influencia y comportamiento sobre las emisiones y rendimiento. Dentro de la amplia variedad de combustibles empleados están los llamados combustibles de referencia (PRFs ingl. *Primary Reference Fuels*), los cuales representan el comportamiento del diesel y la gasolina en lo que respecta a propiedades de encendido, ya que se encuentran en ambos extremos de la escala del número de octano y también poseen números de cetano muy distintos. Una de las desventajas de utilizar gasolina pura o mezclas de diesel-gasolina en motores diesel es el tiempo que toma la mezcla en encender y quemar completamente el combustible. Esto generalmente requiere trabajar con cargas parciales o cargas premezcladas.

Para poder aislar los efectos del combustibles sobre los procesos de un chorro y que sea capaz estudiar los parámetros característicos de tiempo de retraso de encendido, longitud de despegue de llama, penetración de líquido y vapor, entre otros, se han realizado distintos experimentos bajo variaciones paramétricas de condiciones de motor diesel. Los ensayos han sido realizados bajo condiciones inertes y reactivas en un motor óptico de dos tiempos y una instalación de alta presión y alta temperatura de flujo continuo a presión constante (CPF ingl. *Constant-Pressure Flow*) empleando toberas mono-orificio, con aplicación de diversas técnicas ópticas. Para estudiar la influencia de las propiedades de los combustibles se utilizaron distintos mono-componentes, así como mezclas binarias y un sustituto de diesel conformado por seis componentes, el cual fuel comparado con diesel convencional. Adicionalmente, los resultados han sido contrastados con un modelo unidimensional para ayudar a explicar los valores y tendencias encontrados.

Los resultados presentaron una fuerte dependencia de las propiedades de los combustibles en los ensayos realizados bajo condiciones inertes y reactivas. La diferencia entre las propiedades físicas del *n*-decano y *n*-hexadecano mostraron una reducción casi lineal sobre la longitud líquida estabilizada hasta aproximadamente un 60 % bajo ciertas condiciones. Adicionalmente, debido a la composición del combustible de sustitución, el *n*-hexadecano puro demostró tener características de evaporación prácticamente idénticas, probándose a sí mismo como un buen candidato para ser un sustituto mono-componente del diesel convencional. De una manera similar, las propiedades químicas de los PRFs *n*-heptano e *iso*-octano también probaron tener influencia sobre el desarrollo del chorro y radiación emitida. Se obtuvieron valores de tiempo de retraso con diferencias de hasta un orden de magnitud entre ambos extremos del rango de las mezclas, así como longitudes de despegue de llama hasta tres veces más largas. La radiación emitida por la incandescencia del hollín presentó las variaciones más altas, ya que algunas condiciones mostraron reducciones de hasta cuatro órdenes de magnitud dentro del rango de mezclas. Es más, algunos casos no presentaron radiación correspondiente al hollín, e incrementar la sensibilidad de la cámara solo ocasionó que la quimioluminiscencia del radical OH* sea detectada. Por otro lado, la longitud estabilizada de llama calculada mediante la radiación del hollín no presentó mucha variación respecto a las propiedades del combustible o la temperatura del aire. De hecho, la única diferencia apreciable fue causada por los cambios en la composición del oxígeno del aire ambiente.

En conclusión, las propiedades de los combustibles demostraron tener un efecto significativo en los procesos de un chorro diesel. Los combustibles más ligeros favorecieron la evaporación del chorro en un rango de condiciones, mientras que combustibles con números de octano más bajos encendieron más pronto y cerca de la tobera pero con mayor luminosidad del hollín medida.

Resum.

En aquests últims anys, la tendència en motors Diesel ha estat la d'emprar diferents tipus de combustibles per a identificar la seva influència i comportament sobre les emissions i rendiment. Dintre de l'àmplia varietat de combustibles emprats estan els anomenats combustibles de referència (PRFs angl. *Primary Reference Fuels*), els quals representen el comportament del dièsel i la gasolina pel que fa a propietats d'encesa, ja que es troben en ambdós extrems de l'escala del nombre d'octà i també posseeixen nombres de cetà molt diferents. Un dels desavantatges d'utilitzar benzina pura o barreges de Diesel-benzina en motors Diesel és el temps que pren la barreja a encendre i cremar completament el combustible. Això generalment requereix treballar amb càrregues parcials o càrregues premesclades.

Per a poder aïllar els efectes del combustibles sobre els processos d'un doll i que sigui capaç estudiar els paràmetres característics de de temps de retard d'encesa, longitud d'enlairament de flama, penetració de líquid i vapor, entre altres, s'han estudiat diferents experiments sota variacions paramètriques de condicions de motor Diesel. Els assajos han estat realitzats sota condicions inertes i reactives en un motor de dos temps i una instal·lació d'alta pressió i alta temperatura de flux continu a pressió constant (CPF angl. *Constant-Pressure Flow*) emprant toberes mono-orifici, amb aplicació de diverses tècniques òptiques. Per a estudiar la influència de les propietats dels combustibles, van ser utilitzats distints mono-components, així com barreges binàries i un substitut de Diesel conformat per sis components, el qual fuel comparat amb Diesel convencional. Addicionalment, els resultats han estat contrastats amb un model unidimensional per a ajudar a explicar els valors i tendències trobats.

Els resultats van presentar una forta dependència de les propietats dels combustibles en els assajos realitzats sota condicions inertes i reactives. La diferència entre les propietats físiques del *n*-decà i *n*-hexadecà van mostrar una reducció gairebé lineal sobre la longitud líquida estabilitzada fins a aproximadament un 60 % sota certes condicions. Addicionalment, degut a la composició del combustible de substitució, el *n*-hexadecà pur va demostrar ser tindre característiques d'evaporació pràcticament idèntiques a aquell, demostrant ser un bon candidat per a ser un substitut mono-component del dièsel convencional. D'una manera similar, les propietats químiques dels PRFs *n*-heptà i *iso*-octà també provaren tindre influència sobre el desenvolupament del doll i la radiació emesa. Es van obtenir valors de temps de retard amb diferències de fins a un ordre de magnitud entre ambdós extrems del rang de les barreges, així com longituds d'enlairament de flama fins a tres vegades més llargues. La radiació emesa per la incandescència del sutge va presentar les variacions més grans, ja que algunes condicions van mostrar reduccions de fins a quatre ordres de magnitud dintre del rang de barreges. Encara més, alguns casos no van presentar radiació corresponent al sutge, i incrementar la sensibilitat de la càmera solament va ocasionar que la quimioluminiscència del radical OH* sigui detectada. D'altra banda, la longitud estabilitzada de flama calculada mitjançant la radiació del sutge no va presentar molta variació respecte a les propietats del combustible o la temperatura del aire. De fet, la única diferència apreciable va ser causada pels canvis en la composició del oxigen de l'aire ambient.

En conclusió, les propietats dels combustibles van demostrar tenir un efecte significatiu en els processos d'un doll dièsel. Els combustibles més lleugers van afavorir l'evaporació del doll en un rang de condicions, mentres que els combustibles amb nombre d'octà més baixos van prendre més aviat i prop de la tovera però amb més lluminositat del sutge mesurat.

Summary.

This last few years, the trend in diesel engines has been to use different kinds of fuels to identify their influence and behaviour on the emissions and performance. Among the wide variety of fuels employed are the so called Primary Reference Fuels (PRFs), which represent the behaviour of diesel and gasoline in terms of ignition properties, as they are located at both ends of the octane rating scale and also have very different cetane numbers. One of the disadvantages of using pure gasoline or diesel-gasoline blends in diesel engines is the time needed for the mixture to ignite and to completely burn the fuel. This generally requires working with partial loads or with premixed charges.

In order to isolate the fuel effects on the spray processes and to be able to study the characteristic parameters of ignition delay time, lift-off length, vapour and liquid penetration, among others; different experiments under parametric variations of diesel like conditions have been performed. The tests were performed under inert and reactive conditions in a 2-stroke optical engine and a constant-pressure flow (CPF) high-pressure high-temperature vessel using single-hole nozzles, while diverse optical techniques were being employed. To study the influence of the fuel properties, different single-component fuels were employed as well as binary blends and a six-component diesel surrogate, which was also compared to conventional diesel. Additionally, the results have been contrasted with a one-dimensional model in order to further explain the values and trends found.

The results presented a strong dependency on the fuel properties for the tests performed under inert and reactive conditions. The difference in physical properties of *n*-decane and *n*-hexadecane showed an almost linear reduction of the stabilized liquid penetration down to approximately 60 % under some conditions. Additionally, due to the composition of the surrogate fuel, pure *n*-hexadecane was demonstrated to have almost identical evaporation characteristics, hence proving itself as a good candidate for a single-component surrogate of diesel fuel. In a similar way, the chemical properties of the PRFs *n*-heptane and *iso*-octane also proved to be influential on the spray development and radiation emitted. Ignition delay values up to one order of magnitude larger where obtained for both extremes of the blend range, as well as lift-off lengths up to three times longer. The radiation emitted by the soot incandescence presented the highest variations, as some conditions showed a reduction of almost four orders of magnitude among the blend range. Moreover, some cases did not present any radiation corresponding to the soot, and increasing the sensitivity of the camera only caused the chemiluminescence of the OH* radical to be captured. On a different way, the stabilized flame length determined also by the soot radiation did not present much variation as the fuel properties or the air temperature were changed; in fact, the only noticeable differences were caused by the changes in the oxygen composition of the ambient air.

In conclusion, the fuel properties proved to have a significant effect on the spray processes. Lighter fuels favoured the evaporation of the spray under a range of conditions, while fuels with lower octane numbers ignited sooner and closer to the spray tip but with more soot luminosity measured.

Zusammenfassung.

In den letzten Jahren hat sich der Trend bei Dieselmotoren dahingehend entwickelt verschiedene Arten von Kraftstoffen zu verwenden und deren Einfluss auf das Emissionsverhalten und die Leistung zu untersuchen. Unter der Vielzahl von Kraftstoffen, die eingesetzt werden, sind die so genannten Primärbezugskraftstoffe (PRFs engl. *Primary Reference Fuels*), an denen das Verhalten von Diesel und Benzin studiert werden kann, da sie hinsichtlich ihrer Zündungseigenschaften, ihrer Lage an den Extremen der Oktanskala und ihrer Cetanzahlen mit denselbigen vergleichbar sind. Einer der Nachteile der Verwendung von reinem Benzin oder Diesel-Benzin-Mischungen bei Dieselmotoren ist die Zeit, die nötig ist, um das Gemisch zu zünden und um den Kraftstoff vollständig zu verbrennen. Dies erfordert in der Regel die Arbeit mit Teillasten oder mit vorgemischten Chargen.

Um die Auswirkungen des Kraftstoffs auf die Spritzverfahren zu isolieren und die Charakteristika der Parameter u.A. hinsichtlich der Zündungsverzögerungszeit, Lift-off Länge, Dampf- und Flüssigkeitspenetration zu analysieren, wurden unter Dieselmotor ähnlichen Bedingungen verschiedene Versuchsanordnungen untersucht. Die Tests wurden unter inerten und reaktiven Bedingungen in einem Zweitakt-Transparentmotor und einer Hochdrucktemperaturzelle mit Konstantdruckfluss (CPF engl. *Constant-Pressure Flow*) mit Einzellochdüsen unter Anwendung unterschiedlicher optischer Techniken durchgeführt. Um den Einfluss der Kraftstoffeigenschaften zu untersuchen, wurden verschiedene Ein-Komponenten-Kraftstoffe und binäre Mischungen eingesetzt sowie ein Sechs-Komponenten-Diesel-Surrogat, das auch im Vergleich zu herkömmlichen Diesel verwendet wurde. Darüber hinaus wurden die Ergebnisse einem eindimensionalen Modell zur Erläuterung der gefundenen Werte und Trends gegenübergestellt.

Die Ergebnisse zeigen eine starke Abhängigkeit von den Kraftstoffeigenschaften für die unter inerten und reaktiven Bedingungen durchgeführten Tests. Der Unterschied in den physikalischen Eigenschaften von *n*-Decan und *n*-Hexadecan ergab eine nahezu lineare Abnahme der stabilisierten Flüssigkeitspenetration von bis zu 60 % unter verschiedenen Bedingungen. Darüberhinaus konnte gezeigt werden, dass Surrogat-Kraftstoff aufgrund seiner Zusammensetzung und reines *n*-Hexadecan nahezu identische Verdampfungseigenschaften besitzen, und sich daher als ein guter Kandidat für einen Einkomponenten-Surrogat von Dieselkraftstoff erweist. In ähnlicher Weise werden die chemischen Eigenschaften des PRFs *n*-Heptan und Isooktan auch im Hinblick auf die Sprayentwicklung und Strahlenemission beeinflusst. Bis zu einer Größenordnung größere Zündungsverzögerungswerte sowie bis zu dreimal längere Lift-off Längen konnten an beiden Extremen der Skala gemessen werden. Die durch das Rußglühen emittierte Strahlung präsentiert die höchsten Abweichungen, unter bestimmten Bedingungen zeigte sich eine Verringerung von fast vier Größenordnungen unter den Mischungen. Außerdem konnte in einigen Fällen keine rußbedingte Strahlung beobachtet werden. Eine Erhöhung der Kameraempfindlichkeit führte nur zur Erfassung der Chemilumineszenz des OH*-Radikals. Im Gegensatz dazu variierte die ebenfalls durch das Rußglühen beeinflusste stabilisierte Flammenlänge selbst unter veränderten Kraftstoffeigenschaften oder Lufttemperatur kaum; die einzigen merklichen Unterschiede wurden durch Veränderungen in der Sauerstoffzusammensetzung der Umgebungsluft verursacht.

Zusammenfassend konnte gezeigt werden, dass Kraftstoffeigenschaften einen signifikanten Einfluß auf die Spritzverfahren haben. Leichtere Kraftstoffe begünstigen das Verdampfen des Sprays unter einer Vielzahl von Bedingungen, während Kraftstoffe mit niedrigeren Oktanzahlen sowohl schneller als auch näher an der Düse zündeten und dabei mehr Rußglühen gemessen werde konnte.

Table of Contents

Index of Figures

Index of Tables

Nomenclature

Latin

a, b, c, d, e, f	Constants for experimental correlations
A/F	Air/Fuel ratio
A/F_{st}	Stoichiometric Air/Fuel ratio
d_o	Nominal nozzle diameter
d_{eq}	Equivalent nozzle diameter
f	Mixture fraction
$\dot{m}$	Mass flux
$\dot{M}$	Momentum flux
O_2	Air oxygen concentration
P	Air pressure
R_u	Universal ideal gas constant
r	Spray radial coordinate
$\overline{s}$	Standard deviation of the sample of data
Si	Vapour penetration under inert conditions
Sr	Vapour penetration under reactive conditions
t	Time
T	Air temperature
T_{boil}	Specie boiling temperature
u	Axial velocity of the spray
u	Radial velocity of the spray
V	Volume
X	Mole fraction
x	Spray axial coordinate
$\overline{x}$	Average of the sample of data
$\mid x \mid$	Absolute value
Y	Mass fraction

Greek

Δ	Increment / Variation
θ	Spray angle
ρ	Air density

τ	Ignition delay
ϕ	Equivalence ratio

Superscripts

o	Condiciones estándar

Subscripts

air	Relative to the air (standard composition)
a, inf	Relative to the pure ambient gas
cl	Relative to the spray centre line
eq	Equivalent
$delay$	Relative to the ignition delay time
$evap$	Relative to the evaporation conditions
f	Relative to the fuel
$f, evap$	Relative to the total evaporation conditions
f, l	Relative to the liquid phase of the fuel
f, v	Relative to the vapour phase of the fuel
I	Relative inert conditions
inj	Relative to the injection
g	Relative to the gas
max	Maximum
o	Relative to the exit conditions of the nozzle
$O2$	Relative to the oxygen specie
R	Relative reactive conditions

Initials and acronyms

1D	*One dimensional*
aSoI	*after the Start of Injection*
BR	*Broadband Radiation*
CAD	*Crank Angle Degree*
CFD	*Computational Fluid Dynamics*
CPF	*Constant Pressure Flow facility*
CVP	*Constant Volume Pre-burn Chamber*
CWL	*Centre Wavelength*
CN	*Cetane Number*
ECN	*Engine Combustion Network*
EGR	*Exhaust Gas Recirculation*
EoI	*End of Injection*
EoS	*Equation of State*
FL	*Flame Length*

FPS	*Frames per second*
IL	*Intact Length*
LL	*Liquid Length*
HBW	*Half Bandwidth*
HPHT	*High Pressure High Temperature*
LoL	*Lift-off Length*
ON	*Octane Number*
PRF	*Primary Reference Fuel*
S	*Spray vapour penetration*
SI	*International System of Units*
SoC	*Start of Combustion*
SoDC	*Start of Diffusion Combustion*
SoI	*Start of Injection*
SOL	*Soot Onset Length*
TDC	*Top Dead Centre*
TPeak	*Peak Transmittance*

Chapter 1

Introduction

Contents

1.1 Introduction

This introductory chapter has the goal of providing an overview of the whole document. In order to accomplish this, the diesel spray will be situated in the realm of reciprocating internal combustion engines. Additionally, the motivation for this work of research will be explained as well as the objectives that were planned to be fulfilled. Finally, the approach and contents of this document will be explained in detail.

1.2 Motivation of the study

The diesel engine has been around for more than a century, it has very diverse applications like passenger cars, trains, submarines and power plants, among many others. Also, its configurations range from one to over a dozen cylinders, and the power output may be from under 10 kW to over 100 MW. Figure 1.1 shows a Wärtsilä RT-flex96C which is claimesd to be "*The world's most powerful reciprocating engine*" with a power range of 24000 kW to 80080 kW depending on the configuration.

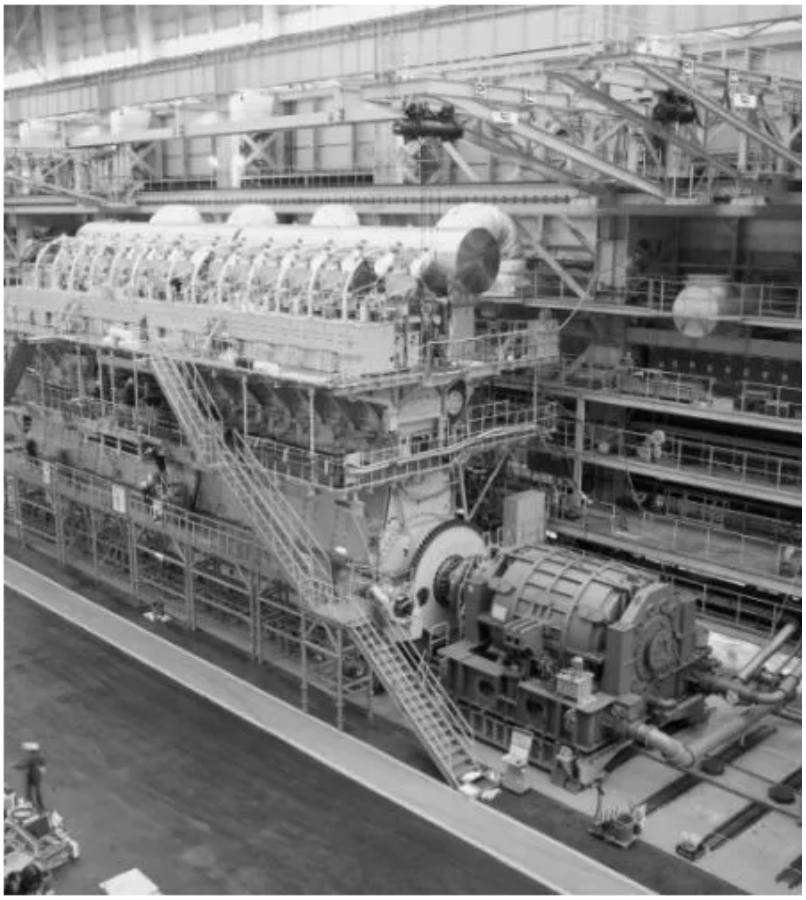

Figure 1.1. *"The world's most powerful reciprocating engine". The Wärtsilä RT-flex96C has a 960 mm cylinder bore with a 2500 mm piston stroke yielding a displacement of 24 litres per cylinder. It is available in 6-cylinder up to 14-cylinder configurations with a power range of 24000 kW to 80080 kW at 92 RPM to 102 RPM. Source: Wärtsilä Corporation [1].*

One of the main features that has traditionally separated the diesel engine from its gasoline counterpart, is how the fuel is delivered into the combustion chamber. In the diesel engine, the fuel is injected into the cylinder, either directly into the combustion chamber ("direct injection") or into a pre-combustion chamber ("indirect injection"). Regardless the injection type, a nozzle is needed to deliver the fuel at high pressure into an already pressurized chamber. One of the drawbacks of this is, that by having a stratified charge, as opposed to the homogeneous charge of the conventional gasoline engine, the mixing of the injected fuel with the entrained air is of paramount importance. Otherwise, the fuel may not evaporate completely and it could also results in zones with local equivalence ratios that are too poor or too rich, which could reduce the performance of the engine and augment the emission of air pollutants. Therefore the importance of studying the mixing and evaporation of a fuel spray.

In recent years, the trend in diesel engines has been to use different kinds of fuels [2, 3] to identify their behaviour and their influence on the performance of the engines and emissions. This has resulted in a large research effort to try to understand the behaviour of different fuels and identify their influence in processes such as mixing, evaporation, ignition and combustion. In this field, two research directions can be identified:

- The first kind is the study regarding bio-fuels, among which is bio-diesel for Compression Ignition Engines and ethanol for Spark Ignition Engines. One of the main advantages of bio-fuels is that due to their nature they are a renewable source of energy, either fully or partially. A recent study about the physical and chemical properties of various fuels was presented as a Ph.D. Thesis [4] at CMT-Motores Térmicos, in which the characteristics and differences of three types of bio-fuels and two synthetics fuels where studied. Among the results shown, under reactive conditions the synthetic fuels demonstrated to have shorter lift-off lengths and ignitions delay times than the bio-diesel ones. Following the same pattern, under inert conditions the fuels mentioned first had shorter liquid lengths that the later ones, as fuel density proved to be the most relevant property on determining the liquid length of the spray, while the fuel properties appeared to have no effect at all on the vapour penetration of the spray.

- Another recent research line is the use of gasoline-diesel blends [5, 6] in diesel engines. Possibly, the most important advantage of these blends is the reduction of emissions and improvement of engine efficiency. Recent studies show that the use of gasoline in diesel engines leads to a reduction of emissions such as NO_X and soot [6, 7]. Nevertheless, the usage of high-octane fuel requires working with partial loads and with pre-mixed charges [7–9], in order to allow more time for the fuel to burn completely. A recent Ph.D. Thesis [10] presented at the Lund Institute of Technology studied many different effects of using various fuel blends on a diesel engine. It was concluded that using gasoline in partially premixed combustion led to high efficiencies and low emissions over the whole load range.

One of the difficulties of working with real fuels is that they are a mixture of a variety of components, which makes knowing their exact composition and properties extremely difficult or very inaccurate. A way to prevent this issues is working with surrogate fuels. These fuels are defined based on blends of pure substances (single-component fuels) that

present a very similar behaviour to their "real" counterparts, but their properties and composition are known in detail.

From many years, the characterization of the influence of the fuel on the processes related with diesel combustion is being performed in High Pressure High Temperature vessels [11] where the contour conditions can be kept steady or with little variation. These vessels are usually equipped with optical accesses so that the visualization of the injection event is possible [12] and therefore the application of different optical techniques. These studies consist mainly in the visualization of the spray and acquisition of images, to determine geometric parameters such as vapour penetration [13], flame lift-off length [14], and the study of evaporation and penetration of the spray [15].

1.3 Objectives of the study

The main goal of this thesis is the analysis and study of the evaporation and combustion processes of a diesel spray under engine conditions using controlled blends of single-component fuels. As mentioned earlier, the advantage of using single-component fuels to real fuels is the elimination of the uncertainty related to their accurate properties and composition. This enables a very straightforward comparison of experimental results to numerical simulation. All this allows the integral use of both, experimental and modelling tools, which in this work are expected to contribute to the detailed knowledge of the different processes that take place during the injection-combustion of a diesel spray.

In order to reach this goal, the following objectives have been defined:

- Study of the processes of mixing and evaporation. To accomplish this, a series of tests will be conducted under INERT conditions in order to isolate the spray from the effects of the combustion. A wide range of fuels at various engine conditions will be studied to help understand the behaviour of the spray under different circumstances. Finally, a 1D model will be used as an additional tool to help calculate complementary parameters.

- Study of the processes of ignition and combustion. In order to fulfil this objective, a different series of test will be conducted under REACTIVE conditions. Again a broad range of single-component blends under a parametric variation of conditions will be tested.

1.4 Approach and contents of the study

Based on the objectives of this research, two fundamental steps have been defined and the following approach will be pursued:

- As the first step, and in order to understand the processes of mixing and evaporation, experiments will be performed using n-decane (n-$C_{10}H_{22}$), n-hexadecane (n-$C_{16}H_{34}$), intermediate blends and a real fuel with its surrogate counterpart due to the fact that their physical properties are very different. The tests will be

performed in a two-stroke single-cylinder engine with an optical head under many ambient conditions that include variations of air temperature, air density, fuel blend composition and injection pressure. All points will be performed under inert conditions, that means 100% nitrogen and 0% oxygen. The results will help quantify the parameters of liquid length using the optical technique of Mie-scattering and vapour penetration by means of schlieren visualization. As a complementary point, 1D simulations will be done to calculate some parameters that were not measured during the experiments as well as to obtain data from points outside the test matrix.

- As the second step, to help understand the processes of auto-ignition and combustion, tests will be done using *n*-heptane (n-C_7H_{16}), *iso*-octane (iso-C_8H_{18}) and blends in-between, because of the great difference in their chemical properties. The tests will be performed in a HPHT vessel with optical accesses under various conditions that involve variations of air temperature, oxygen concentration, fuel blend composition and injection pressure. With these tests the parameters of vapour penetration by means of schlieren visualization, flame lift-off length via the OH* radical chemiluminescence and intensity and soot distribution by broadband radiation will be measured.

Finally, the analysis of the work done for this research and the modifications and validation of the model can be found with more detail in [16–19]. The results of these publications are the fruit of this work of research.

1.5 Structure of the document

In order the accomplish the objectives set and followed the approach presented, the documents is structured as presented:

I. Introduction: The first and current chapter, it has the goal of providing an overview of the whole document.

II. Combustion processes in diesel sprays: The second chapter explains the structure of a diesel spray and the processes involved in it, such as atomization, evaporation, air entrainment, ignition delay, premixed combustion and mixing controlled combustion. Additionally, it will interlace those processes and the parameters involved that will be quantified during the experimental tests.

III. Experimental and theoretical tools and methodological approach: The third chapter gives a complete description of the tools used to gather the information for this work of research. The test facilities in which the experiments were carried on, the optical techniques that were used and the numerical model that was developed to predict the evolution of a spray will be described in detail.

IV. Fuel effects on mixing and evaporation under inert conditions: Following the objectives and approach of the study, the fourth chapter will present the results obtained from the tests under inert conditions. An in depth analysis of the effects of the fuel properties on the processes of mixing and evaporation will be done, as well as the comparison and study of new parameters obtained through modelling.

V. Fuel effects on auto-ignition and combustion: In an analogous way as the previous point and using the information obtained, in the fifth chapter the results from the tests under reactive conditions are going to be presented. An study of the processes of ignition and combustion, as well as the characteristic parameters of a diffusion flame will be done with the addition of results from modelling and some possible trends and correlations obtained.

VI. Conclusions and future work: The sixth and last chapter will summarize the results obtained and will draw the main conclusions of this work. Moreover, suggestions for future works of research will be presented.

Bibliography

[1] *Wärtsilä Corporation*. http://www.wartsila.com/en/Home.

[2] Reitz R.D., R.Hanson, Splitter D. and Kokjohn S. "High-Efficiency, Ultra-Low Emission Combustion in a Heavy-Duty Engine via Fuel Reactivity Control". In *15th Diesel Engine-Efficiency and Emissions Research (DEER) Conference, Dearborn, MI*. Engine Research Center, University of Wisconsin-Madison, August 2009.

[3] Reitz R.D. "High-Efficiency Fuel Reactivity Controlled Compression Ignition (RCCI) Combustion". In *16th Directions in Engine-Efficiency and Emissions Research (DEER) Conference, Detroit, MI*. Engine Research Center, University of Wisconsin-Madison, August 2010.

[4] Nerva J.G. *An assessment of fuel physical and chemical properties in the combustion of a Diesel spray*. Doctoral Thesis, Universitat Politècnica de València, 2013.

[5] Hanson R., Splitter D. and Reitz R.D. "Operating a heavy-duty direct-injection compression-ignition engine with gasoline for low emissions". *SAE Technical Paper*, n^o 2009-01-1442, 2009.

[6] Kalghatgi G.T., Gurubaran R. Kumara, Davenport A., Harrison A.J., Hardalupas Y. and Taylor A.M.K.P. "Some advantages and challenges of running a Euro IV, V6 diesel engine on a gasoline fuel". *Fuel*, Vol. 108, pp. 197–207, 2013.

[7] Hildingsson L., Kalghatgi G., Tait N., Johansson B. and Harrison A. "Fuel Octane Effects in the Partially Premixed Combustion Regime in Compression Ignition Engines". *SAE Technical Paper*, n^o 2009-01-2648, 2009.

[8] Kalghatgi G., Risberg P. and Ångström H.E. "Advantages of Fuels with High Resistance to Auto-ignition in Late-injection, Low-temperature, Compression Ignition Combustion". *SAE Technical Paper*, n^o 2006-01-3385, 2006.

[9] Manente V., Tunestål P. and Johansson B. "Half Load Partially Premixed Combustion, PPC, with High Octane Number Fuels. Gasoline and Ethanol Compared with Diesel". In *Symposium on International Automotive Technology (SIAT), Pune, India*. The Automotive Research Association of India, Research Institution of the Automotive Industry, January 2009.

[10] Manente V. *Gasoline Partially Premixed Combustion - An advanced internal combustion engine concept aimed to high efficiency, low emissions and low acoustic noise in the whole load range*. Doctoral Thesis, Lund Institute of Technology, 2010.

[11] Baert R.S.G., Frijters P.J.M., Somers B., Luijten C.C.M. and de Boer W. "Design and Operation of a High Pressure, High Temperature Cell for HD Diesel Spray Diagnostics: Guidelines and Results". *SAE Technical Paper*, n^o 2009-01-0649, 2009.

[12] Kim T. and Ghandhi J.B. "Characterization of evaporating diesel sprays using exciplex laser-induced fluorescence measurements". *Atomization and Sprays*, Vol. 13, pp. 535–559, 2003.

[13] Settles G.S. *Schlieren and Shadowgraph Techniques: Visualizing Phenomena in Transparent Media*. Springer-Verlag, Berlin, Germany, 2001.

[14] Higgins B. and Siebers D. "Measurement of the Flame Lift-Off Location on DI Diesel Sprays Using OH Chemiluminescence". *SAE Technical Paper*, n^o 2001-01-0918, 2001.

[15] Faeth G.M. "Evaporation and combustion of sprays". *Progress in Energy and Combustion Science*, Vol. 9, pp. 1–76, 1983.

[16] Pastor J.V., García-Oliver J.M., Novella R. and Vera-Tudela W. "Investigation on ignition and combustion characteristics of primary reference fuels under diesel engine conditions". In *Der Arbeitsprozess des Verbrennungsmotors*, pp. 378–393. Institut für Verbrennungskraftmaschinen und Thermodynamik, Technische Universität Graz, September 2013.

[17] Pastor J.V., García-Oliver J.M., Pastor J.M. and Vera-Tudela W. "One-dimensional diesel spray modeling of multicomponent fuels". *Atomization and Sprays*, Vol. 25(2), pp. 485–517, 2015.

[18] Knox B.W., Genzale C.L., Pickett L.M., García-Oliver J.M. and Vera-Tudela W. "Combustion recession after end of injection in diesel sprays". *SAE International Journal of Engines*, Vol. 8(2) n^o 2015-01-0797, 2015.

[19] Pastor J.V., García-Oliver J.M., López J.J. and Vera-Tudela W. "An experimental study of the effects of fuel properties on reactive spray evolution using Primary Reference Fuels". *Fuel*, Vol. 163, pp. 260–270, 2016.

Chapter 2

Combustion processes in diesel sprays

Contents

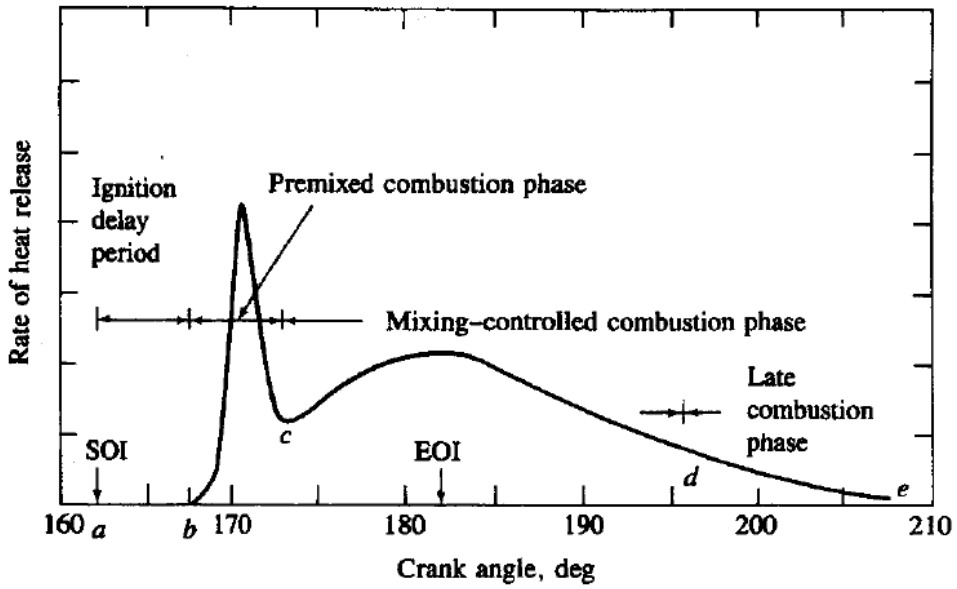

Figure 2.1. *Typical DI engine heat-release-rate diagram identifying different diesel combustion phases as shown in [1].*

2.1 Introduction

This second chapter has the goal of explaining in detail the structure of a diesel spray and the processes involved; as well as describing the differences between an inert and a reactive spray and the variables that affect its behaviour and evolution over time. Additionally, it will provide a link between those processes and the most important parameters involved that provide significant information and were therefore quantified during the experimental campaigns that were carried out in order to produce the information for the elaboration of this document.

This chapter is structured as follows. First, a basic description of the diesel spray phases will be presented to give a general overview. Then, the inert spray will be explained in detail and the atomization, evaporation, mixing and air entrainment are going to the described. After this, the reactive stages will be introduced, this includes the processes occurring during the ignition delay, the premixed combustion and mixing controlled combustion. And last, all the processes will be integrated into a time resolved sequence and the parameters that best help to quantify those processes will be mentioned.

2.2 Classical description of diesel combustion phases

The combustion processes of a diesel spray are best described by analyzing the rate heat release while the fuel is being injected into the combustion chamber. Figure 2.1 shows the typical rate of heat release diagram as it happens in a direct-injection diesel engine. Four phases are clearly distinguishable:

- The first one commences right after the injection has begun, the fuel is being introduced into the combustion chamber and there is no apparent heat released. The fuel is mixing with the air, the processes of atomization, air entrainment and evaporation take place during this phase. Due to the high temperature of the air and the availability of oxygen in it, the fuel starts oxidizing and very low intensity pre-reactions appear, this will give place later to the spontaneous ignition of the mixture that defines the start of combustion. This first phase is known as the *ignition delay* and can be seen in Figure 2.1 from the points a to b as a flat line of value close to zero in the rate of heat release axis.

- The second phase is of a transient state and is defined by a premixed combustion of the fuel-air mixture. As explained in the previous paragraph, the fuel had mixed with the entrained air and even some low temperature pre-reactions had taken place; however, the mixture could not burn due to not being within the flammability limits of the fuel. This phase is characteristic of a combustion with very high heat release, as the combustion of the mixture formed during the ignition delay occurs very rapidly and this is what generates the main peak in Figure 2.1. This phase is known as *premixed combustion* and extends from the start of combustion to the first minimum value after the peak (from the points b to c).

- The third phase begins when the fuel that was mixed during the ignition delay phase burns out completely. During this phase the heat is released at a much lower rate, as it is controlled by the availability of the new mixture formed for burning, hence the name of *Mixing-controlled combustion*. As mentioned in [1], even though many processes are involved in this phase, fuel atomization and vaporization, mixing of vapour with air and chemical pre-reactions, the burning rate is controlled mainly by the air-fuel mixing ratio. The length of the heat release depends on the injection length and may form a second peak, but much lower than the main one, and happen near the EOI. In this phase the flame goes into an almost steady state (as opposed to the premixed combustion). This can be seen from the points c to d in Figure 2.1.

- The fourth and last phase takes place after the injection has ended and it is known as the *Late combustion phase*. The heat released goes on because the injected fuel has not been completely exhausted and the oxidation of some combustion products can still release heat. However, this heat release is considerably lower due to much poorer mixing and the flame behaviour is more erratic, it continues until the remaining fuel inside the chamber disappears (Figure 2.1, points d to e).

2.3 Review of the relevant processes during inert spray evolution

When the liquid fuel is injected into a high pressure environment it starts breaking into very small drops by a process called atomization, the angle of this developing spray will be defined mostly by the density of the environment, as a higher density will make it more difficult for the fuel to go through it, hence the spray angle will be wider. Also, as the fuel penetrates further away from the nozzle, it will start entraining air and the

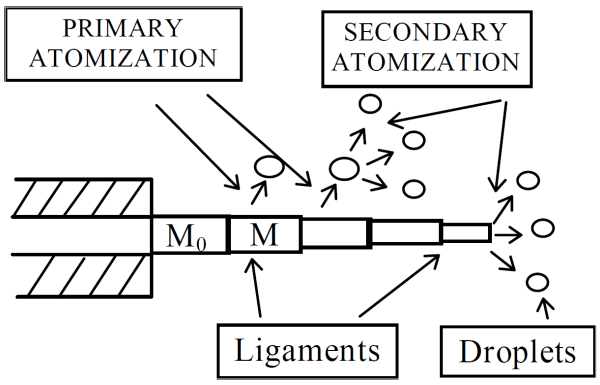

Figure 2.2. *Primary and secondary atomization process scheme [2].*

local mixture fraction will become leaner as the spray tip moves further away. If the temperature of the environment is high enough the fuel will start evaporating wherever the local mixture fraction is lower than the evaporation fraction of a given fuel under the disposed contour conditions. The processes of atomization and entrainment are not affected by the temperature of the environment nor by the composition of the ambient gas; meanwhile, the process of evaporation is affected by the temperature but is unaffected by the composition of the surrounding air. Hence the evolution and processes involved in an inert spray are analogue to those of a reactive spray during the ignition delay phase, in other words, these phases are controlled by the physical properties of the fuel being injected. Each one of the aforementioned processes takes place through the whole injection event and will be explained in this section.

2.3.1 Atomization of the liquid fuel

The phase that takes place after the injection has been initiated is the atomization of the liquid fuel, which consists in the conversion of the liquid core of the fuel into very fine droplets. This process helps increase the area in contact between the fuel and air, and therefore helping the processes of air entrainment and evaporation that follow. In a diesel spray, the atomization process does not start right at the nozzle exit, but instead it takes place at a given distance from the injector tip. This distance is referred to as *intact length* and depends on many factors such as the physical properties of the fuel, injection pressure and ambient density, among others. From this distance on, the break-up of the liquid core of the spray has begun and is no longer intact (hence the name), but instead is a mixture of the entrained air and the droplets of the liquid fuel.

As mentioned in [3], the atomization is basically a process in which an amount of liquid is converted into small drops. However, many of the drops produced by the initial fragmentation may be further disintegrated into smaller drops during the secondary atomization. Figure 2.2 shows a scheme presented in [2], where it is explained that the fuel droplets are formed by the initial ligament breaking up (primary atomization) or by the breaking of the larger droplets into smaller ones (secondary atomization). The ligaments are formed by the fuel mass exiting the nozzle, which suffers a deceleration due to the surrounding air.

This is consistent to what is explained in [3, 4], the disintegration of a liquid jet begins as a cylindrical body exiting the nozzle. Then, due to the perturbations and oscillations that arise due to cohesive and disruptive forces caused by the high relative velocity between liquid and gas, this liquid body begins to fragment into drops. This is referred to as *primary* atomization; successively, and if the drops that have been formed are larger than the critical size, they will further disintegrate into smaller drops by the process of *secondary* atomization. The size of the droplets obtained after the atomization ranges from 10 μm to 20 μm and depends on the orifice diameter, air density and injection pressure [5–7]. Additionally, experimental results [8–10] show that the droplet size is larger in the central part on the spray and closer to the nozzle, meanwhile, being smaller in the periphery and closer to the tip of the liquid spray, which is consistent with the primary and secondary atomization concepts. Although others have reported to have found similar droplet size throughout the liquid core due to coalescence of the smaller drops caused by smaller velocities [11, 12]. Finally, in order to get good atomization, high injection pressure (spray velocity), small nozzle diameter, optimum fuel viscosity and high cylinder pressure (air density) are required [1, 8, 12–14].

Different works of research agree that the extent of this intact length is in the order of a few nozzle diameters [15–18], ranging from a spray fully atomized from the injector tip (i.e. no intact length) to a length of 1 to 3 diameters. Nevertheless, a more recent work [19] presents the possibility of the intact liquid core existing further downstream. An interesting concept presented in [20] is the following: A diesel spray being injected at high pressure into engine-like conditions presents very fast atomization, meaning that the drops of fuel are small and reach a state of dynamic equilibrium with the air stream. This leads to having no velocity gradients between phases and therefore a uniform velocity of the spray with local compositions and thermodynamic conditions. This simplification connotes that the behaviour of an evaporating diesel spray is very similar to that of an isothermal gas jet, and therefore the effect of the atomization on the combustion process is minimum.

2.3.2 Mixing and air entrainment

The air entrainment is one of the most important processes in a diesel spray, specially if a combustion will take place afterwards the evaporation of the fuel. This is because, after the premixed combustion, the subsequent phase is a mixing controlled combustion, so the air entrainment is crucial for the mixing of the injected fuel with the ambient air, as the entrained air will aid the evaporation process and will also provide the oxygen necessary for combustion [21–24]. Additionally, for an atomized liquid spray, the air entrainment plays an important role in the evaporation of the fuel, as it is a process controlled by the mixing [25, 26]. There seem to be two types of air entrainment, regarding the state of the spray. On one hand, the steady spray entrains air only from the sides; on the other hand, the transient spray has the capability to entrain air also from the tip. Hence, a transient spray will entrain more air than a steady one under the same contour conditions [22, 24, 27, 28]. Moreover, the spray angle is related to the amount of air entrained, as a spray with a wider angle covers a larger cross-sectional region and therefore is able to entrain more air [13].

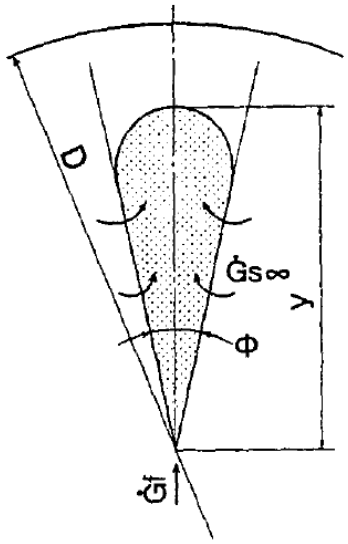

Figure 2.3. *Schema of a free spray [29].*

The air entrainment on a steady spray is defined as the flux of ambient gases drawn into the spray from the radial direction. The entrainment rate has a significant effect on the mixing rate of the injected fuel with the ambient air, and in the reactive cases, the overall chemical reactions are also affected [30]. The behaviour and structure of a fuel spray is similar to that of a gas jet, and the air entrainment of a free spray depends on few variables. Figure 2.3 shows the schematic of a free spray (no wall impinging nor spray interaction). The amount of air entrained at a given distance from the nozzle is equal to the amount of air passing through that same section [29]. Equation 2.1 presents the proportion of air entrained by fuel injected and it can be seen that is does not depend on many parameters.

$$\frac{\dot{G}_{s\infty}}{\dot{G}_f} = 2\tan\left(\frac{\theta}{2}\right)\sqrt{\frac{\rho_a \cdot \nu}{c \cdot \rho_f \cdot d_o}} \tag{2.1}$$

where $\dot{G}_{s\infty}$ is the amount of air entrained, $\dot{G}_f$ is the amount of fuel injected, θ is the spray angle (denoted as Φ on Figure 2.3), ν is the kinematic viscosity of the fuel, c is the discharge coefficient of the nozzle, d_o is the exit diameter and ρ_a and ρ_f are the air and fuel densities, respectively.

Spray penetration

The spray penetration is a parameter almost always measured in diesel sprays; this is due to the fact that the impact of the spray against the cylinder walls may affect the combustion processes and emission of pollutants.

The speed and distance at which the spray penetrates to has a very important effect on the air-fuel mixing and air entrainment. Past results [13, 17] show that the evolution of the spray penetration over time has two very distinctive trends, one of the them being completely linear with time and the other evolving to the square root of time. Moreover,

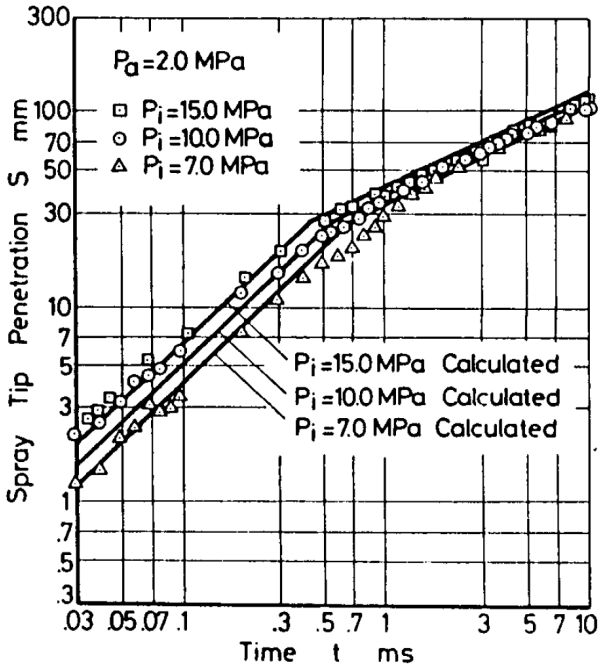

Figure 2.4. *Spray tip penetration at various injection pressures [17].*

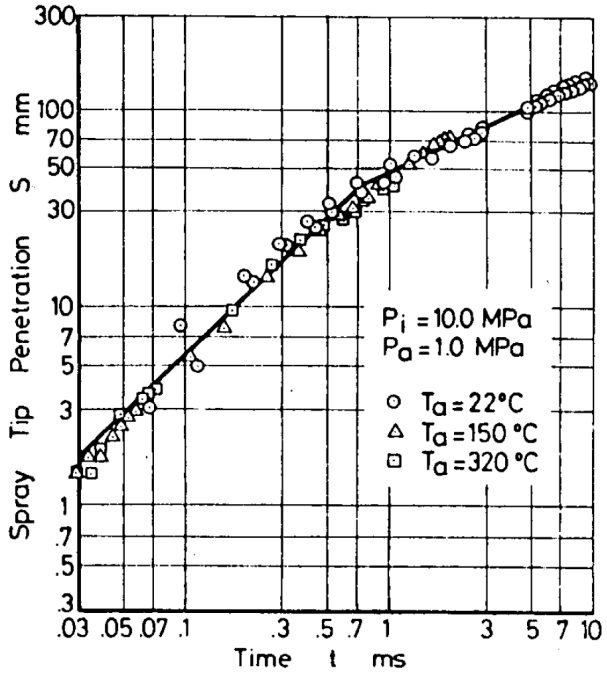

Figure 2.5. *Spray tip penetration at various ambient gas temperatures [17].*

the penetration of the spray tip has been proven to be dependant on the injection pressure and the ambient density; however, the air temperature seems to have a negligible effect on it as do the fuel properties [31]. This can be seen in Figures 2.4 and 2.5, where the evolution of the spray penetration over time under injection pressure and air temperature variations is shown.

Equations 2.2 and 2.3 show the correlation for the spray penetration, before (linear) and after (square root) the time for the change of slope, respectively [17]; and equation 2.4 shows the time at which the slope of the penetration changes. The values calculated from this expressions are also shown in Figures 2.4 and 2.5. The first part of the penetration is linear mostly due to the transient state of the initial injection rate [32], which is consistent with the results presented in [33], where a triangular injection rate (increasing velocity linearly with time) lead to a linear spray penetration along time. And as concluded in [13], the first part of the penetration (linear) is dominated by the injected fuel, while the second part (square root) is by the entrained air.

$$S = 0.39 \cdot \left(\frac{2\Delta P}{\rho_l}\right)^{0.5} \cdot t \tag{2.2}$$

$$S = 2.95 \cdot \left(\frac{\Delta P}{\rho_a}\right)^{0.25} \cdot (t \cdot d)^{0.5} \tag{2.3}$$

$$t_b = 28.65 \cdot \frac{\rho_L \cdot d}{(\rho_a \cdot \Delta P)^{0.5}} \tag{2.4}$$

where ΔP is the difference between injection and chamber pressure, t is the time after injection, d is the nozzle exit diameter, and ρ_a and ρ_l are the air and liquid densities, respectively [17].

Spray angle

In an analogue way as the spray penetration, the spray angle is another parameter widely studied, because, like the spray penetration, it is also easy to measure; however, it is difficult to quantify accurately. The angle of the spray determines the widening of the injected fuel into the ambient air and is therefore directly proportional to the spray radius. A fuel injected into a highly pressurized environment will have a wider angle, as it is "harder" to travel through a denser fluid, and vice-versa. The fuel properties and the nozzle exit diameter also have an effect on the angle, but not as strong as the previous. This means that for a given nozzle-fuel combination, the spray angle depends solely on the chamber density, as it can be seen in Equation 2.5. However, the exponent of this density ratio is not constant among experiments conducted between different works of research, being 0.26 in [17], 0.18 in [34] and in the range of 0.25 and 0.5 in [13].

Another aspect mentioned in [35, 36], is that the spray angle, specially of an atomized liquid, seems to have two different values. Moreover, a recent work [37] demonstrated the presence of the two angles by experimental testing and 1D modelling. Being an *initial* angle near the orifice, that depends mainly on the nozzle geometry and fuel properties, and a *total* angle for the developed spray which depends on the spray dynamics. Reverting

to Equation 2.1 in which the air entrainment depends on the spray angle, and since the angle is not constant throughout the axial coordinate, means that the entrainment will be smaller near the nozzle and will continue growing until it is stabilized along with the fully developed spray.

As an additional point, and since the spray is assumed to be axisymmetrical, for the study and analysis done in this work, the spray angle will be referred to as $\theta/2$ or as $\tan(\theta/2)$ and, unless specified, is the *total* angle of the spray.

$$\theta = 83.5 \cdot \left(\frac{l_o}{d_o}\right)^{-0.22} \cdot \left(\frac{d_o}{d_s}\right)^{0.15} \cdot \left(\frac{\rho_a}{\rho_l}\right)^{0.26} \tag{2.5}$$

where l_o and d_o are the length and diameter of the nozzle hole, d_s is sac chamber diameter of the nozzle, and ρ_a and ρ_l are the air and liquid densities, respectively [17].

2.3.3 Spray evaporation

This phase takes place after the liquid fuel has broken into very small droplets and as opposed to the process of atomization, will take place only if the ambient temperature is high enough for the fuel injected to begin a change of phase.

While the spray keeps on entraining air, heat is being transferred from the ambient gas to the tiny drops of fuel; therefore, their relative velocities decrease as the droplets transfer their momentum to the air and the temperature of the liquid rises. The temperature increase causes the vapour pressure of the droplets surface to decrease, so they start evaporating and the local mixture approaches the adiabatic saturation conditions [4].

It has been widely demonstrated that, even though, the liquid core reaches the tip of the spray at the beginning of the injection event, after a while, the liquid core will stop advancing and will stabilize at a certain position from the injector tip, this distance is known as *liquid length* [6, 25, 26, 31, 38, 39]. This happens because the local composition will become leaner further away from the nozzle, both radially and axially, and in any place that the local mixture fraction is lower than evaporation fraction the fuel will only exist in the vapour phase in a mixing-controlled evaporation. The zone conformed by the coexistence of the liquid and vapour phases is referred to as the *liquid core* of the spray.

Examining the evaporation process in detail, three phenomena area found to determine the evolution of a fuel drop under engine conditions [1]:

- Deceleration of the drop due to aerodynamic drag
- Heat transfer to drop from the air
- Mass transfer of vaporized fuel away from the drop

As the drops travel through the air, their velocity decreases due to aerodynamic drag; this deceleration causes the drop to have more time to exchange heat with the air. Additionally, since the surface area of the drop is largest, the heat transferred from the air is high, leading to a rapidly increasing evaporation rate, as the evaporation is

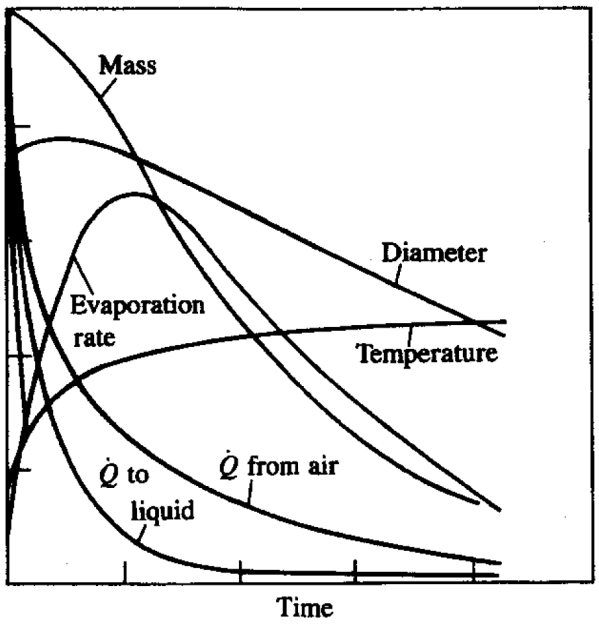

Figure 2.6. *Schematic of variation of mass, diameter, temperature, evaporation rate, heat-transfer rate from air, and hear-transfer rate to liquid drop core as function of time during evaporation process of individual drop in diesel environment at the time of injection as shown in [1].*

a surface phenomenon. The heat transfer also rises the temperature, which causes the vapour pressure to increase and so does the evaporation rate [1]. As time passes by, the drop diameter decreases at a somewhat linear rate, nevertheless, its surface area is decreasing quadratically. This causes the heat transferred from the air to have a drastic change of slope and the evaporation rate to reach a peak as mass transfer also decreases. The temperature of the drop starts reaching an asymptotic state, as its temperature is much closer to that of the air than that of the injected fuel, and also because the surface area of the drop keeps getting smaller until it eventually disappears, causing the heat transferred to keep on lessening. Figure 2.6 shows the evolution of the aforementioned phenomena of a single drop under engine conditions. An important remark to be made is the difference between the heat transferred from the air and the heat transferred to the liquid drop core. The latter is smaller as part of the air energy is spent on the change of phase of the fuel at the surface and the heating of the vaporized fuel.

Liquid length

The rate of evaporation depends largely on the size of the droplets formed during the atomization and their velocity and distribution; additionally, the pressure and temperature inside the chamber along with the fuel volatility play an important role too [1].

As presented by numerous sources in previous researches, among the conditions that influence the liquid length are the nozzle diameter [25, 40, 41], the air density and temperature [25, 26, 39–46], and the fuel properties [25, 31, 39, 40, 47]. The injection

pressure, on the other hand, seems to have an almost negligible effect on the penetration of the liquid core [25, 26, 41–44, 48]. Therefore, and as mentioned in [20, 25, 49], the evaporation is a mixing-controlled process, meaning that the evaporation of the droplets takes place by the energy transferred from the surrounding air. As opposed to the local interphase transport rates of mass, the momentum flux, and energy that control de liquid breakup and droplet evaporation, that do not seem to play an important role in the overall vaporization rate. This stands for the hypothesis that the evaporation is a thermodynamic equilibrium between the species involved; moreover, the enthalpy that allows the evaporation of the fuels comes from the entrained air. From a different perspective, the evaporation can be seen from a simpler point of view, where the liquid length is reached in a point in which the enthalpy entrained by the spray is enough to evaporate all the fuel. Hence, the evaporation process can be reduced to a local mixture fraction [20]. From all of the above and as mentioned in [49, 50], the maximum liquid length can be scaled as presented in Equation 2.6:

$$LL = \frac{k_{LL}}{tan(\frac{\theta}{2})} \frac{d_{eq}}{Y_{f,evap}} \tag{2.6}$$

where θ is the spray angle, d_{eq} is the equivalent exit diameter of the nozzle, $Y_{f,evap}$ is the evaporation fraction for the given mixture and k_{LL} is a correlation constant.

2.4 Review of the relevant processes during the reacting spray evolution

Continuing with the storyline presented at the beginning of Section 2.3, the fuel has evaporated and is well mixed with the air; however, the combustion will not take place immediately. The entrained air will cause the fuel temperature to rise and some low temperature pre-combustion reactions will start taking place in the zones with relatively rich local equivalence ratios. This will give place to an initial premixed combustion, followed by a continuous oxidation of the injected fuel with the remaining air, this last phase is known as mixing-controlled combustion or diffusion flame. Combustion takes place at a certain distance from the injector, and is affected by both the ambient conditions and the injection parameters. On the other hand, the time that goes by from the start of the introduction of the fuel into the chamber and the instant at which the premixed combustion happens seems to be influenced mainly by the contour conditions and not so much by the injection characteristics. The ignition delay takes enough time so that when the combustion happens, a significant amount of fuel has been atomized, evaporated and mixed well with the air. When the ignition finally takes place, the mixture burns at a very high rate, by the multiplication of ignition pockets and the high temperature inside the combustion chamber. After this premixed combustion, the fuel that has been left unburned and any fuel subsequently injected will burn at a controlled rate, mainly dominated by its ability to mix and find oxygen [51].

2.4.1 Ignition delay

During this phase, physical and chemical processes, in that order, have to take place before any important amount of chemical energy of the injected fuel is released [1]. The physical processes mentioned in Section 2.3, will cause the liquid fuel to break up into small droplets, evaporate and mix with the entrained air, creating a hot and reactive mixture. Furthermore, the chemical pre-reactions of the fuel with the air, also known as cool flames, do not release a significant amount of heat, as they involve the formation of free radicals by the breaking up of fuel chains. Nevertheless, they will cause the mixture to be prepared for the subsequent spontaneous combustion. The pre-combustion reactions occur mostly when the fuel is in the vapour phase; additionally, cracking of large hydrocarbon chains to smaller molecules could also take place [1].

An important factor to take into account is that as long as the fuel has not evaporated completely, the full gamut of equivalence ratios will exist, ranging from zero (no fuel) to infinity (no air within the droplets); therefore, the ignition will take place wherever the equivalence ratio is most favourable. Hence, the ignition delay time will depend largely on the ambient conditions, such as air temperature, density and oxygen concentration [51].

As presented in [20, 52] the autoignition process of a diesel spray can be considered as a three phase sequence. The stages are as follows:

I. **Physical induction period:** During this phase all the processes presented in Section 2.3 take place (atomization, evaporation, and mixing and air entrainment). As a consequence, the fuel molecules are being diluted in the increasingly amounts of entrained air which causes their temperature to rise to values that allow the chemical reactions to begin. This start of reaction will mark the end of the physical induction phase. Despite the fact that the chemical reactions have begun, the physical processes area still of great importance, as they separate phenomena that take place in the autoignition of an homogeneous mixture and those on a diesel spray. On the first case, the phase of physical induction does not exist as the mixing was already finished, while on the latter, the local composition evolves as the chemical reactions and the physical process of dilution take place.

II. **First stage ignition:** Throughout this stage the low temperature processes take place, which involve the chemical pre-reactions and the formation of free radicals by the breaking up of fuel chains previously mentioned. Additionally, a low intensity radiation appears that corresponds to the *chemiluminescence*, in which certain molecules are elevated to a excited state due to the exothermic chemical reactions and then return to their equilibrium state emitting radiation. According to the results shown in [53] the chemiluminescence corresponds to the presence of formaldehyde (CH_2O) and the radical CH, as the intensity peaks correspond to the wavelengths emitted by said substances. But once the high temperature phase starts, the concentration of such component completely disappears. The aforementioned phenomena correspond to the formation of *cool flames*. Nevertheless, the injection process keeps on playing an important role in rising the temperature of the mixture as the reactions keep on occurring, which will then lead to the high temperature phase.

III. Second stage ignition - premixed combustion: This step corresponds to the rapid rise of the heat release rate due to the premixed combustion. This begins when the energy transferred from the entrained air to the evaporated fuel and the heat released during the first stage combustion cause the mixture to reach the conditions for the high temperature phase and give place to the autoignition. This phase will be explained with more detail in the next subsection.

Ignition delay time

The ignition delay time in a diesel spray is described as the time that passes from the beginning of the injection until the start of the combustion. The fuel characteristics are extremely important in determining the ignition delay time. Equation 2.7 presents a correlation for the ignition delay time based on the contour conditions:

$$\tau_{id} = \frac{A}{P^n} \exp\left(\frac{E_A}{\tilde{R} \cdot T}\right) \tag{2.7}$$

where τ_{id} is the ignition delay time, E_A is the apparent activation energy of the fuel autoignition process, $\tilde{R}$ is the universal gas constant, A and n are constants dependent on the fuel, and P and T are ambient pressure and temperature, respectively [1].

2.4.2 Premixed combustion

The entrained fuel takes some time to ignite after it has been injected. As explained earlier, it has to go through the evaporation, mixing and pre-reactions before the premixed combustion can take place; this time is know as ignition delay. After the pre-reactions have taken place, and the fuel-air mixture formed during the ignition delay is at the right temperature it burns at a very fast rate, leading to a significant radial expansion of the spray at a given distance from the nozzle tip due to the sudden heat released. The time at which this happens is intimately related to two main factors, one of them being the physical process dominating the formation of the air-fuel mixture, while the other is the chemical process that leads to the heat release [4].

The rate of heat release during this process is very high due to the fact that the fuel has had time to evaporate and mix with the air during the ignition delay. Therefore, the rate and extent of the premixed combustion are closely related to the length of the ignition delay time. Based on this statement, it is expected that the speed and duration of this phase increments as the delay period increases, since both, mixing time and fraction of fuel taking part in the combustion, also augment [51]. Another factor that plays an important role in this second phase, although it is not of significance on the first one, is the time of end of injection. On one hand, if the injection ends before the combustion starts, the pressure rise is going to be smaller as the ignition delay time increases. This is because the mixture will be more diluted, resulting in a weaker premixed combustion. On the other hand, if the ignition takes place before the end of injection, longer ignition delay times would allow more fuel to have been injected into the chamber resulting in a stronger premixed combustion.

2.4.3 Mixing-controlled combustion

After the initial ignition has happened, the spray continues to burn for as long as the fuel is being injected and evaporating; however, the combustion is controlled primarily by the mixing of the fuel with the entrained air. The mixing is also important during the ignition delay phase, as the air mixed with the fuel within its limits of flammability affects the rate at which the pressure rises once ignition happens, even though the ignition time per se is not changed much [1].

In a similar way as with the rate of heat release on the premixed combustion, the injection timing also plays a key role on the mixing-controlled combustion. When the injection duration is shorter than the ignition delay time, the third phase will involve only fuel that did not find enough oxygen to burn during the second phase and the combustion will be limited only by the mixing process, which is controlled mainly by the proportion between the available oxygen and the unburned fuel and by how they are distributed at the end of the second phase. However, if the ignition takes place before the end of injection, as some fuel is still being added to the chamber, the third phase will be affected by the rate of injection as well as the processes of evaporation and mixing [51].

Lift-off length

Once the ignition process has finished, the flame of a diesel spray under quiescent conditions tends to stabilize at a quasi-steady distance from the injector tip during the mixing-controlled phase until the end of injection. Although there may be some fluctuations due to turbulence, the flame will present a quasi-steady mean value [54–56]. This location is known as *lift-off length* and separates de spray into two parts, inert (upstream the LoL) and reactive (downstream the LoL). The air entrained prior to this position mixes with the fuel and after the lift-off length the premixed charge reacts immediately. The lift-off length takes place at a high temperature zone where stoichiometric combustion occurs [54], this type of combustion generates large amounts for the OH* radical at a exited state, and due to the relatively short time of its chemiluminescence is a good indicator of the lift-off length [57].

Past results show that an important amount of the air required for the combustion is entrained before the lift-off length. Then, this mixture reacts downstream the lift-off length in the central region of the spray, where a significant local heat release produces high temperature products rich in partially reacted and/or unburned fuel [13, 55–58]. Therefore, the lift-off length plays and important and almost crucial role in the combustion and formation of pollutants in a diesel spray.

Figure 2.7 presents a comparison of the lift-off and liquid lengths at the same conditions but with different orifice diameters. It show the strong relationship between the vaporization and combustion of the fuel, as smaller diameter will cause the fuel to evaporate faster and to arrive at the reactive part of the spray already in the vapour phase and ready to burn. This also means that the amount of air entrained, which increases as the diameter is reduced, has a stronger effect on the vaporization of the fuel than on the flame stabilization at the lift-off length [55].

The aforementioned concept can be appreciated in Figure 2.8, where the schematics of two extreme cases are shown. Each schematic presents the penetration of the liquid core,

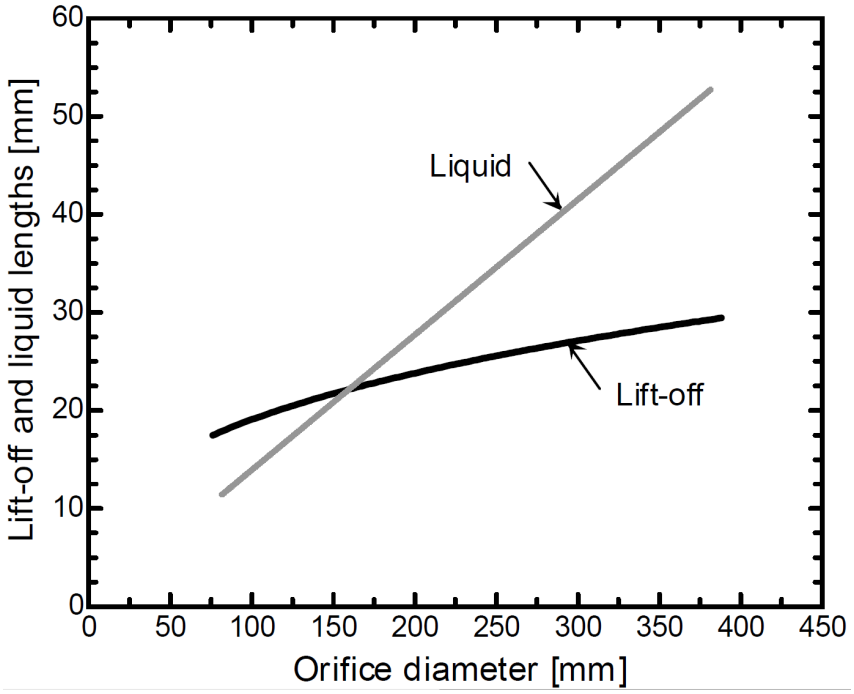

Figure 2.7. *Comparison of lift-off and liquid length at different nozzle diameter [55].*

the mixture of air with the vaporized fuel, the premixed combustion, the stoichiometric diffusion flame sheath which is known to exist in the periphery of the spray [58, 59], the soot formation region (inside this layer) and the combustion products (outside the surface). The schematic on the left, which resembles older technology (low injection pressure and large diameters), shows that there is very little vaporized fuel at the lift-off length and only 8% of the air required for combustion has been entrained. Additionally, as the liquid length is longer than that of the lift-off, the combustion surrounds the liquid region, resulting in a long vaporizing spray with a cool core. This has the consequence of a interaction between the vaporization and combustion processes, thus resulting in the vaporization cooling the gases and causing interaction with the flame stabilization at the lift-off length. On the other hand, the schematic on the right, resembling more recent technology (smaller diameter and higher pressures) represents a spray coming from a nozzle with a smaller diameter and with a larger pressure drop, being injected into a slightly cooler and less dense ambient. All this causes a radical change in the lift-off and liquid lengths proportion. In this case all the fuel has evaporated before the lift-off length, as a result of more air entrainment (relative to the fuel injected) and a smaller orifice. Also, there is no interaction between the evaporation and combustion processes, as the lift-off is longer that the liquid length and much more air is entrained. All this results in a reaction zone that is much more intense and with less soot formed [55]. This concept is consistent with the results presented in [60, 61], where the use of a micro-hole nozzle (as opposed to the standard nozzle) and/or higher injection pressures, yielded much lower smoke emissions.

Finally, Equation 2.8 presents a simplified correlation for the lift-off length depending on ambient conditions, fuel properties and injection parameters, based on correlations previously found [55, 56, 62].

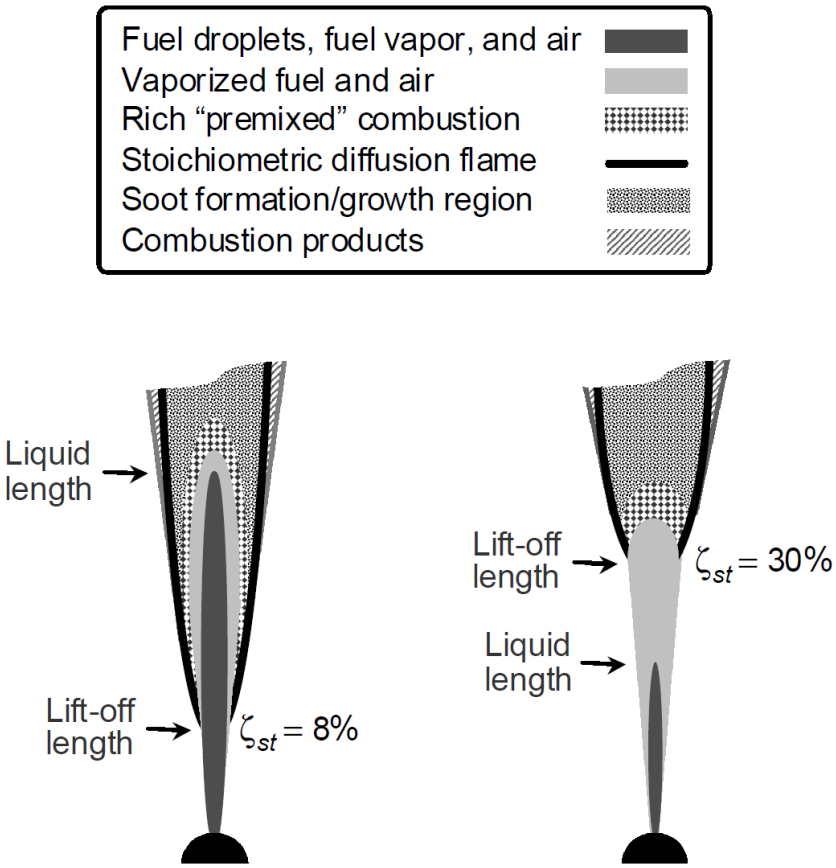

Figure 2.8. *Schematic of stoichiometric air entrained up to the lift-off length under quiescent conditions. The schematic on the left has an ambient gas at 1100 K and 23 kg/m^3 with a pressure drop and orifice diameter of 40 MPa and 250 µm. The schematic on the right has an ambient gas at 1000 K and 20 kg/m^3 with a pressure drop and orifice diameter of 200 MPa and 100 µm [55].*

$$LoL = C \cdot \frac{d_o^{0.34} \cdot U^1}{T^{3.74} \cdot \rho^{0.85} \cdot Z_{st}^1} \tag{2.8}$$

where LoL is the lift-off length, d_o is the nozzle exit diameter, U is the injection velocity, Z_{st} is the stoichiometric mixture fraction, C is the proportionality constant, and T and ρ are the ambient temperature and density, respectively.

Soot formation

Another important aspect of the diffusion flame is the formation and oxidation of soot, because combustion may happen and the spray may enter the phase of diffusion flame even if soot is not being generated.

The thermal decomposition of the fuel during the ignition delay phase may cause acetylene (C_2H_2) to be formed. This compound is an unsaturated hydrocarbon that reacts with its other molecules under high temperature to form poly-aromatic hydrocarbons

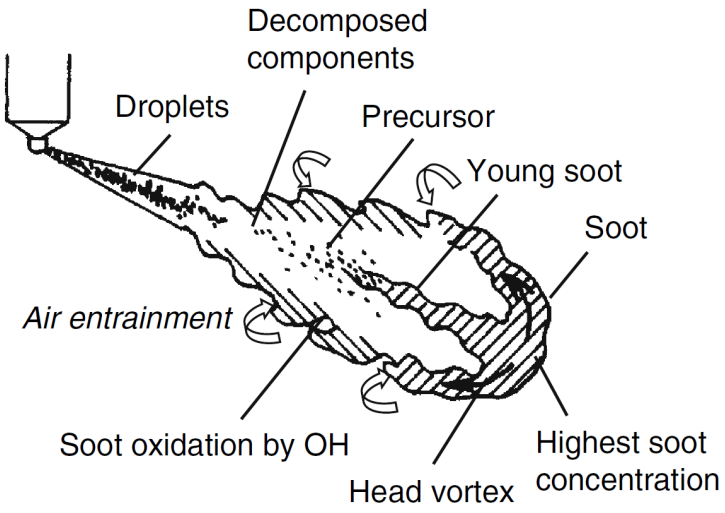

Figure 2.9. *Mechanism of soot formation and oxidation in a transient reacting spray [4].*

(PAH) that are known as soot precursors [63]. The soot starts forming then at the head of the spray as the fuel concentration is too rich in the centre of the flame [64]. Soot formation is dominated by the air temperature and local compositions, and they are most favourable at the flame tip [65]. The oxidation of soot is highly dominated by the reaction of the OH* radical, which is one of the intermediate combustion products [4]. This takes place downstream, as the soot is transported by the air flow to the centre of the spray, resulting in a zone with high temperature of soot [65].

Figure 2.9 helps the understanding of the processes of soot formation and oxidation in a reactive spray by summarizing what was explained previously. The fuel that is introduced into the combustion chamber atomizes into small droplets and then evaporates. The fuel vapour generates many saturated and unsaturated split hydrocarbons due to thermal cracking, such as acetylene from PAHs, which is a soot predecessor. Soot particles are formed at the periphery of the flame tip from poly-aromatic hydrocarbons, as the equivalence ratio and gas temperature favour it and fuel mixing is poor due to the soot clouds travelling in a direction parallel to the air current. Then, the particles start piling up and growing in size and begin travelling downstream, so the soot concentration increases and therefore the highest concentration of soot takes place in the spray tip, which then moves along the spray surface by the generated vortex. Finally, the soot batches that flow upstream along the spray perimeter are re-entrained into the spray core and oxidized by the OH* radical [4, 65].

2.5 Sequence of the spray processes under engine conditions

In order to summarize the phases of the diesel spray and put them together in a time (or crank angle) resolved context, a sequential explanation of the processes will be presented. This sequence is as similar to that presented by Dec [58] using a heavy duty

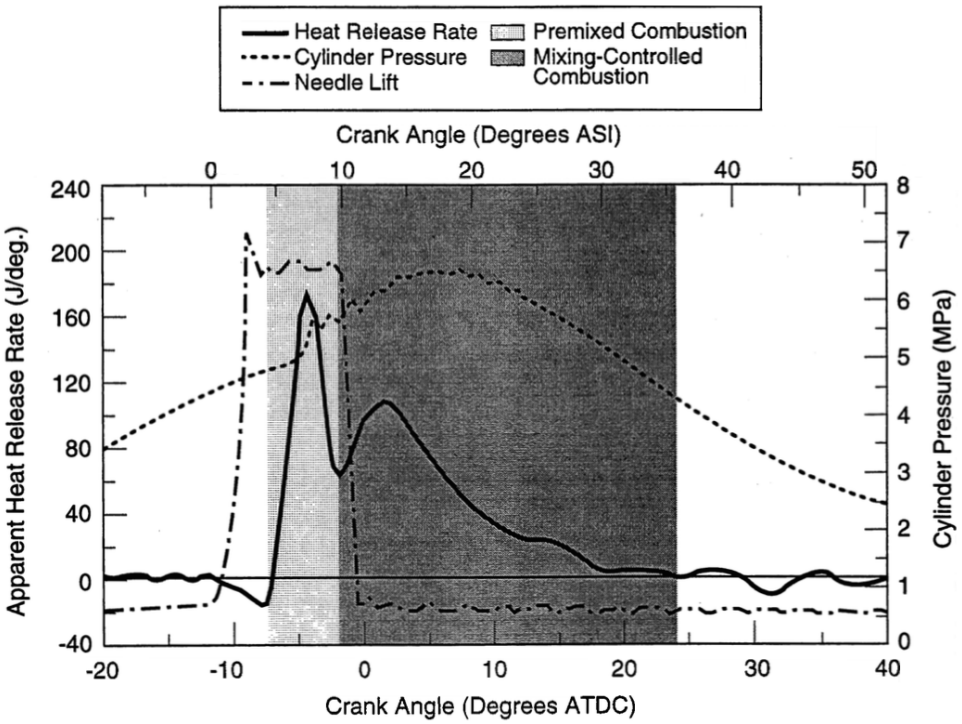

Figure 2.10. *Evolution of the apparent heat release rate, cylinder pressure and needle lift [58].*

engine with 2 l of displacement at 1200 RPM, therefore the resolution in CAD and not seconds.

Ignition delay (0-4 CAD ASI)

1.0° ASI The needle lift begins and the liquid starts penetrating into the chamber, the liquid region is comprised of droplets, ligaments and the intact core. (Figures 2.10 and 2.11)

2.0° ASI The liquid continues penetrating as the needle keeps on lifting. Additionally, as the spray entrains hot air a layer of fuel vapour forms on the sides of the liquid core. (Figures 2.10 and 2.11)

3.0° ASI The injector is fully open and coincidentally the liquid penetration has reached its maximum (*liquid length*); also, fuel keeps on evaporating and the vapour layer on the sides thickens. Some pre-reactions may be occurring along the sides of the spray, in the vapour region. (Figures 2.10 and 2.11)

4.0° ASI As the liquid core has reached its maximum penetration, the vapour phase of the spray (evaporated fuel + entrained air) keeps on penetrating as the injection event is still ongoing. Some pre-reactions are taking place and radicals are being formed. (Figures 2.10 and 2.11)

No apparent heat release is visible up to this point. On the contrary, there is a small decrease in the curve as the heat is absorbed by the liquid fuel in order to evaporate.

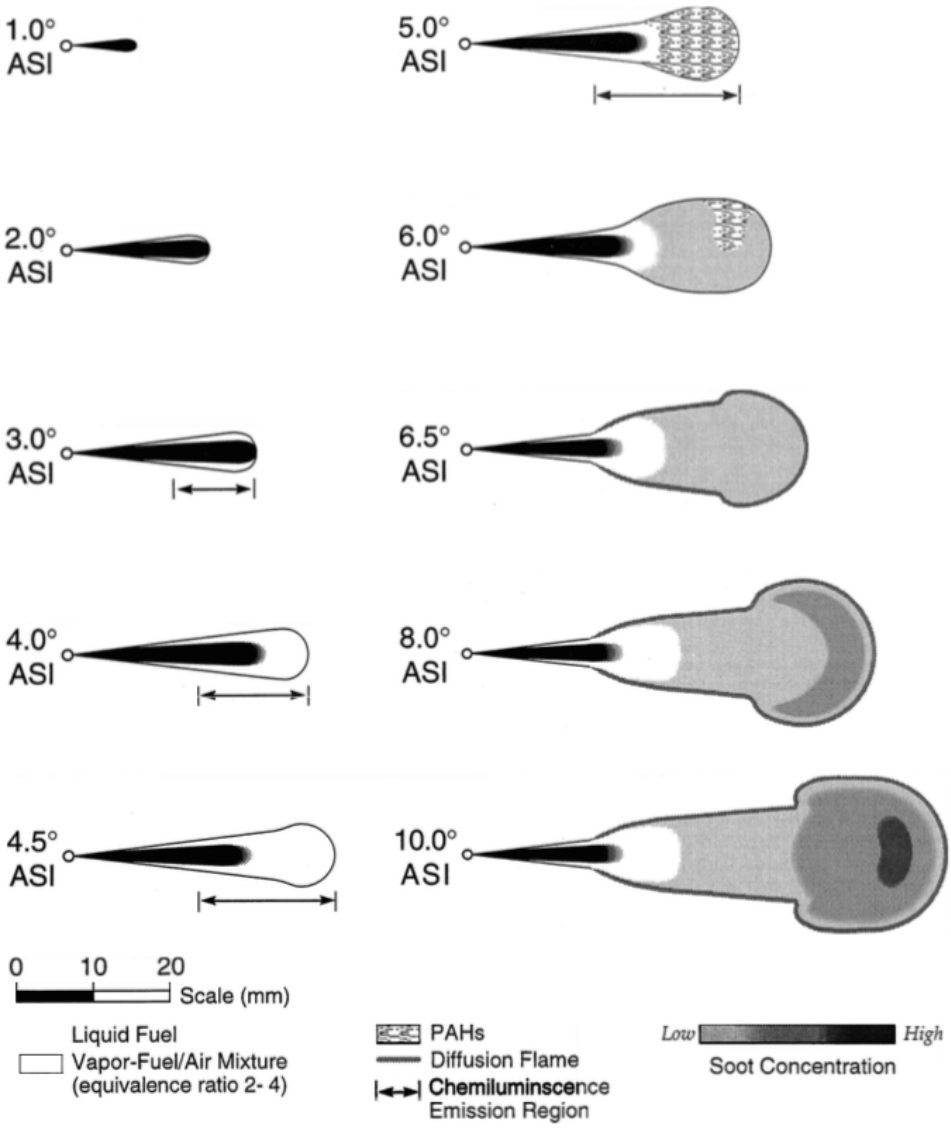

Figure 2.11. *Time resolved (1° = 139 μs) sequence of schematics showing the evolution of a reactive diesel from the start of injection up through the early part of the mixing-controlled combustion [58].*

(Figures 2.10)

Premixed combustion (4-9 CAD ASI)

4.5° ASI The initial part of the fuel oxidation takes place, and as consequence the heat release begins and the spray starts widening. The zone of chemiluminescence of radicals (OH*/CH*) keeps on growing and most of it comes from the leading portion of the spray. The time between the start of injection and this instant is the *ignition delay time*. (Figures 2.10 and 2.11)

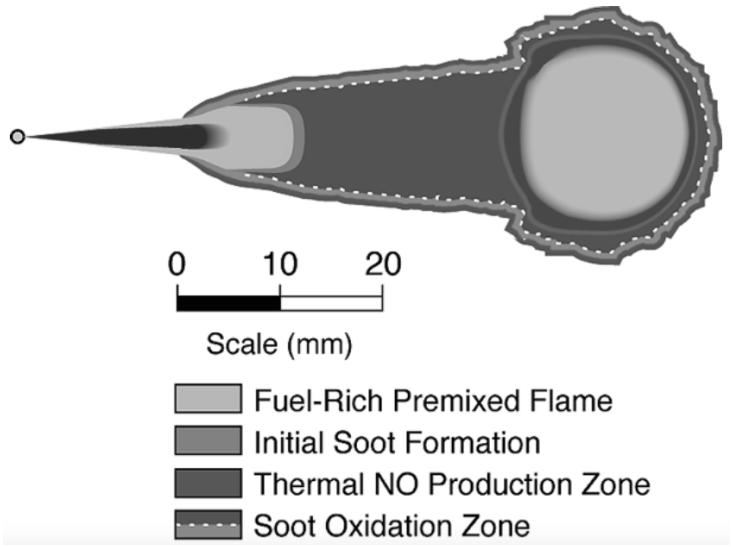

Figure 2.12. *Schematic of quasi-steady burning jet [66].*

5.0° ASI The rate of heat release grows rapidly and large PAHs start to form on the tip of the spray as fuel breaks down. The zone of chemiluminescence has reached a maximum value (*lift-off length*). (Figures 2.10 and 2.11)

6.0° ASI Soot formation begins in large portions of the spray as the oxygen is depleting, but the rate of heat release keeps on rising. (Figures 2.10 and 2.11)

6.5° ASI Soot formation is complete and is found throughout the downstream region as the oxygen has been exhausted, the apparent rate of heat release has reached its maximum. The oxidation is now taking place on the periphery of the spray, from where the air is being entrained. (Figures 2.10 and 2.11)

8.0° ASI The flame front is defining itself and the soot concentration on the flame tip increases as the injected fuel keeps on burning. (Figures 2.10 and 2.11)

The phase of premixed combustion has ended as the rate of heat release reaches its first minimum after the peak. The subsequent heat released will be a product of the mixing of the new fuel injected. (Figures 2.10)

Mixing-controlled combustion (9-15 CAD ASI)

10.0° ASI The spray is a about to reach an stabilized phase, the amount of soot on the head vortex region keeps on rising due to the lack of oxygen for the newly vaporized fuel. (Figures 2.10 and 2.11)

The flame has reached an steady state. As the fuel keeps on being injected, the combustion is a process controlled by the evaporation of the fuel and the mixing of this vapour with the entrained air. As the fuel continues evaporating a rich premixed flame

will be present near the liquid core; additionally, this rich mixture will cause the soot to be formed. Due to the low availability of oxygen inside the spray, the soot oxidation will take place on the contour of the spray, from where the air is entrained. Also, the OH* radical concentrations are highest in the diffusion flame, as the attack of the OH* radical is the main method for soot oxidation [58]. Finally, concerning the premixed flame on the flame front, where the temperature is highest, the formation of nitrous oxides may also take place. (Figures 2.12)

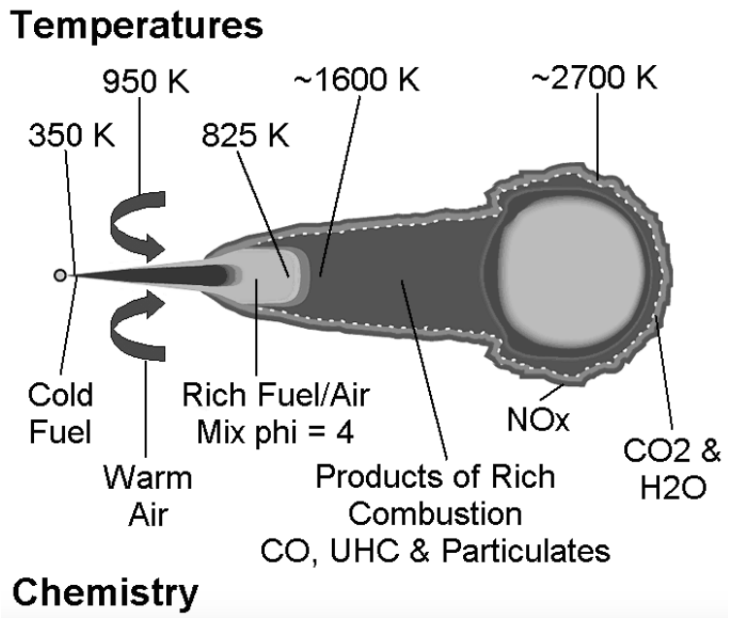

Figure 2.13. *Summary of fuel burning processes [66].*

Finally, an overview of the thermal and chemical variations inside a reactive spray is presented in Figure 2.13. The reactive diesel spray is basically a cold jet of liquid fuel entraining hot air; this mixture supplies the reactants to form a diffusion flame layer which surrounds the spray. Inside this layer there will be rich combustion products as carbon monoxide and unburned hydrocarbons due to the lack of oxygen; additionally, the high temperatures provide a good environment for the formation of nitrous oxides and particulate matter. These products will then go through the diffusion flame where they will achieve complete oxidation, and therefore turning into carbon dioxide and water vapour [66].

2.6 Effects of the fuel properties on the spray processes

Different types of fuel are being used in diesel engines in order to measure their effect on the emissions and performance; additionally, the study of different fuels under diesel-like conditions in combustion vessels is also an important field in the research of the different spray processes. Various fuel types are being used such as bio-diesel, synthetic Fischer-Tropsch fuels, Primary Reference Fuels, oxygenated fuels, diesel-gasoline blends

and surrogate fuels, to mention a few. In order to do this, different combustion strategies and fuel types have been studied in order to improve the engine efficiency and reduce the emission of pollutants. For example, a study with direct diesel injection and port gasoline injection showed that the higher amount of gasoline retarded the combustion phasing. This in turn lowered the heat transferred and allowed for the lowest fuel consumption, which also resulted in low NO_X and PM emissions [67]. Another study replaced entirely the diesel fuel with gasoline and also obtained less specific fuel consumption while obtaining lower smoke levels [68]. Blends of gasoline and ethanol have also been used in diesel engines in order to study the effects on combustion and reduce the amount of diesel injected [69]. Results have shown reduction of soot levels, but at the cost of higher NO_X and compromised combustion stability under some conditions. Furthermore, a similar study with blends and changes in the contour conditions also presented improvements in the combustion efficiency [70].

Regarding the study of the spray processes under diesel-like conditions in combustion vessels, past studies have shown that the physical properties of the fuel have very little effect on the vapour spray penetration [31, 71–74]. On the other side, such properties have proven to have a very important effect on the evaporation of the liquid fuel and therefore the liquid penetration of the spray [25, 26, 31, 47, 75, 76]. This last parameter is often correlated with the liquid density or boiling point, as they have demonstrated to be good indicators of the evaporation characteristics and volatility of the fuel. Nevertheless, the fuel effects on the reactive spray are a bit more complex than on the inert case, as not all chemical properties affect the spray processes in the same direction.

Ignition delay times and lift off lengths have been shown to be shorter for the synthetic fuels than those when using bio-diesel. Meanwhile, the flame opacity caused by the amount of soot present in the flame shows no clear trend when using the aforementioned fuels [71, 77]. Moreover, another work studied seven fuels with many different ignition characteristics (cetane number), physical properties (liquid density) and oxygen content under various conditions [62]. As mentioned, the fuels with higher cetane numbers also yielded the shorter lift-off lengths and ignition delay times.

Two oxygenated diesel fuels where compared to a non-oxygenated blend of primary reference fuels in a past work of research [78]. Both oxygenated fuels presented less natural luminosity than the non-oxygenated reference fuel, which could mean less soot within the flame. However, there where also some differences among the oxygenated compounds, which indicated that the oxygen was not the only important factor governing the soot reduction, as they both had the same amount of oxygen in their composition. A contemporary publication, presented the effect on the spray combustion of three oxygenated fuels with different mass contents versus conventional diesel. The results showed that all three oxygenated fuels presented lower ignition delay times at all conditions; nevertheless, the differences in delay times among them did not lead any clear trends [79]. Finally, a more recent work used diesel and blends of oxygenated fuels with a wide range of cetane numbers to study the relation of flame lift-off length and soot production with ignition delay [80]. Results show that short lift-off lengths are often related to small ignition delay times, while the trend is inverse when referring to soot luminosity. Regarding the fuel effects, diesel presented the highest soot luminosity and longer lift-off lengths than some of the oxygenated fuels. This means that, despite the relation previously described, the oxygenated fuels yielded shorter lift-off lengths due to

their increased reactivity, but the higher amounts of soot obtained with diesel are due to its composition.

Another type of fuels are those known as Primary Reference Fuels or PRFs, which represent both ends of the octane rating scale; namely *n*-heptane ($ON = 0$) and *iso*-octane ($ON = 100$). Said fuels also have very different cetane numbers and are good representatives of diesel and gasoline, respectively, in terms of ignition and combustion. A very recent study [81] presents the ignition mechanism of *n*-heptane and *iso*-octane under various conditions and it can be seen that for all cases the ignition delay times corresponding to *iso*-octane are always longer than those of *n*-heptane. Such results are also verified by experimental investigations [82], as the ignition delay of four different PRF blends was shown to increase as the composition of *iso*-octane augmented in the blends. Furthermore, engine tests also report an increase in the ignition delay times as the octane number of the fuel is greater [83–85]. Another work done with PRFs, diesel and gasoline, investigated the combustion recession after the end of injection [86]. The results showed that the fuels with higher cetane numbers presented the least lifted flames and the shortest combustion recession times. A similar study using just Primary Reference Fuel blends studied the influence of the fuel properties on the lift-off length, ignition delay times and soot luminosity [87]. The chemical properties of the fuel showed to be of paramount importance on the ignition and combustion of a spray, as the blends with highest cetane numbers presented the shorter lift-off lengths, smaller ignition delay times and the most soot luminosity. Analogously, the lift-off length and ignition delay time relationship was also studied under a wider range of conditions using conventional diesel and a PRF blend of similar properties [88]. Although the trend was not very clear, there was a interaction implying that the point with longer lift-off lengths also presented the greater ignition delay times.

2.7 Outlook

As mentioned throughout this chapter, there are many parameters to be taken into account in order to characterize a diesel spray. Moreover, for a fuel spray injected under non-reactive conditions, no other processes, besides the aforementioned ones along Section 2.3, would take place.

Figure 2.14 presents a block diagram of diesel combustion, similar to one found in [17]. On one hand, there are the air characteristics, starting with EGR, which in this research has been simulated by adding nitrogen to the air in order to decrease the amount of oxygen and reduce the reactivity of the air. Then, there are the effects of the ambient air such as temperature and density; in this case the latter has been regulated with the ambient pressure. On the other hand, there are the properties of the fuels, both physical and chemical, such a cetane and octane numbers, density, boiling point, enthalpy of vaporization, among others. The paths of the air and fuel merge in the combustion chamber, and in order to study the spray characteristics, the spray penetration and cone angle have been measured; additionally, the liquid length has been determined too under inert conditions to study the vaporizing characteristics of the fuels. The time and distance from the nozzle at which the premixed combustion takes place will be analyzed with the measurements of ignition delay time and the lift-off length; the spray penetration has

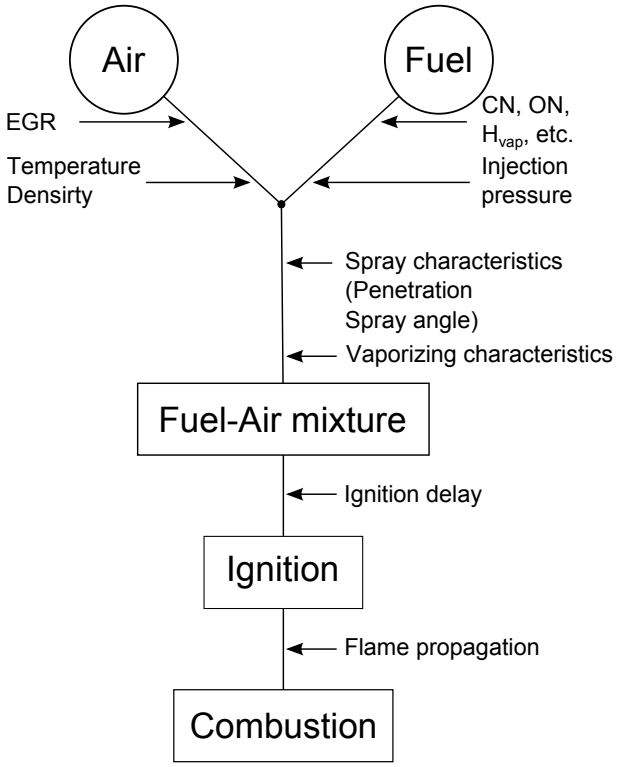

Figure 2.14. *Block diagram of diesel combustion.*

also been measured under reactive conditions to help further understand the premixed combustion. The mixing controlled combustion and the flame propagation and subsequent combustion of the injected fuel will be also studied by analyzing the flame evolution, both soot onset length and maximum stabilized flame penetration, and the generation and luminosity of soot.

Bibliography

[1] Heywood J. *Internal Combustion Engine Fundamentals*. McGraw-Hill Education, 1988.

[2] Tinaut F.V., Melgar A. and Giménez B. "A model of atomization of a transient evaporative spray". *SAE Technical Paper*, n^o 1999-01-0913, 1999.

[3] Lefebvre A.H. *Atomization and Sprays*. Hemisphere Publishing Corporation, 1989.

[4] Arcoumanis C. and Kamimoto T. *Flow and Combustion in Reciprocating Engines*. Springer-Verlag, 2009.

[5] Kamimoto T., Yokota H. and Kobayashi H. "A new technique for the measurement of sauter mean diameter of droplets in unsteady dense sprays". *SAE Technical Paper*, n^o 890316, 1989.

[6] Hodges J.T., Baritaud T.A. and Heinze T.A. "Planar liquid and gas fuel and droplet size visualization in a DI diesel engine". *SAE Technical Paper*, n^o 910726, 1991.

[7] Som S., Ramirez A.I., Longman D.E. and Aggarwal S.K. "Effect of nozzle orifice geometry on spray, combustion, and emission characteristics under diesel engine conditions". *Fuel*, Vol. 90(3), pp. 1267–1276, 2011.

[8] Hiroyasu H. and Kadota T. "Fuel droplet distribution in diesel combustion chamber". *SAE Technical Paper*, n^o 740715, 1974.

[9] Arcoumanis C. and Cutter P.A. "Flow and heat transfer characteristics of impinging diesel sprays under cross-flow conditions". *SAE Technical Paper*, n^o 950448, 1995.

[10] Arcoumanis C. and Gavaises M. "Linking nozzle flow with spray characteristics in a diesel fuel injection system". *Atomization and Sprays*, Vol. 8(3), pp. 307–347, 1998.

[11] Huh K.Y., Lee E. and Koo J. "Diesel spray atomization model considering nozzle exit turbulence conditions". *Atomization and Sprays*, Vol. 8(4), pp. 453–469, 1998.

[12] Arrègle J. *Análisis de la estructura y dinámica interna de chorros Diesel*. Doctoral Thesis, Universitat Politècnica de València, 1997.

[13] Naber J. and Siebers D.L. "Effects of gas density and vaporization on penetration and dispersion of diesel sprays". *SAE Technical Paper*, n^o 960034, 1996.

[14] López J.J. *Estudio teórico-experimental del chorro libre diesel no evaporativo y de su interacción con el movimiento del aire*. Doctoral Thesis, Universitat Politècnica de València, 2003.

[15] Reitz R.D. and Bracco F.V. "Mechanism of atomization of a liquid jet". *Physics of Fluids*, Vol. 25(10), pp. 1730–1742, 1982.

[16] Gülder Ö.L. "Views on the structure of transient diesel sprays". *Atomization and Sprays*, Vol. 10(3-5), pp. 355–386, 2000.

[17] Hiroyasu H. and Arai M. "Structures of fuel sprays in diesel engines". *SAE Technical Paper*, n^o 900475, 1990.

[18] Arai M., Tabata M., Hiroyasu and Shimizu M. "Disintegrating process and spray characteristics of fuel jet injected by a diesel nozzle". *SAE Technical Paper*, n^o 840275, 1984.

[19] Pickett L., Manin J., Kastengren A. and Powell C. "Comparison of near-field structure and growth of a diesel spray using light-based optical microscopy and x-ray radiagraphy". *SAE International Journal of Engines*, Vol. 7(2), pp. 1044–1053, 2014.

[20] García J.M. *Aportaciones al estudio del proceso de combustión turbulenta de chorros en motores diesel de inyección directa*. Doctoral Thesis, Universitat Politècnica de València, 2004.

[21] Ricou F.P. and Spalding D.B. "Measurements of entrainment by axisymetrical turbulent jets". *Journal of Fluid Mechanics*, Vol. 11, pp. 21–32, 1961.

[22] Cossali G.E, L. G. Brunello and Coghe A. "LDV characterization of air entrainment in transient diesel sprays". *SAE Technical Paper*, n^o 910178, 1991.

[23] Cossali G.E., Gerla A., Coghe A. and Brunello G. "Effect of gas density and temperature on air entrainment in a transient diesel spray". *SAE Technical Paper*, n^o 960862, 1996.

[24] Araneo L., Coghe A. and Cossali G.E. "Experimental analysis of structure and characteristics of a diesel spray head vortex". In *Proceedings of the thirteen ICLASS*, pp. 103–109, 1997.

[25] Siebers D.L. "Liquid-phase fuel penetration in diesel sprays". *SAE Technical Paper*, n^o 980809, 1998.

[26] Siebers D.L. "Scaling liquid-phase fuel penetration in diesel sprays based on mixing-limited vaporization". *SAE Technical Paper*, n^o 1999-01-0528, 1999.

[27] Cho I.Y., Fujimoto H., Kuniyoshi H., Ha J.Y, Tanabe H. and Sato G.T. "Similarity law of entrainment into diesel spray and steady spray". *SAE Technical Paper*, n^o 900447, 1990.

[28] Obokata T., Hashimoto T. and Takahashi H. "LDA analysis of diesel spray and entrainment air flow". In *Comodia international symposium*, pp. 231–236, 1990.

[29] Chikahisa T. and Murayama T. "Theory and experiments on air-entrainment in fuel sprays and their application to interpret diesel combustion processes". *SAE Technical Paper*, n^o 950447, 1995.

[30] Han D. and Mungal M.G. "Direct measurement of entrainment in reacting/nonreacting turbulent jets". *Combustion and Flame*, Vol. 124(3), pp. 370–386, 2001.

[31] Kook S. and Pickett L.M. "Liquid length and vapor penetration of conventional, Fischer-Tropsch, coal-derived, and surrogate fuel sprays at high-temperature and high-pressure ambient conditions". *Fuel*, Vol. 93, pp. 539–548, 2012.

[32] Correas D. *Theoretical and experimental study of isothermal diesel free sprays.* Doctoral Thesis, Universitat Politècnica de València, 1998.

[33] Wan Y. and Peters N. "Scaling of spray penetration with evaporation". *Atomization and Sprays*, Vol. 9(2), pp. 111–132, 1999.

[34] Arrègle J., Pastor J.V. and Ruiz S. "The Influence of injection parameters on diesel spray characteristics". *SAE Technical Paper*, n^o 1999-01-0200, 1999.

[35] Reitz R.D. and Bracco F.V. "On the dependence of spray angle and other spray parameters on nozzle design and operating conditions". *SAE Technical Paper*, n^o 790494, 1979.

[36] Tindal M.J., Williams T.J. and Harcombe A.T. "Fuel spray formation in an experimental swirl chamber". *SAE Technical Paper*, n^o 870451, 1987.

[37] Pickett L.M., Manin J., Payri R., Bardi M. and Gimeno J. "Transient rate of injection effects on spray development". *SAE Technical Paper*, n^o 2013-24-0001, 2013.

[38] Bower G.R. and Foster D.E. "The effect of split injection on fuel distribution in an engine-fed combustion chamber". *SAE Technical Paper*, n^o 930864, 1993.

[39] Espey C. and Dec J.E. "The effect of TDC temperature and density on the liquid-phase fuel penetration in a DI diesel engine". *SAE Technical Paper*, n^o 952456, 1995.

[40] Browne K.R., Partridge I.M. and Greeves G. "Fuel property effects on fuel/air mixing in an experimental diesel engine". *SAE Technical Paper*, n^o 860223, 1986.

[41] Martínez S. *Desarrollo de una instalación experimental para el estudio de chorros diesel evaporados en atmósfera inerte y reactiva.* Doctoral Thesis, Universitat Politècnica de València, 2003.

[42] Verhoeven D., Vanhemelryck J.L. and Baritaud T. "Macroscopic and ignition characteristics of high-pressure sprays of single-component fuels". *SAE Technical Paper*, n^o 981069, 1998.

[43] Kamimoto T., Yokota H. and Kobayashi H. "Effect of high pressure injection on soot formation processes in a rapid compression machine to simulate diesel flames". *SAE Technical Paper*, n^o 871610, 1987.

[44] Payri. R., Gimeno J., Bardi M. and Plazas A. "Study liquid length penetration results obtained with a direct acting piezo electric injector". *Applied Energy*, Vol. 106, pp. 152–162, 2013.

[45] Malbec L.M., Egúsquiza J., Bruneaux G. and Meijer M. "Characterization of a set of ECN Spray A injectors: Nozzle to nozzle variations and effect of spray characteristics". *SAE International Journal of Engines*, Vol. 6(3) n^o 2013-24-0037, pp. 1642–1660, 2013.

[46] Payri R., García-Oliver J.M., Bardi M. and Manin J. "Fuel temperature influence on diesel sprays in inert and reacting conditions". *Applied Thermal Engineering*, Vol. 35, pp. 185–195, 2012.

[47] Higgins B., Mueller C. and Siebers D. "Measurements of fuel effects on liquid-phase penetration in DI sprays". *SAE Technical Paper*, n^o 1999-01-0519, 1999.

[48] Yeh C.N., Kamimoto T., Korobi S. and Kosaka H. "2-D imaging of fuel vapor concentration in a diesel spray via excuplex-based Fluorescence technique". *SAE Technical Paper*, n^o 932652, 1993.

[49] González C. *Estudio de la influencia de la geometría de la tobera de inyección en la combustión y emisión de contaminantes de un motor diesel*. Doctoral Thesis, Universitat Politècnica de València, 2005.

[50] Desantes J.M., Pastor J.V., Payri R. and Pastor J.M. "Experimental Characterization of Internal Nozzle Flow and Diesel Spray Behavior. Part II. Evaporative Conditions". *Atomization and Sprays*, Vol. 15, pp. 517–543, 2005.

[51] Taylor C.F. *The Internal-Combustion Engine in Theory and Practice*. MIT Press, 1985.

[52] Higgins B., Siebers D. and Aradi A. "Diesel-spray ignition and premixed-burn behavior". *SAE Technical Paper*, n^o 2000-01-0940, 2000.

[53] Dec J.E. and Espey C. "Chemiluminescence imaging of autoignition in a DI diesel engine". *SAE Technical Paper*, n^o 982685, 1998.

[54] Peters N. *Turbulent Combustion*. Cambridge University Press, 2000.

[55] Siebers D. and Higgins B. "Flame lift-off on direct-injection diesel sprays under quiescent conditions". *SAE Technical Paper*, n^o 2001-01-0530, 2001.

[56] Siebers D., Higgins B. and Pickett L. "Flame Lift-off on direct-injection diesel fuel jets: Oxygen concentration effects". *SAE Technical Paper*, n^o 2002-01-0890, 2002.

[57] Higgins B. and Siebers D. "Measurement of the Flame Lift-Off Location on DI Diesel Sprays Using OH Chemiluminescence". *SAE Technical Paper*, n^o 2001-01-0918, 2001.

[58] Dec J.E. "A conceptual model of DI diesel combustion based on laser-sheet imaging". *SAE Technical Paper*, n^o 970873, 1997.

[59] Kosaka H., Nishigaki T., Kamimoto T., Sano T., Matsutani A. and Harada S. "Simultaneous 2-D imaging of OH radicals and soot in a diesel flame by laser sheet techniques". *SAE Technical Paper*, n^o 960834, 1996.

[60] Kobori S., Kamimoto T. and Kosaka H. "Ignition, combustion and emissions in a DI diesel engines equipped with a micro-hole nozzle". *SAE Technical Paper*, n^o 960321, 1996.

[61] Yokota H., Kamimoto T., Kosaka H. and Tsujimura K. "Fast burning and reduced soot formation via ultra-high pressure diesel fuel injection". *SAE Technical Paper*, n^o 910225, 1991.

[62] Pickett L.M., Siebers D.L. and Idicheria C.A. "Relationship between ignition processes and the lift-off length of diesel fuel jets". *SAE Technical Paper*, n^o 2005-01-3843, 2005.

[63] Kitamura T., Ito T., Senda J. and Fujimoto H. "Mechanism of smokeless diesel combustion with oxygenated fuels based on the dependence of the equivalence ratio and temperature on soot particle formation". *International Journal of Engine Research*, Vol. 3(4), pp. 223–248, 2002.

[64] Won Y.H., Kamimoto T., Kobayashi H. and Kosaka H. "2-D visualization in unsteady spray flame by means of laser sheet scattering technique". *SAE Technical Paper*, n^o 910223, 1991.

[65] Won Y.H., Kamimoto T. and Kosaka H. "A study on soot formation in unsteady spray flames via 2-D soot imaging". *SAE Technical Paper*, n^o 920114, 1992.

[66] Flynn P.F., Durrett R.P., Hunter G.L., zur Loye A.O., Akinyemi O.C., Dec J.E. and Westbrook C.K. "Diesel combustion: An intengrated view combining laser diagnostics, chemical kinetics, and empirical validation". *SAE Technical Paper*, n^o 1999-01-0509, 1999.

[67] Hanson R., Kokjohn S., Splitter D. and Reitz R. "An experimental investigation of fuel reactivity controlled PCCI combustion in a heavy-duty engine". *SAE Technical Paper*, n^o 2010-01-0864, 2010.

[68] Kalghatgi G.T., Gurubaran R. Kumara, Davenport A., Harrison A.J., Hardalupas Y. and Taylor A.M.K.P. "Some advantages and challenges of running a Euro IV, V6 diesel engine on a gasoline fuel". *Fuel*, Vol. 108, pp. 197–207, 2013.

[69] Benajes J., Molina S., García A. and Monsalve-Serrano J. "Effects of direct injection timing and blending ratio on RCCI combustion with different low reactivity fuels". *Energy Conversion and Management*, Vol. 99, pp. 193–209, 2015.

[70] Desantes J., Benajes J., García A. and Monsalve-Serrano J. "The role of the in-cylinder gas temperature and oxygen concentration over low load reactivity controlled compression ignition combustion efficiency". *Energy*, Vol. 78, pp. 854–868, 2014.

[71] Nerva J.G. *An assessment of fuel physical and chemical properties in the combustion of a Diesel spray.* Doctoral Thesis, Universitat Politècnica de València, 2013.

[72] Pastor J.V., García-Oliver J.M., Pastor J.M. and Vera-Tudela W. "One-dimensional diesel spray modeling of multicomponent fuels". *Atomization and Sprays*, Vol. 25(2), pp. 485–517, 2015.

[73] Payri R., García A., Domenech V., Durrett R. and Plazas A.H. "An experimental study of gasoline effects on injection rate, momentum flux and spray characteristics using a common rail diesel injection system". *Fuel*, Vol. 97, pp. 390–399, 2012.

[74] Galle J., Defruyt S., de Maele C. Van, Rodriguez R. Piloto, Denon Q., Verliefde A. and Verhelst S. "Experimental investigation concerning the influence of fuel type and properties on the injection and atomization of liquid biofuels in an optical combustion chamber". *Biomass and Bioenergy*, Vol. 57, pp. 215–228, 2013.

[75] Pastor J.V., García-Oliver J.M., Nerva J.G. and Giménez B. "Fuel effect on the liquid-phase penetration of an evaporating spray under transient diesel-like conditions". *Fuel*, Vol. 90(11), pp. 3369–3381, 2011.

[76] Canaan R.E., Dec J.E., Green R.M. and Daly D.T. "The influence of fuel volatility on the liquid-phase fuel penetration in a heavy-duty DI diesel engine". *SAE Technical Paper*, n^o 980510, 1998.

[77] Payri F., Pastor J.V., Nerva J.G. and García-Oliver J. "Lift-off length and KL extinction measurements of biodiesel and Fischer-Tropsch fuels under quasi-steady diesel engine conditions". *SAE International Journal of Engines*, Vol. 4(2) n^o 2011-24-0037, pp. 2278–2297, 2011.

[78] Mueller C.J. and Martin G.C. "Effects of oxygenated compounds on combustion and soot evolution in a DI diesel engines: Broadband natural luminosity imaging". *SAE Technical Paper*, n^o 2002-01-1631, 2002.

[79] Ito T., Ueda M., Matsumoto T., Kitamura. T., Senda J. and Fujimoto H. "Effects of ambient gas conditions on ignition and combustion process of oxygenated fuel sprays". *SAE Technical Paper*, n^o 2003-01-1790, 2003.

[80] Donkerbroek A.J., Boot M.D., Luijten C.C.M., Dam N.J. and ter Meulen J.J. "Flame lift-off length and soot production of oxygenated fuels in relation with ignition delay in a DI heavy-duty diesel engine". *Combustion and Flame*, Vol. 158, pp. 525–538, 2011.

[81] Han W.Q. and Yao C.D. "Research on high cetane and hig octane number fuels and the mechanism for their common oxidation and auto-ignition". *Fuel*, Vol. 150, pp. 29–40, 2015.

[82] Machrafi H., Cavadia S. and Gilbert P. "An experimental and numerical analysis of the HCCI aiuto-ignition process of primary reference fuels, toluene reference fuels and diesel fuels in an engine, varying the engine parameters". *Fuel Processing Technology*, Vol. 89, pp. 1007–1016, 2008.

[83] Lü X.C., Chen W., Hou Y.C. and Huang Z. "Study on the ignition, combustion and emissions of a HCCI combustion engines fueled with primary reference fuels". *SAE Technical Paper*, n^o 2005-01-0155, 2005.

[84] Xionq Q., Inaba K., Ogawa H. and Shibata G. "Influence of fuel properties on opoperation range and thermal efficiency of premixed diesel combustion". *SAE International Journal of Fuels and Lubricants*, Vol. 6(3) n^o 2013-32-9054, pp. 1005–1013, 2013.

[85] López J.J., García-Oliver J.M., García A. and Domenech V. "Gasoline effects on spray characteristics, mixing and auto-ignition processes in a CI engine under partially premixed combustion conditions". *Applied Thermal Engineering*, Vol. 70(1), pp. 996–1006, 2014.

[86] Knox B.W., Genzale C.L., Pickett L.M., García-Oliver J.M. and Vera-Tudela W. "Combustion recession after end of injection in diesel sprays". *SAE International Journal of Engines*, Vol. 8(2) n^o 2015-01-0797, 2015.

[87] Pastor J.V., García-Oliver J.M., Novella R. and Vera-Tudela W. "Investigation on ignition and combustion characteristics of primary reference fuels under diesel engine conditions". In *Der Arbeitsprozess des Verbrennungsmotors*, pp. 378–393. Institut für Verbrennungskraftmaschinen und Thermodynamik, Technische Universität Graz, September 2013.

[88] Persson H., Andersson Ö. and Egnell R. "Fuel effects on flame lift-off under diesel conditions". *Combustion and Flame*, Vol. 158, pp. 91–97, 2011.

Chapter 3

Experimental and theoretical tools and methodological approach

Contents

3.1 Introduction

The purpose of this third chapter is to give a comprehensive explanation of the tools that contributed to the gathering of information for this work of research. The test rigs in which the experiments were carried on, the optical techniques that were used for the visualization of the characteristic parameters of the spray and the numerical model for the calculation of additional parameters will all be described in detail.

3.2 Experimental facilities

For this research, two different test rigs were used. A two-stroke engine for the experiments under inert conditions and constant pressure vessel for the reactive ones. All tests were carried out using single-hole nozzles in order to eliminate the effects caused by spray-to-spray interaction.

3.2.1 2-Stroke optical engine

The experiments under inert conditions for the study of spray mixing and evaporation were conducted in the hot spray test rig described in [1, 2]. This facility is based on a modified loop-scavenged single cylinder two-stroke direct injection diesel engine (Jenbach JW 50), with a displacement of 3 litres (bore 150 mm, effective stroke 108 mm), low rated rotational speed (500 RPM) and a compression ratio of 15.6:1. The engine does not generate any positive net work per cycle due to the amount of fuel injected for an engine of this given displacement (4-18 $mg/cycle$), so it could be thought of as a "passive compression machine" [3, 4]. So in order to rotate and keep a constant speed it is coupled to an electrical motor.

Due to the absence of inlet or exhaust valves, optical access to the combustion chamber can be easily achieved through the cylinder head, which encloses a cylindrical combustion chamber (diameter 45 mm, height 91 mm). This chamber has an upper access where the fuel injector is mounted and four lateral orthogonal accesses. One of them is used to install a pressure transducer, whereas the other three accesses are equipped with elliptical quartz windows, 88 mm high, 37 mm wide and 28 mm thick (Figure 3.1). Taking into account the peripheral obstruction of the sealing and the injector penetration, the useful line-of-sight area for imaging is 78 mm long and 29 mm wide. The details of the engine are shown in Table 3.1.

The hot spray test rig can be operated under inert or reacting ambient conditions. For the latter configuration, the rig is operated as a conventional engine, that is, ambient air is aspirated through the intake system. In the inert atmosphere configuration, nitrogen is supplied to the rig instead of air, so that fuel combustion is avoided. A roots compressor is used as an intake supercharging system to increase intake air pressure up to 0.3 MPa. Additionally, the intake air temperature is controlled by means of two conditioning units and a small settling chamber up to values of 400 K. The set-up makes it possible to reproduce thermodynamic conditions (pressure, temperature and density) similar to those in a direct injection diesel engine. The current setup is configured for the visualization of a spray by using a single-hole nozzle injecting the fuel downwards (Figure 3.1).

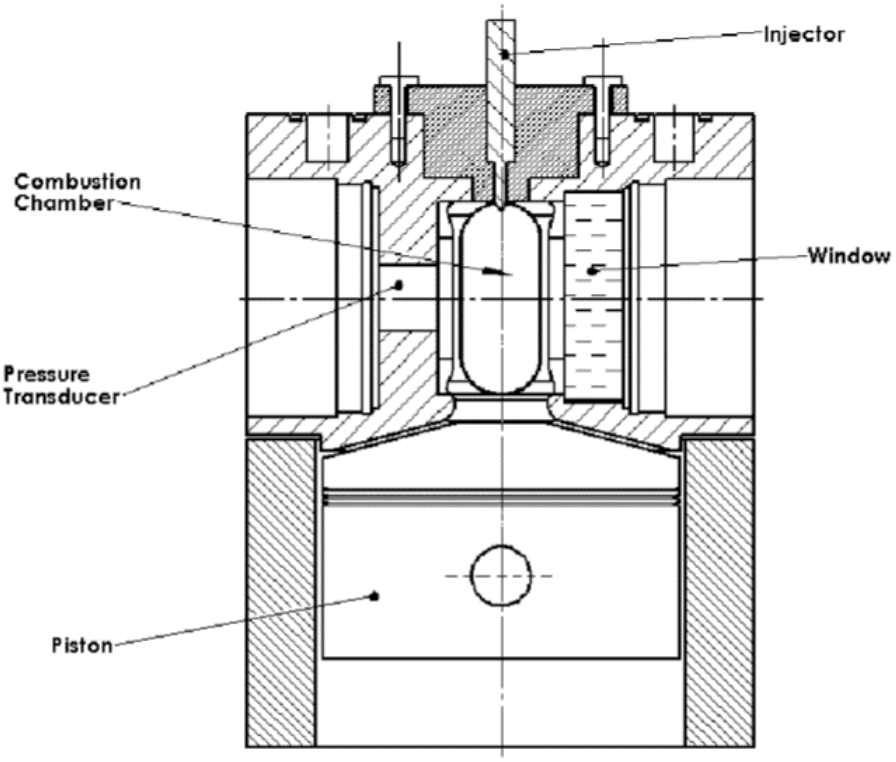

Figure 3.1. *Cross-section of the two-stroke engine with optical head (Side view).*

Table 3.1. *Hot spray test rig characteristics.*

Type	Single-cylinder two-stroke loop-scavenged engine
Displacement	3000 cm^3
Bore	150 mm
Stroke	170 mm
Effective stroke	108 mm
Distance between injector tip and piston head at TDC	87.7 mm
Compression ratio	15.6:1
Speed	500 RPM
Electric motor power	37 kW
Chamber diameter	45 mm
Chamber height	91 mm
Window height	88 mm
Window width	37 mm

3.2.2 High Pressure High Temperature Vessel

The reactive tests for the study of spray auto-ignition and combustion were performed in a high pressure and high temperature (HPHT) test chamber, in which the thermodynamic conditions similar to a diesel engine at the instant of injection can be obtained. As presented in [5], the vessel is classified as a constant-pressure flow (CPF) facility, as the conditions are reached by a continuous flow of high-pressure high-temperature gas through the chamber. The vessel is equipped with three large optical accesses (128 mm of diameter) arranged in an orthogonal manner so that there is a full vision of the injection event (Figure 3.2). The limits of the vessel are 15 MPa of air pressure and 1000 K or air temperature, and it is possible to obtain nearly quiescent and steady thermodynamic conditions in the test chamber [6–8]. A summary of the details of the vessel is shown in Table 3.2. This equipment is also comprised of an injection system that allows to change the fuel injection pressure and duration of injection. Furthermore, the facility is prepared for single- and multi-hole injector; however, for the tests presented here a single-hole nozzle has been used, injecting the fuel horizontally (Figure 3.2).

The pressurized gas is supplied to the vessel by two volumetric compressors working in parallel, providing a continuous feed of 70 Nm^3/h. Additionally, and in order to allow temporary variations of the gas flow without acting on the compressors, two high pressure tanks of a total volume of 0.1 m^3 have been placed in-between the test vessel and the compressors. Due to the configuration of the layout, it is possible to work in open or closed circuits in order to simulate EGR and testing under inert conditions. On one hand, under open circuit operation, the intake gas to the compressors is ambient air, which has an oxygen concentration of 21 %, and the outlet gases of the vessel are discharged to the atmosphere. On the other hand, under closed circuit operation, the intake to the compressors is a mixture of atmospheric air and pure nitrogen, allowing the oxygen concentration to be varied from 0 % to 21 %. In this case, the outlet gases from the vessel are recirculated instead of being discharged to the atmosphere, and the gas oxygen content is measured with a lambda sensor. The content of oxygen in the combustion chamber is then adjusted by either adding air or nitrogen by a reintegration system. It is important to note that even though the injected fuel and combustion products remain in the system when working under closed circuit operation, they do not affect the subsequent tests for two reasons. The first one is that there is an air-liquid separator that removes the injected fuel from the circulating air mixture. The second, is that the combustion products are of no significance on the composition and density of the chamber air, as those few milligrams of burnt gases are negligible when compared to the kilograms of pressurised air that are being circulated for all the tests.

In order to heat the flowing air, two electrical heaters of 15 kW each are placed upstream the chamber, allowing a maximum outlet temperature of 1173 K. Also, a secondary heater of 2.5 kW is placed at the bottom of the chamber to help maintain the temperature. Additionally, a 3 kW heating liner is placed in the periphery of the chamber to minimize the heat losses from the in-chamber air to the outside of the vessel.

Finally, the conditions inside the combustion chamber are controlled by a closed loop PID system that adjusts the pressure and the power of the heaters to obtained the temperature required for the experiments. A more detailed description of the gas circuit,

heating system, test chamber, temperature control and nozzle temperature control of the facility can be found in [8].

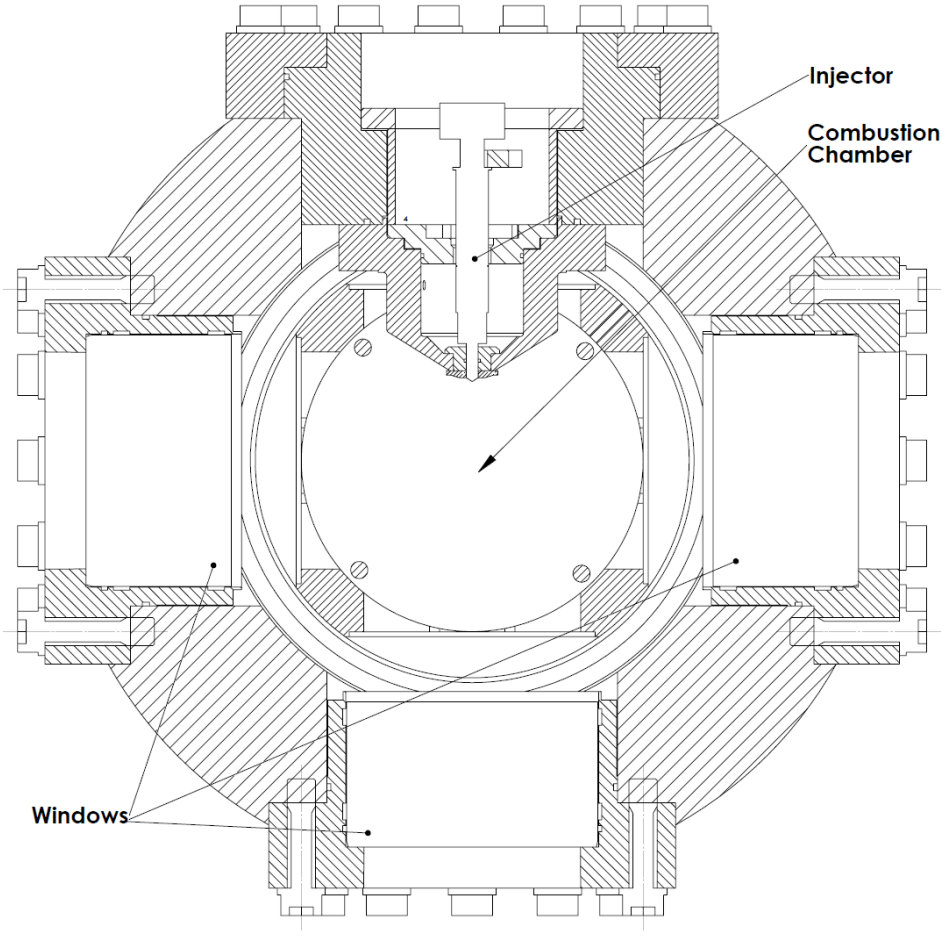

Figure 3.2. *Cross-section of the high temperature high pressure vessel (Top view).*

Table 3.2. *Characteristics of the HPHT vessel.*

Facility type	CPF
Chamber diameter	200 mm
Chamber height	250 mm
Window diameter	128 mm
Max. pressure	150 MPa
Max. temperature	1000 K
Max. density (@ 900 K)	53 kg/m^3
Main heater power	30 kW
Gas velocity	<0.3 m/s

3.3 Optical techniques

In this sections the applied optical techniques will be described. For the study of the inert spray, only schlieren and Mie-scattering were used, because only the parameters of spray vapour penetration and maximum liquid length were quantified. On the other hand, for the experiments under reactive conditions, schlieren was used again for vapour penetration but now with the addition of autoignition delay time, as well as OH* radical chemiluminescence for the flame lift-off length and broadband radiation imaging for different measurements.

The digital images have been analysed by means of purpose-developed processing software, which delivers the spray/flame geometrical parameters. Examples of Mie-scattering, schlieren, broadband radiation and OH* chemiluminescence images are shown in Figures 3.3 to 3.6.

3.3.1 Mie-scattering

The penetration of the liquid core of the spray has been captured by Mie-scattering imaging, which relies on the light reflected by liquid droplets. In practice, two types of light scattering are happening. On one hand, the spherical particles larger than one tenth of the incident wavelength are scattering the light under the hypothesis of kinetic energy conservation, also known as "elastic scattering", and most of it is reflected in the same direction of the incident wavelength; this is Mie-scattering. On the other hand, the particles that are much smaller than the wavelength, even on a molecular scale, are diffusing the light in a more homogeneous way, this is Rayleigh-Scattering. Therefore, an evaporating spray presents both types of scattering [4]; nevertheless, the intensity of the light reflected by the vapour phase is so low compared to that of the liquid that their effect is negligible, making this technique appropriate to measure liquid length.

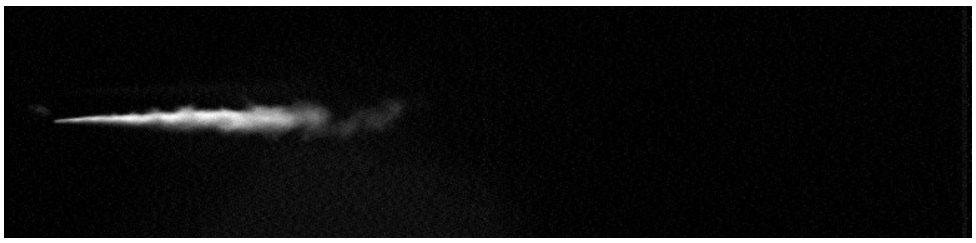

Figure 3.3. *Sample image of the Mie-scattering technique at 1000 μs after SoI.*

An example of a Mie-scattering image can be seen in Figure 3.3. The processing routine first subtracts the background, which is calculated by averaging the images taken prior the start of injection. Then, the contour of the liquid core is determined by means of a thresholding algorithm reported in [9, 10]. Finally, the maximum liquid length is obtained by averaging the distance to the nozzle of the contour points that are ± 1 mm around the intersection of the liquid spray axis and the calculated contour. No connectivity algorithm has been applied, so some liquid ligaments that sometimes are detached from the continuous liquid core are not accounted for to calculate liquid length.

3.3.2 Schlieren

The spray evolution inside the combustion chamber has been recorded by schlieren imaging [11]. This technique is sensitive to the first spatial derivative of density within the combustion chamber, which makes it useful to detect spray boundaries and thus evaluate macroscopic spray scales. This technique shows the boundary between vaporized liquid and background gas because of the refractive index differences that exist between them, additionally, density gradients are also created in the chamber as the vaporized liquid cools the ambient gas [12, 13]; such refractive index gradients are also present during combustion, as the high temperature creates low density regions. Therefore, this method is valid for inert and reactive conditions. For this technique, the spray has to be illuminated from one side by a collimated light beam. The shadow produced by the spray is then gathered with a lens and at its focal length a diaphragm is positioned to produce the schlieren effect by eliminating the diverted light beams, otherwise it would be just shadowgraphy without the diaphragm. The image produced is then captured by a high speed camera in order to obtain a time resolved evolution of the spray.

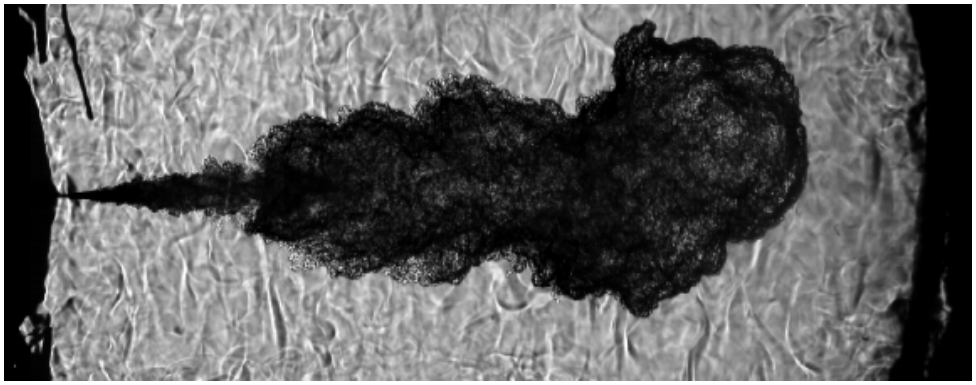

Figure 3.4. *Sample image of the schlieren technique at 3000 μs after SoI.*

An example of an schlieren image can be seen in Figure 3.4. The routine used for the processing was developed by Sandia National Laboratories as part of the ECN group and is available on-line [14]. The code is based on the successive calculation of two standard deviation images to remove the schlieren effect of the hot ambient gases and to detect the spray boundary. For every instant (I_t), the processing routine subtracts the two preceding images (I_{t-1} & I_{t-2}), then a two-step derivative process highlights the zones where the pixels have changed due to either spray or background gas movement, then the image is segmented [15–17]. Once the boundaries have been defined, the spray penetration is calculated by the procedure shown in [13]. Additionally, the ignition delay has also been determined using the schlieren method, which relies on the change in refractive index of the mixture and the shortening of the penetration [7, 12, 18].

3.3.3 Broadband radiation

The soot distribution and intensity inside the combustion chamber have been recorded by direct imaging. This technique records the flame broadband radiation, which

corresponds to the soot thermal luminosity during the diffusion combustion phase. This type of radiation may have to kinds of contributions, chemiluminescence and incandescence. Under most of the operating conditions, the second is the fundamental one as it depends on the amount of soot and its temperature, therefore it will be used for a qualitative analysis of such parameters. Moreover, the soot onset length and flame length will be calculated from this radiation. Nevertheless, on some operating points the incandescence disappears and the only radiation captured by the camera is the chemiluminescence.

Figure 3.5. *Sample of the broadband radiation imaging at 3000 μs after SoI.*

Figure 3.5 shows a sample image of broadband radiation. An average background image is calculated for each repetition and based on that image and a two constant thresholds, a mask is generated to define the region of interest. It is important to clarify that given the strong difference between the intensity levels in the soot onset area (in the vicinity of the lift-off length) and further downstream, two threshold values (a lower one for the onset and a higher one for the tip) were selected in order to accurately detect the contour. Then, the area of the flame and cumulative digital intensity are computed, and based on those two values the specific intensity is obtained. Also, and in a similar way to the spray penetration, the soot onset length and soot penetration (or flame length) are obtained as the distance from the nozzle to the points closest and furthest away from the injector, respectively. After all cases have been processed, the normalized intensity and specific intensity are calculated taking into account the camera settings of exposure time and aperture. It is worth noting that the soot onset length is not a replacement of the lift-off length calculated by means of OH* chemiluminescence, because significant amounts of soot do not form until downstream from the lift-off location [19].

3.3.4 OH* chemiluminescence

The lift-off length (LoL) was recorded by OH* chemiluminescence imaging. This technique records radiation at 310 nm, which is controlled by the OH* radical, being a marker of the diffusion flame limits, and thus of the lift-off length for diesel sprays [19]. The OH* chemiluminescence occurs at stoichiometric conditions and high temperatures, therefore being a good marker of the lift-off length [20]. Additionally, the wavelength band of 310 nm that corresponds to the chemiluminescence of the OH* radical is the strongest one and therefore best for determining the lift-off length [19, 20]. Although soot radiation could also be contributing to the recorded signal in the images, previous studies in the literature [19] also indicate that there should exist a spatial separation in both contributions. Therefore, while the downstream radiation will most probably be dominated by soot, the most upstream one is assumed to be essentially related to OH* chemiluminescence.

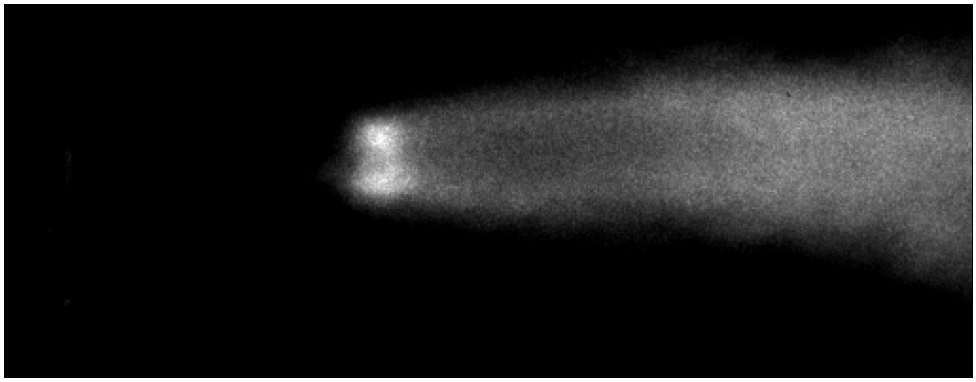

Figure 3.6. *Sample image of the OH* chemiluminescence technique from 2000 μs to 5000 μs after SoI.*

Figure 3.6 shows an image of OH* radiation. These images are similar in appearance to the broadband ones, but with different spectral information. Additionally, these images have been taken with a long exposure (3000 μs), starting 2000 μs after the start of injection in order to allow the lift-off length to stabilize; as opposed to the broadband radiation where the exposure times were much shorter ($\sim$20 μs). The field of view in this case is located closer to the injector, in order to be able to measure the lift-off length with an adequate resolution. The processing algorithm for OH* images is similar, but lift-off length is calculated as the closest zone to the nozzle where flame can be found [19]. The algorithm divides the image in two parts, based on the injector axis, because the time averaged images show two bright bands of light corresponding to the OH* chemiluminescence from the cylindrical diffusion flame. Nevertheless, these bands do not imply that the combustion extends further on the edges of the spray, but instead, they correspond to line-of-sight averaging of the light from flame that surrounds the spray [21, 22]. Carrying on with the processing, the values per row and side are added up so two curves Digital level vs Axial distance can be obtained. Finally, the lift-off length is calculated as the average level between valley and first peak of each curve, as this gives the mean location of the turbulently fluctuating lift-off length [19].

3.4 1D Spray model for multicomponent fuels

A one-dimensional model helps to simplify the problems involved in a three-dimensional real-world spray while providing accurate results in relatively short times compared to much more complex CFD models. Originally, the model was conceived for the use of a single component as the injected fuel and the calculation of the state relationships as the mixing of ideal gases. As part of this work and in order to improve the accuracy and versatility of the model, the code was modified in order to be able to work with mixtures of single-components as the injected fuel. Moreover, the state relationships have been modified to calculate the enthalpy by using the Peng-Robinson equation of state and the liquid-vapour equilibrium as a real substance via a fugacity based model. As future modifications, the inclusions of chemical equilibrium and reaction kinetics for the modelling of the spray under reactive conditions are being planed.

An overview of the model will be presented in this section, explaining the general description of the model as well as the modifications done as part of this work and their validation. For further reference, an in depth description of each modification done over the years can be found in [23–25].

3.4.1 General model description

The spray is assumed to be injected into a quiescent air volume, which is large enough so that flow evolution does not modify air conditions far away from the nozzle. Figure 3.7 shows a depiction of the basic configuration of this type of problem. Fuel stream is assumed to have a uniform velocity profile at the nozzle exit. This flow exchanges momentum with the ambient air and sets it in motion, so that it increases in width with the axial distance. The spray cone half angle (or spreading angle) $\theta/2$ defines this radial growth, and will be an input to the model. Together with the nozzle diameter d_0, the spray angle defines the virtual origin of the spray in terms of $x_0 = d_0/2/\tan(\theta/x)$.

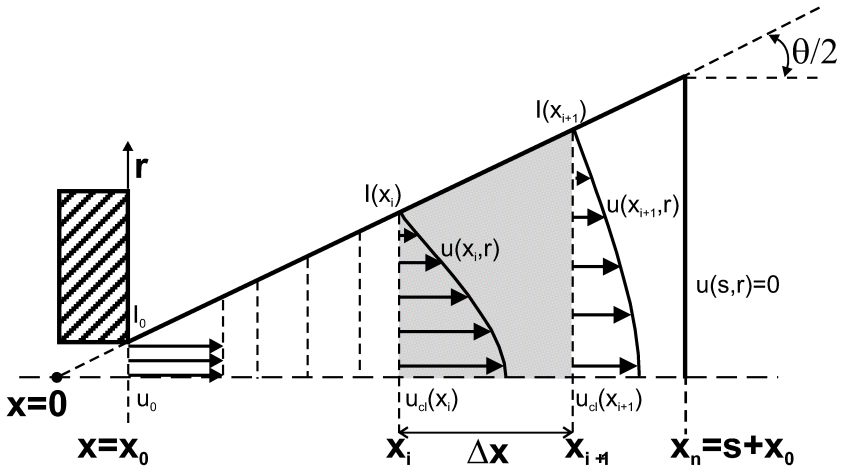

Figure 3.7. *Schematic of spray structure.*

The spray domain is divided axially into a number of cells with a certain thickness (Δx) spanning the whole spray cross section. Each cell is limited by the inlet and the outlet sections ("i" and "$i+1$", respectively) so that $x_{i+1} = x_i + \Delta x$. At every time instant, the spray size is defined in terms of the tip penetration (S), which is the farthest cell from the nozzle where inlet velocity is different from zero and outlet velocity is zero.

In order to accomplish these, the following hypotheses are made:

1. Symmetry on the spray axis [26], i.e. no air swirl.
2. A fully developed turbulent flow is assumed, which means that self-similar radial profiles can be defined for the conserved variables. In the present approach, a radial Gaussian profile is assumed, so that

$$\frac{u(x,r)}{u_{cl}(x)} = \left[\frac{f(x,r)}{f_{cl}(x)}\right]^{1/Sc} = \exp\left[-k\left(\frac{r}{x}\right)^2\right] \tag{3.1}$$

where $u_{cl}(x)$ and $f_{cl}(x)$ are values on the spray axis of the axial component of the velocity vector and mixture fraction, respectively; k is a constant and Sc is the turbulent Schmidt number.

3. Linked to the previous assumption, the spray cone angle is defined as the location where the axial velocity is ζ=1 % of the value on the spray axis, so that

$$k = \frac{\ln(1/\zeta)}{\tan^2(\theta/2)} \tag{3.2}$$

4. Turbulent Lewis number is assumed to be equal to one. Consequently, the local enthalpy, for which no conservation equation is solved, can be expressed as:

$$h(x,r,t) = h_{a,\infty} + f(x,r,t)(h_{f,0} - h_{a,\infty}) \tag{3.3}$$

where $f(x,r,t)$ is the local mixture fraction value and $h_{f,0}$ and $h_{a,\infty}$ are the enthalpy of pure fuel (nozzle outlet conditions) and pure air (far away from nozzle), respectively.

This relationship is independent of the general flow calculations, so that state relationships can be calculated *a priori*, as will be shown below.

5. Pressure is assumed to be constant all over the spray.

6. Locally homogeneous flow is assumed, i.e. local equilibrium exists both in thermal and velocity conditions. This allows for the consideration of the spray as a single-fluid jet.

Conservation equations of axial momentum and fuel mass are formulated for each cell (Figure 3.7), which leads to the following expressions:

$$I(x_i,t) - I(x_{i+1},t) = \frac{d}{dx}\int \rho u dV \tag{3.4}$$

$$M_f(x_i,t) - M_f(x_{i+1},t) = \frac{d}{dx}\int \rho f dV \tag{3.5}$$

The terms on the left-hand side of the equations correspond to the conserved property fluxes across the cell inlet and outlet surfaces. Thus, I and M_f stand for the axial momentum (related to local axial velocity, u) and mixture fraction (related to local mixture fraction, f) fluxes, respectively. The right-hand side terms represent the temporal variation of the integral over the whole cell, which quantifies the process of accumulation or de-accumulation of momentum and fuel within a cell. By means of corresponding radial integration of self-similar profiles, such equations can be expressed in terms of on-axis unknowns u_{cl} and f_{cl}, which can be solved starting from the nozzle exit, where injection conditions are known. After solving both unknowns, local values of u and f at any radial position can be retrieved from the on-axis properties by means of the corresponding self-similar radial profile.

To solve the previous equations, a definition of local density has to be made. Formally, this is expressed as a function of the type $\rho = f(f)$, which falls into the category of the so-called state relationships. In a more general way, such relationships define the local

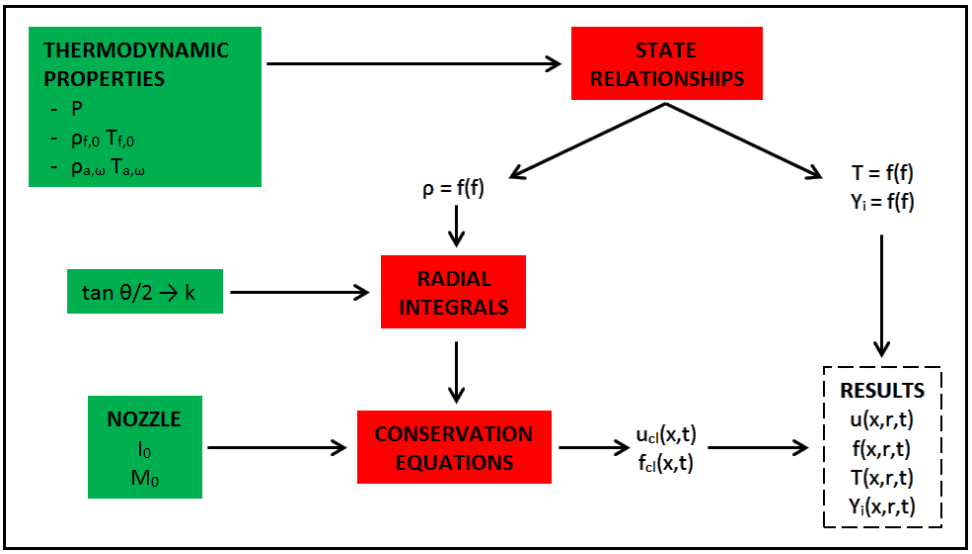

Figure 3.8. *General overview of the model.*

composition, temperature and density of the spray in terms of the mixture fraction, by means of ideal adiabatic-mixing processes of pure fuel stream (nozzle conditions, subscripted as $(f, 0)$) and pure air (subscripted as (a, ∞)). These boundary conditions can be considered either constant or variable with time. Calculation of state relationships is independent of the solution of the flow conservation equation and will be described in the following section.

Figure 3.8 summarizes the model structure, showing explicitly the link between boundary conditions (inputs for each calculation) and the solution procedure. The conservation equations are solved at each cell, to obtain u_{cl} and f_{cl}, from which u and f can be obtained at any other location. Required information consists of momentum I_0 and mass M_0 fluxes at the nozzle exit, and the radial integration of radial profiles coupled to the local density. To calculate such integrals, the spray cone angle (θ) is needed (to define the self-similar profile function) as well as the local density (ρ), which is obtained from the state relationships module. Eventually, once f is obtained at one location, local temperature, density and composition can also be calculated from state relationships.

Finally, Figure 3.9 presents a sample of some of the results obtained by the model. Figure 3.9 (top) shows the evolution of the penetration of the vapour and liquid phases along time and it can be seen that the vapour penetration keeps on penetrating while the liquid reaches a maximum value and stabilizes. This happens because the increasing radius due to the air entrainment causes the velocity to drop, and therefore, the penetration also slows down. The liquid length on the other side is controlled mostly by the mixing and is affected by the local mixture fraction which doesn't depend on the velocity. Figure 3.9 (bottom) shows the progress of the fuel mass fraction in the centre line along the spray axis. It shows that the value remains unaltered in the vicinity of the nozzle, which is the zone corresponding to the intact length. After that point, it begins to decrease as the radius grows due to the entrainment of air.

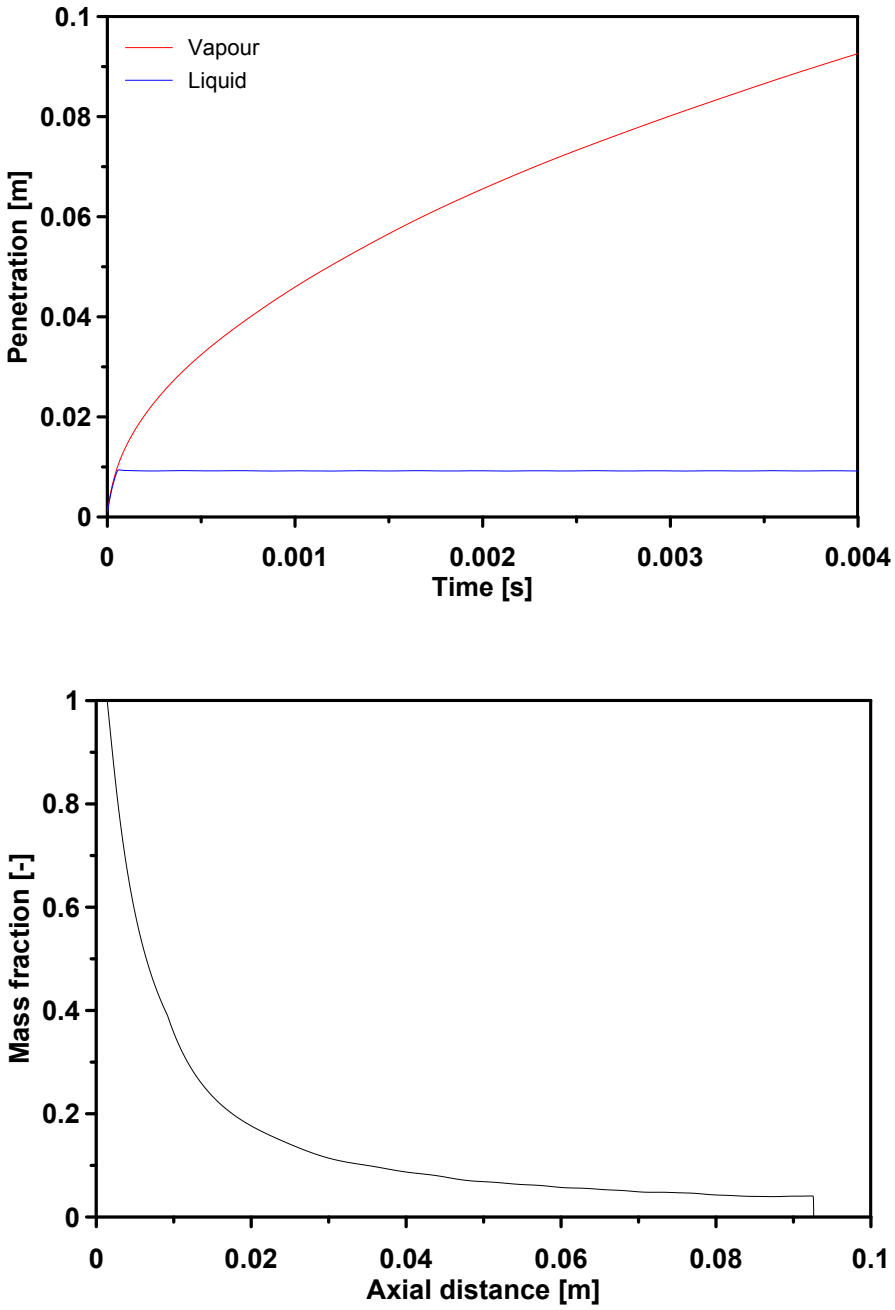

Figure 3.9. *Liquid and vapour penetration (top) and fuel mass in the centre line (bottom).*

3.4.2 State relationships

As previously defined, state relationships consist of composition (Y_i), temperature (T) and density (ρ) tabulations as a function of mixture fraction (f). To calculate these dependencies, the following general procedure has been developed:

1. The main underlying assumption is that mixture state corresponds to the result of an adiabatic mixing. For inert sprays, this hypothesis results in the following considerations:

   (a) Local mixture enthalpy is calculated by means of Equation 3.3.

   (b) Local composition can be obtained from the mixture fraction from:

   $$Y_i = Y_{i,\infty} + f \cdot (Y_{i,0} - Y_{i,\infty}) \tag{3.6}$$

   where Y_i is the mass fraction of species i in the mixture, when adding contribution of both liquid and vapour phases.

2. To define the local composition, the contribution of both liquid (Y_i^L) and vapour/gas (Y_i^V) phases to each of the components has to be found, with $Y_i = Y_i^L + Y_i^V$. If the mixture is in a single phase region of the spray, then, the solution is trivial, ($Y_i = Y_i^V$ or $Y_i = Y_i^L$). In the liquid-vapour region, the spray is assumed to be in adiabatic saturation conditions, and therefore, liquid and vapour phase conditions are those of the bubble and dew curves, respectively. This demands for a detailed calculation of the L-V equilibrium. In practice, local composition for each phase will be obtained from a L-V flash calculation as a function of pressure, local temperature and mixture fraction, i.e. $(Y_i^L, Y_i^V) = f(P, T, f)$.

3. A real-gas mixture is assumed by means of the following equation:

   $$h(T, f) = \sum_{i=1}^{n} Y_i \cdot \bar{h}_i(T) \tag{3.7}$$

   where $\bar{h}_i$ is the partial enthalpy of component i in the mixture and n is the number of components.

   This partial enthalpy is obtained by means of the equation:

   $$\overline{h}_i = h_i^0 - RT^2 \left(\frac{dln\hat{\phi}_i}{dT} \right)_{P,x_i} \tag{3.8}$$

   where h_i^0 is the perfect gas enthalpy, and $\hat{\phi}_i$ is the fugacity coefficient of component i in the mixture.

4. In the single-phase region of the spray, where composition is fully defined, local temperature is the only unknown when equating enthalpy from Equation 3.3 to the real gas mixture enthalpy in Equation 3.7. In the two-phase region, where composition of both liquid and vapour phases are also unknown, L-V equilibrium is coupled to the previous enthalpy calculations to fully resolve both temperature and composition for each phase.

5. Once temperature and composition are known, mixture density can be obtained by means of the equation

$$\frac{1}{\rho} = \frac{\sum_{i=1}^{n} Y_i^L}{\rho^L} + \frac{\sum_{i=1}^{n} Y_i^V}{\rho^V} \tag{3.9}$$

where ρ^L and ρ^V are the liquid and vapour phase densities, respectively; which are obtained from local temperature, pressure, composition and compressibility factor for each phase, respectively z^L and z^V; and n is the total number of components.

The previous formulation is valid for any Equation of State (EoS), from which the following necessary parameters can be derived:

- Fugacity coefficients of each component in the mixture for the L-V equilibrium $\hat{\phi}_i$ (Equation 3.10).
- Departure terms in the real enthalpy calculation, i.e. $\left(\frac{dln\hat{\phi}_i}{dT}\right)_{P,x_i}$ (Equation 3.8).
- Compressibility factors z^L and z^V of the liquid and vapour phases to derive ρ^L and ρ^V (Equation 3.9).

In the present work, the Peng-Robinson EoS has been applied to both the liquid and vapour phases, due to its simplicity and extended use in the spray literature [27–32].

The previous general formulation is similar to the previous version of the model [23]. However, some important steps have been modified within the present Ph.D. work. First, L-V equilibrium has been improved by means of the fugacity formulation. The second major difference is the use of a single EoS for the definition of all fluid properties, while in the previous version both enthalpies and liquid phase densities were calculated by means of generalized correlations based upon the principle of corresponding states.

Figures 3.10 and 3.11 show an example of state relationships for a 50/50 blend of n-decane and n-hexadecane spray injected into an ambient of air as calculated by the 1D model. This will show the potential of the model to calculate a multicomponent fuel, as well as the solubility of gas into the liquid phase. Mixture temperature and composition have been plotted as a function of mixture fraction. Values for $f = 1$ and $f = 0$ correspond to the pure fuel $(f, 0)$ and air (a, ∞) properties, respectively. For intermediate f values, the state relationships reach values between the extreme ones, due to the adiabatic mixing hypotheses. In Figure 3.10, both dew and bubble curves have been added to get a more clear insight into the mixture evolution compared to the L-V equilibrium. From the intersection of the temperature state relationship and such curves, two characteristic points can be defined, in terms of the corresponding fuel mass fractions and temperature (f_{evap}, T_{evap}) and (f_{evap_s}, T_{evap_s}).

The first point lays on the dew curve, which defines the limit between vapour and liquid-vapour equilibrium. This curve indicates conditions where the last liquid disappears and vapour is still at saturation conditions. From a point of view of mixing-controlled evaporation, this is precisely the fuel mass fraction (or fuel-air ratio) that would be present

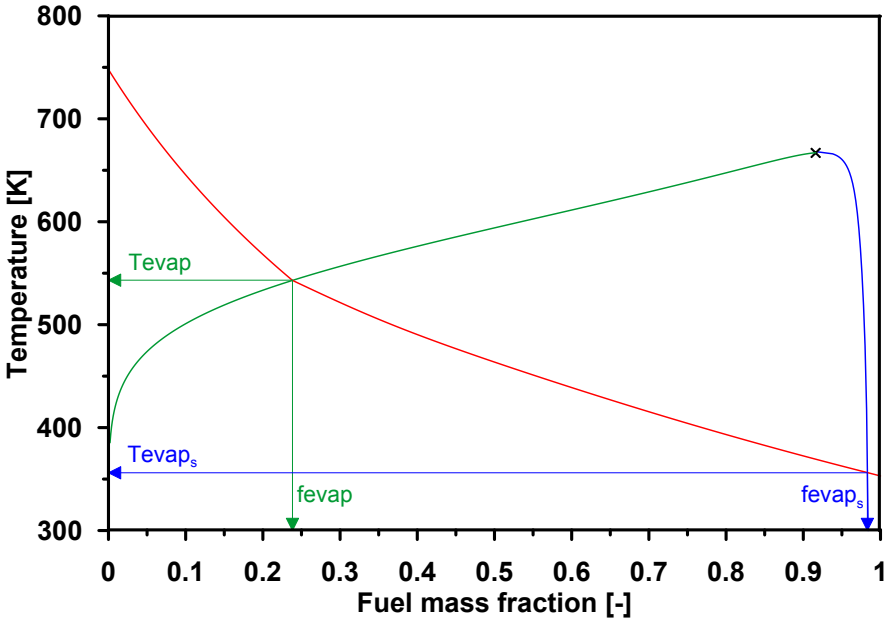

Figure 3.10. *Dew and bubble curves along with temperature evolution for a 50/50 blend of n-decane and n-hexadecane into an ambient of air at P=5.3 MPa; $T_{f,0}$=353 K and $T_{a,\infty}$=765 K.*

at the maximum liquid length, the liquid-vapour spray being contained by an iso-line of f_{evap}.

Analogously, the second point (f_{evap_s}, T_{evap_s}) lays on the bubble curve, which defines the limit between liquid and liquid-vapour equilibrium. The curve indicates conditions where vapour first appears within the liquid phase, which is at saturation conditions. From a mixing-controlled evaporation point of view, f_{evap_s} is precisely a characteristic fuel mass fraction (or fuel-air ratio) where fuel vapour is starting to be formed.

After the definition of these two characteristic points, three well defined zones can be observed within the spray space of states, namely one of pure liquid ($f > f_{evap_s}$), one of pure vapour ($f < f_{evap}$), and one where both liquid and vapour coexist $f_{evap} < f < f_{evap_s}$.

The zone $f > f_{evap_s}$ corresponds to the vicinity of the injector, the fuel is fully liquid, and the ambient air is also in liquid phase, due to its solubility into the liquid fuel. Under the conditions shown in this case, nitrogen solubility in the fuel in terms of mass is maximum 1.7 %. Figure 3.11 (top and bottom) shows that for f values higher than f_{evap_s} there is no vapour of any of the components and that there is an increasing liquid fraction of nitrogen as f decreases (i.e. more air is entrained). The temperature of the mixture will keep rising while in the liquid phase up to f_{evap_s} and its corresponding temperature T_{evap_s}.

The zone with $f_{evap} < f < f_{evap_s}$ would correspond to the two-phase spray region, near the nozzle and up to the maximum liquid length, where both liquid and vapour are present and vaporization process is occurring. In this zone, moving toward lower f values means that more air has been entrained, which transfers enthalpy into the mixture, increasing local temperature up to a certain limit, defined by f_{evap} and its corresponding temperature,

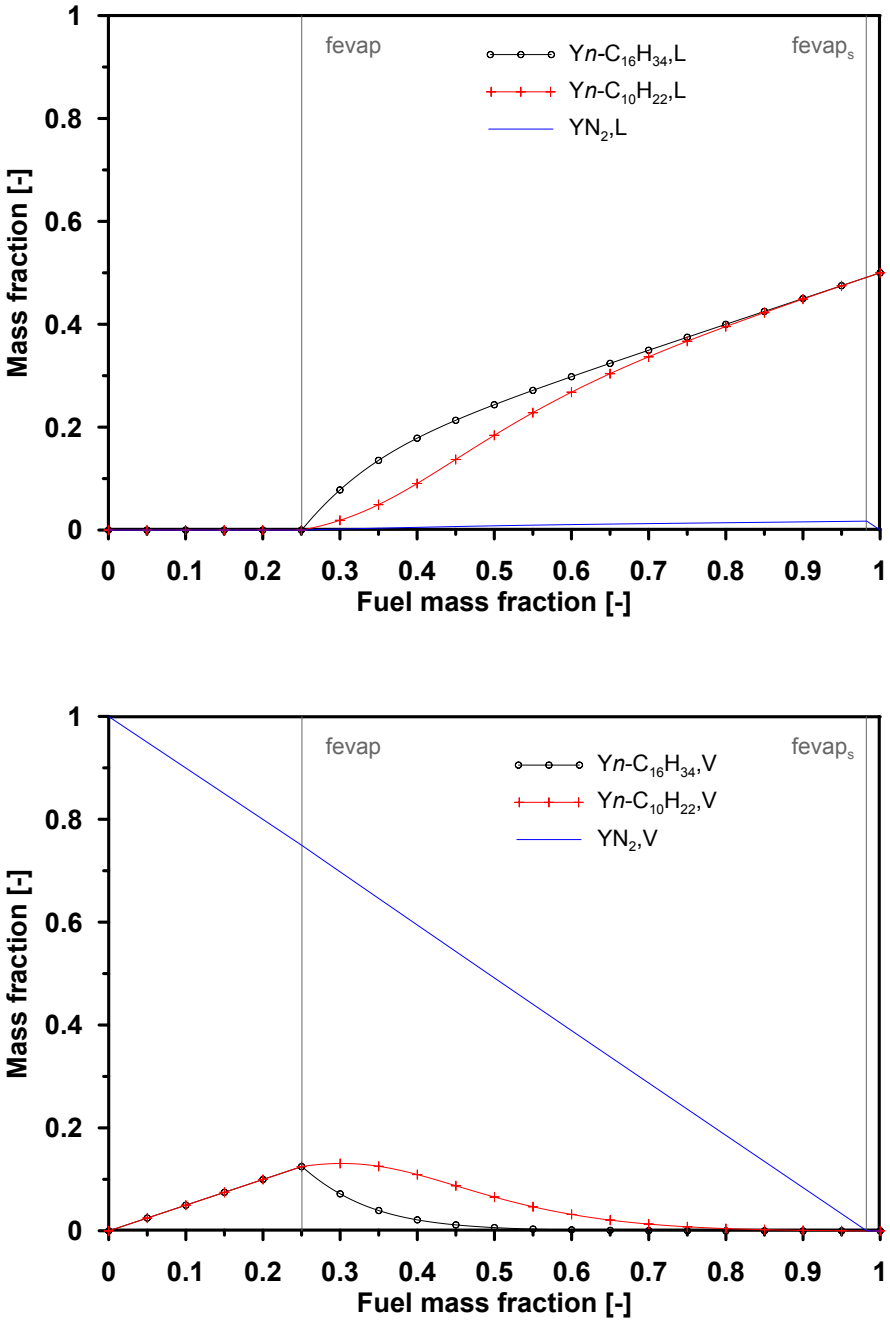

Figure 3.11. *Spray liquid and vapour mass fractions (top and bottom) from the state relationships for a 50/50 blend of n-decane and n-hexadecane into an ambient of air at P=5.3 MPa; $T_{f,0}$=353 K and $T_{a,\infty}$=765 K.*

T_{evap}. The composition curves show that most of the evaporation takes place between $f = 0.5 - 0.7$ and f_{evap}, even though the mass of entrained air is always proportional to $(1 - f)$. This is due to the fact that in the range $0.7 < f < f_{evap_s}$ evaporation rates are not very high, due to the low temperature. On the other hand, no matter how little, there is always some liquid nitrogen dissolved in the liquid fuel. Calculations in the examples correspond to a 50/50 mixture of n-decane and n-hexadecane. Results indicate that n-decane, which is the more volatile fuel, vaporizes faster than n-hexadecane. However, there is always some small quantity of n-decane in the liquid mixture, which only disappears together with the whole liquid phase.

For $f < f_{evap}$ complete evaporation has been achieved, and the liquid phase is no longer present. Figure 3.11 shows that there is no liquid fraction of any of the components and, as expected, the fraction of each fuel component is linearly decreasing, and the corresponding air component is increasing, as mixture fraction approaches zero.

The change in the slope of the temperature curve is closely related to the vaporization process. If liquid and vapour are present ($f_{evap} < f < f_{evap_s}$), the energy increase by air entrainment is spent on fuel evaporation, and thus the latent heat incorporates the enthalpy from the air. Once vaporization is over ($f < f_{evap}$), no energy is spent on the phase change. As a consequence, the enthalpy from the air is directly used to rise the temperature, and the slope of the temperature curve increases.

3.4.3 Validation of the liquid-vapour equilibrium

A central point for the calculation of the state relationships under vaporizing conditions is the Liquid-Vapour (L-V) equilibrium. Previous models by this research group made use of two different approaches: (i) In [23] and [33] an approach based upon a ratio of compressibility coefficients was used, which is thermodynamically inconsistent as shown in [28], (ii) In [29] a more elaborated description of local L-V equilibrium was used, which was however only valid for single-component fuels and neglected solubility of the gas phase into the liquid. The current approach solves a full high pressure L-V equilibrium by means of fugacity coefficients:

$$x_i^L \hat{\phi}_i^L(x_i^L, P, T) = x_i^V \hat{\phi}_i^V(x_i^V, P, T) \tag{3.10}$$

where x_i denotes the molar fraction of component i in the liquid phase (L superscript) or vapour phase (V superscript).

This equation can be solved for multi-component fuels, and also accounts for solubility of ambient gases into the liquid. By means of this approach, both dew and bubble routines have been developed [34, 35], which have been validated with independent L-V equilibrium data in the literature, as follows in the present section. Additionally, flash equilibrium routines have also been implemented for calculations within the two-phase region of the spray.

To validate the liquid-vapour equilibrium algorithm, a small parametric study has been carried out at different pressures using two fuels and two ambient gases, as shown in Table 3.3. Experimental data have been taken from [36–38].

Table 3.3. *Fuel and ambient gas combinations for L-V equilibrium validation.*

	CO_2	N_2
n-$C_{10}H_{22}$		X [36]
n-$C_{16}H_{34}$	X [38]	X [37]

Figure 3.12 shows an example of L-V results for a CO_2/n-$C_{16}H_{34}$ mixture at 5 MPa of ambient pressure. Although L-V equilibrium is solved in terms of mole fractions, results throughout this section will be shown in terms of the mass fractions, which is in an equivalent metrics of local composition. Furthermore, mixture fraction will be used instead of fuel mass fraction, which is a more coherent variable when analysing spray results. For a binary inert system (such as the ones shown in Table 3.3), the problem has only two unknowns (temperature and composition of one species), and mixture fraction is equivalent to the fuel mass fraction. When using a multi-component fuel, or when ambient consists of more than one species (e.g. oxygen or combustion products are included) L-V equilibrium problem includes N+1 unknowns. To reduce the dimensionality of the problem, only compositions that fall upon the adiabatic mixing assumption are considered.

For all cases plotted, solid and dashed lines represent the dew and bubble curves, respectively; dots (•) correspond to experimental data of L-V equilibrium (i.e. dew or bubble curves) and crosses (×) to the calculated mixture critical points, which occur due to the fact that ambient pressure is higher than the critical pressure of any component within the mixture. When using the Peng-Robinson EoS together with the mixing rules as described in Appendix 3.A, the so-called binary interaction coefficient k_{ij} appears, which can be used to fit the EoS results with the use of experimental L-V values. The effect of this parameter is clearly shown in Figure 3.12, a higher k_{ij} value will lead to a higher dew or bubble temperature at a given mixture fraction. k_{ij} values are different for each possible combinations of species, however, they do not depend on temperature, pressure or composition. In order to achieve the most accurate value for a given gas-fuel system, an optimization procedure has been carried out for each binary combination based upon the minimization of the difference between experimental and modelled temperatures upon the dew curve. This criterion has been followed because the dew curve is the one used to calculate the evaporation mass fraction (f_{evap}) as will be shown in next section, and, therefore, it is directly linked to the liquid length prediction, which is the quantitative parameter to be later compared when using the spray model. Table 3.4 shows the k_{ij} values calculated for the three combinations studies. Figure 3.12 shows the improvement in prediction of the L-V equilibrium when using the optimized k_{ij} compared to the baseline $k_{ij} = 0$.

The optimized k_{ij} results have also been used in Figures 3.13 to 3.15. All combinations result in a similar behaviour to pressure changes. As the ambient pressure increases, the maximum temperature decreases. In these cases, in which the conditions are supercritical for the components used, the maximum temperature corresponds to that of the critical point. Not only the temperature of the critical point is affected by the pressure, but also its composition. It can be seen that as the pressure increases the critical point is shifted to the left; in other words, the highest temperature of the dew-bubble curves is reached

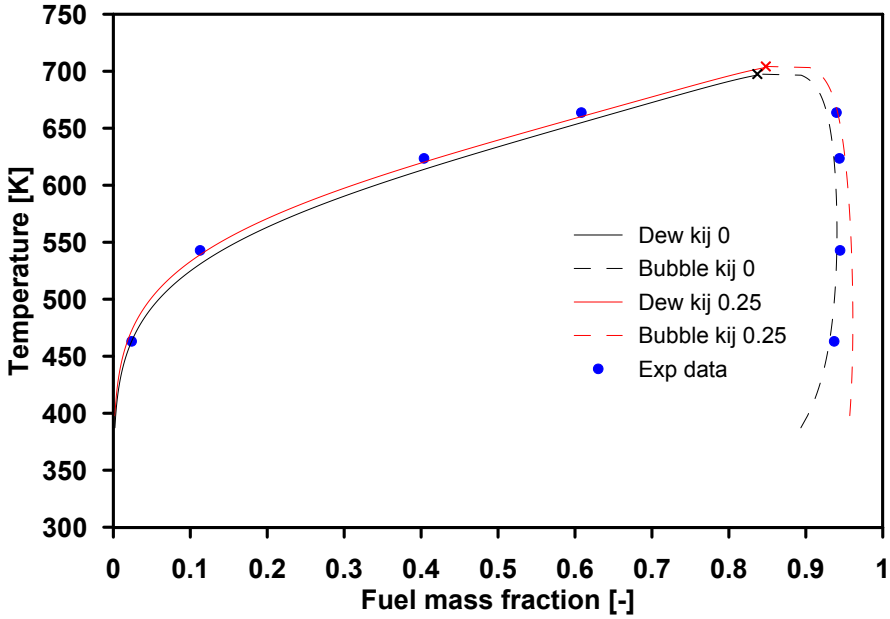

Figure 3.12. *Comparison of experimental data and calculated values with and without k_{ij} for a CO_2/n-$C_{16}H_{34}$ mixture at 5 MPa of ambient pressure.*

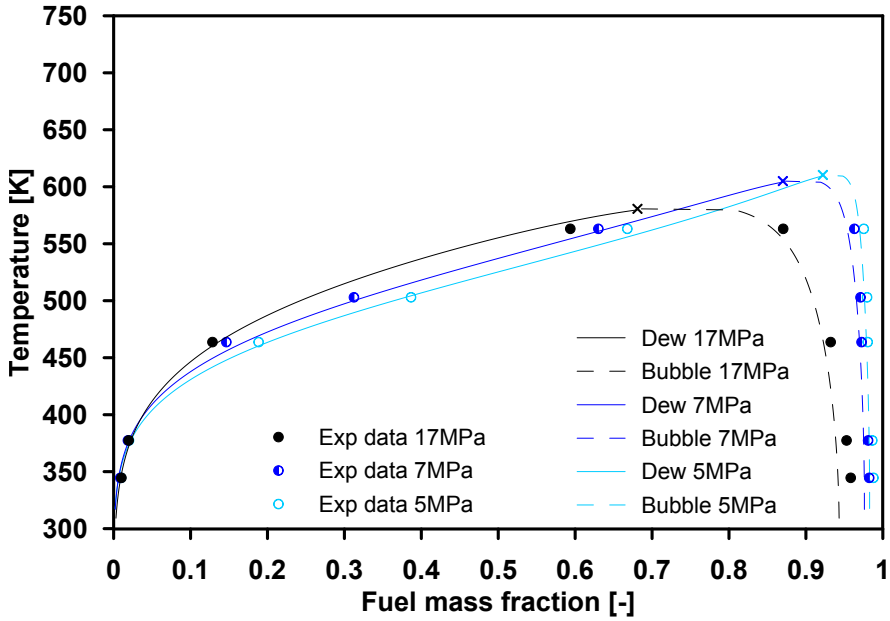

Figure 3.13. *Dew and bubble curves and experimental data for N_2/n-$C_{10}H_{22}$ at different pressures.*

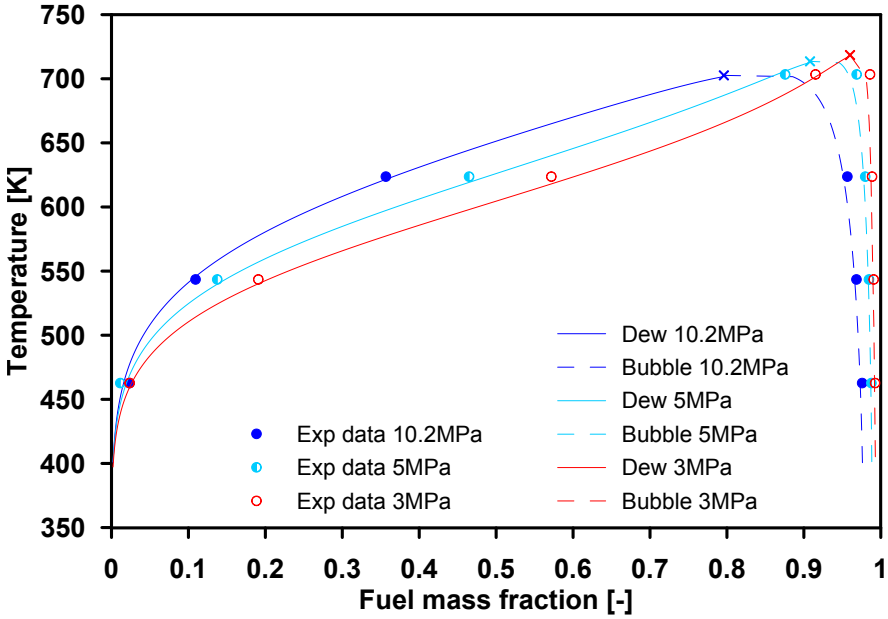

Figure 3.14. *Dew and bubble curves and experimental data for N_2/n-$C_{16}H_{34}$ at different pressures.*

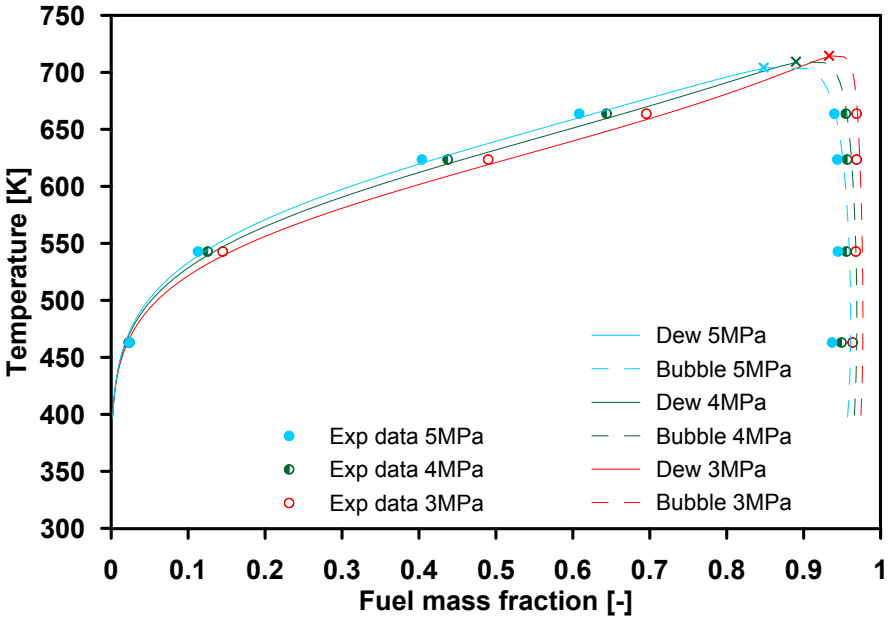

Figure 3.15. *Dew and bubble curves and experimental data for CO_2/n-$C_{16}H_{34}$ at different pressures.*

Table 3.4. *k_{ij} values for all fuel and ambient gas combinations that fit best to the experimental data.*

Combination	k_{ij}
$N_2/n\text{-}C_{10}H_{22}$	0.06
$N_2/n\text{-}C_{16}H_{34}$	0.10
$CO_2/n\text{-}C_{16}H_{34}$	0.25

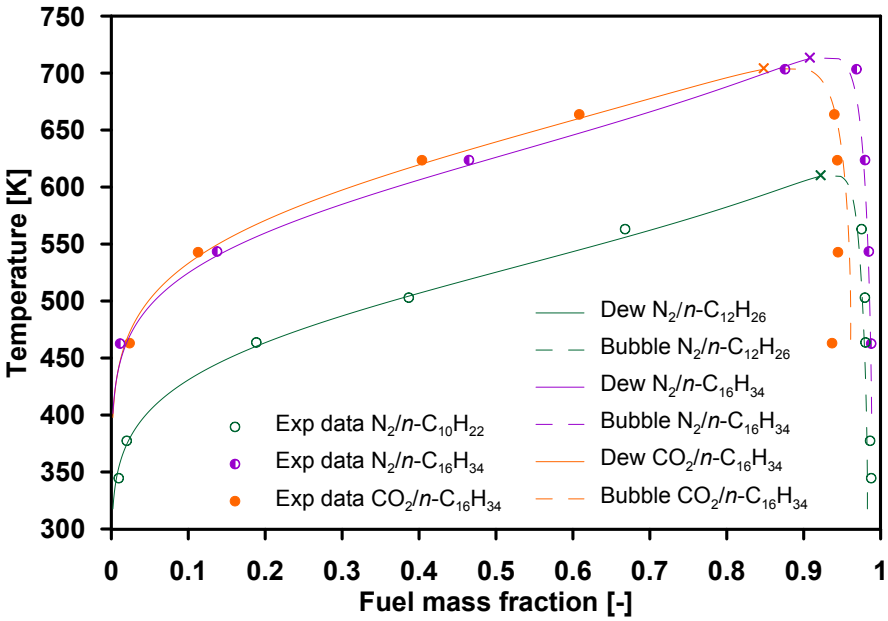

Figure 3.16. *Ambient gas-fuel comparison at 5 MPa.*

at a lower fuel mass fraction, mainly due to the increasing solubility of gas in the liquid phase.

Figure 3.16 shows the effect of the fuel and the ambient gas on the shape of the dew and bubble curves and on the temperature and composition of the critical point. Both, $N_2/n\text{-}C_{16}H_{34}$ and $CO_2/n\text{-}C_{16}H_{34}$, curves have very similar dew curves, which shows that their behaviour is mostly controlled by n-hexadecane. That is also the reason why the critical point is similar in temperature but not so much in composition. On the other hand, looking at the $N_2/n\text{-}C_{10}H_{22}$ and $N_2/n\text{-}C_{16}H_{34}$ curves, it can be seen that the dew curves have a steady offset and that the composition of the critical point is very similar. Additionally, it is evident that both bubble curves are akin, that is because their behaviour is dominated by the nitrogen.

The results presented from the liquid-vapour equilibrium validation correspond with the experimental data, which confirms the thermodynamic consistency of the model. Moreover, the binary interaction coefficient (k_{ij}) values calculated have also proven to affect the calculation and bring the values slightly closer to those from the experiments

by changing the slope of the dew and bubble curves, and therefore, yielding an evaporation fraction value (f_{evap}) that is more accurate.

3.A Appendix: Equation of state

The Peng-Robinson EoS has been used [39], which can be expressed as:

$$P = \frac{RT}{v-b} - \frac{a(T)}{v^2 + 2bv - b^2} \tag{3.11}$$

where a and b are obtained from the following mixing rules

$$\begin{aligned} a &= \sum_i \sum_j x_i x_j \left(a_i a_j\right)^{1/2} (1 - k_{ij}) \\ b &= \sum_i x_i b_i \\ a_i &= 0.45724 \frac{(RT_{ci})^2}{P_{ci}} \left[1 + f\omega_i \left(1 - T_r^{1/2}\right)\right]^2 \\ f\omega_i &= 0.37464 + 1.54226\omega_i - 0.26992\omega_i^2 \\ b_i &= 0.07780 \frac{RT_{ci}}{P_{ci}} \end{aligned} \tag{3.12}$$

The previous equation can be written in terms of the compressibility factor, which is more convenient to be able to resolve the liquid or vapour density, as:

$$z^3 + (B-1)z^2 + (A - 3B^2 - 2B)z + (-AB + B^2 + B^3) = 0 \tag{3.13}$$

where

$$\begin{aligned} A &= aP/(RT)^2 \\ B &= bP/RT \end{aligned} \tag{3.14}$$

On the other hand, to solve the L-V equilibrium, the following equation for the fugacity coefficient of a component in the mixture can be derived from the departure function of Helmholtz energy:

$$\begin{aligned} ln(\hat{\phi}_i) = \frac{b_i}{b}(z-1) - ln(z-B) \\ + \frac{A}{2\sqrt{2}B}\left(\frac{b_i}{b} - \delta_i\right) ln\left(\frac{z + B(1+\sqrt{2})}{z + B(1-\sqrt{2})}\right) \end{aligned} \tag{3.15}$$

with

$$\delta_i = \frac{2a_i^{1/2}}{a} \sum_j x_j a_j^{1/2} (1 - k_{ij}) \tag{3.16}$$

Finally, to enable real gas enthalpy calculations, the following expression can be derived:

$$\begin{aligned}\left(\frac{dln\hat{\phi}_i}{dT}\right)_{P,x_i} &= \frac{b_i}{b}\frac{\delta z}{\delta T} - \frac{1}{z-B}\left(\frac{\delta z}{\delta T}+\frac{B}{T}\right) \\ &\quad - \left(\frac{b_i}{b}-\delta_i\right)\frac{A}{(z+B)^2-2B^2}\left[\frac{\delta z}{\delta T}+\frac{z}{T}\right] \\ &\quad + \left[\left(\frac{1}{A}\frac{\delta A}{\delta T}+\frac{1}{T}\right)\left(\frac{b_i}{b}-\delta_i\right)\right. \\ &\qquad - \left[\frac{1}{a_i^{1/2}}\frac{\delta a_i^{1/2}}{\delta T}-\frac{1}{a}\frac{\delta a}{\delta T}\right]\delta_i \\ &\qquad \left. - \frac{2a_i^{1/2}}{a}\sum_j x_j\frac{\delta a_j^{1/2}}{\delta T}(1-k_{ij})\right] \\ &\quad \cdot \frac{1}{2\sqrt{2}}\frac{A}{B}ln\left(\frac{z+B(1+\sqrt{2})}{z+B(1-\sqrt{2})}\right)\end{aligned}$$

with

$$\begin{aligned}\frac{\delta z}{\delta T} &= \frac{(B-z)\frac{\delta A}{\delta T}+\frac{B}{T}\left(z^2-(6B+2)z-A+3B^2+2B\right)}{3z^2+2(B-1)z+(A-3B^2-2B)} \\ \frac{\delta A}{\delta T} &= A\left(\frac{1}{a}\frac{\delta a}{\delta T}-\frac{2}{T}\right) \\ \frac{\delta a}{\delta T} &= \sum_i\sum_j x_i x_j(1-k_{ij})\frac{1}{2}\left(\sqrt{\frac{a_i}{a_j}}\frac{\delta a_j}{\delta T}+\sqrt{\frac{a_j}{a_i}}\frac{\delta a_i}{\delta T}\right) \\ \frac{\delta a_i}{\delta T} &= -a_{ci}\left[1+f\omega_i\left(1-T_r^{1/2}\right)\right]f\omega_i\frac{1}{\sqrt{TT_{ci}}}\end{aligned} \tag{3.17}$$

Bibliography

[1] Bermúdez V., García J.M., Juliá E. and Martínez S. "Engine with Optically Accessible Cylinder Head: A Research Tool for Injection and Combustion Processes". *SAE Technical Paper*, n^o 2003-01-1110, 2003.

[2] Martínez S. *Desarrollo de una instalación experimental para el estudio de chorros diesel evaporados en atmósfera inerte y reactiva*. Doctoral Thesis, Universitat Politècnica de València, 2003.

[3] García J.M. *Aportaciones al estudio del proceso de combustión turbulenta de chorros en motores diesel de inyección directa*. Doctoral Thesis, Universitat Politècnica de València, 2004.

[4] Nerva J.G. *An assessment of fuel physical and chemical properties in the combustion of a Diesel spray*. Doctoral Thesis, Universitat Politècnica de València, 2013.

[5] Baert R.S.G., Frijters P.J.M., Somers B., Luijten C.C.M. and de Boer W. "Design and Operation of a High Pressure, High Temperature Cell for HD Diesel Spray Diagnostics: Guidelines and Results". *SAE Technical Paper*, n^o 2009-01-0649, 2009.

[6] Payri R., García-Oliver J.M., Bardi M. and Manin J. "Fuel temperature influence on diesel sprays in inert and reacting conditions". *Applied Thermal Engineering*, Vol. 35, pp. 185–195, 2012.

[7] Bardi M., Payri R., Malbec L.M., Bruneaux G., Pickett L.M., Manin J., Bazyn T. and Genzale C. "Engine Combustion Network: Comparison of spray development, vaporization, and combustion in different combustion vessels". *Atomization and Sprays*, Vol. 22(10), pp. 807–842, 2012.

[8] Bardi M. *Partial needle lift and injection rate shape effect on the formation and combustion of the diesel spray*. Doctoral Thesis, Universitat Politècnica de València, 2014.

[9] Pastor J.V., Arrègle J. and Palomares A. "Diesel spray image segmentation with a likelihood ratio test". *Applied Optics*, Vol. 40(17), pp. 2876–2885, 2001.

[10] Pastor J.V., Arrègle J., García J.M. and Zapata L.D. "Segmentation of diesel spray images with log-likelihood ratio test algorithm for non-Gaussian distributions". *Applied Optics*, Vol. 46(6), pp. 888–899, 2007.

[11] Settles G.S. *Schlieren and Shadowgraph Techniques: Visualizing Phenomena in Transparent Media*. Springer-Verlag, Berlin, Germany, 2001.

[12] Pickett L.M., Kook. S. and Williams T. "Visualization of diesel spray penetration, cool-flame, ignition, high-temperature combustion, and soot formation using high-speed imaging". *SAE International Journal of Engines*, Vol. 2(1) n^o 2009-01-0658, pp. 439–459, 2009.

[13] Naber J. and Siebers D.L. "Effects of gas density and vaporization on penetration and dispersion of diesel sprays". *SAE Technical Paper*, n^o 960034, 1996.

[14] *Engine Combustion Network*. http://www.sandia.gov/ecn.

[15] Pickett L.M., Manin J., Genzale C.L., Siebers D.L., Musculus M.P.B. and Idicheria C.A. "Relationship between diesel fuel spray vapor penetration/dispersion and local fuel mixture fraction". *SAE International Journal of Engines*, Vol. 4(1) n^o 2011-01-0686, pp. 764–799, 2011.

[16] Pastor J.V., Payri R., García-Oliver J.M. and Nerva J.G. "Schlieren measurements of the ECN-Spray A penetration under inert and reacting conditions". *SAE Technical Paper*, n^o 2012-01-0456, 2012.

[17] Pastor J.V., Payri R., García-Oliver J.M. and Briceño F. "Schlieren methodology for the analysis of transient diesel flame evolution". *SAE International Journal of Engines*, Vol. 6(3) n^o 2013-24-0041, pp. 1661–1676, 2013.

[18] Pickett L.M., Genzale C.L., Bruneaux G., Malbec L.M., Hermant L., Christiansen C. and Schramm J. "Comparison of diesel spray combustion in different high-temperature, high-pressure facilities.". *SAE International Journal of Engines*, Vol. 3(2) n^o 2010-01-2106, pp. 156–181, 2010.

[19] Higgins B. and Siebers D. "Measurement of the Flame Lift-Off Location on DI Diesel Sprays Using OH Chemiluminescence". *SAE Technical Paper*, n^o 2001-01-0918, 2001.

[20] Gaydon A.G. *The Spectroscopy of Flames*. Chapman and Hall, 1974.

[21] Dec J.E. "A conceptual model of DI diesel combustion based on laser-sheet imaging". *SAE Technical Paper*, n^o 970873, 1997.

[22] Kosaka H., Nishigaki T., Kamimoto T., Sano T., Matsutani A. and Harada S. "Simultaneous 2-D imaging of OH radicals and soot in a diesel flame by laser sheet techniques". *SAE Technical Paper*, n^o 960834, 1996.

[23] Pastor J.V., López J.J., García J.M. and Pastor J.M. "A 1D model for the description of mixing-controlled inert diesel sprays". *Fuel*, Vol. 87, pp. 2871–2885, 2008.

[24] Desantes J.M., Pastor J.V., García-Oliver J.M. and Pastor J.M. "A 1D model for the description of mixing-controlled reacting diesel sprays". *Combustion and Flame*, Vol. 156, pp. 234–249, 2009.

[25] Pastor J.V., García-Oliver J.M., Pastor J.M. and Vera-Tudela W. "One-dimensional diesel spray modeling of multicomponent fuels". *Atomization and Sprays*, Vol. 25(2), pp. 485–517, 2015.

[26] Borée J., Atassi N. and Charnay G. "Measurements and image analysis of the turbulent field in an axisymmetric jet subject to a sudden velocity decrease". *Experimental Thermal and Fluid Science*, Vol. 14, pp. 45–51, 1997.

[27] Qiu L., Wang Y., Wang H., Jiao Q. and Reitz R.D. "Simulating Condensation in a Supercritical Gas Jet". In *25th Annual Conference on Liquid Atomization and Spray Systems*. ILASS Americas, May 2013.

[28] Luijten C.C.M. and Kurvers C. "Real gas effects in mixing-limited diesel spray vaporization models". *Atomization and Sprays*, Vol. 20(7), pp. 595–609, 2010.

[29] Desantes J.M., López J.J., García J.M. and Pastor J.M. "Evaporative diesel spray modeling". *Atomization and Sprays*, Vol. 17, pp. 193–231, 2007.

[30] Zhang L. and Kong S.C. "High-pressure vaporization modeling of multi-component petroleum-biofuel mixtures under engine conditions". *Combustion and Flame*, Vol. 158, pp. 1705–1717, 2011.

[31] Qiu L., Wang Y., Jiao Q., Wang H. and Reitz R.D. "Development of a thermodynamically consistent, robust and efficient phase equilibrium solver and its validations". *Fuel*, Vol. 115, pp. 1–16, 2014.

[32] Oefelein J., Dahms R. and Lacaze G. "Detailed modeling and simulation of high-pressure fuel injection processes in diesel engines". *SAE International Journal of Engines*, Vol. 5(3) n^o 2012-01-1258, pp. 1410–1419, 2012.

[33] Siebers D.L. "Scaling liquid-phase fuel penetration in diesel sprays based on mixing-limited vaporization". *SAE Technical Paper*, n^o 1999-01-0528, 1999.

[34] Reid R. C., Prausnitz J. M. and Poling B. E. *The properties of gases and liquids*. McGraw-Hill, fourth edition, 1998.

[35] Elliott J. R. and Lira C.T. *Introductory Chemical Engineering Thermodynamics*. Prentice Hall International Series in the Physical and Chemical Engineering Sciences. Prentice Hall, 2nd edition, 2012.

[36] García-Sánchez F., Eliosa-Jiménez G., Silva-Oliver G. and García-Flores B. E. "Vapor-Liquid equilibrium data for the Nitrogen + n-Decane system from (344 to 563) K and at pressures up to 50 Mpa". *Journal of Chemical & Engineering Data*, Vol. 54, pp. 1560–1568, 2009.

[37] García-Sánchez F., Eliosa-Jiménez G., Silva-Oliver G. and Vázquez-Román R. "Vapor-Liquid Equilibria of Nitrogen-Hydrocarbon Systems Using the PC-SAFT Equation of State". *Fluid Phase Equilibria*, Vol. 217, pp. 241–253, 2004.

[38] Sebastian H.M., Slmnick J.J., Lin H.M. and Chao K.C. "Vapor-Liquid Equilibrium in Binary Mixtures of Carbon Dioxide + n-Decane and Carbon Dioxide + n-Hexadecane". *Journal of Chemical & Engineering Data*, Vol. 25, pp. 138–140, 1980.

[39] Peng D. and Robinson D. B. "A New Two-Constant Equation of State". *Industrial Engineering Chemistry Fundamentals*, Vol. 15 (1), pp. 59–64, 1976.

Chapter 4

Fuel effects on mixing and evaporation under inert conditions

Contents

4.1 Introduction

This present chapter will report the results obtained from the tests under an inert environment and study the influence of the fuel properties on the processes of mixing and evaporation under various conditions. The aforementioned processes will be studied under non-reactive conditions in order to isolate the spray from the effects of the combustion and analyze more precisely the influence of the contour conditions. In order to do this, two different types of fuel have been employed. First, five blends of *n*-decane and *n*-hexadecane were used due to their different physical properties, such blends represent a smooth variation between diesel and gasoline. As the second study, a seven component surrogate fuel for conventional diesel was studied with the same setup and under similar conditions. This surrogate is then compared to results from real diesel, followed by a single component and results from a 1D model.

4.2 Optical setup

Two different optical techniques have been simultaneously employed for the experimental measurements under inert conditions: schlieren imaging and Mie-scattering; the first one was used to measure the vapour spray penetration and the second one for the liquid length. Digital images have been analyzed by means of purpose-developed processing software, which delivers the spray geometrical parameters (Section 3.3). The schematic shown in Figure 4.1 corresponds to the setup of the 2-stroke optical engine, which was used for the tests presented in this chapter. The optical setup for the inert and reactive tests performed in the high-pressure high-temperature vessel will be explained in Chapter 5.

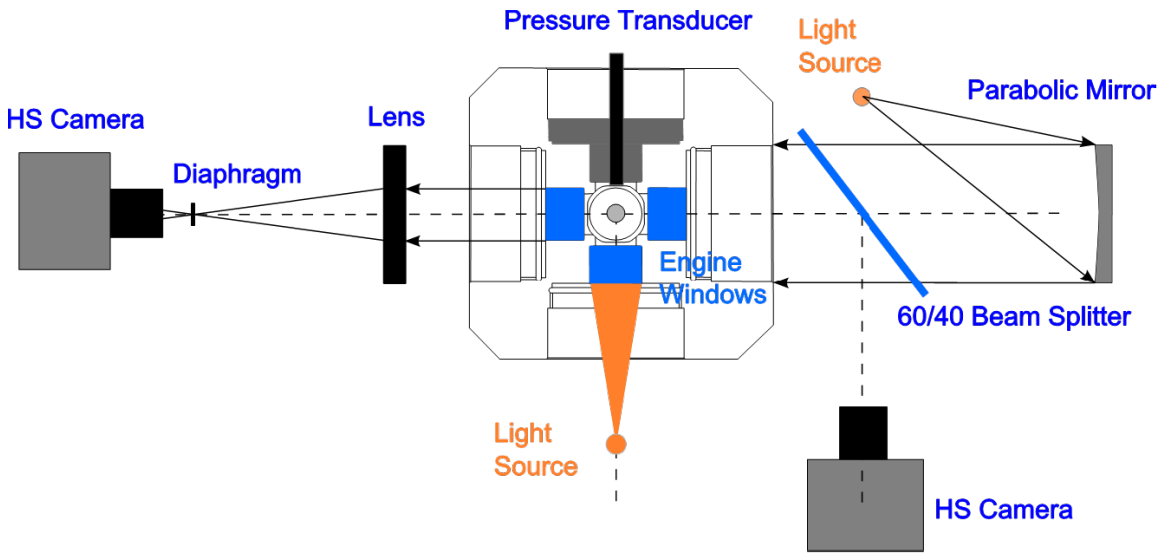

Figure 4.1. *Schematic of the experimental setup for the study of the inert spray.*

Schlieren

An schematic of the optical arrangement for the schlieren technique is shown in Figure 4.1. The spray is illuminated from the right side of the combustion chamber, whereas the shadow is being recorded from the other side by means of a CMOS camera. Illumination is achieved by means of a continuous Xenon lamp, and to reduce the size of the light source and improve sensitivity, an iris diaphragm is placed just at the bundle exit, in order to form a light source with a diameter of 1 mm. The light source is located at the focal length of a parabolic mirror in order to generate collimated light beams. On the other side of the combustion chamber, a 150 mm biconvex lens collects the light beams to form an image that will be projected onto the camera lens and then recorded by the sensor. A diaphragm is placed at the focal point of the beam to filter the light beams that have been diverted from their original parallel direction due to density gradients. A 12-*bit* Photron SA-5 CMOS high-speed camera equipped with a Zeiss 100 mm $f/2$ lens were used, image acquisition frequency was 20000 FPS with a exposure time of 14 μs and 10.35 of pixel/mm ratio.

Mie-scattering

Figure 4.1 also shows an schematic of the optical setup for Mie-scattering. The spray has been illuminated from the front of the combustion chamber, and the image has been recorded from the right side via a CMOS camera. The light source was also a Xenon lamp and was fitted with a collimator in order to have homogeneous illumination of the spray. On the collecting side, which is the illumination side of the schlieren set-up, a 60/40 beam splitter is placed between the cylinder head and the parabolic mirror in order to redirect the light reflected by the spray to the camera and still be able to let some light through for the other technique. The beam splitter is placed with a 45° angle, so the camera axis could be parallel to the spray axis but the reflected image perpendicular to it. A Phantom 10-*bit* V12 CMOS high-speed camera equipped with a Zeiss 100 mm $f/2$ lens was used; with an image acquisition frequency was 20000 FPS with an exposure time of 10 μs and 9.92 of pixel/mm ratio.

Finally, the synchronization of both cameras was done using the *phase lock* feature of the Photron SA-5. This camera was used as the "*master* camera" as it received the triggering signal from the injection system and the Phantom was used as a "*slave* camera" as it received the output signal of the Photron. Moreover, since both cameras used the same acquisition frequency, the synchronization of both apparatuses was further corroborated when comparing the first frames of an image sequence and checking the times at which the spray started to appear.

4.3 Test conditions and fuel selection

As mentioned in Section 1.3, in order to understand the processes of mixing and evaporation, experiments will be performed using n-decane (n-$C_{10}H_{22}$), n-hexadecane (n-$C_{16}H_{34}$) and intermediate blends, due to the fact that their physical properties are very different (Table 4.1). The tests will be performed in the 2-stroke optical test rig

Table 4.1. *Boiling temperatured, vaporization enthalpies and densities for single-component fuels employed. Source: NIST Chemistry WebBook [1].*

Fuel	T_{boil} $[K]$	H_{vap} $[kJ/mol]$	ρ_f $[kg/m^3]$
n-heptane	371.5	36	680
iso-octane	372.4	35.1	690
n-decane	447.2	51.3	730
n-dodecane	489.2	61	750
n-butylbenzene	456	50.8	860
n-hexadecane	554.1	81.3	770
n-octadecane	589.3	92	777
n-eicosane	616.2	102	789
1-methylnaphthalene	515	59	1001

Table 4.2. *Test matrix for binary blends. Combustion chamber temperature and pressure at top dead centre.*

$T \setminus P$	4.28 MPa	5.28 MPa	7.26 MPa
748 K	X	X	X
881 K	X	X	X

described in Section 3.2.1. All points will be carried out under inert conditions (0% oxygen concentration) to isolate the spray from the possible combined effects that may take place during combustion. The experimental matrix is shown in Table 4.2, only two temperatures have been chosen as it is expected to have an effect only on the liquid penetration, and none on that of the vapour phase. On the other hand, three ambient pressures, leading to three air density values for each temperature, were selected as its effect is reflected on the penetration of both phases. All conditions will be done at three injection pressures of 50 MPa, 100 MPa and 150 MPa using a single-hole nozzle with an orifice diameter of 140 μm; for each operating condition 15 repetitions were performed. Finally, fuel composition will vary from pure *n*-decane to pure *n*-hexadecane, the detailed nomenclature and composition of the blends is presented in Table 4.3. Those two fuels were selected because of the differences among their properties, and also as the *n*-hexadecane is a good representative of the behaviour of diesel in terms of evaporation. Moreover, mixing it with a lighter component would provide with blends that have properties similar to possible diesel-gasoline mixtures.

Additionally, a parametric study has also been carried out using a much more complex blend composed of six hydrocarbons, composition shown in Table 4.4. The formulation of the multi-component fuel came as a result of the search for a surrogate for a real diesel fuel in terms of evaporation properties; a comparison of their distillation curves is shown

Table 4.3. *Fuel composition of binary n-decane/n-hexadecane blends (in mass).*

Fuel \ Blend	D0	D30	D50	D70	D100
n-decane [%]	0	32	54	77	100
n-hexadecane [%]	100	68	46	23	0

Table 4.4. *Fuel composition of diesel surrogate (in mass).*

Component	[%]
n-dodecane	10
n-butylbenzene	3
n-hexadecane	29
n-octadecane	20
n-eicosane	13
1-methylnaphthalene	25

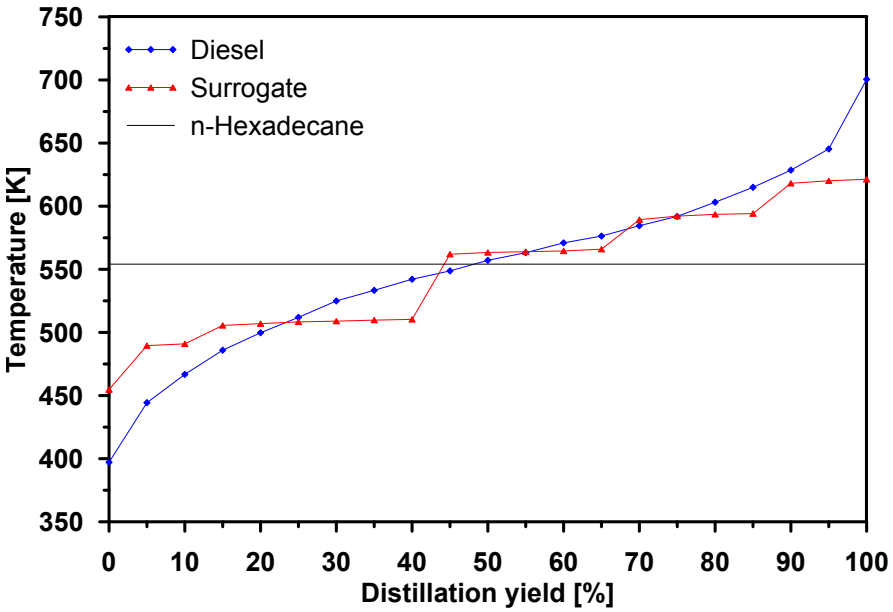

Figure 4.2. *Distillation curves of the conventional diesel fuel and its surrogate and the boiling point of n-hexadecane.*

in Figure 4.2 and the evaporation properties of each component are presented also in Table 4.1.

In order to be able to use the results of the 1D model presented in the previous chapter, the validation of such model will be done using *n*-dodecane as fuel. To do

Table 4.5. *Test matrix for model validation. "A" indicates Spray-A standard conditions. *For 1000K, only results at 50MPa were used.*

$\rho \backslash T$	700 K	800 K	900 K	1000 K*
7.6 kg/m^3			X	
15.2 kg/m^3			X	
22.8 kg/m^3	X	X	**A**	X

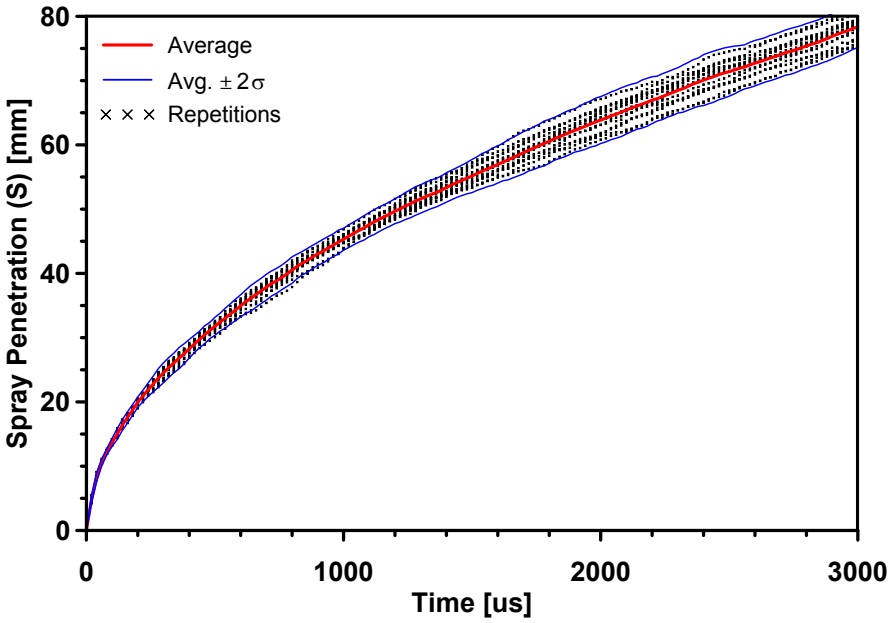

Figure 4.3. *Spray penetration scattering of all repetitions and average value at Spray A standard conditions; 900 K and 22.8 kg/m^3 of air temperature and pressure, and 150 MPa of injection pressure.*

that, experimental results from spray penetration under ECN Spray A conditions were used [2]. A parametric variation of air density and temperature at three injection pressures (50 MPa, 100 MPa & 150 MPa) as shown in Table 4.5 was performed.

Finally, Figure 4.3 shows an example of the experimental scattering in the spray tip penetration for 15 different injections. It shows all the values are within two standard deviations (blue lines), which should enclose approximately 95 % of the values according to the two-sigma (2σ) rule of the Normal distribution. Since the tests have proven to be repetitive, the results shown throughout the rest of the document will only present the average values of all the repetitions (red line). For time-averaged values such as lift-off lengths and ignition delay times, the error bars presented also correspond to two standard deviations (95 %).

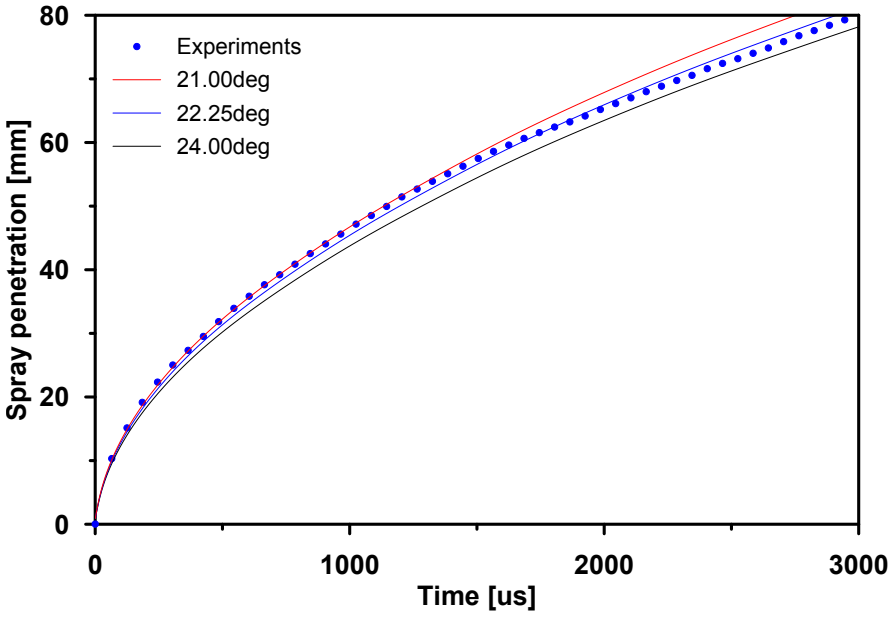

Figure 4.4. *Experimental vapour penetration and modelled values for three angles under Spray A standard conditions; 900 K and 22.8 kg/m^3 of air temperature and pressure, and 150 MPa of injection pressure.*

4.4 Model calibration with single-component fuels

As was mentioned in the model description (Section 3.4.1) the only unknown input of the model is the spray angle; therefore, it needs to be determined by adjusting the results of the modelled vapour penetration to the experimental one. The experimental penetration values used for the fitting of the model were those corresponding to the Spray A conditions using *n*-dodecane as fuel. The Spray A is a set of operating conditions set by the Engine Combustion Network (ECN) working group in order to study the processes involved in a diesel spray [3]. Therefore, a wide range of results under numerous contour conditions is available for researchers worldwide [2]. Spray A boundary conditions are based upon engine operation at moderate EGR levels; additionally, different values for parametric variations of oxygen concentration, ambient temperature, air density and injection pressure, among others have been included. Reference injection pressure, chamber density, temperature and oxygen concentration in volume for Spray A are 150 MPa, 22.8 kg/m^3, 900 K and 15 %, respectively.

To validate the model and to determine the adequate spray angle for a given set of conditions, a series of calculations were made at small angle increments; then, the deviation from the experimental curves was determined, and based on that the angle value was chosen. Figure 4.4 shows the experimental vapour penetration for the Spray A standard conditions and the curves for three different values of spray angle as predicted by the model. It can be seen that a wider angle (ie. 24°) tends to under-predict the penetration, while a narrower value (ie. 21°) may seem appropriate at the beginning but in the end over-predicts it. Therefore, the angle selected (ie. 22.25°) is one that

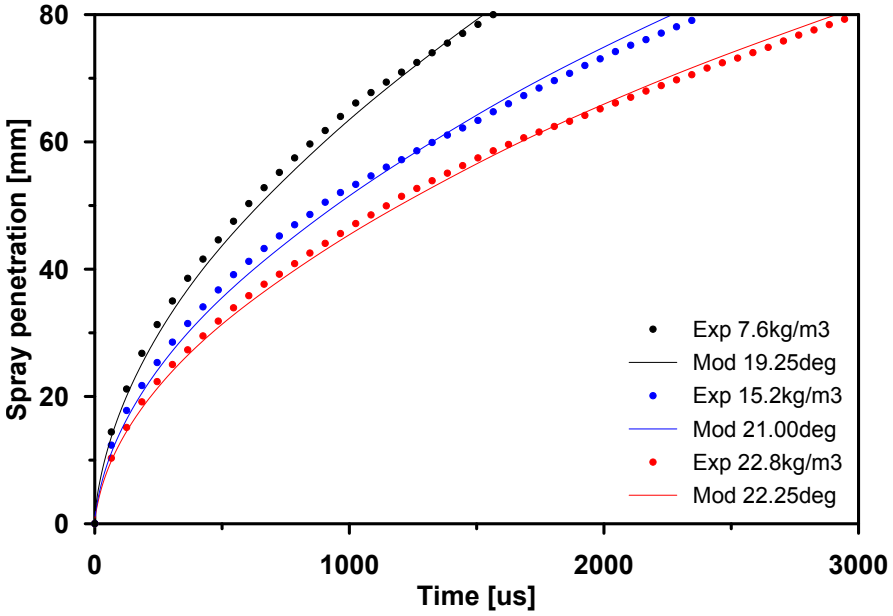

Figure 4.5. *Model-fitted angles for ambient densities at Spray A parametric variation; 900 K of air temperature and 150 MPa of injection pressure.*

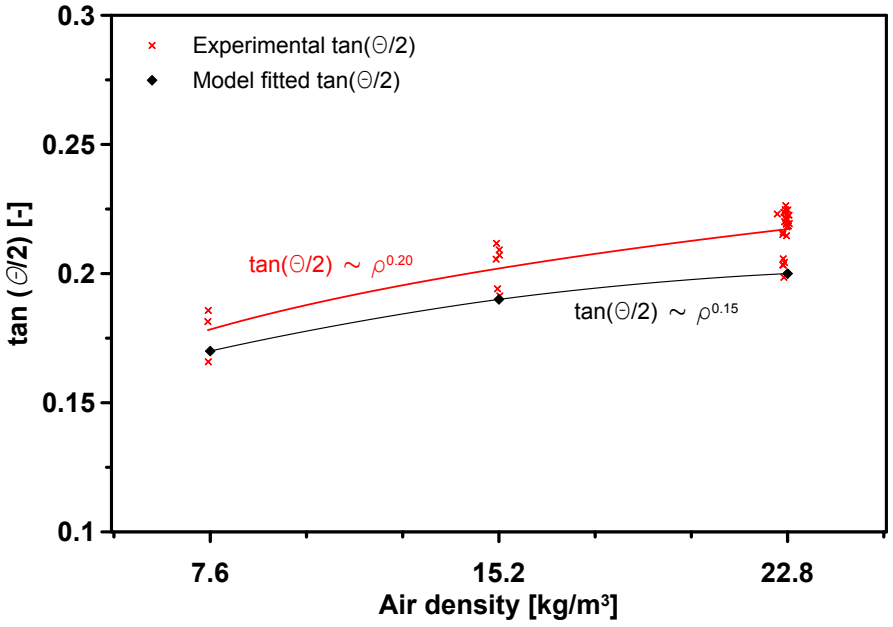

Figure 4.6. *Experimental and model-fitted angles as a function of the density at Spray A parametric variation; 900 K of air temperature and 150 MPa of injection pressure.*

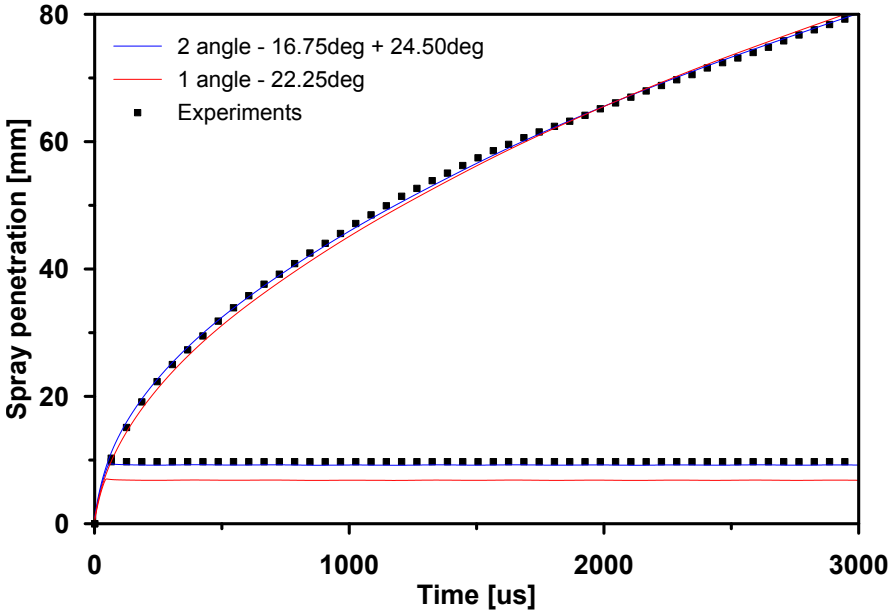

Figure 4.7. *Experimental liquid and vapour penetration and modelled values with one and two angles under Spray A standard conditions; 900 K and 22.8 kg/m^3 of air temperature and pressure, and 150 MPa of injection pressure.*

presents a good balance between the near and far regions of the spray from the nozzle. Additionally, it was found that the spray angle depended mainly on the ambient density and not on other values as injection pressure or air temperature. Figure 4.5 presents the different model cone angle values determined for three ambient densities. The values not only correspond to the smallest error, but also are a good compromise between the penetration close and far from the nozzle. It can be seen that the best fits correspond to the cases of higher densities, this is because mixing controlled hypothesis are less valid at low density and injection pressure. Past results have also shown the effect of the gas density on the spray spreading angle [4]; furthermore, the calculation of the angle as a function of the ambient gas to the power of a constant has been previously used in the literature [5, 6]. Figure 4.6 presents the experimental and model-fitted tangents of the half-angle as a function of the ambient density. The experimental values are an average of all repetitions in a time range in which the spray angle has stabilized. The angle has been calculated by fitting a line passing through the injector tip on the spray contour. The values presented for the experimental case are in agreement with values previously presented, $\tan(\theta/2) \sim \rho^{0.2}$ [4]. Moreover, the exponent of 0.15 for the fitted values is also in agreement with the experimental results, as the fitted-angle slightly under-predicted the penetration in the near field while slightly over-predicting it in the far field (Figure 4.5). As a result of this compromise the model-fitted angle was more acute than the experiments, therefore a smaller exponent for the correlation.

One of the drawbacks found by using single angle values fitted to the vapour penetration is that the liquid length was severely under predicted as the model (models in general) tends to over-entrain air. This issue and the aforementioned compromise

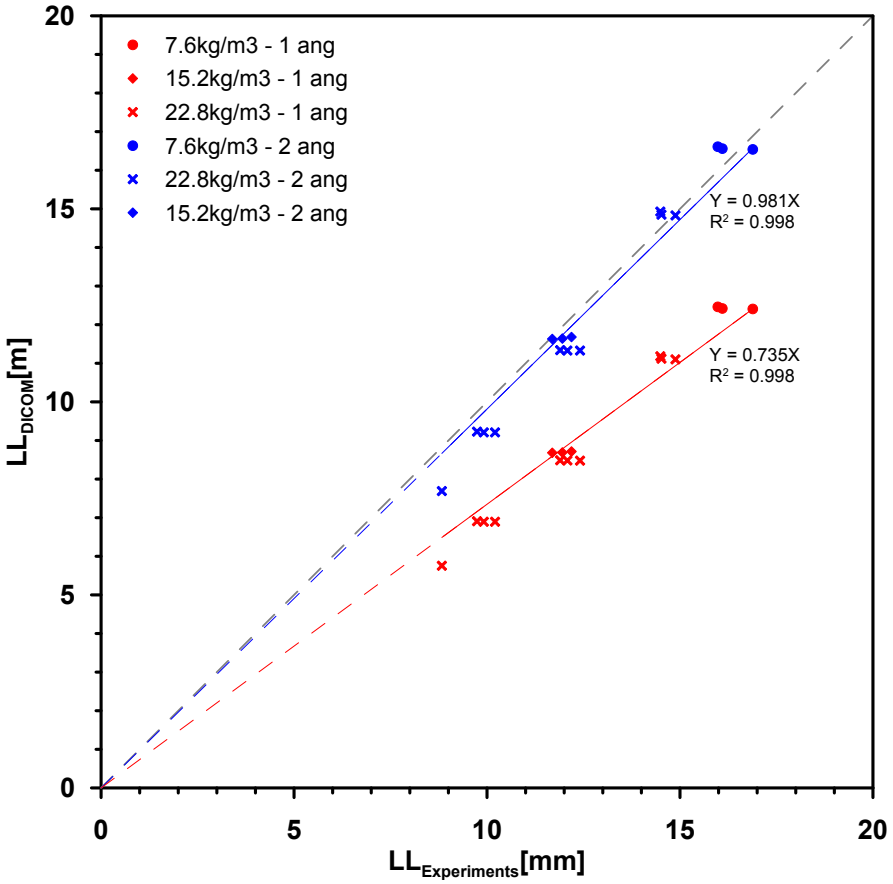

Figure 4.8. *Experimental and modelled liquid penetration with n-dodecane at Spray A parametric variation; 900 K of air temperature and 150 MPa of injection pressure.*

between close and far regions, which is worse at lower densities (Figure 4.5), led to considering the need for two different spray angles: (1) A narrower angle for rapid penetration near the nozzle and a good fitting of the liquid length and, (2) A wider angle for the steady penetration of the vapour phase far from the nozzle. This issue has already been discussed in a paper where the spray angle was studied under vaporizing and non-vaporizing conditions [7], as well as in a similar validation of the model [8]. Additionally, two previous Ph.D. theses have studied the spray angle in the near-field [9] and far-field [10] and the results also show the angle closer to the nozzle to be narrower. Figure 4.7 shows the experimental liquid and vapour penetrations and the modelled curves using one and two angles. The first angle was fitted using the penetration upto a fixed distance in the vicinity of the nozzle for all the cases. The second angle was obtained by fitting the rest of the penetration curve. It can be seen that for the single-angle case, the spray penetration was as shown in Figures 4.4 and 4.5, overall a good fit, but slightly over-prediction in the near region and slightly over-predicting far from the nozzle; however, the liquid length is under predicted. On the other hand, the double-angle case not only fits the liquid penetration with much more accuracy, but the evolution of the vapour phase also seems more according to the experiments in the near and far regions, proving that

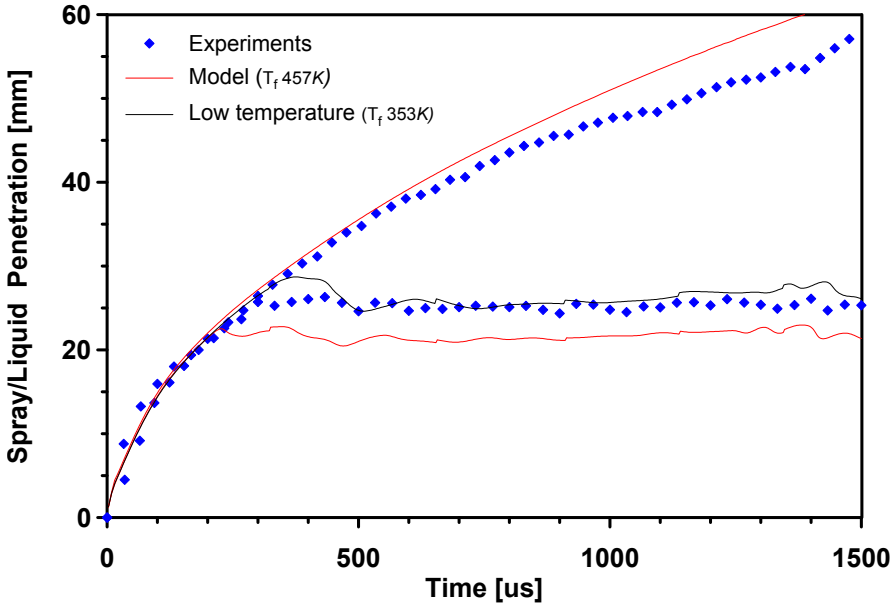

Figure 4.9. *Experimental and modelled vapour and liquid penetration for the D50 blend at 748 K and 5.28 MPa. Angle values of 15.00° (close) and 26.75° (far) were used.*

the two angle strategy is not only positive for the liquid phase but for the evolution of the spray under both phases. Finally, the liquid length has been calculated with one and two angles for a wide range of Spray A conditions in order to further validate the model and the bi-angle strategy. Figure 4.8 shows that the liquid length calculated with only one angle reaches just 73 % of the experimental values in average, whereas the two angle penetrations achieve values of 98 % in average.

As a result and in order to produce a reliable source for comparison, the liquid and vapour penetration presented along this chapter have been calculated using the two angle strategy.

4.5 Studies with binary blends

In this section the results corresponding to the tests performed with *n*-decane, *n*-hexadecane and the three intermediate blends will be presented (Table 4.3). As mentioned in Section 4.3, a parametric variation was performed under the conditions shown in Table 4.2. As a starting point, an analysis of the general trends caused by the boundary conditions will be done with an intermediate blend. Then the effects of the fuel properties will be studied with the help of the 1D model presented in Section 3.4.

Figure 4.9 shows the experimental results of liquid and vapour penetration for the D50 blend at 748 K, 5.28 MPa and 100 MPa of injection pressure, along with the output of the model using the double-angle strategy. As opposed to Figure 4.7, where the penetration of both phases showed a very accurate fit along the whole time scale as the conditions where nearly quiescent and the fuel temperature was accurately estimated [11]

because the tests were performed on the HPHT vessel, the results for the binary blends are slightly different for two reasons. On one hand, the 2-stroke optical engine has a piston moving upwards and creating a counter-flow that tends to flatten the penetration of the spray, therefore the growing differences in the penetration curves as time passes. On the other hand, despite the double angle strategy the stabilized liquid length remains shorter than the experimental, this is because of the uncertainty on determining the actual fuel temperature, which is an important parameter for the calculation of the state relationships and the evaporation fraction, which will define the liquid length values. This effect has been seen for all five blends, as will be shown later in this chapter. Even though the injector temperature has been characterized and a correlation for the temperature was obtained in function of the contour conditions [11], the actual temperature of the fuel is thought to be lower than the values obtained. Figure 4.9 also shows a simulated liquid length at a lower fuel temperature. The estimated fuel temperature for the given conditions has a value of 457 K, which is thought to be higher than the actual fuel temperature. However, if a lower temperature is used, for example 353 K which is the cooling water temperature, the model returns a liquid penetration that has a very similar shape but a longer value. Therefore, the simulations shown have been calculated with the estimated temperature as it is the most accurate value available, even though the actual fuel temperature is thought to be in-between those two values. Nevertheless, the stabilized liquid penetrations calculated with the cooling water temperature will also be shown as a reference.

Figure 4.10 shows an example of the effect of the in-cylinder pressure on the liquid and vapour penetration. Experiments show that there is a decrease in spray tip penetration (top) with in-cylinder pressure rise due to the increase in air density [12–17]. This results in a higher air entrainment into the spray and, by conservation of momentum flux, in a reduced velocity within the spray; which is also in agreement with the results from the model. A reduction is also observed for the stabilized liquid length, Figure 4.11 (bottom). The state relationships as calculated by the 1D model under the same pressure variation show that the higher ambient pressures cause the dew curves to be above the ones corresponding to lower pressures, which means that the liquid-vapour equilibrium will still be achieved at higher temperatures and lower fuel mass fractions, Figure 4.11 (top). Analogously, the temperature curves are also shifted upwards; however, since not all curves start at the same fuel temperatures nor end at the same ambient temperatures, when intersected with their respective dew curves, the changes in evaporation fractions are not as straight forward. This fluctuations are due to the nature of the test rig, which is a reciprocating engine and not a constant volume (CVP) or pressure (CPF) vessel. Therefore, the conditions obtained at TDC affect the chamber conditions at the SOI and also the fuel temperature. It can be seen that for the cases of 4.28 MPa and 7.26 MPa the values of f_{evap} are very similar, 0.2797 and 0.2791, respectively; while the other case has a lower value at 0.2686. This could mean that the liquid lengths of the highest and lowest pressures would be similar and shorter than the intermediate one. Nevertheless, since the lower ambient density is also causing the spray to penetrate faster into the chamber, the liquid penetration differences are inverse to those of the pressures, since the increase in air entrainment offsets the aforementioned effect and justifies the reduction of the stabilized liquid penetration [4, 11, 15–23]. Figure 4.11 (bottom) shows the fuel mass fraction along the center line, this further proves that the increased air ambient pressure augments

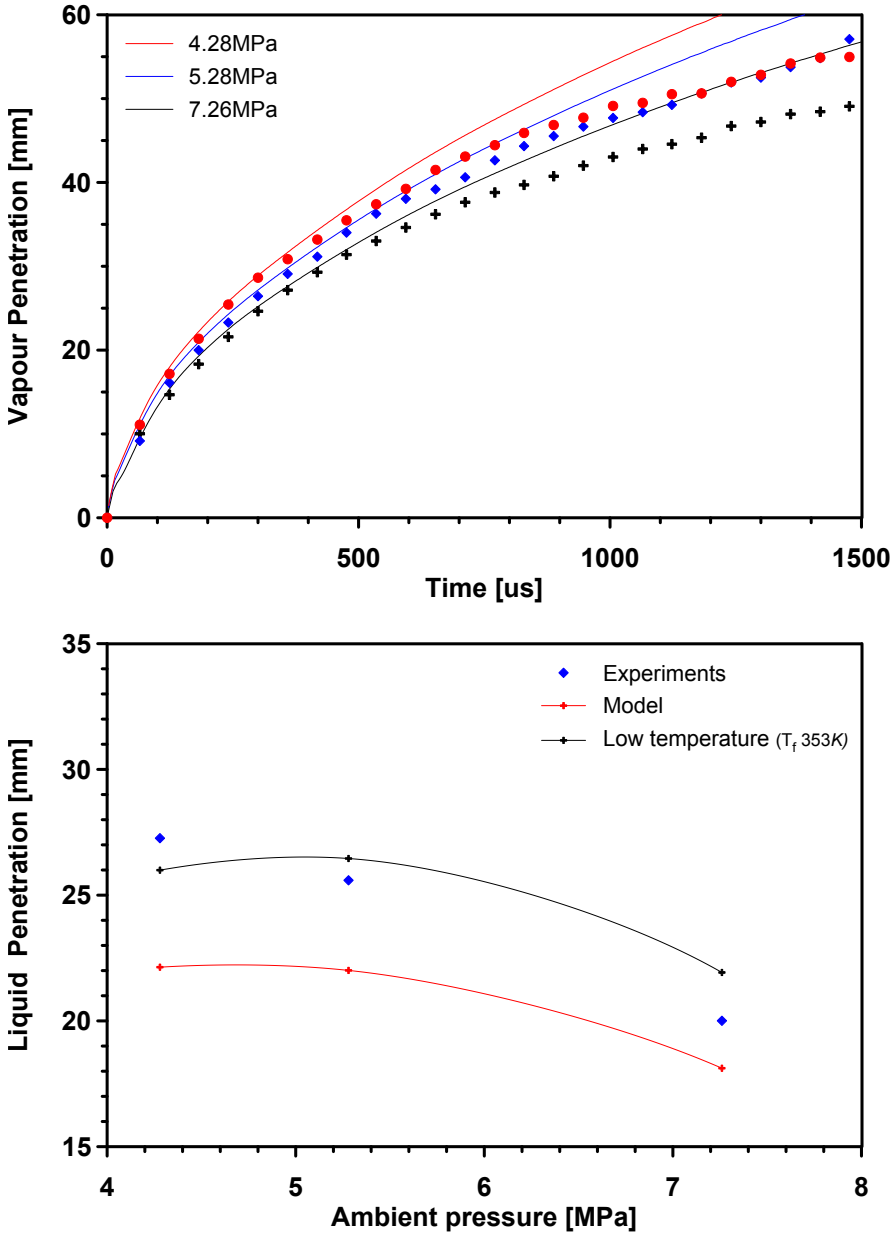

Figure 4.10. *Experimental and modelled vapour (top) and liquid (bottom) penetration under ambient pressure variation at 748 K of ambient temperature for the D50 blend, time after SOI.*

the amount of air entrained, leading to leaner mixtures at the same axial position. As increasing the ambient pressure increases the LV equilibrium temperature, but also the ambient and fuel temperatures increase as a collateral effect due to the nature of the test rig. And increasing the ambient density leads to more air entrainment, so f_{evap} is reached at shorter distances leading to shorter liquid lengths. Summarizing, in order to predict the liquid length the model calculates the evaporation fraction from the state relationships using the enthalpy balance and the liquid-vapour equilibrium. On the other hand, the spatial distribution of mass fractions in the spray depends on the air entrainment. So,

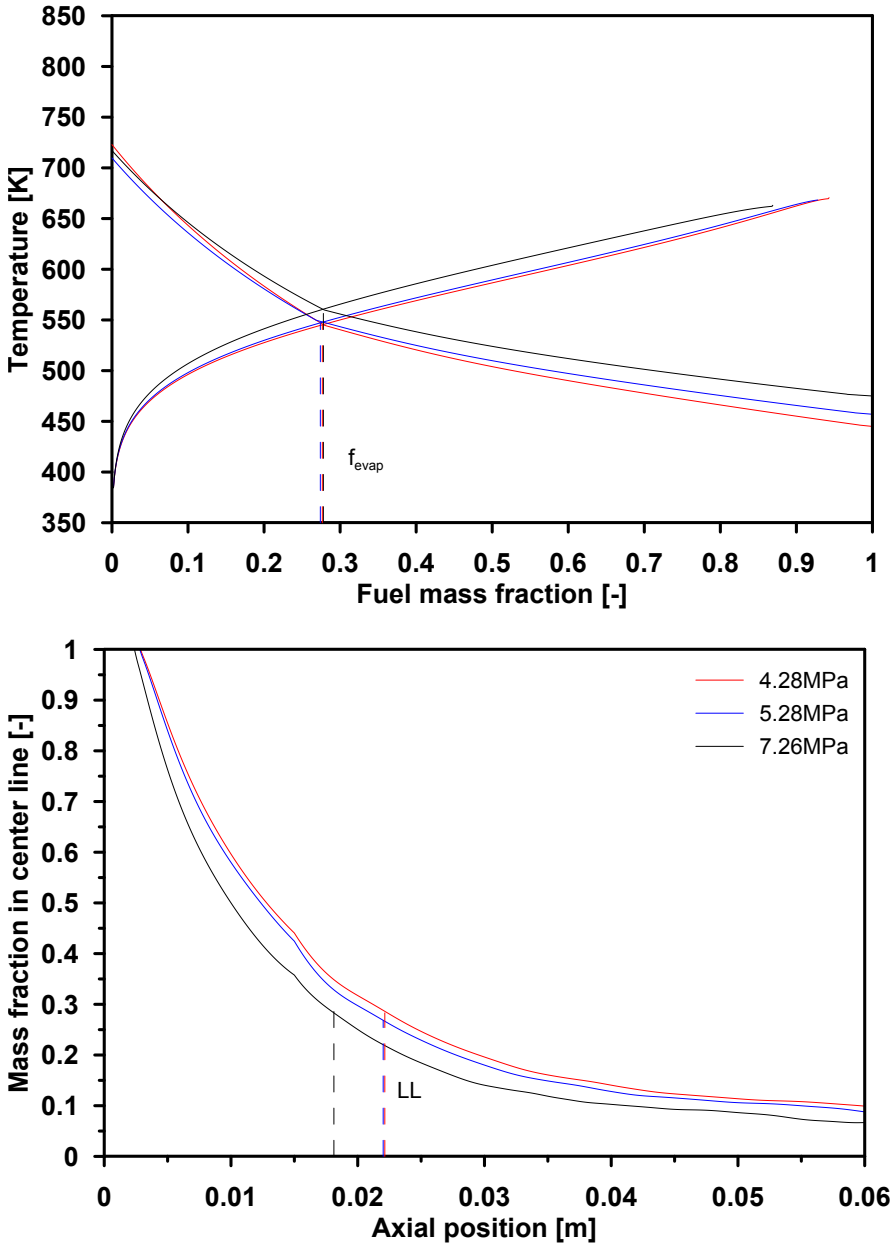

Figure 4.11. *Modelled dew curve and temperature evolution (top) and mass fraction in center line (bottom) under ambient pressure variation at 748 K of ambient temperature for the D50 blend, time after SOI.*

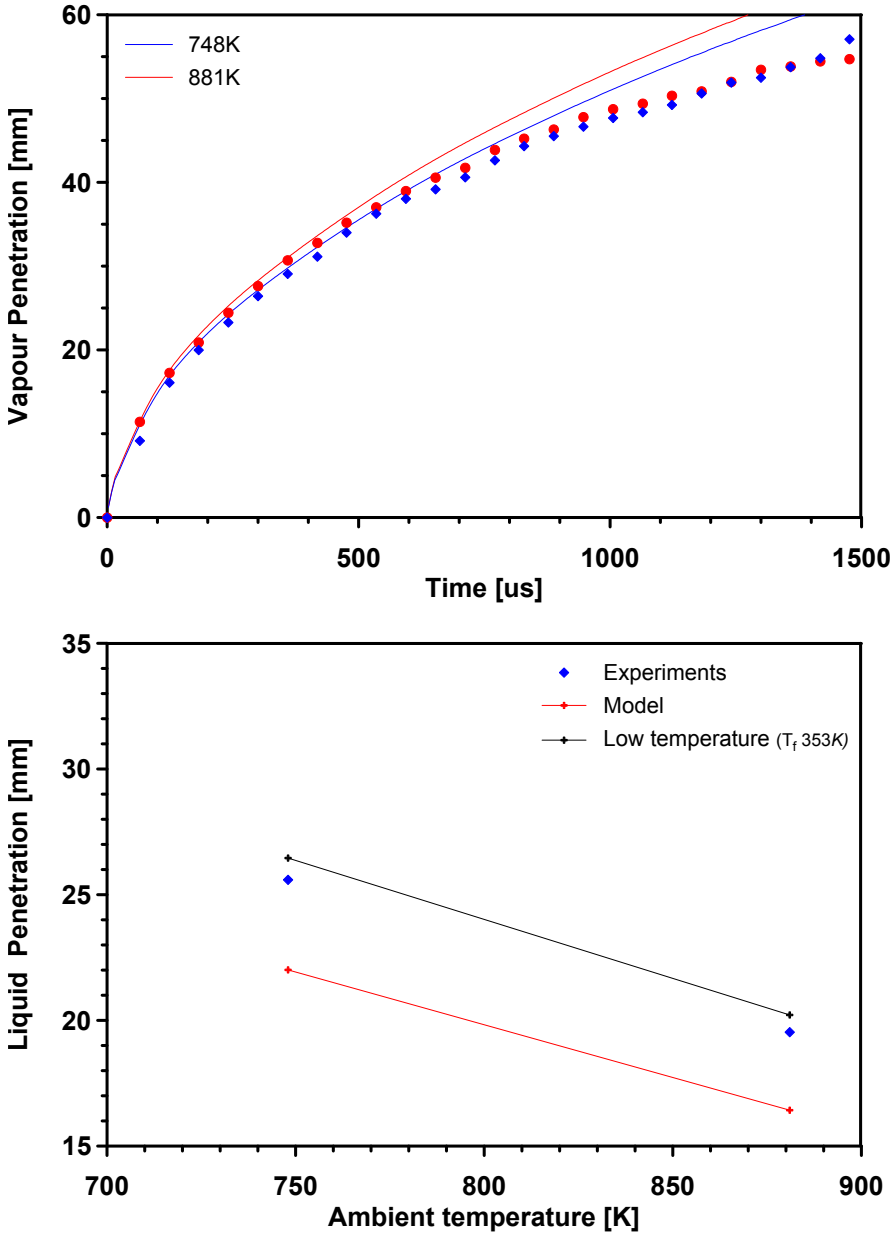

Figure 4.12. *Experimental and modelled vapour (top) and liquid (bottom) penetration under ambient temperature variation at 5.28 MPa of ambient pressure for the D50 blend, time after SOI.*

the liquid length is determined by how far away from the nozzle the f_{evap} is found in such distribution.

The vapour tip penetration is not significantly affected by the change of air temperature, as shown in Figure 4.12 (top). An slight increment can be seen on the high temperature point, as the increase in temperature at constant pressure reduces the density of the combustion chamber, which has been observed to have an effect on vapour tip penetration (Figure 4.10). On the other hand, Figure 4.12 (bottom) shows that the

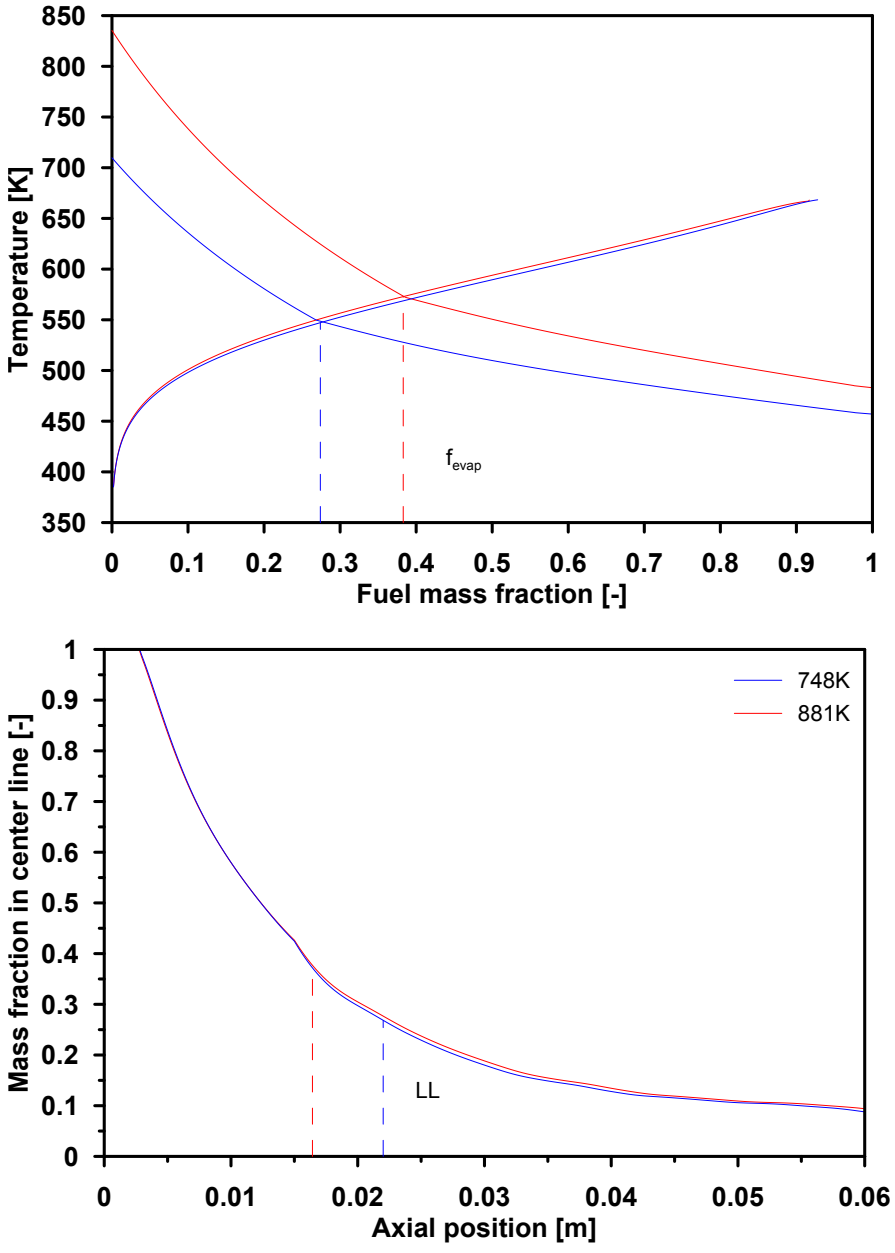

Figure 4.13. *Modelled dew curve and temperature evolution (top) and mass fraction in center line (bottom) under ambient temperature variation at 5.28 MPa of ambient pressure for the D50 blend, time after SOI.*

stabilized liquid length is reduced because of the higher air temperature. Figure 4.13 (top) shows the state relationships as calculated by the 1D model under the same temperature variation. The dew curves are almost identical, as they are only affected by the air pressure and not the temperature. The temperature curves are obviously different, as the hotter air will cause the fuel to heat up faster as more enthalpy is being entrained into the spray (in spite of the commented drop in density). Figure 4.13 (bottom) shows that the ambient temperature has no effect on the air entrainment nor the spatial distribution of mass fractions, as both center lines are almost identical. Therefore, the higher evaporation fraction will be found closer to the nozzle than on the low temperature case. This will result in shorter liquid lengths as it is an indicator of the faster evaporation of the fuel [4, 16, 18, 19, 21–25].

The injection pressure has an important effect on the vapour tip penetration, as the increased pressure is reflected in a higher fuel exit velocity from the nozzle, increasing the momentum of the spray and causing it to penetrate faster into the combustion chamber [13, 16, 17, 26]. This can be seen in Figure 4.14 (top) where the higher injection pressures correspond to the curves with higher penetration rates for both, the experiments and the model. On the other hand, Figure 4.14 (bottom) shows a decrease in the liquid lengths as the injection pressure rises as opposed to others that show very little to no change at all [4, 16, 22, 23, 27]; nevertheless some other experimental studies have also reported a reduction in the maximum liquid penetration with increasing injection pressures [11, 17, 21, 28–30]. This could be contradictory to the hypothesis of the fuel injection pressure not having an effect on the stabilized liquid penetration as the evaporation is a mixing controlled phenomenon and the liquid length would be limited only by the air entrainment. However, in cases where the role of the atomization is more important than the entrainment of air, which could be cases of lower density or low injection pressures, the liquid length is seen to change. Additionally, such hypothesis assumes that the higher injection pressure is causing the fuel flow rate to increase and this effect is compensated by the same change in the evaporation rate, hence no change in the liquid penetration [23]. Figure 4.17 presents the state relationships (top) and the mass fraction along the center line (bottom) as calculated by the 1D model under the same injection pressure variation. It can be seen that all curves are identical for the three injection pressures, which implies that no change will be obtained in the liquid length as the evaporation fractions are also the same for all conditions as well as the spatial distribution of mass fractions. Nevertheless, in the experiments performed the effect of the evaporation rate caused by the air entrainment seems to be more important than the increase in mass flow, thus leading to shorter liquid length values.

Figure 4.16 (top) shows that the fuel composition and properties have a negligible effect on vapour penetration, as was expected from previous results [15, 20, 31]. As already commented, this parameter depends mainly on nozzle momentum flux, spray cone angle and ambient density. The latter variable does not change within the test series on the plot, leaving momentum flux as the only parameter that could change with fuel type. However, measurements and theoretical justifications [31] show that this parameter is independent of fuel type (in particular of fuel density) when operating at constant injection pressure, which justifies the independence of the vapour tip penetration regarding the fuel. This result is in agreement with other studies in the literature [20]. For example, from the definition that the momentum flux is proportional to the fuel density, area and

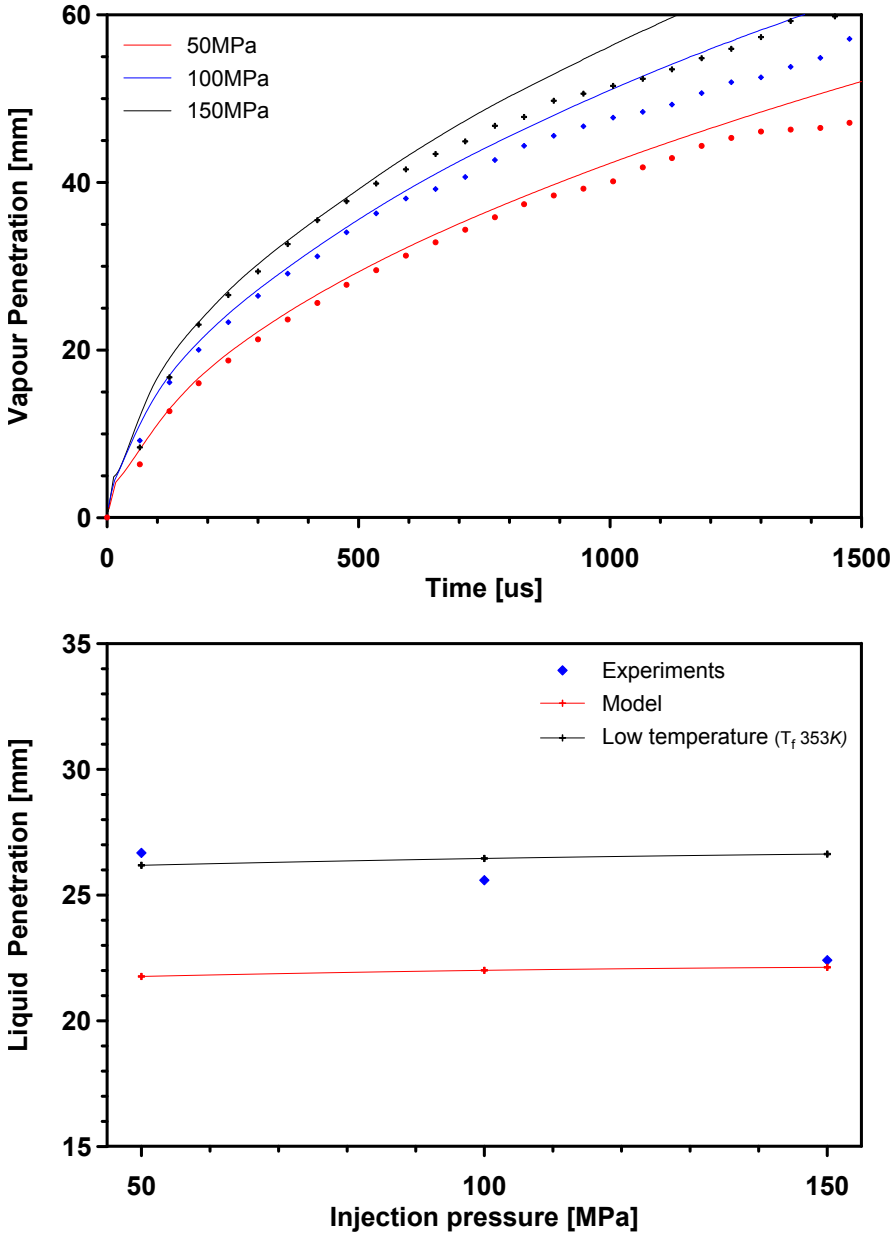

Figure 4.14. *Experimental and modelled vapour (top) and liquid (bottom) penetration under injection variation at 5.28 MPa and 748 K of ambient pressure and temperature for the D50 blend, time after SOI.*

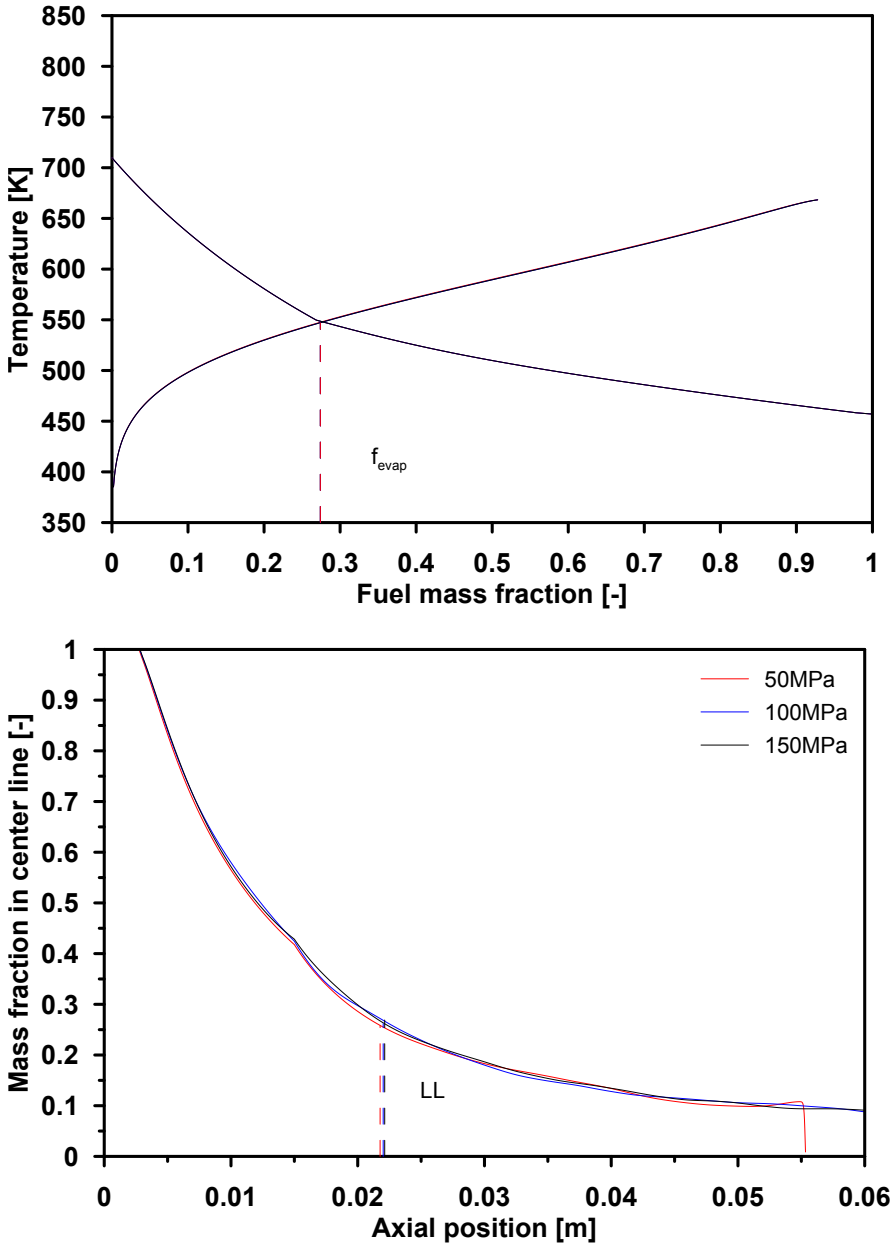

Figure 4.15. *Modelled dew curve and temperature evolution (top) and mass fraction in center line (bottom) under injection variation at 5.28 MPa and 748 K of ambient pressure and temperature for the D50 blend, time after SOI.*

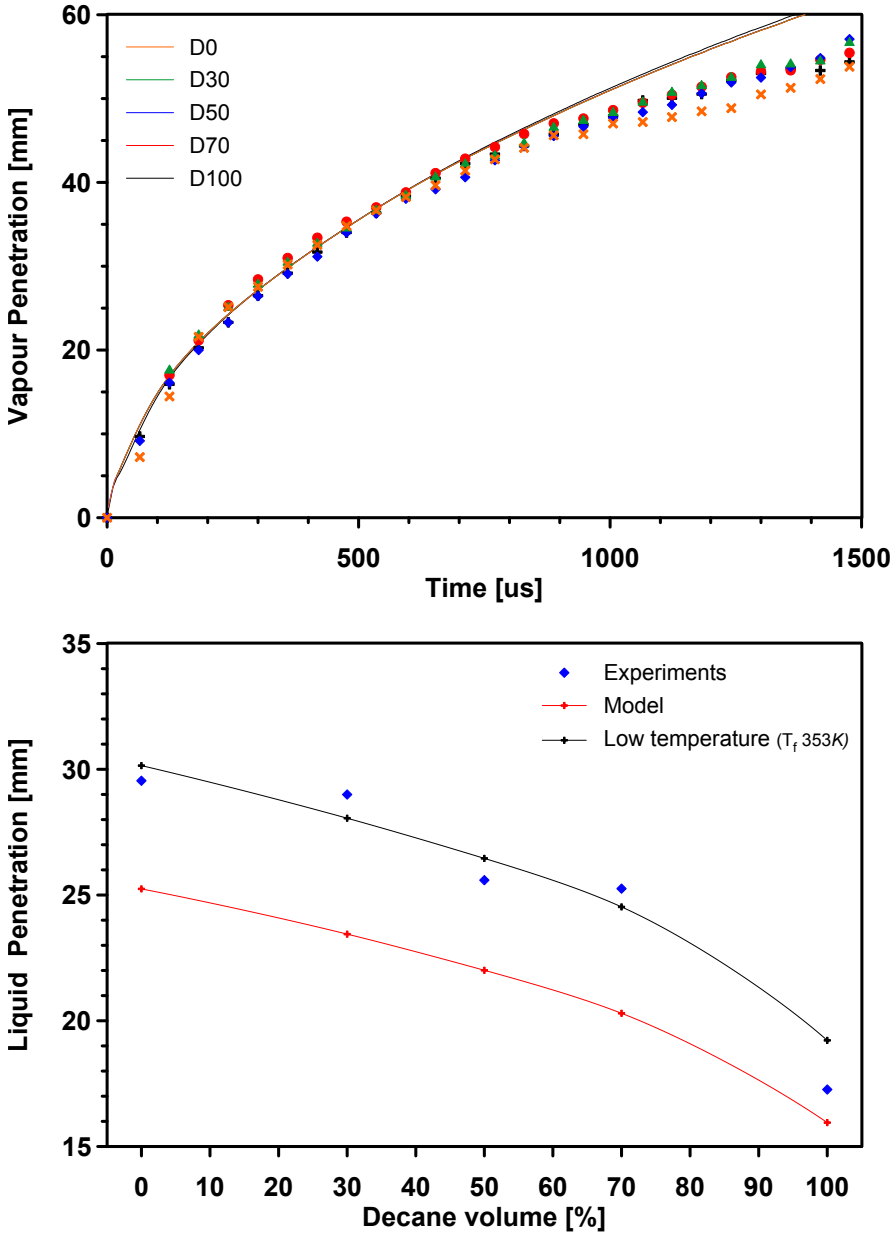

Figure 4.16. *Experimental and modelled vapour (top) and liquid (bottom) penetration for all blends at 5.28 MPa and 748 K of ambient pressure and temperature, time after SOI.*

square of the exit velocity ($\dot{M} \sim \rho_f \cdot A \cdot u_0^2$) and the exit velocity is equal to the square root of twice the pressure drop divided by the fuel density ($u_0 = 2\sqrt{\frac{\Delta P_{inj}}{\rho_f}}$), then the momentum flux would depend only on the area and pressure drop ($\dot{M} \sim A \cdot \Delta P_{inj}$). Since the fuel comparison is performed at constant injection pressure, there should not be a noticeable effect of the fuel on the spray penetration. On the other hand, the liquid penetration does present a dependency on the properties of the fuel, being the longest value corresponding to *n*-hexadecane (D0), which is the fuel with the highest boiling

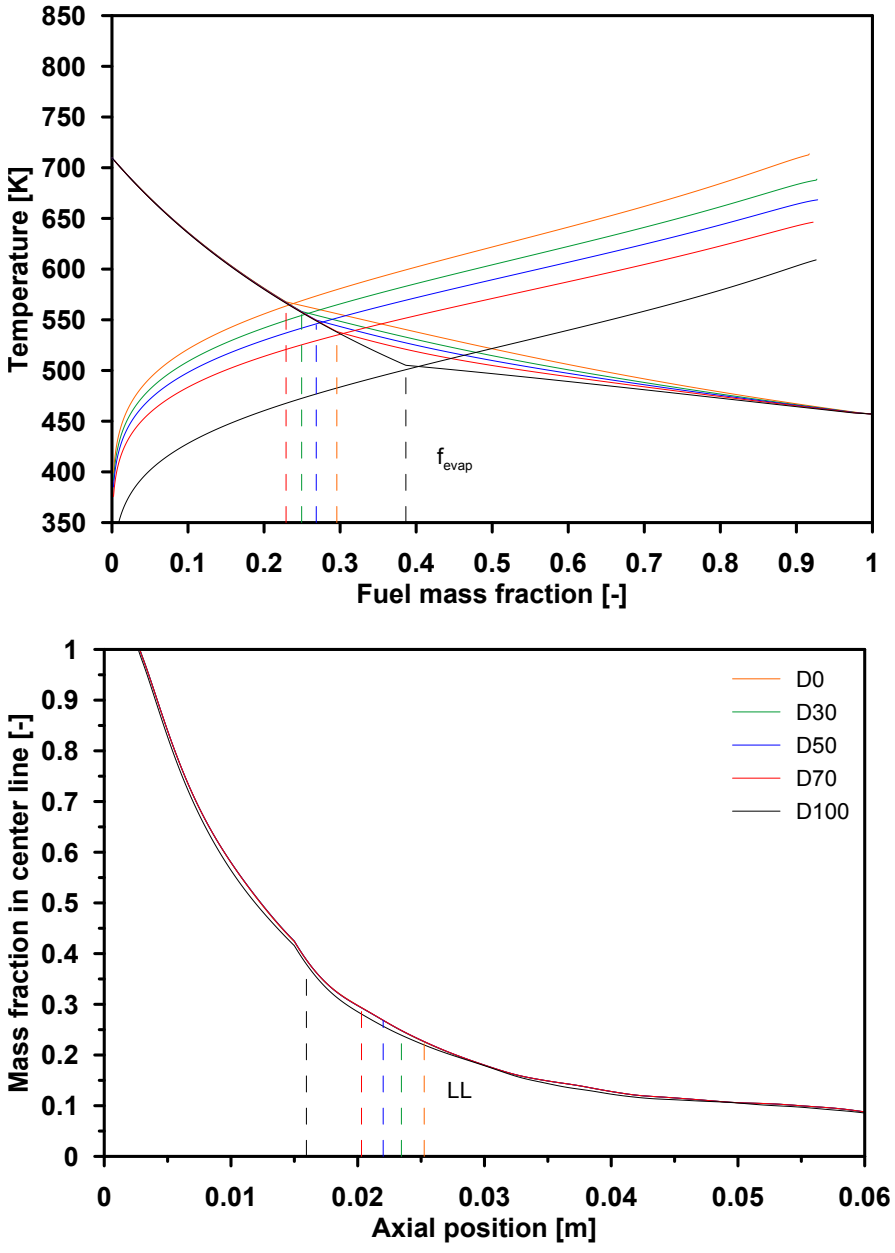

Figure 4.17. *Modelled dew curve and temperature evolution (top) and mass fraction in center line (bottom) for all blends at 5.28 MPa and 748 K of ambient pressure and temperature, time after SOI.*

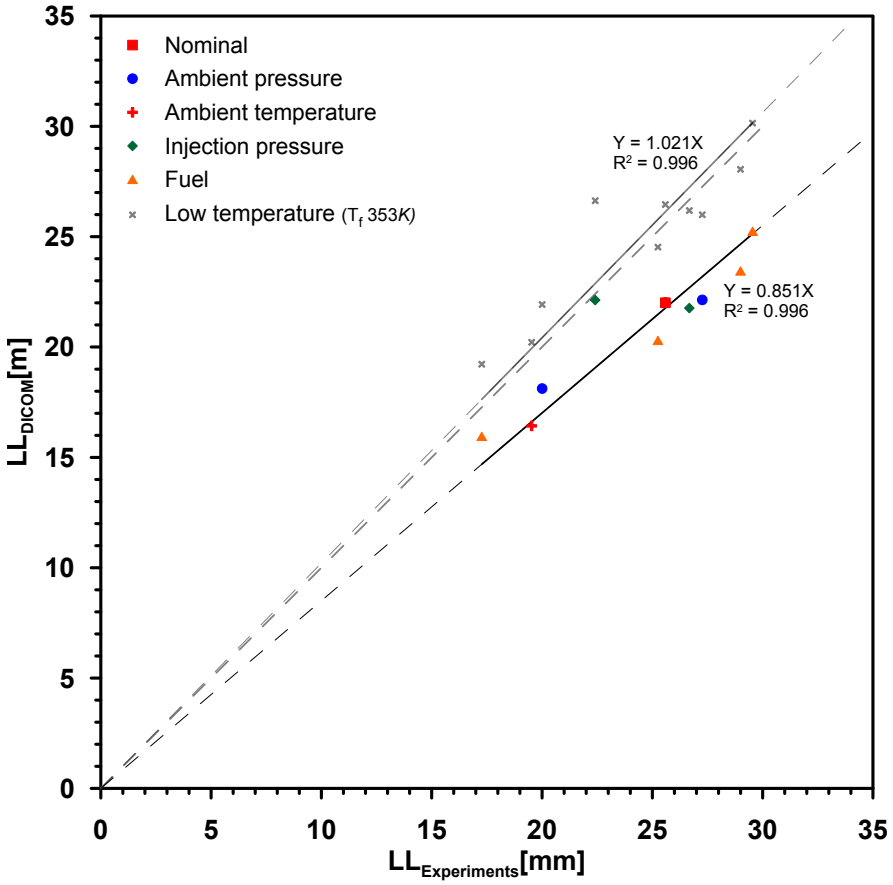

Figure 4.18. *Experimental and modelled liquid penetration for the parametric variations with binary blends.*

point and enthalpy of vaporization. From Figure 4.16 (bottom) it can be appreciated that increasing the percentage of *n*-decane, which is the most volatile component (Table 4.1), reduces the liquid length; this is in agreement to previous studies where the volatility of the fuel proved to be a determining parameter on the stabilized liquid penetration [4, 19, 20, 23, 32]. Experiments and calculations show the same trends, although the trend in the experiments is not totally monotonic with the composition, probably due to uncertainties in the experiments. However, calculations do show a well-defined trend which is relatively linear for the D0-D70 blends, while being lower for D100. Figure 4.17 (top) presents the state relationships as calculated by the 1D model for the five different blends. The linear trend for the four heavier blends and the slight offset for *n*-decane seen in the liquid length is also present here; this could mean that the *n*-hexadecane continues to be the dominant component of the blend even if its composition is less than 50 %. It can be seen that as the fuel volatility decreases, the dew curves are shifted upwards, meaning that the liquid-vapour equilibrium can exist at higher temperatures and lower fuel mass fractions, thus leading to longer liquid lengths. Additionally, Figure 4.17 (bottom) shows that the mass fraction distribution is not affected by the fuel composition, therefore the larger values of f_{evap} will be found closer to the nozzle.

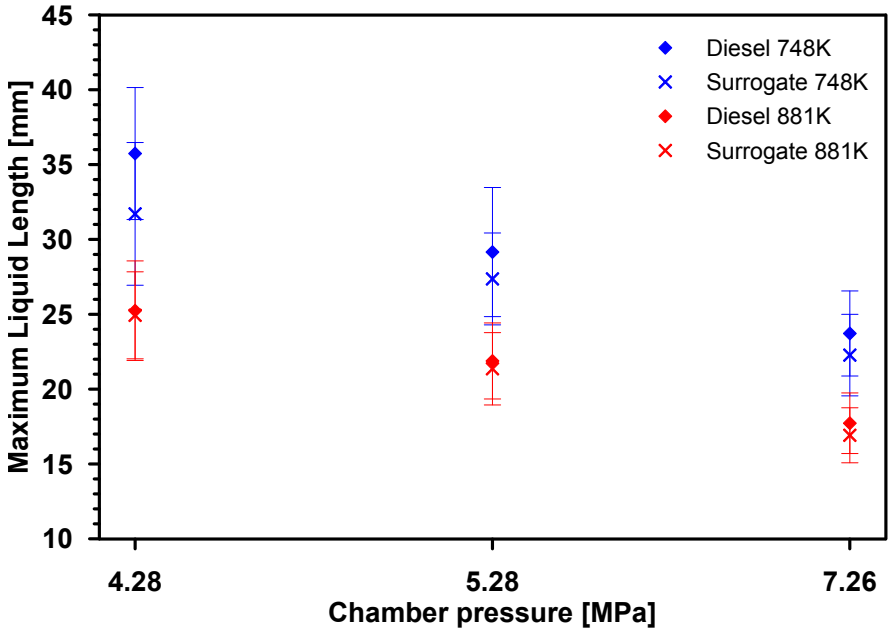

Figure 4.19. *Liquid length comparison of diesel and surrogate fuels under chamber temperature and pressure variations.*

As a final comparison using the experimental results and the simulations with the 1D model, Figure 4.18 shows the values of liquid penetration under the parametric variation presented. As was mentioned throughout this section the model under predicted the liquid length due to the uncertainty on the actual fuel temperature. Figures 4.10, 4.12, 4.14 and 4.16 also showed the values calculated with the cooling water temperature and in Figure 4.18 they do show a better fit in average; however, they over predict the liquid penetration as the assumed temperature of the cooling water is too low. This can be corroborated by looking back at Figure 4.8, where the fuel temperature was accurately estimated and the model slightly under predicted the penetration but the results were still a very good calculation for the given boundary conditions.

4.6 Studies with a diesel surrogate

The surrogate fuel was formulated to be able to predict the behaviour of a conventional diesel but with much more controlled properties and composition than a real fuel (Tables 4.1 and 4.4). The distillation curves of the conventional diesel and its surrogate are presented in Figure 4.2. As expected, the diesel showed a continuously increasing line due to its large number of components, whereas the surrogate presented well defined temperatures for a finite range of the recovered volume agreeing with the values already mentioned. For this study, the tests were performed under the same conditions as the binary blends, shown in Table 4.2.

As was studied in the previous section, the fuel properties play a negligible effect on the evolution of the vapour penetration [15, 20, 31]. While the liquid penetration was greatly affected by them, specifically by the boiling point and enthalpy of vaporization [4, 19, 20, 23, 32]; therefore, the analysis in this section is focused on the liquid length. Figure 4.19 shows the stabilized liquid penetration for both fuels under all tested conditions. The trends seen are the same as presented in the previous section, further demonstrating that an increase of air temperature will cause the fuel to evaporate faster and reduce the liquid length (red vs. blue points). And an ambient pressure rise will also cause the liquid length to decrease, but because the spray would entrain more air and the fuel would be evaporating faster. As expected, a combination of both factors will result in even shorter stabilized liquid penetration values.

Regarding the properties of the fuel, it can be appreciated that for the points of high temperature, the results obtained with the surrogate fuel are almost identical to those of the diesel. On the other hand, on the low temperature values the points are close to each other and become further apart as the pressure decreases, this is due to the combined effect of the ambient pressure and temperature, as explained in the previous paragraph. Nevertheless, as expected from the distillation curve (Figure 4.2), the narrower temperature range and the lower maximum temperature of the surrogate were indicators that the liquid length of the diesel would be expected to be longer [4, 19, 20, 23, 32].

4.6.1 *n*-Hexadecane as a diesel surrogate

An interesting result that was found, is the similarity between the liquid penetrations of the six-component surrogate and *n*-hexadecane among the different conditions tested. Figure 4.20 shows a comparison of modelled and experimental stabilized liquid lengths for *n*-hexadecane and the six-component fuel. Experimental results show that the differences between both fuel types are within experimental uncertainty. This is confirmed by the model, which shows no real difference between both fuels. To clarify this result, information from the state relationships will be used.

The evolution of the cumulative liquid mass fraction on the spray axis is shown in Figure 4.21 (top). According to these results, the fraction of all the components starts to decrease gradually when moving towards the liquid length, at approximately 27 *mm*, after which the liquid fraction of all the components is zero. Solubility effects of ambient air have not been plotted due to the small relevance under these particular conditions. Comparing the different contributions, *n*-hexadecane and *1*-methylnaphthalene are seen to last with a larger proportion in the vicinity of the liquid length. However, it is important to note that, no matter how small, there is always liquid mass of every component of the fuel throughout the liquid core. This fact is due to the presence of the heavier components that prevent the lighter ones from evaporating completely while those are still in the liquid phase. This may seem surprising, as the results from the distillation curves (Figure 4.2) show the lighter components evaporating completely after reaching their respective boiling temperatures, while the heavier ones remained in the liquid phase. However, the results of the state relationships behave in such a way due to the approach of the model, which is based on phase change equilibrium. In a similar way, Figure 4.21 (bottom) shows the evolution on the spray axis of the cumulative vapour mass fraction of all components. This value increases steadily after the spray intact length, reaching a maximum value

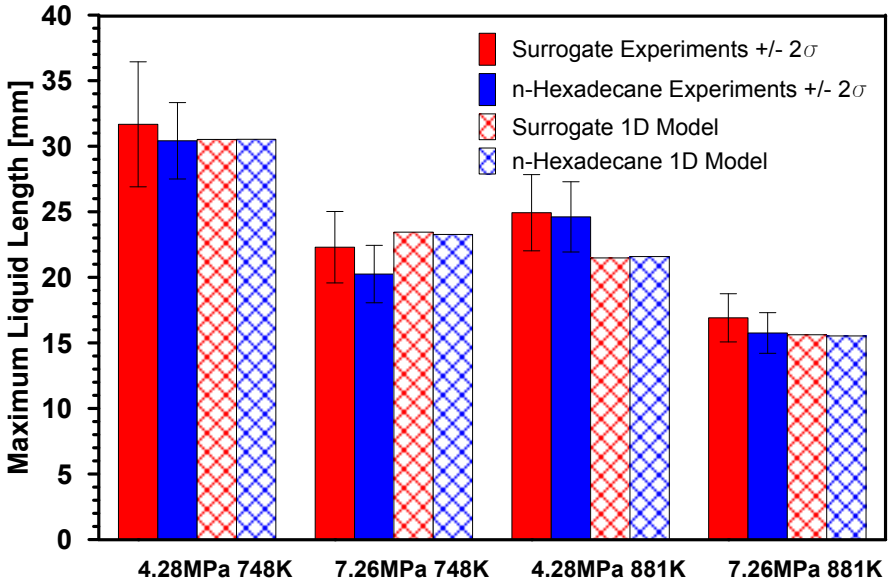

Figure 4.20. *Comparison of modelled and experimental stabilized liquid lengths for n-hexadecane and surrogate fuel.*

at the liquid length (27 mm) due to the evaporation process. On both plots the mass fraction in the center line is also shown for the multi-component fuel and n-hexadecane, this line represents the total fraction of all components in both phases. This parameter is an output of the model that is obtained by solving the conservation equation of fuel mass as presented in Section 3.4.1. It can be seen that the cumulative mass of the liquid is equal to the f_{cl} and equal to unity during the intact length because air has not been entrained and none of the fuel has evaporated. In a similar way, the total mass of vapour is equal to the total fuel mass after the liquid length, as liquid has completely evaporated and the fuel mass fraction drops with axial distance solely due to the air entrainment process. Therefore, only one phase is existing in either region; however, in the zone between IL and LL, the cumulative mass will never be equal to the f_{cl} as both phases are coexisting.

The case of n-hexadecane can be seen to follow the same pattern of the six-component fuel. The evolution of the liquid and vapour fractions of n-hexadecane is slightly higher and lower, respectively, than the total liquid and vapour fraction of the six-component fuel. Additionally, Figure 4.22 (top) shows the state relationship temperature curves for both fuels, together with the dew temperature ones. It can be seen that the L-V equilibrium curves are very similar for single- and multi-component fuels. This means that, in spite of having components lighter and heavier, which are almost as important in mass proportion as n-hexadecane (Table 4.4), the six-component fuel L-V equilibrium is highly similar to n-hexadecane alone. Furthermore, the solution of the state relationship for both fuels confirms that the thermal properties are not that different among both fuels, and therefore almost identical evaporation mass fraction and temperature values (f_{evap}, T_{evap}) are obtained. These characteristic values define the predicted liquid length, which confirms that both fuels should have similar values of liquid penetration. Additionally, Figure 4.22

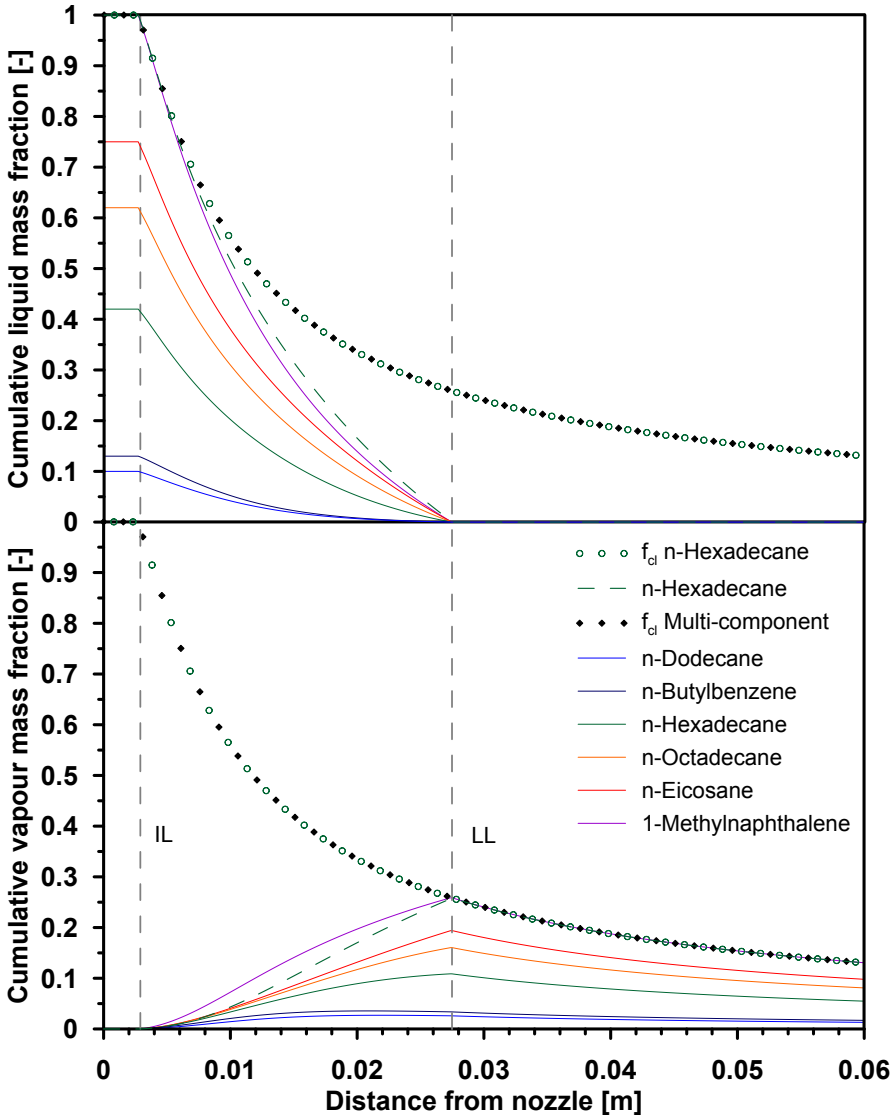

Figure 4.21. *Cumulative liquid mass fraction (top) and cumulative vapour mass fraction (bottom) for all the elements of the multi-component fuel and n-hexadecane at 5.28 MPa and 748 K.*

(bottom) shows the dew and bubble temperature curves for each components of the surrogate fuel alone with nitrogen. It can be seen that the dew curves of *n*-hexadecane and *1*-methylnaphthalene are very close to one another and are right in the middle of all the components, while the rest are separated in two pairs, *n*-butylbenzene and *n*-dodecane at the bottom and *n*-octadecane and *n*-eicosane at the top. The previous arguments, along with the fact that the components with the higher mass percentage are also *n*-hexadecane and *1*-methylnaphthalene (29 % and 25 %, respectively) further explains why the evaporation of the multi-component fuel is so similar to that of the *n*-hexadecane.

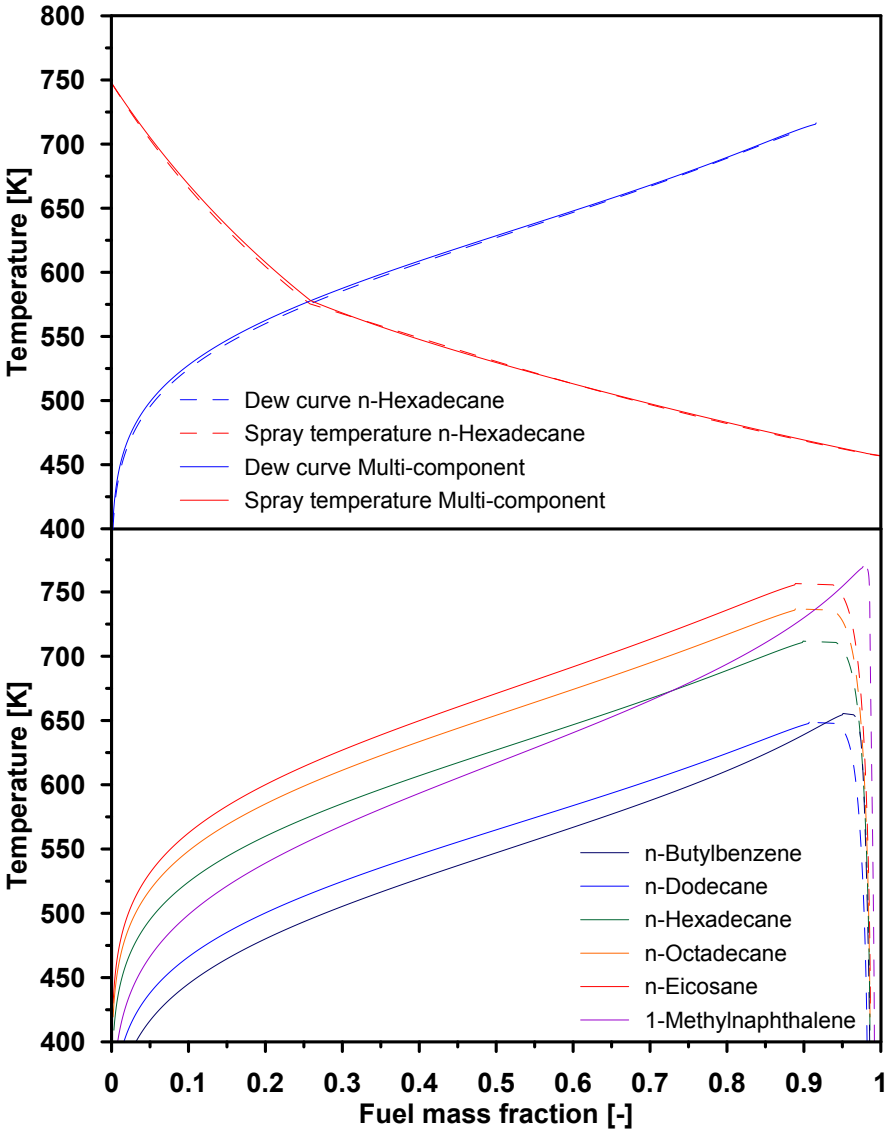

Figure 4.22. *Spray temperature and dew curves (top) for all the elements of the multi-component fuel and n-hexadecane, and dew-bubble curves for every component of the surrogate fuel alone with nitrogen; both plots at 5.28 MPa and 748 K.*

4.7 Normalization of the spray vapour penetration

The evolution of the spray penetration over time has a shape corresponding to the square root of time ($S \propto \sqrt{t}$) as was explained in Section 2.3.2. However, the values of a penetration curve are influenced by other parameters like injection pressure [13, 16, 17, 26] and ambient pressure or density [12–17] as has been analysed in the previous sections of this chapter. Therefore, and in order to be able to compare the trends, a normalization of penetration and time has been done for the binary blends and the primary reference fuels. In order to keep the plot clean and easy to read not all conditions have been plotted, so to condensate the wide range of results into a few conditions the following selection has been

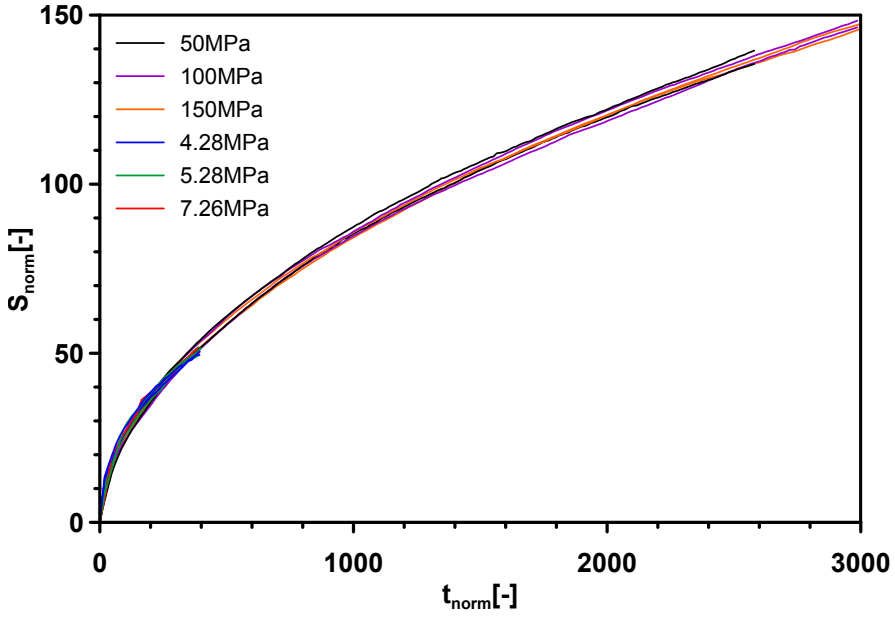

Figure 4.23. *Normalized spray penetration versus normalized time comparison for all fuels and conditions.*

made: For the primary reference fuels, an injection pressure variation is presented under the Spray A nominal conditions for both fuels. And for the binary blends, the ambient pressure variation is presented under low temperature for both pure components and the intermediate blend.

Figure 4.23 shows the normalized spray tip penetration (spray penetration divided by the equivalent diameter) versus the normalized time (time multiplied by the injection velocity divided by the equivalent diameter). Expressions for the calculation of such parameters are presented in Equations 4.1 to 4.3.

$$S_{norm} = \frac{S}{d_{eq}} \tag{4.1}$$

$$t_{norm} = \frac{t \cdot u_0}{d_{eq}} \tag{4.2}$$

$$d_{eq} = d_0 \cdot \sqrt{\frac{\rho_f}{\rho_a}} \tag{4.3}$$

where S is the spray penetration, d_{eq} is the equivalent diameter, t is the time after SoI, u_0 is the nozzle exit velocity, d_0 is the nozzle exit diameter and ρ_f and ρ_a are the fuel and ambient air densities, respectively.

It can be seen that all curves collapse onto one another. This is because the injection pressure has an effect on the spray velocity which affects the normalized time. On the other hand the air density affects the equivalent diameter, hence modifying both, the

normalized penetration and time. While the air temperature or the fuel composition have no effect on any of the aforementioned parameters, thus not affecting the shape of the curves. All this further demonstrates that the spray penetration under inert conditions is steadily growing and depends only on air density and injection pressure.

4.8 An engineering correlation for the stabilized liquid penetration

As initially explained in Section 2.3.3 and demonstrated throughout this chapter, the liquid length reaches a maximum value and remains steady for as long as the injection event continues and the contour conditions do not change. Moreover, Equation 2.6 presented a correlation for the stabilized liquid length based on only three parameters (d_{eq}, $tan(\theta/2)$ and $Y_{f,evap}$) and a constant. However the spray angle ($tan(\theta/2)$) has not been measured for the results shown and the evaporation fraction ($Y_{f,evap}$) is a value that *a priori* can not be experimentally determined, leaving the equivalent diameter (d_{eq}) as the only quantifiable value (Equation 4.3).

In order to be able to compare the stabilized liquid length for all the fuels under the different conditions, an engineering correlation based on the experimental parameters and fuel properties will be obtained in the form of Equation 4.4. Additionally and in order to further complement the experimental database for this correlation, results performed under inert conditions with the fuel and nozzle of the next chapter will also be used. The spray angle has not been included in the correlation not only because it is not a contour condition, but a consequence of them. Moreover, its effect would be indirectly included in the air density ($\tan(\theta/2) \sim \rho^{0.2}$) [4].

$$LL = k_{LL} \cdot {d_o}^a \cdot {P_{inj}}^b \cdot {T_a}^c \cdot {P_a}^d \cdot {H_{vap}}^e \tag{4.4}$$

where k_{LL} is the correlation constant, d_o is the nozzle exit diameter, P_{inj} is the injection pressure, T_a and P_a are the ambient temperature and pressure, respectively, H_{vap} is the enthalpy of vaporization of each blend tested and a, b, c, d and e are the exponents of each parameter.

With an equation of this form, the liquid length should be determined with more precision as all the parameters are measurable or available through experimental data. It is important to keep in mind that the utility of this correlation is to obtain an initial estimation of the stabilized liquid penetration from the boundary and fuel properties without the need of 1D or CFD modelling, which are in fact more accurate. Although the ambient density has been chosen for the PRFs, while for the binary blends and surrogate fuel the parametric variation has been done with the ambient pressure, this latter value has been selected for the correlation, as it is a parameter that has been measured while testing in both experimental facilities, as opposed to the density where it had to be calculated.

The exponents of the correlation are displayed in Table 4.6 and can be seen from the R^2 value of 96.7 % that the correlation is fairly accurate in predicting the liquid penetration. Moreover, Figure 4.24 shows the comparison between the predicted and experimental values for all conditions tested and it can be seen that, although there are

Table 4.6. *Exponents for the liquid length correlation.*

Parameter	k_{LL}	d_o	P_{inj}	T_a	P_a	H_{vap}	R^2
Units	$[A.U.]$	$[\mu m]$	$[MPa]$	$[K]$	$[MPa]$	$[kJ/mol]$	–
Exponent	–	a	b	c	d	e	–
Value	640.9	0.606	-0.060	-1.461	-0.662	1.123	96.7%

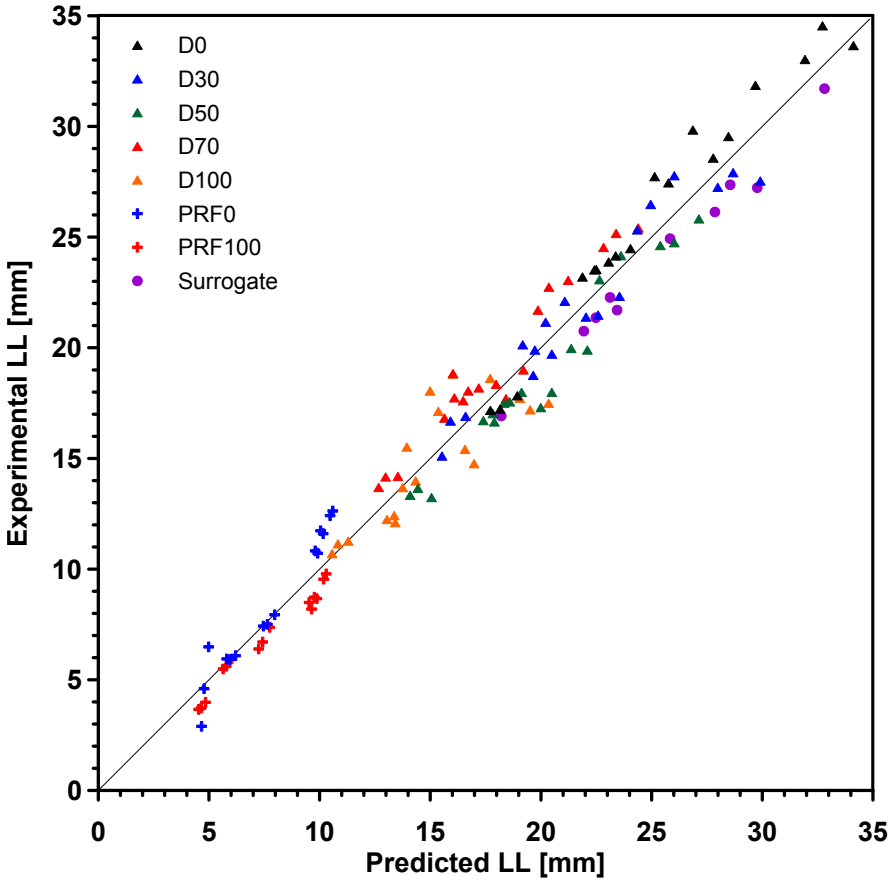

Figure 4.24. *Predicted and experimental liquid penetration comparison.*

some differences due to experimental uncertainties, the cloud of points follows a well-defined trend in the shape of a $Y = X$ straight line. The detail of all the experimental and predicted values is shown in Appendix 4.A.

As was expected and studied in the previous sections, a larger nozzle diameter (d_o) will increase the liquid penetration due to more fuel mass being injected. Moreover, the exponent of 0.606309 means that it will have a somehow asymptotic behaviour, so the larger the diameter gets, the longer the LL will be, with smaller differences. This is a bit surprising, as past correlations have found the exponent of the diameter close to

unity [33] and past results have also shown the liquid length to linearly grow with the orifice diameter [4, 23].

A similar effect but with the opposite behaviour is the vaporization enthalpy (H_{vap}), which will also causes the liquid length to grow, as was seen from the study with the binary blends. However, the exponent of 1.12273 implies that the growth will have an almost linear effect.

On a completely different trend to the aforementioned values, the ambient pressure (P_a) will reduce the liquid length but with an asymptotic trend due to the values of -0.662322, so increasing the pressure too much will have less effect on the liquid penetration. This effect is consistent with others presented in the literature [23, 33].

On the same direction, the air temperature (T_a) will have a slightly parabolic effect on the liquid length, as the value of -1.46097 implies, and has also been seen from this and previous studies [4, 11, 16, 18, 19, 21–23, 25, 33] that increasing the air temperature will cause more noticeable differences on the penetration of the liquid core.

And last, the effect of the injection pressure (P_{inj}) seems to be not very important, like the value of -0.060412 implies. As was reported earlier, some have experimented a reduction of the liquid length with increasing injection pressures [11, 17, 21, 28, 29], while others have reported no change at all [4, 16, 22, 23, 27]. Either way, a negative value close to zero (-0.060412) proves that even though the trend of the liquid length is to decrease as the injection pressure rises, the changes will be very subtle.

Previous studies [11, 33] have reported a similar correlation with values comparable to the ones presented. This means that the trends found and importance of each parameter in the final liquid length value are very reasonable. The only discrepancy is the exponent of the injection pressure, because it was positive, meaning that the LL grows as the injection pressure is increased. However, the value was also very small, which implies that its effect is minimal on the stabilized liquid penetration. As opposed to a correlation presented in a doctoral thesis [30], the choice of enthalpy instead of fuel density or boiling point, was done because is the best representative of the fuel propensity to evaporate and thus determine the liquid length. Also, since the fuels involved in this research are both, straight- and branched-chained alkanes, the latter values could have provided erroneous trends. This has already been mentioned in a previous work, where scaling the liquid length with the fuel boiling point was not accurate for some fuels [19].

4.9 Recapitulation and Synthesis

A wide range of fuels has been employed under different conditions in order to understand the effect of their physical properties in the processes of evaporation and mixing. In order to accomplish this, the parameters of vapour spray penetration and maximum liquid length have been quantified by means of the optical techniques of schlieren and Mie-scattering. Table 4.7 presents a summary of the trends found throughout the analysis, each contour condition affects the measured parameters in the following way:

- Higher injection pressures cause the tip penetration to increase as a consequence of the rise in the nozzle exit velocity. On an opposite direction, the injection pressure

Table 4.7. *Summary of trends per parameter.*

Parameter	Si	LL
$\uparrow P_{inj}$	$\uparrow$	$\approx$
$\uparrow T_a$	$\approx$	$\downarrow$
$\uparrow \rho_a/P_a$	$\downarrow$	$\downarrow$
$\uparrow H_{vap}$	$\approx$	$\uparrow$

will have a minimal effect on the liquid penetration as the increased flow rate is compensated by a similar change in evaporation rate. Nevertheless, the liquid penetration does seem to decrease slightly as the injection pressure rises. Results from the model show that the injection pressure has no effect on the temperature evolution or the LV equilibrium, therefore, the liquid length, which is consistent with past results showing no change at all and the results presented where the change is very small. On the other hand, the increased injection pressure is translated into increased velocity, so the model also shows a much faster penetration of the vapour phase.

- The air temperature has a negligible effect on the air entrainment and spray velocity, as a result the vapour penetration remains unaltered. Although, from the binary blends an small variation on the vapour penetration was reported, this was due to the change of the air density by increasing the temperature and maintaining the pressure, which was corroborated with the model. On the other hand, higher temperatures will result in shorter liquid lengths, as the increased available enthalpy in the surrounding air will cause the fuel to evaporate faster. The hotter ambient air causes the mixture temperature to rise much faster according to the model, therefore the change of phase took place at higher mass fractions, which are achieved closer to the nozzle, resulting in shorter stabilized liquid penetrations.

- An increase in the ambient pressure or density causes both the liquid and vapour penetration to be reduced due to the higher entrainment of air. On one hand, the spray angle is increasing, resulting in reduced penetration values for both phases. On the other hand, this higher entrainment will cause the fuel to evaporate sooner, thus resulting in shorter liquid lengths. Although the effect of the pressure is very clear for the model keeping all other boundary conditions constant; meaning that for a higher ambient pressure full evaporation would take place at slightly leaner local equivalence ratios, which would be found farther from the nozzle. However, since the increased air entrainment is causing a different distribution of mass fractions, the evaporation takes place closer to the nozzle, resulting in shorter liquid lengths. Nevertheless, since for the actual experiments modelled the fuel and air temperatures were different for the three cases, a clear trend is not shown as too many variables are affecting the LV equilibrium and temperature distributions on the spray.

The results proved that the fuel properties have no effect on the penetration of the vapour phase of the spray as the air entrainment remained unaltered; on the other

hand, the liquid length did show a strong dependency on the properties. Moreover, the vaporization enthalpy was demonstrated to be the most important property for evaporation of the fuel, as it indicates how much energy is needed for a component to change phases independently of other properties such as boiling temperature or liquid density. Although the experiments showed longer liquid lengths for heavier blends, a clear trend was not evident as some blends presented very similar stabilized liquid penetrations. However, the results of the model did show a monotonic evolution of the liquid length, this was further confirmed by the temperature evolution along the spray and liquid vapour equilibrium. Finally, the model also did not show any variation on the vapour penetration among the fuels tested, as the tip penetration depended only on the spray momentum and ambient density, which were kept constant for the analysis of fuel effects.

Expanding the explanation of the previous paragraph, and in order to find a single parameter that would involve the effect of the fuel properties in the stabilized liquid penetration, the enthalpy of vaporization was selected and proven to be of high importance in the correlation obtained. This is because this variable is an indicator of the energy required by the liquid in order to change to the vapour phase, regardless of the other properties. It is important to bear that this property is easy to obtain for single-component fuels or blends of them, for "real" or commercial fuels the evaporation enthalpy may not be available and would have to be experimentally determined or simply rely on the distillation curves of the blend [30].

The spray penetration presented a very marked trend with the different contour conditions, as was explained in Chapter 2. Furthermore, the normalization presented in Section 4.7 showed that all curves collapsed onto one another, proving such trend under different conditions and injection parameters.

Finally, results have confirmed that the behaviour of the surrogate fuel is highly similar to that of *n*-hexadecane. Experimental results and detailed analysis of the model information showed that both L-V equilibrium and enthalpies are similar, in spite of the fact that lighter and heavier components are present in the diesel surrogate. Additionally, being all the contour conditions the same, the correlation presented very similar values as the vaporization enthalpies of the surrogate fuel and *n*-hexadecane are close to one another (Appendix 4.A).

4.A Appendix: Experimental and correlated liquid length values

The experimental results used for the liquid length correlation and the predicted values are presented in Tables 4.8 to 4.15. The vaporization enthalpy for the binary blends and the surrogate fuel has been calculated using Equation 4.5.

$$H_{vap,mix} = \sum_{i=1}^{n} X_i \cdot H_{vap,i} \tag{4.5}$$

where $H_{vap,mix}$ is the vaporization enthalpy of the mixture and X_i and $H_{vap,i}$ are the molar fraction and vaporization enthalpy of each component.

Table 4.8. *Experimental and predicted liquid length values PRF0.*

Blend	d_o $[\mu m]$	P_{inj} $[MPa]$	T_a $[K]$	P_a $[MPa]$	H_{vap} $[kJ/mol]$	LL_{exp} $[mm]$	LL_{corr} $[mm]$
PRF0	89.4	50	800	3.66	36	12.4	10.5
PRF0	89.4	100	800	3.66	36	11.7	10.0
PRF0	89.4	150	800	3.66	36	10.8	9.8
PRF0	89.4	50	800	5.53	36	7.9	8.0
PRF0	89.4	100	800	5.53	36	7.5	7.6
PRF0	89.4	150	800	5.53	36	7.4	7.5
PRF0	89.4	50	800	11.23	36	6.5	5.0
PRF0	89.4	100	800	11.23	36	4.6	4.8
PRF0	89.4	150	800	11.23	36	2.9	4.7
PRF0	89.4	50	700	4.83	36	12.6	10.6
PRF0	89.4	100	700	4.83	36	11.6	10.2
PRF0	89.4	150	700	4.83	36	10.7	9.9
PRF0	89.4	50	900	6.23	36	6.1	6.2
PRF0	89.4	100	900	6.23	36	5.9	5.9
PRF0	89.4	150	900	6.23	36	5.9	5.8

Table 4.9. *Experimental and predicted liquid length values PRF100.*

Blend	d_o $[\mu m]$	P_{inj} $[MPa]$	T_a $[K]$	P_a $[MPa]$	H_{vap} $[kJ/mol]$	LL_{exp} $[mm]$	LL_{corr} $[mm]$
PRF100	89.4	50	800	3.66	35.1	9.5	10.2
PRF100	89.4	100	800	3.66	35.1	8.7	9.8
PRF100	89.4	150	800	3.66	35.1	8.5	9.5
PRF100	89.4	50	800	5.53	35.1	7.4	7.7
PRF100	89.4	100	800	5.53	35.1	6.7	7.4
PRF100	89.4	150	800	5.53	35.1	6.4	7.2
PRF100	89.4	50	800	11.23	35.1	4.0	4.8
PRF100	89.4	100	800	11.23	35.1	3.7	4.6
PRF100	89.4	150	800	11.23	35.1	3.7	4.5
PRF100	89.4	50	700	4.83	35.1	9.8	10.3
PRF100	89.4	100	700	4.83	35.1	8.7	9.9
PRF100	89.4	150	700	4.83	35.1	8.2	9.6
PRF100	89.4	50	900	6.23	35.1	5.9	6.0
PRF100	89.4	100	900	6.23	35.1	5.6	5.8
PRF100	89.4	150	900	6.23	35.1	5.5	5.6

Table 4.10. *Experimental and predicted liquid length values D0.*

Blend	d_o $[\mu m]$	P_{inj} $[MPa]$	T_a $[K]$	P_a $[MPa]$	H_{vap} $[kJ/mol]$	LL_{exp} $[mm]$	LL_{corr} $[mm]$
D0	140	50	748	4.28	81.3	33.7	34.1
D0	140	100	748	4.28	81.3	34.5	32.7
D0	140	150	748	4.28	81.3	33.0	31.9
D0	140	50	748	5.28	81.3	31.9	29.7
D0	140	100	748	5.28	81.3	29.5	28.5
D0	140	150	748	5.28	81.3	28.6	27.8
D0	140	50	748	7.26	81.3	24.5	24.0
D0	140	100	748	7.26	81.3	23.9	23.1
D0	140	150	748	7.26	81.3	23.5	22.5
D0	140	50	881	4.28	81.3	29.8	26.9
D0	140	100	881	4.28	81.3	27.5	25.8
D0	140	150	881	4.28	81.3	27.7	25.1
D0	140	50	881	5.28	81.3	24.2	23.4
D0	140	100	881	5.28	81.3	23.5	22.4
D0	140	150	881	5.28	81.3	23.2	21.9
D0	140	50	881	7.26	81.3	17.8	18.9
D0	140	100	881	7.26	81.3	17.2	18.2
D0	140	150	881	7.26	81.3	17.2	17.7

Table 4.11. *Experimental and predicted liquid length values D30.*

Blend	d_o $[\mu m]$	P_{inj} $[MPa]$	T_a $[K]$	P_a $[MPa]$	H_{vap} $[kJ/mol]$	LL_{exp} $[mm]$	LL_{corr} $[mm]$
D30	140	50	748	4.28	72.3	27.5	29.9
D30	140	100	748	4.28	72.3	27.9	28.7
D30	140	150	748	4.28	72.3	27.2	28.0
D30	140	50	748	5.28	72.3	27.8	26.0
D30	140	100	748	5.28	72.3	26.5	25.0
D30	140	150	748	5.28	72.3	25.3	24.4
D30	140	50	748	7.26	72.3	22.1	21.1
D30	140	100	748	7.26	72.3	21.2	20.2
D30	140	150	748	7.26	72.3	19.9	19.7
D30	140	50	881	4.28	72.3	22.3	23.5
D30	140	100	881	4.28	72.3	21.5	22.6
D30	140	150	881	4.28	72.3	21.4	22.0
D30	140	50	881	5.28	72.3	19.7	20.5
D30	140	100	881	5.28	72.3	18.8	19.7
D30	140	150	881	5.28	72.3	20.1	19.2
D30	140	50	881	7.26	72.3	16.9	16.6
D30	140	100	881	7.26	72.3	16.7	15.9
D30	140	150	881	7.26	72.3	15.1	15.5

Table 4.12. *Experimental and predicted liquid length values D50.*

Blend	d_o $[\mu m]$	P_{inj} $[MPa]$	T_a $[K]$	P_a $[MPa]$	H_{vap} $[kJ/mol]$	LL_{exp} $[mm]$	LL_{corr} $[mm]$
D50	140	50	748	4.28	66.3	25.8	27.1
D50	140	100	748	4.28	66.3	24.7	26.0
D50	140	150	748	4.28	66.3	24.6	25.4
D50	140	50	748	5.28	66.3	24.2	23.6
D50	140	100	748	5.28	66.3	23.1	22.6
D50	140	150	748	5.28	66.3	19.9	22.1
D50	140	50	748	7.26	66.3	18.0	19.1
D50	140	100	748	7.26	66.3	17.5	18.3
D50	140	150	748	7.26	66.3	16.6	17.9
D50	140	50	881	4.28	66.3	20.0	21.4
D50	140	100	881	4.28	66.3	18.0	20.5
D50	140	150	881	4.28	66.3	17.3	20.0
D50	140	50	881	5.28	66.3	17.6	18.6
D50	140	100	881	5.28	66.3	17.0	17.8
D50	140	150	881	5.28	66.3	16.7	17.4
D50	140	50	881	7.26	66.3	13.2	15.1
D50	140	100	881	7.26	66.3	13.6	14.4
D50	140	150	881	7.26	66.3	13.3	14.1

Table 4.13. *Experimental and predicted liquid length values D70.*

Blend	d_o $[\mu m]$	P_{inj} $[MPa]$	T_a $[K]$	P_a $[MPa]$	H_{vap} $[kJ/mol]$	LL_{exp} $[mm]$	LL_{corr} $[mm]$
D70	140	50	748	4.28	60.3	25.4	24.4
D70	140	100	748	4.28	60.3	25.2	23.4
D70	140	150	748	4.28	60.3	24.5	22.8
D70	140	50	748	5.28	60.3	23.0	21.2
D70	140	100	748	5.28	60.3	22.7	20.4
D70	140	150	748	5.28	60.3	21.7	19.9
D70	140	50	748	7.26	60.3	18.2	17.2
D70	140	100	748	7.26	60.3	17.6	16.5
D70	140	150	748	7.26	60.3	17.7	16.1
D70	140	50	881	4.28	60.3	19.0	19.2
D70	140	100	881	4.28	60.3	17.7	18.4
D70	140	150	881	4.28	60.3	18.3	18.0
D70	140	50	881	5.28	60.3	18.0	16.7
D70	140	100	881	5.28	60.3	18.8	16.0
D70	140	150	881	5.28	60.3	16.8	15.6
D70	140	50	881	7.26	60.3	14.2	13.5
D70	140	100	881	7.26	60.3	14.2	13.0
D70	140	150	881	7.26	60.3	13.7	12.7

Table 4.14. *Experimental and predicted liquid length values D100.*

Blend	d_o $[\mu m]$	P_{inj} $[MPa]$	T_a $[K]$	P_a $[MPa]$	H_{vap} $[kJ/mol]$	LL_{exp} $[mm]$	LL_{corr} $[mm]$
D100	140	50	748	4.28	51.3	17.5	20.3
D100	140	100	748	4.28	51.3	17.2	19.5
D100	140	150	748	4.28	51.3	17.7	19.0
D100	140	50	748	5.28	51.3	18.6	17.7
D100	140	100	748	5.28	51.3	14.8	17.0
D100	140	150	748	5.28	51.3	15.4	16.6
D100	140	50	748	7.26	51.3	14.0	14.3
D100	140	100	748	7.26	51.3	13.7	13.8
D100	140	150	748	7.26	51.3	12.1	13.4
D100	140	50	881	4.28	51.3	18.8	16.0
D100	140	100	881	4.28	51.3	17.1	15.4
D100	140	150	881	4.28	51.3	18.0	15.0
D100	140	50	881	5.28	51.3	15.5	13.9
D100	140	100	881	5.28	51.3	12.4	13.4
D100	140	150	881	5.28	51.3	12.2	13.0
D100	140	50	881	7.26	51.3	11.3	11.3
D100	140	100	881	7.26	51.3	11.1	10.8
D100	140	150	881	7.26	51.3	10.7	10.6

Table 4.15. *Experimental and predicted liquid length values surrogate fuel.*

Blend	d_o $[\mu m]$	P_{inj} $[MPa]$	T_a $[K]$	P_a $[MPa]$	H_{vap} $[kJ/mol]$	LL_{exp} $[mm]$	LL_{corr} $[mm]$
Surrogate	140	100	748	4.28	81.5	31.7	32.8
Surrogate	140	50	748	5.28	81.5	27.2	29.8
Surrogate	140	100	748	5.28	81.5	27.4	28.6
Surrogate	140	150	748	5.28	81.5	26.1	27.9
Surrogate	140	100	748	7.26	81.5	22.3	23.1
Surrogate	140	100	881	4.28	81.5	24.9	25.8
Surrogate	140	50	881	5.28	81.5	21.7	23.4
Surrogate	140	100	881	5.28	81.5	21.4	22.5
Surrogate	140	150	881	5.28	81.5	20.8	21.9
Surrogate	140	100	881	7.26	81.5	16.9	18.2

Bibliography

[1] *National Institute of Standards and Technology (NIST) Chemistry WebBook*. http://webbook.nist.gov/chemistry/.

[2] *Engine Combustion Network*. http://www.sandia.gov/ecn.

[3] Pickett L.M., Genzale C.L., Bruneaux G., Malbec L.M., Hermant L., Christiansen C. and Schramm J. "Comparison of diesel spray combustion in different high-temperature, high-pressure facilities.". *SAE International Journal of Engines*, Vol. 3(2) n^o 2010-01-2106, pp. 156–181, 2010.

[4] Siebers D.L. "Scaling liquid-phase fuel penetration in diesel sprays based on mixing-limited vaporization". *SAE Technical Paper*, n^o 1999-01-0528, 1999.

[5] Siebers D. and Higgins B. "Flame lift-off on direct-injection diesel sprays under quiescent conditions". *SAE Technical Paper*, n^o 2001-01-0530, 2001.

[6] Siebers D., Higgins B. and Pickett L. "Flame Lift-off on direct-injection diesel fuel jets: Oxygen concentration effects". *SAE Technical Paper*, n^o 2002-01-0890, 2002.

[7] Pickett L.M., Manin J., Payri R., Bardi M. and Gimeno J. "Transient rate of injection effects on spray development". *SAE Technical Paper*, n^o 2013-24-0001, 2013.

[8] Pastor J.V., García-Oliver J.M., Pastor J.M. and Vera-Tudela W. "One-dimensional diesel spray modeling of multicomponent fuels". *Atomization and Sprays*, Vol. 25(2), pp. 485–517, 2015.

[9] de la Morena J. *Estudio de la influencia de las características del flujo interno en tobera sobre el proceso de inyección diésel en campo próximo*. Doctoral Thesis, Universitat Politècnica de València, 2011.

[10] Gimeno J. *Desarrollo y aplicación de la medida del flujo de cantidad de movimiento de un chorro diesel*. Doctoral Thesis, Universitat Politècnica de València, 2008.

[11] Payri R., García-Oliver J.M., Bardi M. and Manin J. "Fuel temperature influence on diesel sprays in inert and reacting conditions". *Applied Thermal Engineering*, Vol. 35, pp. 185–195, 2012.

[12] Naber J. and Siebers D.L. "Effects of gas density and vaporization on penetration and dispersion of diesel sprays". *SAE Technical Paper*, n^o 960034, 1996.

[13] Pickett L.M., Manin J., Genzale C.L., Siebers D.L., Musculus M.P.B. and Idicheria C.A. "Relationship between diesel fuel spray vapor penetration/dispersion and local fuel mixture fraction". *SAE International Journal of Engines*, Vol. 4(1) n^o 2011-01-0686, pp. 764–799, 2011.

[14] Desantes J.M., Payri R., Salvador F.J. and Gil A. "Development and validation of a theoretical model for diesel spray penetration". *Fuel*, Vol. 85, pp. 910–917, 2006.

[15] Galle J., Defruyt S., de Maele C. Van, Rodriguez R. Piloto, Denon Q., Verliefde A. and Verhelst S. "Experimental investigation concerning the influence of fuel type and properties on the injection and atomization of liquid biofuels in an optical combustion chamber". *Biomass and Bioenergy*, Vol. 57, pp. 215–228, 2013.

[16] López J.J., García-Oliver J.M., García A. and Domenech V. "Gasoline effects on spray characteristics, mixing and auto-ignition processes in a CI engine under partially premixed combustion conditions". *Applied Thermal Engineering*, Vol. 70(1), pp. 996–1006, 2014.

[17] Manin J. *Analysis of mixing processes in liquid and vaporized diesel sprays through LIF and Rayleigh scattering measurements*. Doctoral Thesis, Universitat Politècnica de València, 2011.

[18] Espey C. and Dec J.E. "The effect of TDC temperature and density on the liquid-phase fuel penetration in a DI diesel engine". *SAE Technical Paper*, n^o 952456, 1995.

[19] Higgins B., Mueller C. and Siebers D. "Measurements of fuel effects on liquid-phase penetration in DI sprays". *SAE Technical Paper*, n^o 1999-01-0519, 1999.

[20] Kook S. and Pickett L.M. "Liquid length and vapor penetration of conventional, Fischer-Tropsch, coal-derived, and surrogate fuel sprays at high-temperature and high-pressure ambient conditions". *Fuel*, Vol. 93, pp. 539–548, 2012.

[21] Pastor J.V., García-Oliver J.M., Nerva J.G. and Giménez B. "Fuel effect on the liquid-phase penetration of an evaporating spray under transient diesel-like conditions". *Fuel*, Vol. 90(11), pp. 3369–3381, 2011.

[22] Payri. R., Gimeno J., Bardi M. and Plazas A. "Study liquid length penetration results obtained with a direct acting piezo electric injector". *Applied Energy*, Vol. 106, pp. 152–162, 2013.

[23] Siebers D.L. "Liquid-phase fuel penetration in diesel sprays". *SAE Technical Paper*, n^o 980809, 1998.

[24] Jung Y., Manin J., Skeen S. and Pickett L. "Measurement of liquid and vapour penetration of diesel sprays with a variation in spreading angle". *SAE Technical Paper*, n^o 2015-01-0946, 2015.

[25] Malbec L.M., Egúsquiza J., Bruneaux G. and Meijer M. "Characterization of a set of ECN Spray A injectors: Nozzle to nozzle variations and effect of spray characteristics". *SAE International Journal of Engines*, Vol. 6(3) n^o 2013-24-0037, pp. 1642–1660, 2013.

[26] Arrègle J., Pastor J.V. and Ruiz S. "The Influence of injection parameters on diesel spray characteristics". *SAE Technical Paper*, n^o 1999-01-0200, 1999.

[27] Wang X., Kuti Z. HuaZ. Huang.A., Zhang W. and Nishida K. "An experimental investigation on spray, ignition and combustion characteristics of biodiesels". *Proceedings of the Combustion Institute*, Vol. 33(2), pp. 2071–2077, 2011.

[28] Som S., Ramirez A.I., Longman D.E. and Aggarwal S.K. "Effect of nozzle orifice geometry on spray, combustion, and emission characteristics under diesel engine conditions". *Fuel*, Vol. 90(3), pp. 1267–1276, 2011.

[29] Kuti O.A., Zhu J., Nishida K., Wang X. and Huang Z. "Characterization of spray and combustion processes of biodiesel fuel injected by diesel engine common rail system". *Fuel*, Vol. 104, pp. 838–846, 2013.

[30] Nerva J.G. *An assessment of fuel physical and chemical properties in the combustion of a Diesel spray*. Doctoral Thesis, Universitat Politècnica de València, 2013.

[31] Payri R., García A., Domenech V., Durrett R. and Plazas A.H. "An experimental study of gasoline effects on injection rate, momentum flux and spray characteristics using a common rail diesel injection system". *Fuel*, Vol. 97, pp. 390–399, 2012.

[32] Canaan R.E., Dec J.E., Green R.M. and Daly D.T. "The influence of fuel volatility on the liquid-phase fuel penetration in a heavy-duty DI diesel engine". *SAE Technical Paper*, n^o 980510, 1998.

[33] Payri R., Salvador F.J., Gimeno J. and Zapata L.D. "Diesel nozzle geometry influence on spray liquid-phase fuel penetration in evaporative conditions". *Fuel*, Vol. 87(7), pp. 1165–1176, 2008.

Chapter 5

Fuel effects on auto-ignition and combustion

Contents

5.1 Introduction

In this fifth chapter, an experimental investigation on the ignition and combustion behaviour of fuel sprays under Spray A conditions [1] is presented with a detailed focus on fuel properties. For that purpose, *n*-heptane and *iso*-octane, which are Primary Reference Fuels (PRFs), and four intermediate blends have been tested. The choice of components was done in order to represent the transition from conventional diesel fuel to a gasoline-like one in terms of ignition behaviour, being *n*-heptane similar to a conventional diesel and *iso*-octane to a gasoline.

The main objective of this study is the experimental characterization of spray mixing, ignition and sooting processes. Therefore, parametric variations of oxygen concentration, air temperature and injection pressure have been performed for each fuel, since these have the largest effect on spray ignition behaviour. The experiments have been conducted in a constant pressure vessel, where high ambient pressure and temperature conditions typical of diesel engines can be reproduced.

In the previous chapter, similar tests were conducted to study the effect of contour conditions and fuel properties on the stabilized liquid length and spray vapour penetration. Therefore, when studying the spray penetration under reactive conditions some trends will be compared to those of Section 4.5. Additionally, for the normalization of the spray penetration presented in Section 4.7 and the correlation of stabilized liquid length presented in Section 4.8, results done with PRFs under inert conditions were also used in order to complement the experimental database.

5.2 Optical setup

Several optical techniques have been used, Schlieren was used to measure spray penetration, broadband luminosity to measure soot distribution and intensity, and OH* radical chemiluminescence to measure flame lift-off length simultaneously in the tests unde reactive conditions. Additionally, schlieren and Mie-Scattering measurements were also employed synchronously for the pure components (PRF0 & PRF100) under some inert conditions as presented in Section 5.4.

Schlieren

A schematic of the schlieren optical arrangement is shown in Figure 5.1. The spray is being illuminated from the left window and the light is captured by a CMOS camera from the opposite side. The light from a Xenon lamp is passing through a 1 mm pinhole simulating a single-point light source. The light is then reflected on a 150 mm parabolic mirror to obtain a collimated light beam. On the other side of the spray, the light is being collected by a biconvex 150 mm lens and at its focal point a 4 mm diaphragm has been positioned to produce the schlieren effect. A BG39 bandpass filter (360 nm - 580 nm) was used to minimize soot radiation effects. A Photron 12-*bit* SA-5 CMOS high-speed camera equipped with a Nikon 50 mm $f/1.8$ lens were used, image acquisition frequency was 42000 FPS (50000 FPS for inert tests) with a exposure time of 4.18 μs and a 5.26 pixel/mm ratio leading to a field of view of 97 mm.

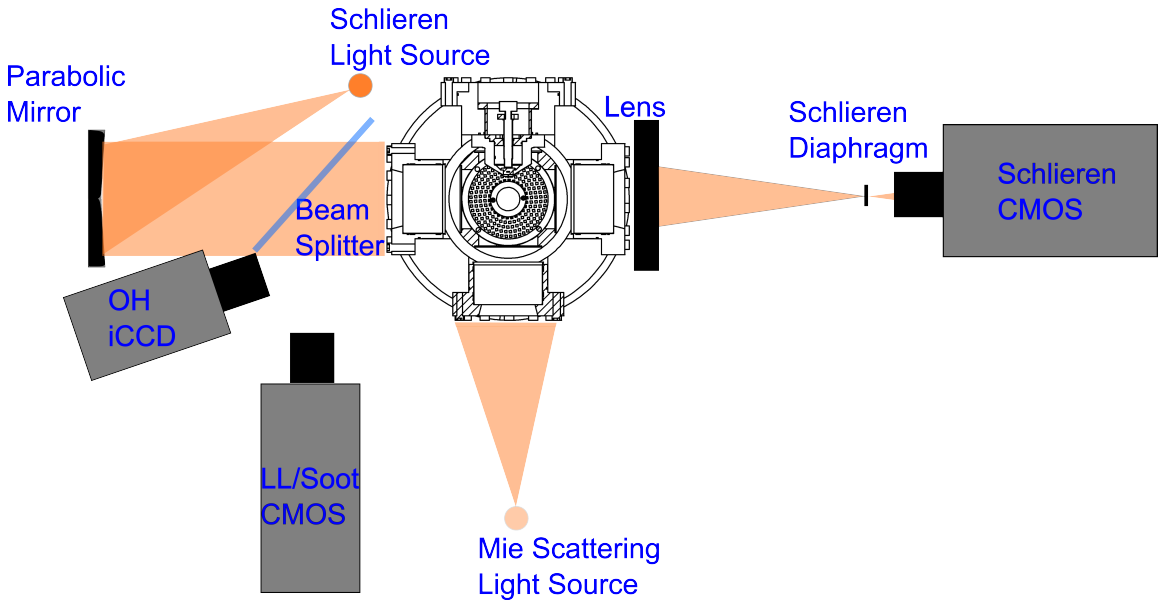

Figure 5.1. *Schematic of the experimental setup for the study of the reactive spray.*

Broadband radiation

Figure 5.1 shows a schematic of the optical arrangement for broadband radiation as well. A 50/50 beam splitter is positioned in between the parabolic mirror and the left window with a 45° angle so the camera axis could be parallel to the spray axis but the reflected image perpendicular to it. A 10-*bit* Phantom V12 CMOS high-speed camera equipped with a Zeiss 100 mm $f/2$ lens were used, image acquisition frequency was 42000 FPS with exposure times ranging from 0.4 μs to 23.29 μs and 7.23 of pixel/mm ratio leading to a field of view of 105 mm.

OH* Chemiluminescence

A schematic of the OH* chemiluminescence optical arrangement is also shown in Figure 5.1. Due to the lack of available optical accesses, the camera is placed next to the parabolic mirror and at a small angle in order to image the spray properly. A 16-*bit* Andor iStar ICCD intensified camera equipped with a 100 mm focal length $f/2$ UV objective (by Bernhard Halle Nachfolger GmbH) and a 310 nm bandpass filter (CWL = 311.50 nm, TPeak = 53.07 %, HBW = 9.60 nm) was used to eliminate any additional radiation such as the soot luminosity, the photo-cathode of the camera has an spectral range from 180 nm to 850 nm which makes it appropriate for OH* imaging. Because of the quasi-steady nature of the diffusion flame, only one image was recorded per injection event with an exposure time of 3000 μs starting 2000 μs after SOI and 5.85 of pixel/mm ratio leading to a field of view of 78 mm.

Mie-Scattering

Figure 5.1 also shows a schematic of the optical arrangement for Mie-Scattering. The camera used was the same as for the broadband radiation with the same pixel/mm ratio and field of view, but the technique was different. The spray was illuminated from the tip by a Xenon lamp (to produce the light scattering), an image acquisition frequency of 50000 FPS and exposure times of 7 μs and 10 μs.

Finally, the synchronization of all three cameras was done using an in-house made signal generator with multiple outputs. Therefore, the same signal intensity and timing goes to the Phantom, Photron and Andor cameras, as well as the injection system. Moreover and in the same way as mentioned in Section 4.2, since both high speed cameras (Photron and Phantom) used the same acquisition frequency and acquired the images simultaneously, the synchronization was further checked by comparing the first frames of an image sequence to see when the spray started to appear.

5.3 Test conditions and fuel selection

As was also mentioned in Section 1.3, to help understand the processes of auto-ignition and combustion, tests will be done using n-heptane (n-C_7H_{16}), *iso*-octane (*iso*-C_8H_{18}) and blends in-between; the detailed composition and nomenclature of each blend is presented in Table 5.1. Those two components were specifically chosen because they represent the two extremes on the octane rating scale and also have very different cetane number (Table 5.2); therefore, they are known as Primary Reference Fuels. The ignition behaviour of such fuels should be representative of a range of diesel-gasoline blends. Some of their physical properties were also presented (Table 4.1), as some tests under inert conditions were carried on to use as reference points. The aforementioned fuels have very similar vaporizing characteristics, therefore, they are appropriate to study the changes in chemical reactivity with more or less constant physical properties.

Table 5.1. *Fuel composition of binary n-heptane/iso-octane blends (in mass).*

Fuel \ Blend	PRF0	PRF20	PRF40	PRF60	PRF80	PRF100
n-heptane [%]	100	80	60	40	20	0
iso-octane [%]	0	20	40	60	80	100

The tests will be performed in the HPHT vessel described in Section 3.2.2. The so-called Spray A injector has been used (Serial No. 210675); this is a standard within the Engine Combustion Network (ECN) group [3] as was explained in Section 4.4. The injector has a single-hole nozzle with a nominal diameter of 90 μm, as opposed to the one used in Chapter 4 where it was 140 μm. Reference injection pressure, chamber density, temperature and oxygen mole fraction for Spray A are 150 MPa, 22.8 kg/m^3, 900 K and 15 $\%O_2$, respectively. The only difference of the present study compared to the standard Spray A is the use of n-heptane/*iso*-octane blends, instead of the standard n-dodecane. Nevertheless, results with n-dodecane from the ECN database will be included

Table 5.2. *Cetane and octane numbers for pure PRFs, blends and n-dodecane. Source: NIST Chemistry WebBook [2] and Engine Combustion Network [3].*

Fuel	CN [-]	ON [-]
n-$C_{12}H_{16}$	87	-40
PRF0	53	0
PRF20	45.2	20
PRF40	37.4	40
PRF60	29.6	60
PRF80	21.8	80
PRF100	14	100

Table 5.3. *Test matrix for reactive conditions. "A" indicates Spray-A standard conditions. *For PRF0, high temperature tests were performed at 1000K.*

$O_2 \backslash T$	800 K	900 K	950 K*
15 %	X	**A**	X
18 %		X	
21 %		X	

Table 5.4. *Test matrix for inert conditions (i.e. 0 %O_2). "A" indicates Spray-A standard conditions.*

$\rho \backslash T$	700 K	800 K	900 K
15.2 kg/m^3		X	
22.8 kg/m^3	X	X	**A**
45.6 kg/m^3		X	

for comparison [3, 4], as it has a higher reactivity than the fuels present in the blends. Parametric variations of temperature and oxygen concentration have been performed as shown in Table 5.3. In this case, the full range of fuels has been tested. For every ambient condition, three injection pressure values (50 MPa, 100 MPa and 150 MPa) have been used, with an injection duration of 5.4 ms. Additionally, for some experimental conditions and only for the pure components (PRF0 & PRF100) the study was also carried out under inert conditions (i.e. with no oxygen in the ambient) with the main purpose of having a reference for the comparison of spray tip evolution; the test matrix is shown in Table 5.4. For each operating condition 15 repetitions were performed

The general effect of the air temperature and injection pressure on the inert spray apply also to the the reactive jet. However, the ignition time is now introduced and it is influenced by such parameters. As opposed to the inert test matrix, where there was an air density variation, in the reactive experiments the density was held constant at the

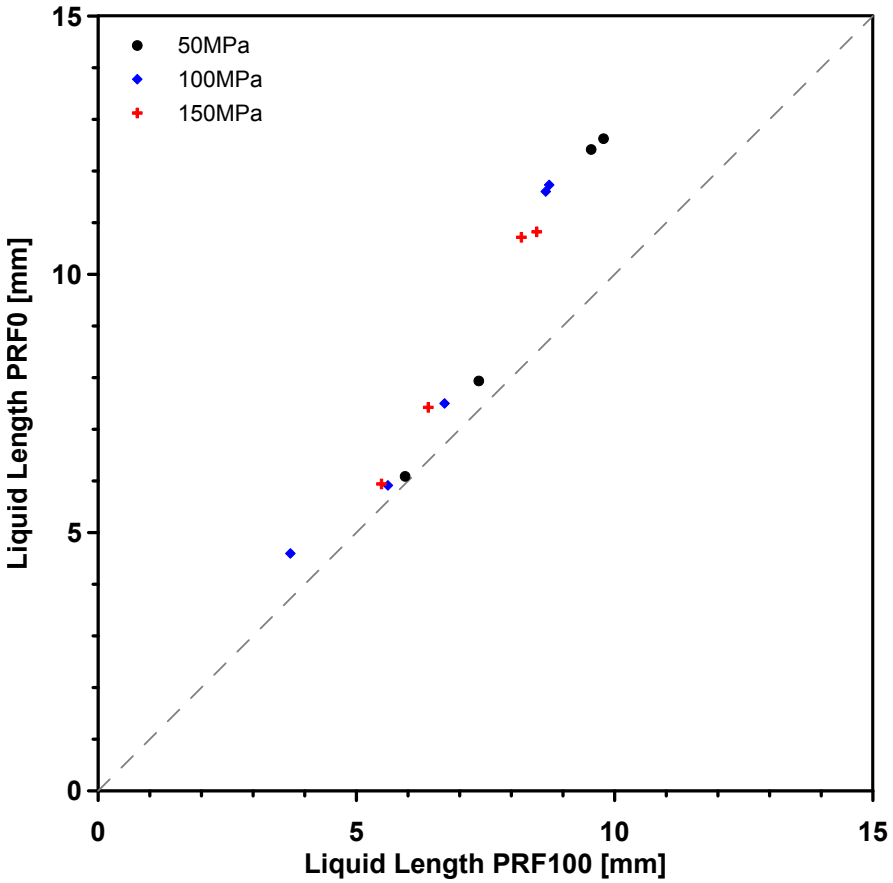

Figure 5.2. *Maximum Liquid Length comparison for iso-octane and n-heptane under all conditions.*

ECN standard value of 22.8 kg/m^3, so the effect of the oxygen concentration was studied instead (Table 5.3).

5.4 Studies under inert conditions

This section presents a small set of tests done as a complement to the reactive condition ones shown in the following sections. The main purpose of these test were to obtain reference points for comparison with the results under reactive conditions. Due to the fairly similar physical properties, only *n*-heptane and *iso*-octane were used instead of the six blends that will be presented later. Nevertheless these results showed interesting trends regarding the fuel properties, as will be explained throughout this section.

Measured liquid penetration showed trends in agreement with the literature [5–8] and with the results presented in Chapter 4, being a shorter stabilized liquid length by increasing the air temperature or air density [9, 10] and a very small variation due to changes in the injection pressure [11]. Nevertheless, a very interesting result was the difference between fuels, where the liquid length of *iso*-octane (PRF100) was shorter than

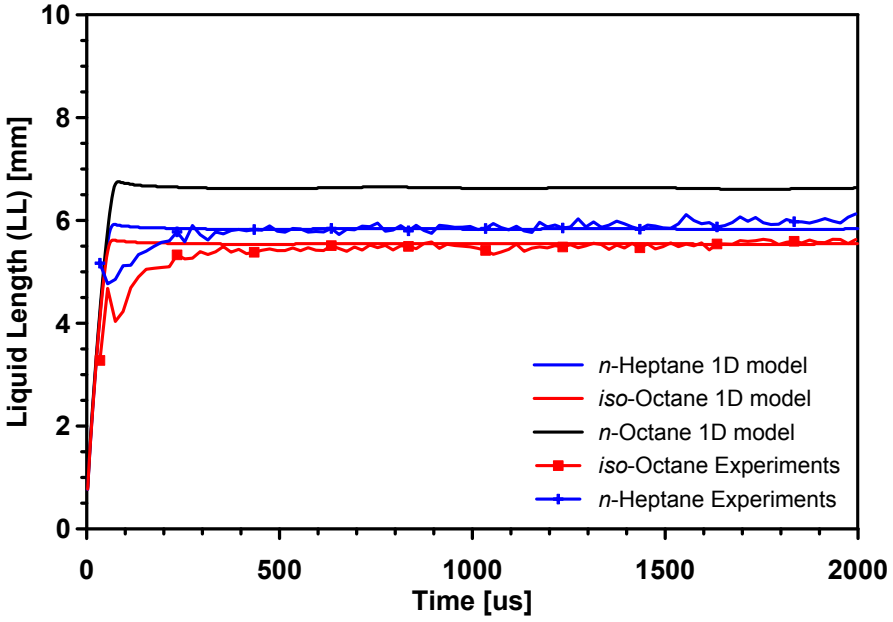

Figure 5.3. *Comparison of experimental and simulated liquid lengths for n-heptane, iso-octane and n-octane at 900 K, 22.8 kg/m^3 and 150 MPa, time after SOI.*

that of *n*-heptane (PRF0) under all ambient conditions and injection pressures. Figure 5.2 shows the relationship between the liquid penetration of both fuels.

Even though *iso*-octane is a heavier component than *n*-heptane, the penetration of the liquid core is shorter due to different molecular structures. The *n*-heptane is a straight-chain alkane, while the *iso*-octane is a branched-chained one. This difference is important, because a straight-chain alkane will have a higher boiling point than a branched-chain alkane of the same number of carbons; also, the more ramifications it has, the lower the boiling point will be. Additionally, a straight-chain alkane will have a lower boiling point (Table 4.1) due to the greater surface area in contact (greater Van der Waals forces) between adjacent molecules [12].

Figure 5.3 shows the experimental results for the baseline conditions (900 K, 22.8 kg/m^3 and 150 MPa), and the penetrations of *n*-heptane, *iso*-octane and *n*-octane as predicted by a 1D model to simulate the mixture and evaporation of diesel sprays under engine conditions. It can be seen that, as explained in the previous paragraph, the liquid length of the *n*-octane is longer than those of *n*-heptane and *iso*-octane. This differences of liquid penetration between fuels with different densities are consistent with what is shown in [13].

5.5 Analysis of the baseline case

Figure 5.4 shows a sequence of instantaneous half-images that describes the evolution of the spray penetration throughout the whole injection event for the inert and reactive

sprays; the lift-off length is also shown in all frames as a reference. For this example, Spray A nominal conditions and PRF0 fuel have been selected.

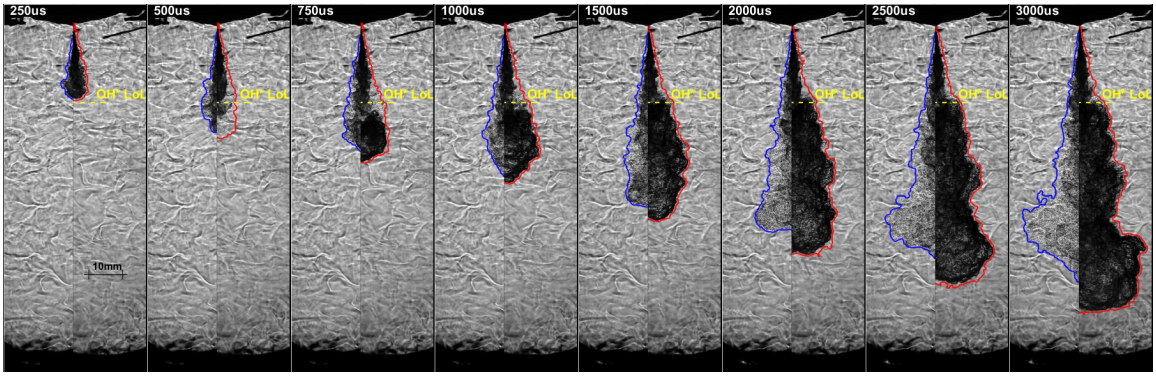

Figure 5.4. *Evolution of inert (blue) and reactive (red) spray penetration for PRF0 at 900 K, 15 %O_2 and 150 MPa, time after SOI. Lift-off length is shown in all frames as a reference.*

From the start of injection (SoI), the spray penetrates as a clearly defined shadow under both, inert and reactive, conditions. At around 500 μs after SoI, the tip of the reactive spray starts becoming transparent, this is due to the low temperature pre-reactions (also known as "cool flames") that precede the start of high temperature heat release. Such reactions result in the spray having similar refraction index as the surrounding air, and therefore becoming transparent [14, 15]. At 750 μs after SoI, the spray tip of the reactive spray becomes visible again, even though some parts are still transparent; also a widening of the spray tip is evident, this indicates that the ignition has begun as the premixed combustion of the air-fuel mixture has caused a sudden increase in the spray volume due to the lower density of the products from the high temperature reactions taking place. After 1000 μs, the whole reactive spray shadow is visible again.

The reactive spray is narrow in the non-reacting region, closer to the nozzle and up to the lift-off length (23 mm for the present operating conditions and marked as a yellow dashed lined in all frames); after this point its width increases abruptly due to combustion, which expands the original flow as explained in the previous paragraph. This difference can clearly be seen by comparing the contours of the inert and reactive sprays after the ignition has taken place and the spray is fully visible again (1500 μs). The inert spray maintains a constant angle and an steadily increasing radius all the way to the transient tip, while the reactive one is very similar to the inert up to the lift-off length, then the radius increases suddenly and the heat release region extends up to the spray tip. The combustion also causes the tip of the reactive spray to accelerate and penetrate at a faster rate than its inert counterpart, which can be observed on the images from 1500 μs onwards. This means that the subsequent spray evolution is also governed by the combustion process. The reactive spray structure remains similar until the end of injection, with the spray tip penetrating steadily with time.

Figure 5.5 shows the broadband radiation images corresponding to the same spray evolution sequence along with the reactive penetration; broadband luminosity is an indicator of the presence of soot in a reactive spray. Lift-off length is also shown in all frames as a reference. At around 1000 μs after SoI the combustion has already started, as explained in the previous paragraph; however, soot is not visible yet up to this time,

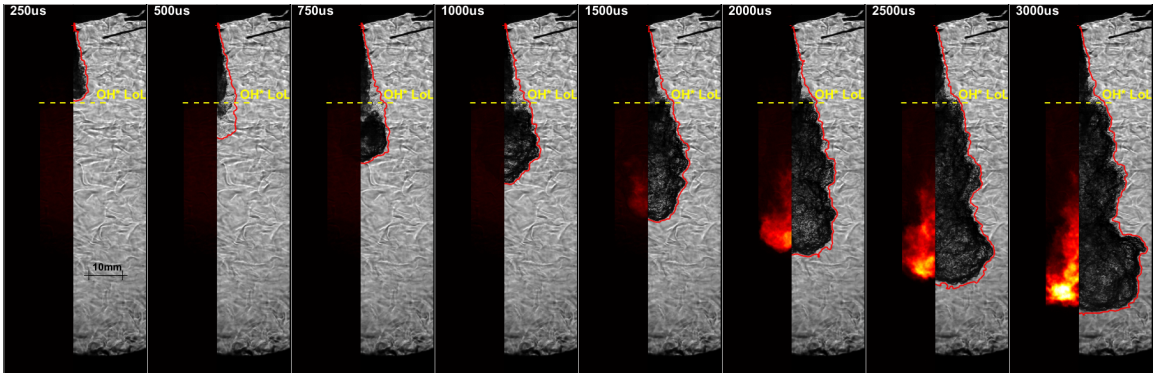

Figure 5.5. *Evolution of soot luminosity and spray penetration simultaneous images for PRF0 at 900 K, 15 %O_2 and 150 MPa, time after SOI. Lift-off length is shown in all frames as a reference.*

either due to the low flame temperature or because not enough soot is formed yet to deliver an incandescence signal high enough to be detected by the camera. After 1500 μs from the SoI, soot starts to become visible at the tip of the spray; and as the spray keeps on penetrating further, the sooting region also grows axially. Nevertheless, the soot region widths are narrower than those of the spray due to the fact that schlieren marks the whole spray region, while soot radiation mainly occurs within the stoichiometric diffusion flame front [16].

Figure 5.6 (top) also shows the spray tip penetration for inert and reactive conditions and the flame length and soot onset length measured from image sequences such as the ones shown in Figures 5.4 and 5.5. From Figure 5.6 (top), it can be seen that the measured inert and reactive penetrations are close to one another until de autoignition. Looking back at the 500 μs frame in Figure 5.4, corresponding to the cool flame period, one can already discern some differences, which become evident after the high-temperature start of combustion (SoC) at 582 μs. After this point, the reactive spray enters the acceleration phase and its tip penetration separates from the inert case. This can be appreciated in Figure 5.6 (bottom), where the ratio between the reacting and inert penetration has been plotted. This variable has a peak near the SoC, it decreases slightly and then starts increasing steadily until it reaches a maximum value and stabilizes under the given conditions. Although for this nominal case the stabilized maximum is found close to the end of the observation window, the parametric variations of ambient temperature and oxygen in the following sections will show a similar behaviour, with a first well defined acceleration followed by a second more stable period. This means that after the acceleration period of the reactive spray has ended, the ratio between reactive and inert velocities is approximately constant and no longer increasing [17, 18]. Theoretically, before the SoC the inert and reactive sprays should be identical, resulting in a ratio of exactly one. However, the experimental uncertainties and cycle-to-cycle scattering is causing this value to oscillate. And since the penetration is so small at the beginning, this "minor" oscilations ($\sim$1 mm) can create variations of up to 10 %. Therefore, in the following plots, the penetration ratios will be plotted from the start of combustion onwards and not on the whole axis range.

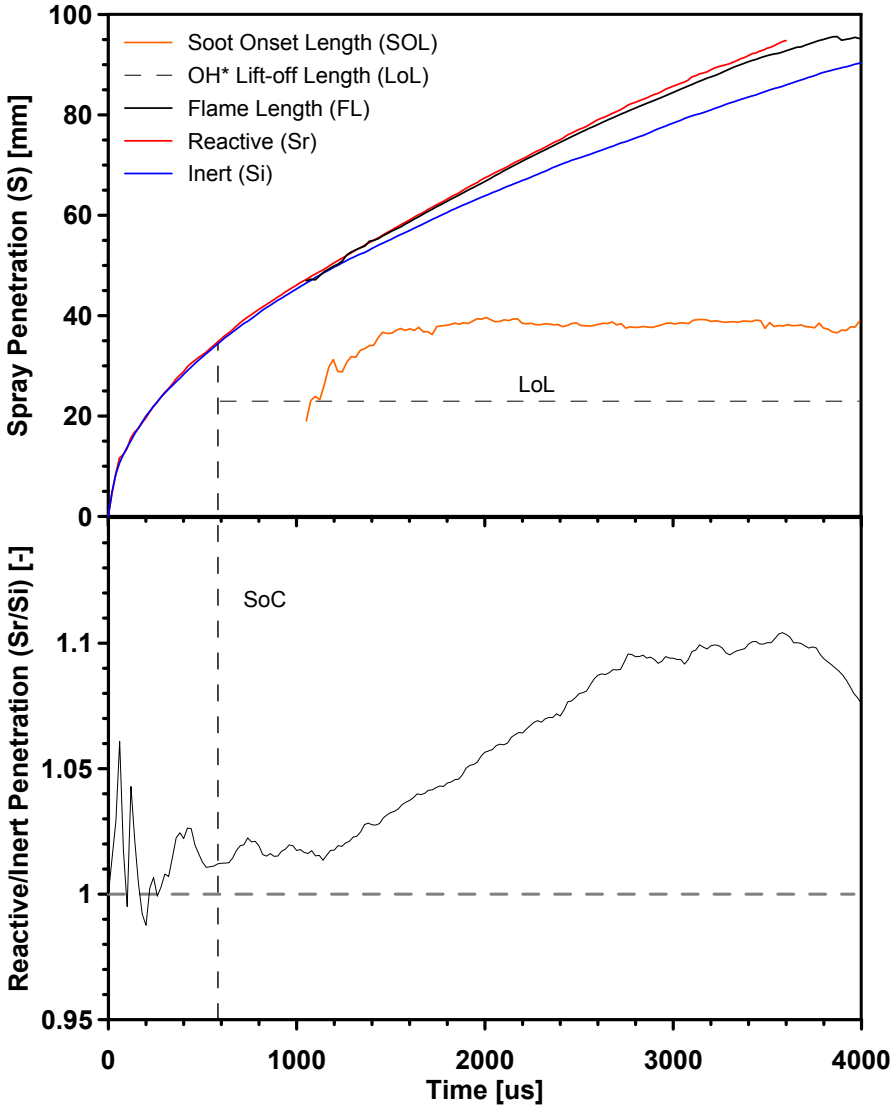

Figure 5.6. *Time resolved evolution of the inert and reactive penetrations, along with flame length, soot onset length and lift-off length (top) and reactive/inert spray penetration ratio (bottom) for PRF0 at 900 K, 15 %O_2 and 150 MPa, time after SOI.*

As explained earlier, the sooting region of the spray tends to reach a steady value after a certain time. This can be seen in Figure 5.6 (top), where the soot onset length (SOL) reaches a stabilized value fairly quickly while the flame length (FL) keeps on penetrating along with the vapour until it starts deviating to come to a steady length which under this nominal condition occurs close to 4000 μs. Although this is close to the end of the observation window, the subsequent study of this FL under oxygen concentration variation (Figure 5.23) will confirm that also for the present nominal condition stabilization occurs.

The OH* lift-off length (LoL) is also shown in Figure 5.6 (top), but unlike the other parameters shown, this value is not time resolved as explained in Section 5.2. A remark worth to be made is the difference between the LoL and SOL, while both parameters

measure the position of the flame, their spectral information is different. The broadband luminosity comes from the radiation of the soot, as opposed to the chemiluminescence of the OH* radical. The latter value is the best indicative that a combustion is taking place within a spray and is always present. The soot, on the other hand, depends strongly on the conditions and fuel used, and may not be present even if a spray is reacting.

Summarizing, the reactive spray evolution can be broken down into five well defined phase:

I Non-reacting phase: There is no combustion and the behaviour of the reactive penetration is like the inert one. In this phase the ratio between penetrations should be one. Figure 5.6 (bottom) shows some deviations due to experimental scattering.

II Auto-ignition phase: Once the ignition has taken place, the spray goes through a wide radial increase and a small axial one. This latter, causes a small peak in the penetration ratios.

III Stabilization phase: The ratios between penetrations is similar again. The duration of this phase depends greatly on the reactivity of the mixture, as shown in [17, 18].

IV Acceleration phase: The reactive penetration separates from the inert case, so the ratio also increases with time.

V Quasi-steady phase: The acceleration phase of the reacting case compared to the inert one ends, and the spray reaches a quasi-steady state where its tip speed is similar to the inert one.

This five stages are consistent to observations in previous studies [17, 18].

5.6 Spray tip penetration

The spray evolution inside the combustion chamber has been measured to quantify the rate at which the spray penetrates into the chamber. This has been done with the aim of studying the influence of the boundary conditions and fuel properties on the evaporating and reacting spray.

The air temperature has no effect at all on the non-reacting part of the spray under reactive conditions, as the density has been kept constant. This can be seen in Figure 5.7 (top) where all penetration curves overlap the inert one up to 600 μs approximately, this was already observed in the previous chapter (Section 4.5, Figure 4.12). At this point all reactive curves seem to go astray due to the pre-reactions occurring at the spray front, this is shown more clearly in Figure 5.7 (bottom) where the ratio between reactive and inert penetrations is depicted. Once the ignition has taken place, the reactive spray will continue deviating from the inert case at a higher rate during the acceleration phase; but when it reaches the quasi-steady phase, the acceleration will cease and the ratio between reactive/inert penetration will remain fairly constant. It can be seen that the higher the temperature of the air, the sooner the acceleration period will begin and, therefore, the quasi-steady period will be reached earlier as the combustion is faster. Nevertheless, it

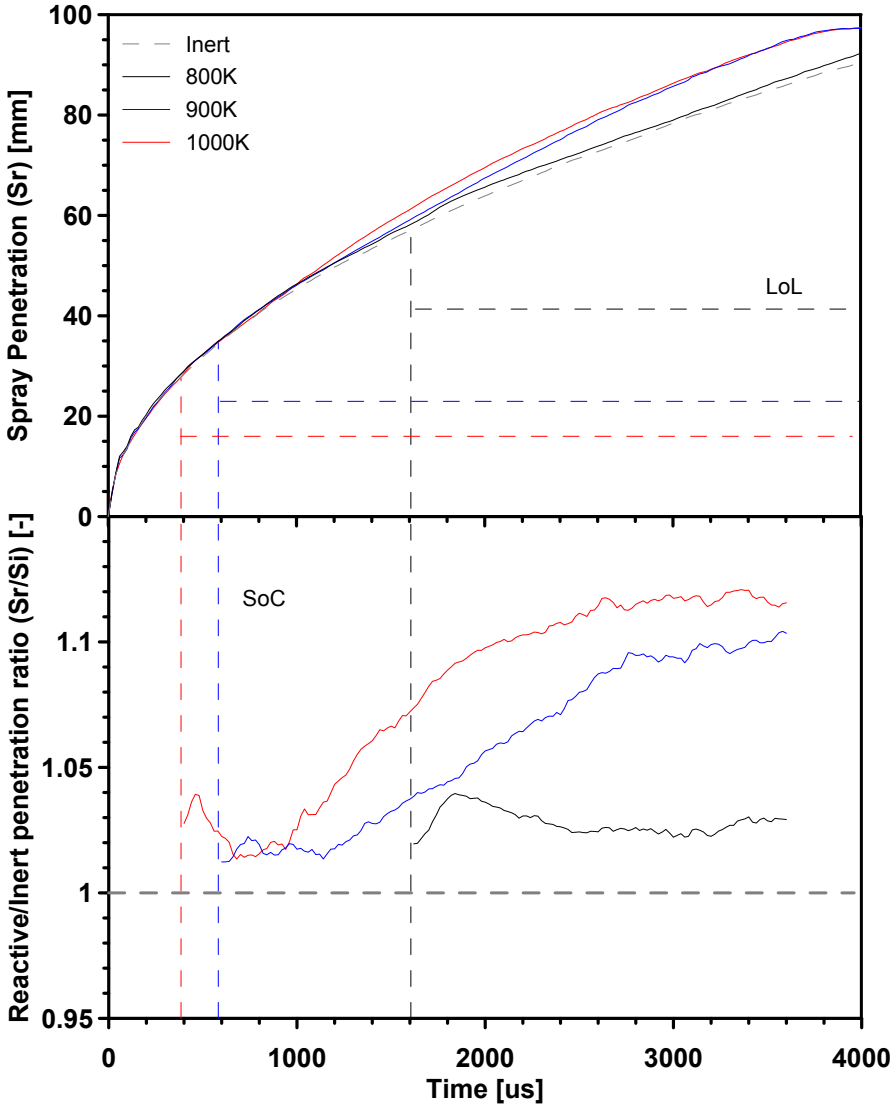

Figure 5.7. *Reactive spray penetration (top) and reactive/inert spray penetration ratio (bottom) comparison for PRF0 under air temperature variation at 15 $\%O_2$ and 150 MPa, time after SOI.*

can also be seen that for the case at 800 K, the reactive penetration remains very close to the inert reference. This leads to a non-increasing curve of the penetration ratios, where neither the acceleration nor the quasi-steady phases are clear. Like it was mentioned earlier, the temperature does not have an effect on the non-reacting region, but will affect the ignition delay time and hence the point at which the acceleration of the tip commences [17]. As mentioned in a recent study, the closer to the nozzle that a spray ignites will cause the ambient density to be lower and therefore a faster acceleration of the spray [19]. This is corroborated in Figure 5.7 (top), where the higher air temperature causes the lift-off length to be shorter for the same injection pressure, as the mixture ignites earlier and therefore closer to the nozzle.

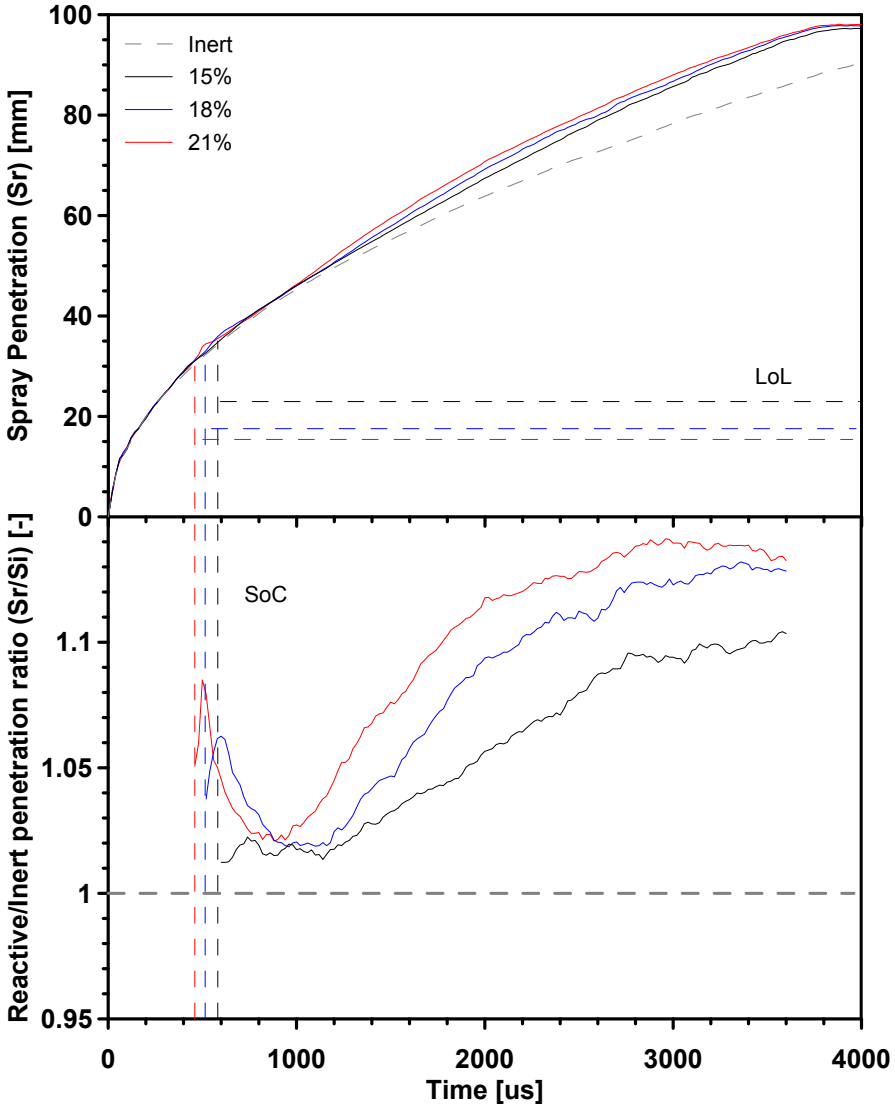

Figure 5.8. *Reactive spray penetration (top) and reactive/inert spray penetration ratio (bottom) comparison for PRF0 under oxygen concentration variation at 900 K and 150 MPa, time after SOI.*

The oxygen concentration has an effect on the start of combustion of a spray and it does not affect the mixing or evaporation of the non-reactive phase directly, but the local equivalence ratios do change. Figure 5.8 (top) shows the comparison of the penetrations under the parametric variation of oxygen. It can be seen that not only the reactivity of the air causes the curves to depart at different positions, but the more pronounced slopes as the oxygen fraction increases is an indicator of a combustion happening more aggressively. Estimations of adiabatic flame temperature for a stoichiometric mixture, initially at the adiabatic mixing conditions, indicate that it changes from around 2337 K for the lowest oxygen case to 2524 K and 2681 K for the medium and highest cases. This approximate 350 K temperature variation with oxygen is much stronger than that

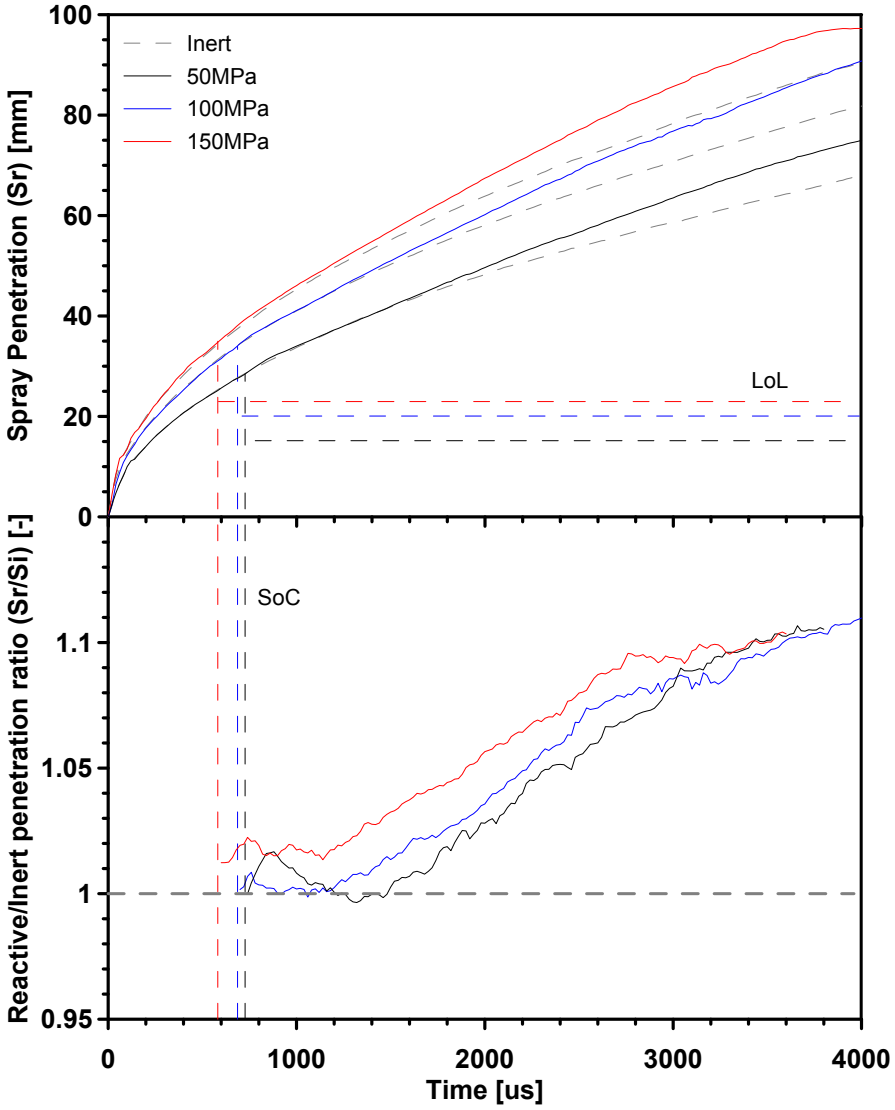

Figure 5.9. *Reactive spray penetration (top) and reactive/inert spray penetration ratio (bottom) comparison for PRF0 under injection pressure variation, at 900 K and 15 %O_2, time after SOI.*

observed when changing the ambient air temperature, 2256 K, 2337 K and 2405 K for the 800 K, 900 K and 1000 K cases shown in Figure 5.7. Therefore it can be hypothesized that the corresponding acceleration of the reacting vs. the inert case is dependent on the combustion-induced temperature variation, which will create a corresponding density drop. Figure 5.8 (bottom) allows to see that the reactivity of the mixture is causing the spray to ignite faster and accelerate more strongly, however, it is no so obvious that the three curves will converge to the same values. The cases with 21 % and 18 % oxygen seem to be getting very close around 3600 μs, but the case with 15 % is still a bit lower. Finally, Figure 5.8 (top), also shows the lift-off length to be shorter as the oxygen increases, this proves that the increased reactivity of the mixture is shifting the reactive region of the spray closer to the nozzle.

The effect of the injection pressure is not of much significance on the spray autoignition delay [20]. Figure 5.9 (top) shows that all three reactive penetrations start to deviate from its inert equivalent very close to one another, although the higher injection pressures start slightly earlier. It is interesting to see that all three injection pressures cause similar trends in the ratio between the inert and reacting penetrations during the quasi-steady period, while the two lower pressures seem to be one on top of the other. This means that the proportionality between inert and reacting penetration does not depend much on injection pressure. Figure 5.9 (bottom) shows the difference among injection pressures on the penetration ratios. Since the injection does not affect much the ignition time, the curves start to deviate very close to each other, starting with the highest pressure due to better mixing. Also, since the injection pressure does not affect the combustion process, all three curves accelerate with the same slope. And last, two of them arrive at the same stabilized value; however, it is not clear that this will always be the case, as the higher injection pressure has concluded its acceleration phase sooner but is higher than the other two. The last statement is contradictory to the results presented in a recent study [17]. This is also consistent with the lift-off length, as the higher injection pressure causes the spray to penetrate faster and therefore ignite further away from the nozzle, resulting in a longer lift-off length; this is show in Figure 5.9 (top).

The fuel effect on the reactive penetration is very similar to that of the oxygen, because it will modify the reactivity of the mixture. The fuel has very little effect on the inert spray [13, 21, 22]; and as mentioned in the previous chapter the liquid length is affected, but not the tip penetration (Section 4.5, Figure 4.16). On the other hand, the reactive penetration shows a strong dependency on the fuel due to different ignition delay times. Figure 5.10 (top) shows the penetration of the baseline case for all fuels and the inert penetration of PRF0 as a reference point. It can be seen that as the octane number increases, the penetration starts deviating form the inert case at a later time and with a less pronounced slope, and for some cases it does not seem to separate at all. This last phenomenon could be due to two factors, either the ignition takes place much later than the time window studied, or because it does not occur at all. This also explains why the stabilized penetrations for all fuels do not converge on the same values. Figure 5.10 (bottom) shows the penetration ratios for all fuels. In a similar trend to that of the oxygen, being that a more reactive mixture will cause the curve to deviate earlier and faster, not all curves start deviating although the ignition has taken place, meaning that either the quasi-steady phase is too long or the radial expansion is so large that the conservation of momentum is preventing the spray tip to accelerate. Moreover, the blends that burn do not seem to reach the same steady value. Finally, the effect of the fuel on the lift-off length can be appreciated in Figure 5.10 (top), where the lower the octane number the longer the lift-off length is. This is analogue with increasing the air temperature or the oxygen concentration, which results in a more reactive mixture and hence a shorter lift-off length.

5.7 Ignition delay time

In this subsection, the analysis of the ignition delay time under the parametric variations (Table 5.3) is presented.

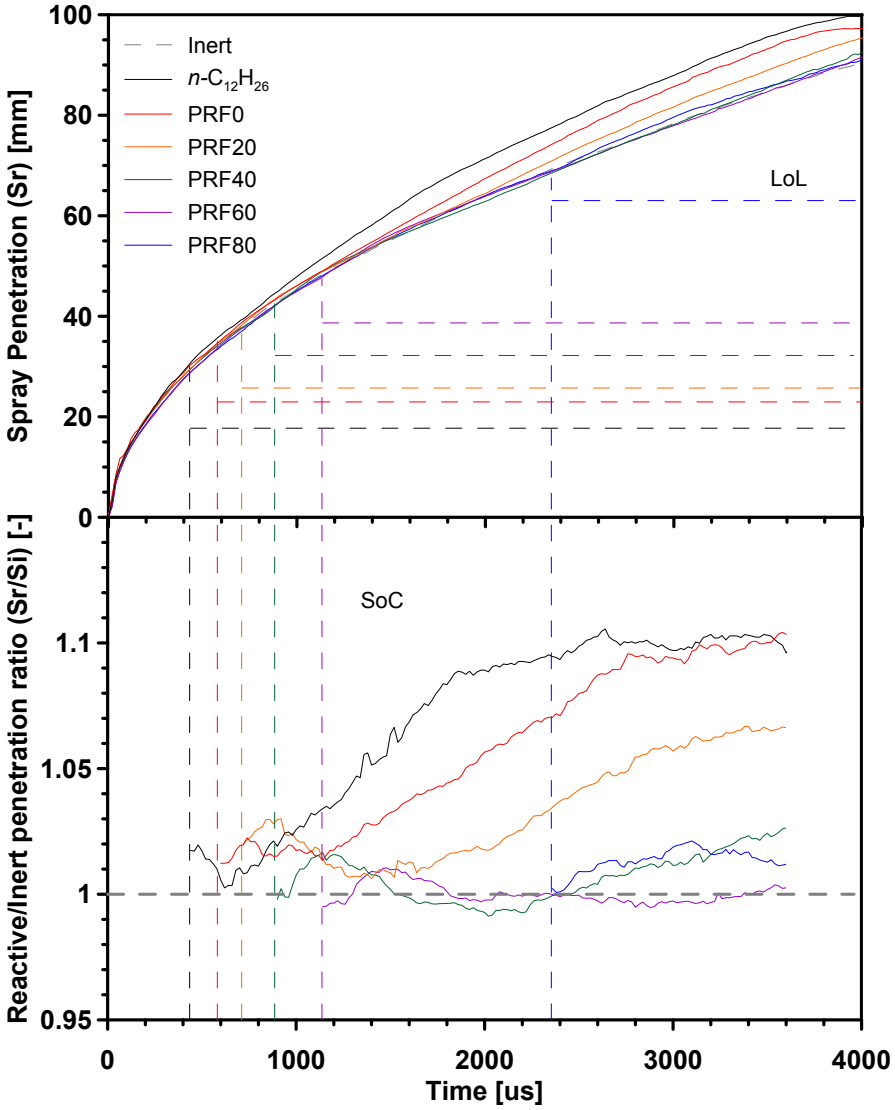

Figure 5.10. *Reactive spray penetration (top) and reactive/inert spray penetration ratio (bottom) comparison for PRF0 to PRF80 and n-dodecane, at 900 K, 15 %O_2 and 150 MPa, time after SOI. n-dodecane data (ON = −40) from [3, 4]. PRF100 is not shown as it does not react under the given conditions.*

The injection pressure appears to have very little effect on the ignition delay [5, 23, 24], this is presented in Figure 5.11, where the effect of the injection pressure on the ignition delay for the different blends is shown. It can be seen that, even though there is a difference among the injection pressures, being the 150 MPa case the shortest time due to a slight improvement of the fuel-air mixing [25], the difference in pressure causes a small effect regardless the fuel used. Although, the ignition delay for PRF60 at 50 MPa is missing, the trend seems to be the same as for PRF0-20-40. However, the fact that for PRF80-100 the trend is reversed is still uncertain. It could have to do with the combination of fuel reactivity and mixing rate controlled by the injection pressure. Where using a fuel with

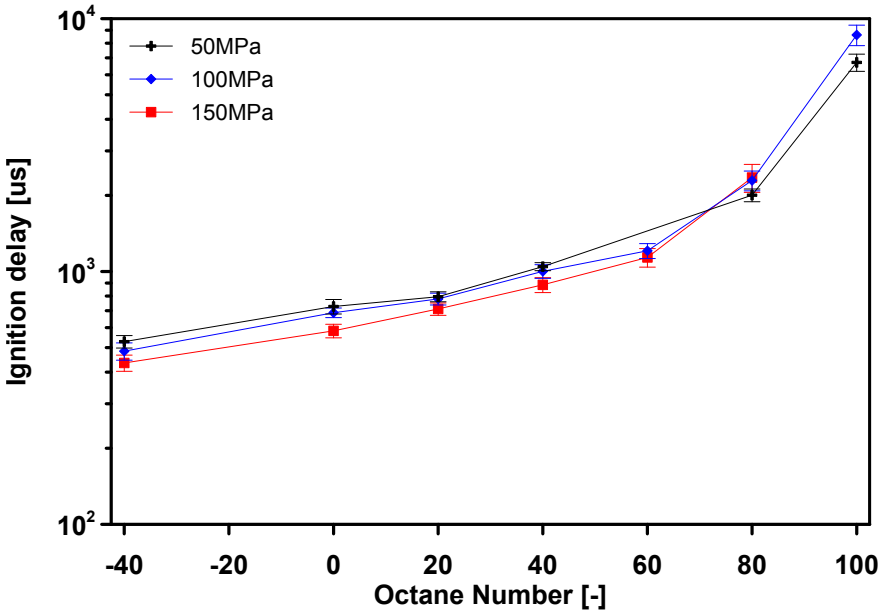

Figure 5.11. *Ignition delay comparison for all blends under injection pressure variation, at 900 K and 15 %O_2, time after SOI. n-dodecane data ($ON = -40$) from [3, 4].*

high reactivity, an increasing injection pressure will cause the mixing rate to improve and the fuel will burn earlier. On the opposite side, using a fuel with low reactivity with increasing mixing rates will make the mixture harder to burn. This was demonstrated in a previous Ph.D. thesis [26], increasing the injection pressure can affect negatively the ignition, leading to lower ignition probabilities, larger ignition delay times and lower flame intensities.

On the other hand, the oxygen concentration appears to have a stronger effect on the start of combustion. This is because while the same amount of air is being entrained, more oxygen is available, leading to a more reactive air-fuel mixture, so the ignition can happen sooner [10, 27]. Figure 5.12 shows the effect of varying the oxygen concentration for each blend tested. Altering the fuel reactivity and the oxygen concentration at the same time has a combined effect, where the higher octane number causes the differences in ignition delay to be greater among oxygen concentrations. As mentioned previously, this combined effect is related to the reactivity of the air-fuel mixture and it seems to have a non-linear trend.

Air temperature has the strongest effect on the ignition delay than any of the other parameters [10, 28–32]. Although oxygen concentration seems to have a somewhat linear effect (for a given fuel) on the ignition delay time, the effect of the air temperature is almost exponential. Figure 5.13 shows an Arrhenius plot of the effect of the air temperature on the ignition delay time. Missing points for the low temperature cases for PRF60 to PRF100, as well as the intermediate temperature for PRF100 are due to combustion not occurring within the investigated conditions. This is due to the fact that the temperature plays a very important role in the start of combustion, because even though there may be enough air to oxidize the fuel, if the temperature is too low, the combustion will never

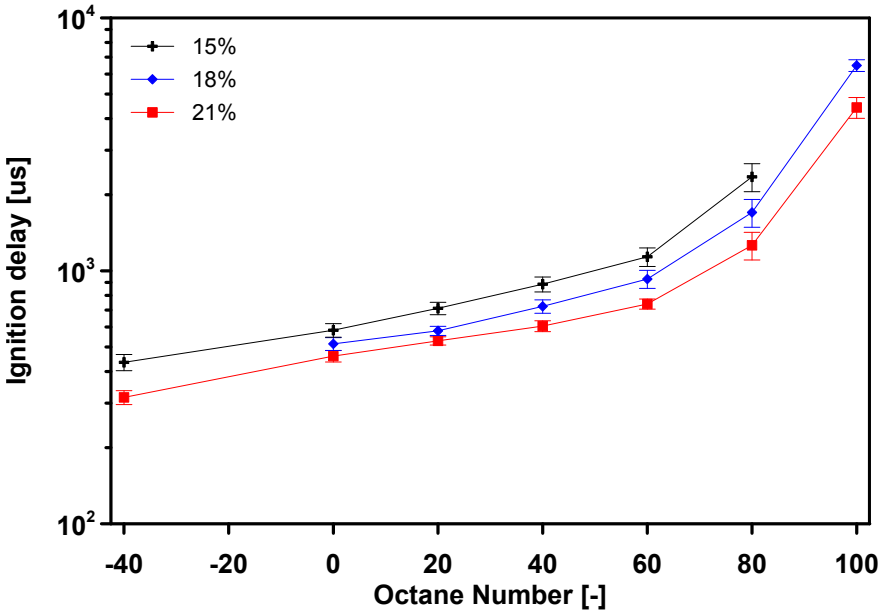

Figure 5.12. *Ignition delay comparison for all blends under oxygen concentration variation, at 900 K and 150 MPa, time after SOI. n-dodecane data (ON = −40) from [3, 4].*

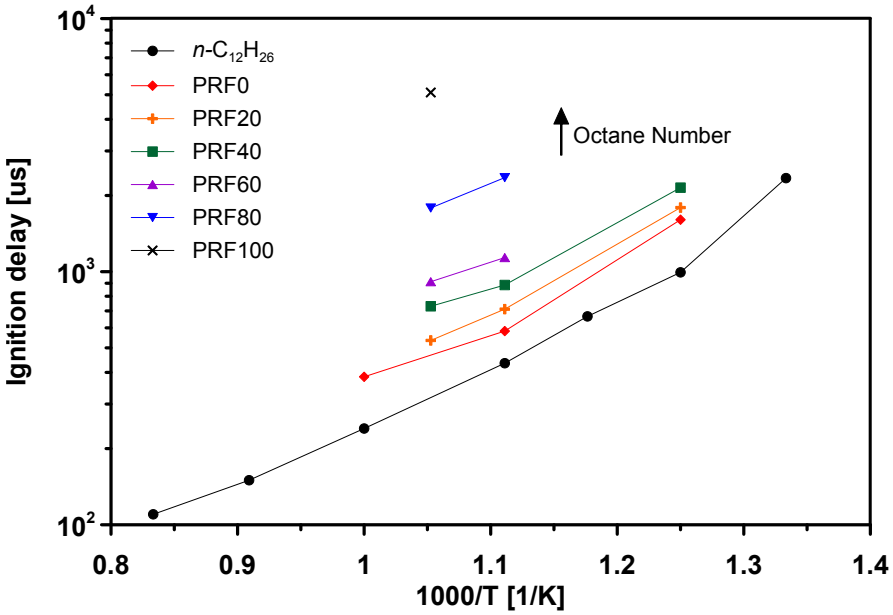

Figure 5.13. *Ignition delay comparison for all blends under air temperature variation, at 15 %O_2 and 150 MPa, time after SOI. n-dodecane data (ON = −40) from [3, 4].*

take place [33]. It can be seen that the drop from 1000 K to 900 K (1/T from 1 to 1.11) seems smaller (around 200 μs for PRF0) compared to the effect of reducing the temperature from 900 K to 800 K (1/T from 1.11 to 1.25) (approx. 1000 μs for PRF0). The explanation for this non-linear effect is that at low temperatures the rate of chemical reaction is slow enough to ignore the time required to form the ignitable mixture, while at high temperatures the ignition delay chemistry progresses very fast, and the delay is mainly dominated by the physical processes [31]. Additionally, it can be seen that the difference in ignition delay between 15 % and 18 % of oxygen is similar to changing the temperature from 900 K to 950 K for PRF20.

The effect of the fuel properties can also be seen in Figures 5.11 to 5.13 and specially on the latter. The ignition delay grows when the octane number increases, in fact, for some PRF100 cases the spray does not ignite at all, while for n-dodecane most cases present ignition and it happens earlier than any other blend. This was expected, as the cetane number of the blend increases as the composition of n-heptane grows, and shorter ignition delay times have been found to correspond to higher cetane numbers [24, 30, 34–39]. This can be seen clearly in Figure 5.13, where the differences in ignition delay times grow dramatically as the octane number does. Additionally, the molecular structure of the fuel plays a significant role on the autoignition as it did on the liquid length. However, in this case straight chain alkanes (n-heptane) improve the ignition quality, while isoalkanes (*iso*-octane) tend to degrade it [36].

5.8 Flame lift-off length

As was also seen during the study of the penetration, the boundary conditions not only affected the time at which the reactive curve started deviating from the inert one (ignition delay time), but also the axial position at which this happened, which is known as the flame lift-off length and will be analyzed in the present section. This phenomenon occurs as the fuel exit velocity causes the flame to *lift-off* and stabilize downstream within the jet [40]; nevertheless, there are also other theories regarding its stabilization. One of them says that shorter lift-off lengths are related to smaller ignition delay times [28]. Another has observed the development of small ignition kernels at the flame base which could connect the stabilization of the lift-off length with local ignition processes, thus suggesting that the lift-off stabilization is not by flame propagation [30]. Finally, a very interesting study forced the ignition to take place earlier by using a laser pulse upstream the lift-off length. This resulted in a stabilized lift-off length close to the laser ignition spot during a relatively long period of time ($\sim$10 ms) before returning to its "original" place [41]; this latter study also suggests a relationship between the lift-off length and the autoignition.

The effect of the injection pressure on the lift-off length can be seen in Figure 5.14. As opposed to the effect it caused on the ignition delay, where it was very little, the lift-off length seems to be much more affected by the injection pressure. This is due to the increased velocity of the spray, causing the flame to stabilize further away from the nozzle tip, and therefore having a longer lift-off distance [4, 5, 24, 27, 40, 42–44]. However, although higher velocities led to longer lift-off lengths, if the velocity is too high and it exceeds a critical value, the flame will be completely blown out [40].

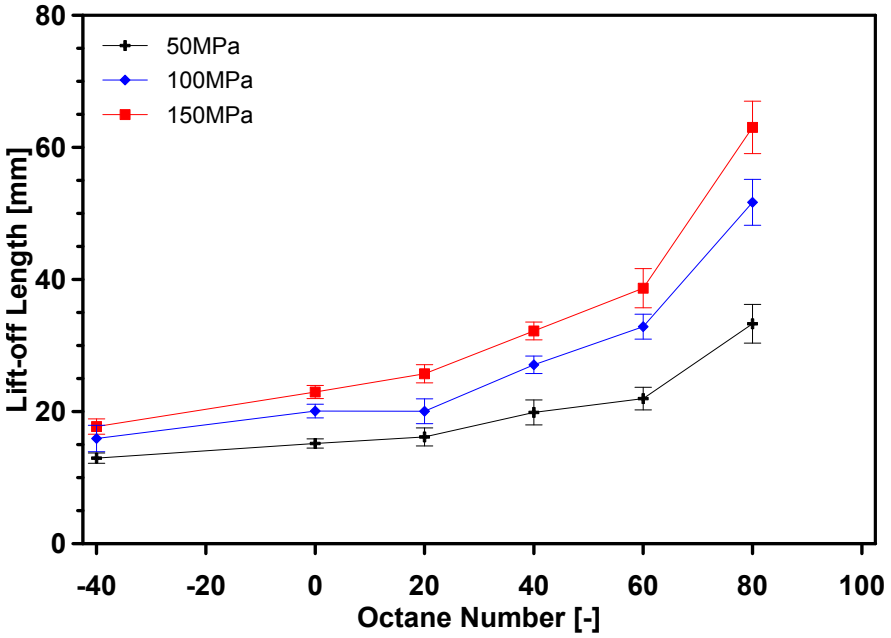

Figure 5.14. *Lift-off length comparison for all blends under injection pressure variation, at 900 K and 15 %O_2. n-dodecane data ($ON = -40$) from [3, 4].*

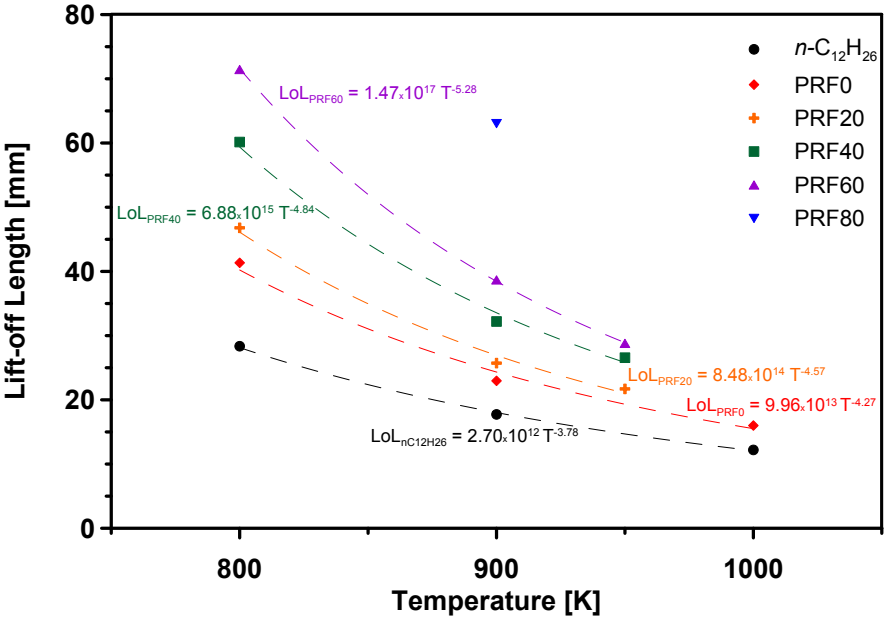

Figure 5.15. *Lift-off length comparison for all blends under air temperature variation, at 15%O_2 and 150MPa. n-dodecane data ($ON = -40$) from [3, 4].*

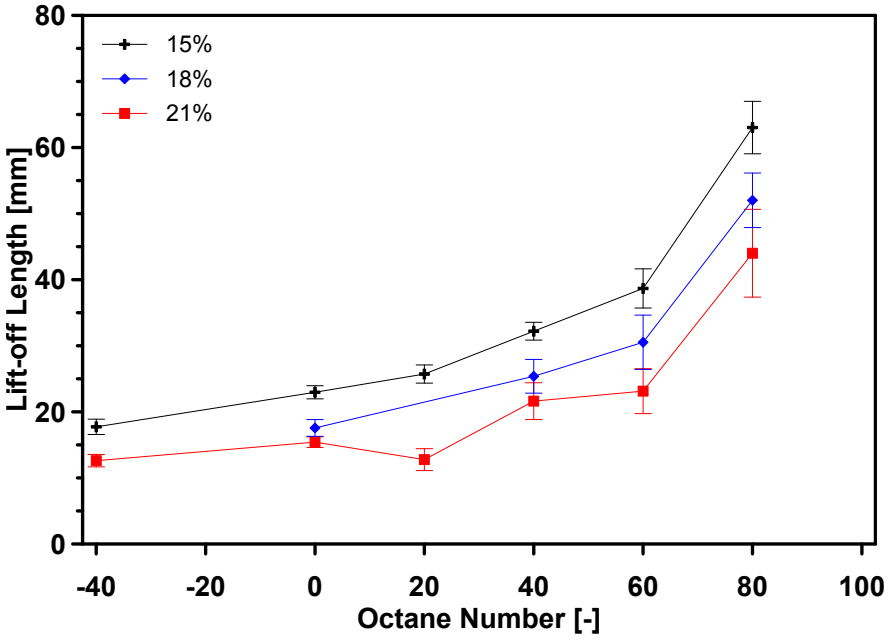

Figure 5.16. *Lift-off length comparison for all blends under oxygen concentration variation, at 900 K and 150 MPa. n-dodecane data (ON = −40) from [3, 4].*

The lift-off length seems to be dramatically affected by changes in the air temperature, as was also mentioned in [5]. This is very clear to see in Figure 5.15, where the lower the temperature the longer the lift-off length is going to be because of the temperature effects on the laminar flame speed and the thermal diffusivity [4, 10, 28, 43–45]. A statistical regression fitting of the results shown in Figure 5.15 indicates that the temperature dependence of the lift-off length occurs with an exponent of −3.78, −4.27, −4.57, −4.84 and −5.28 for *n*-$C_{12}H_{26}$ and PRF0 to PRF60, which indicates that the lower the fuel reactivity, the more important the temperature dependence is. The fitted lines are also presented in Figure 5.15 as dashed lines along with the expressions. Compared to a reference work [30] with a temperature dependence exponent of −3.74, the temperature sensitivity is higher for all cases in the present study. However, the present results are coherent with previous results obtained in the same experimental facility (−5.0 to −5.4 as reported in [20]).

The oxygen concentration causes an similar effect to that of the air temperature [10]. Figure 5.16 shows that the higher the oxygen concentration, the shorter the lift-off length is due to the higher reactivity of the mixture causing the spray to burn earlier (shorter ignition delay) and since the velocity of the spray is not altered (same injection pressure), this happens closer to the injector [4, 45].

Figures 5.14 to 5.16 also show the effect of the fuel composition, and it can be seen that it has a strong effect on the lift-off length [46]. Like it was mentioned earlier, the percentage of *iso*-octane on the blend reduces the reactivity of the mixture tremendously, especially when the composition is over 50 %. Moreover, the results shown only present values up to PRF80, as the cases for PRF100 did not ignite and the ones that burned

did not register any values due to ignition delay times longer than the camera exposure window, so greater stabilization times of the lift-off length were not able to be registered. Additionally, some conditions were not favourable for the ignition of PRF100 such as 800 K and 900 K at 15 % oxygen. In a similar way as the effect on the ignition delay, the variations of the lift-off length by changing the oxygen concentration between 15 % and 18 % are similar to changing the temperature from 900 K to 950 K.

The previous results also help at the understanding of lift-off stabilization mechanism. Although originally thought as based upon a flame front velocity balance, extensive evidences starting from [30] indicate that lift-off stabilizes based upon the autoignition of fuel elements being injected. In this particular case, the fuel composition has been swept from *n*-heptane to *iso*-octane, both of which have very similar laminar flame speeds [47] but highly different autoignition properties. From a point of view of flame stabilization by velocity equilibrium, both fuels should produce the same lift-off length. However, experimental results presented here confirm that both lift-off and autoignition delay change with operating conditions in a highly similar fashion, which indicates the leading role of autoignition on lift-off stabilization.

5.8.1 Relationship between lift-off length and ignition delay time

Lift-off length trends have usually been compared to those of auto-ignition delay [10, 28, 30, 41, 48]. As explained in Section 2.4, the second stage ignition or premixed combustion corresponds to the high rise of the heat release rate and the time that happens since the fuel has been injected to this point is known as the ignition delay time. Moreover, after the ignition has finished the flame of the spray tends to stabilize at a quasi-steady distance from the nozzle, which is known as lift-off length. In this sense, long lift-off lengths would be related to lower reactivity, in other words, larger ignition delay times. When comparing parametric results with temperature and oxygen concentration, relative trends are similar, meaning a nearly proportional effect of oxygen concentration and a highly non-linear trend for temperature. Similar experiments [30, 44, 49, 50] have pointed at the relationship between lift-off length and ignition delay times for diesel sprays. The oxygen concentration seemed to affect the ignition delay and lift-off length in the same way. The higher reactivity of the mixture caused by the increased amount of oxygen available for combustion made the spray reach the stoichiometric ratio much sooner, and because air-entrainment and spray velocity were not affected by this parameter, the ignition took place closer to the nozzle. In a similar way to the effect of the oxygen concentration, the air temperature caused both, the lift-off length and ignition delay time, to be shortened as the temperature was increased. This was similar to the oxygen case but with a more obvious trend, the hotter the air meant that the mixture was more reactive, and since the spray velocity was not affected by the air temperature, if the spray started burning earlier, it burned closer to the injector tip [30].

Figure 5.17 (top) shows that such a relationship exists for the present study as well. Using a less reactive fuel for fixed ambient conditions results in an increase in both ignition delay time and lift-off length. As was seen for the oxygen and temperature sweeps, the effect of the parameter can be reduced to "simply" the reactivity of the mixture. In this

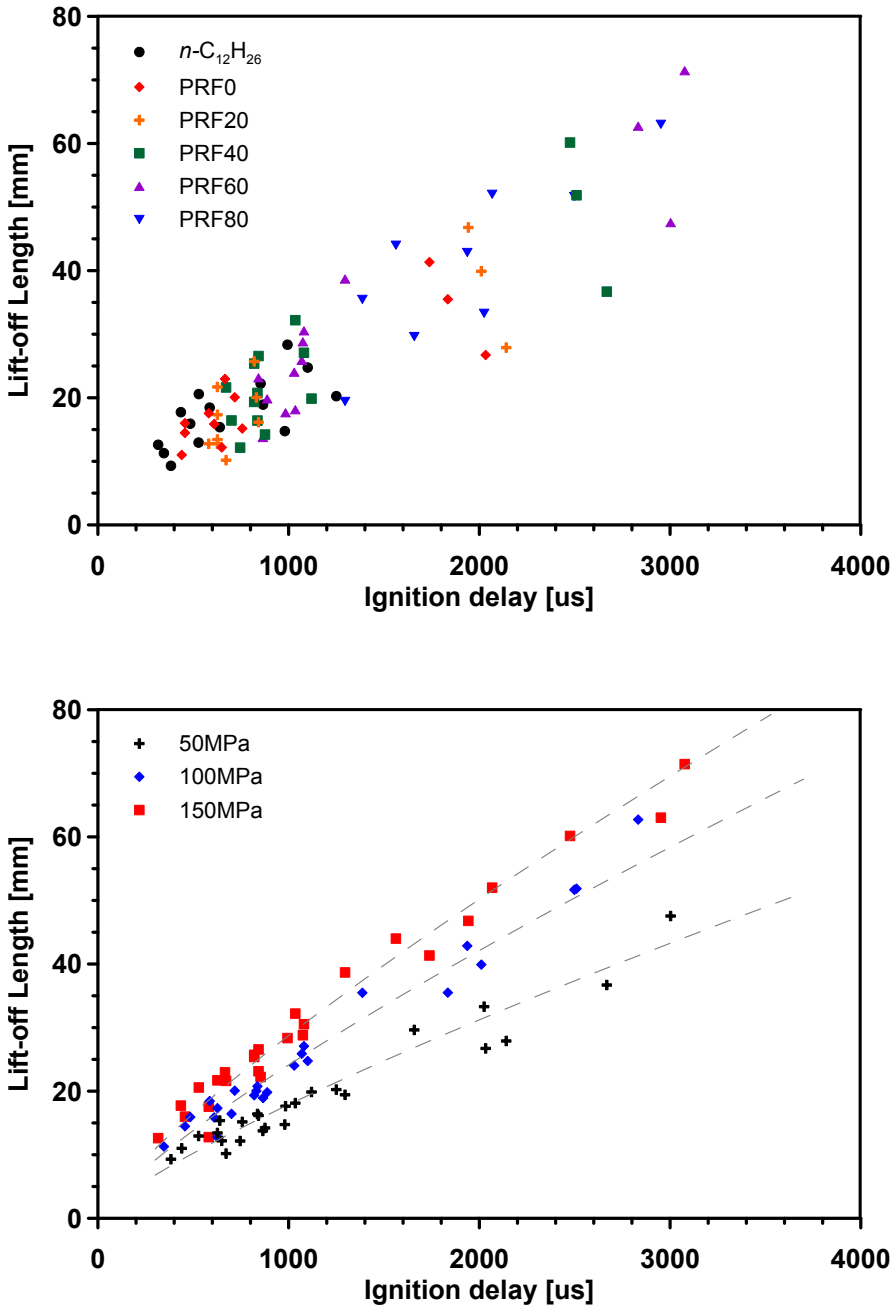

Figure 5.17. *Ignition delay and lift-off length relationship for all fuels under all conditions grouped by fuel (top) and injection pressure (bottom), time after SOI. n-dodecane data (ON = −40) from [3, 4].*

Table 5.5. *Exponents for the lift-off length correlation according to Equation 5.1.*

Parameter	k_{LoL}	P_{inj}	τ	R^2
Units	$[A.U.]$	$[MPa]$	$[\mu s]$	$-$
Exponent	$-$	a	b	$-$
Value	0.0127	0.432	0.804	97.2%

case, the higher octane number means a less reactive blend. Hence, for each parametric point (same oxygen concentration, air temperature and injection pressure) the effect of the fuel employed will be reflected on the start of the combustion, resulting in longer lift-off lengths and ignition delay times for blends with lower cetane number.

In agreement with [44, 49], results are mainly stratified in terms of injection pressure, which has a strong effect on the lift-off length, but not on ignition delay time. As explained earlier, a higher injection pressure had a minimum effect on the ignition delay time. This was because even though more fuel mass was being injected, the higher speed of the spray allowed more air to be entrained, hence the fuel/air ratio remained very similar to other pressures. On the other hand, the higher velocity of the spray caused it to penetrate faster, and since the ignition time was almost the same, the combustion occurred further away from the nozzle tip, which resulted in longer lift-off lengths (Figure 5.17) (bottom). This trend was very interesting and led to think a sort of correlation for the lift-off length as a function of the injection pressure ignition delay time could be obtained in the form of Equation 5.1. This assumption proved to be true and the parameters of such correlation are presented in Table 5.5. It shows that a one-to-one relationship between the lift-off length and the ignition delay time does not exist, as the exponent of 0.804 indicates that the lift-off length grows as ignition delay time increases, but not linearly, which is consistent with a previous study [28]. Moreover, the effect of the injection pressure was also consistent with a similar analysis presented previously in a Ph.D. thesis [48], where the exponent for the fuel exit velocity was 0.88, which is coherent with the value of 0.432 presented here. If the velocity can be related to the square root of the injection pressure ($u_0 = 2\sqrt{\frac{\Delta P_{inj}}{\rho_f}}$), then the term $u_0^{0.88} \sim \Delta P_{inj}^{0.44}$ has the same influence as in the correlation presented in this work. Therefore, the stratification by injection pressure for all fuels under all conditions is further demonstrated when ploting the correlated functions in Figure 5.17 (bottom), where the experimental values follow the calculated trends.

$$LoL = k_{LoL} \cdot P_{inj}^{a} \cdot \tau^{b} \tag{5.1}$$

where k_{LoL} is the correlation constant, P_{inj} is the injection pressure, τ is the ignition delay time and a and b are the exponents of each parameter.

5.9 Flame broadband radiation

One indicative of the presence of soot in a reactive spray is the emission of very intense broadband radiation, as soot luminosity depends on first instance on the temperature

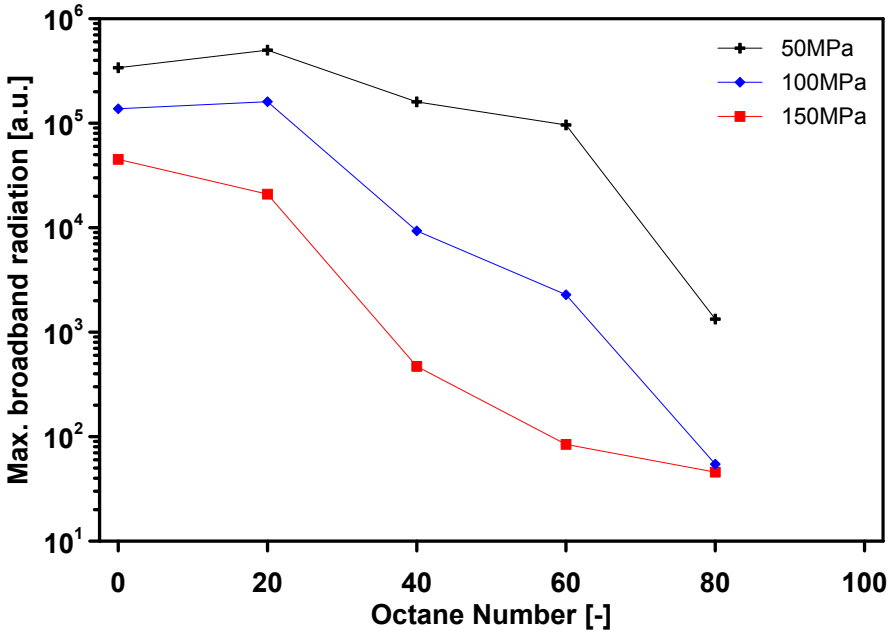

Figure 5.18. *Broadband luminosity for all blends under injection pressure variation, at 900 K and 15 %O_2.*

and the amount of soot within the flame. The effects of the parameters studied (air temperature, oxygen concentration and fuel composition) seem to cause trends on the radiation on the opposite direction of ignition delay time and lift-off length.

Lower injection pressures tend to produce more soot as the injection pressure does not affect the temperature much, but it does the amount of soot generated [51, 52]. This is because the lower the injection pressure, the shorter the lift-off length will be (as shown previously), leading to higher equivalence ratios at the instant of ignition. The lower injection pressure also causes the flame residence time to increase [53], so there is more time for the chemical reactions to take place, hence producing higher soot. Figure 5.18 shows how the radiation generated decreases around one order of magnitude between the highest and lowest injection pressures.

The effects of the air temperature and oxygen concentration cause similar effects on the soot generated and, therefore, on the broadband radiation emitted. Although the trends of these parameters could be compared to their effect on the lift-off length and ignition delay time, these are controlled by the reactivity of the mixture, which is not necessarily related to the formation of soot. In this case, the lower ambient temperature or oxygen concentration will cause the adiabatic flame temperature to be lower, this will generate less soot as the soot formation rate is affected; also, the lower combustion temperature will cause the soot radiation to be less intense. Finally, as was previously explained, a lower oxygen concentration or ambient temperature are related to longer lift-off lengths, therefore, the equivalence ratio will be lower at the flame base, which will in turn generate less soot.

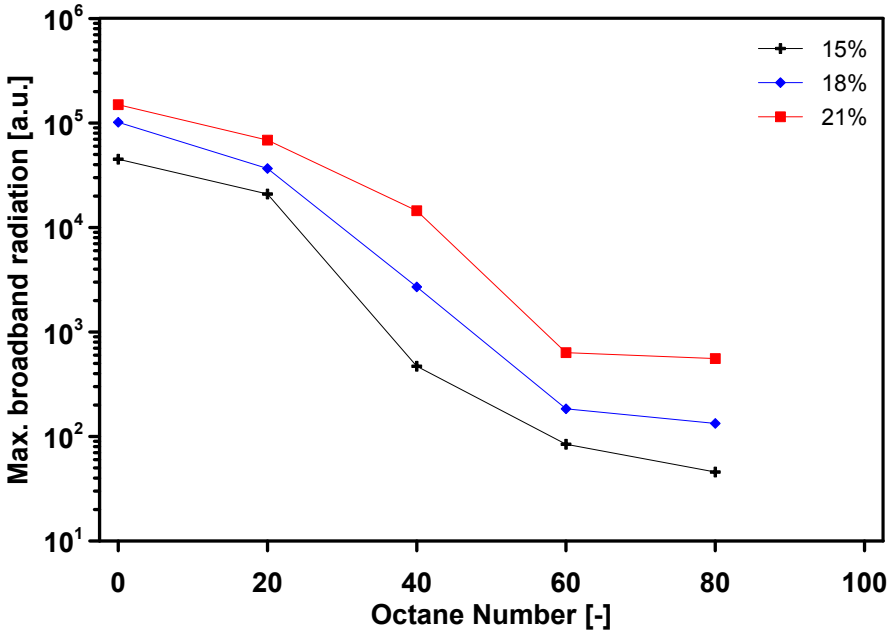

Figure 5.19. *Broadband luminosity for all blends under oxygen concentration variation, at 900 K and 150 MPa, time after SOI.*

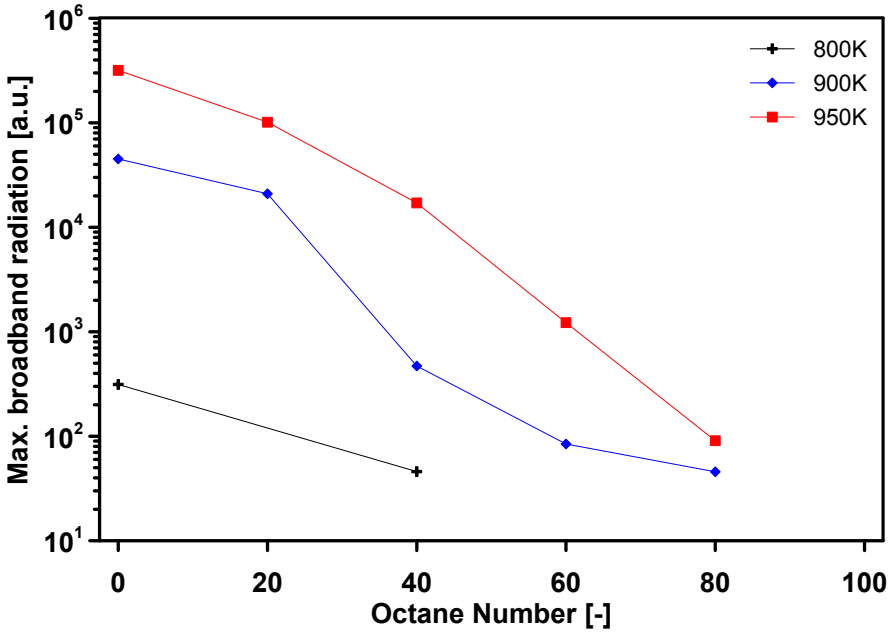

Figure 5.20. *Broadband luminosity for all blends under air temperatures variation, at 15 $\%O_2$ and 150 MPa, time after SOI.*

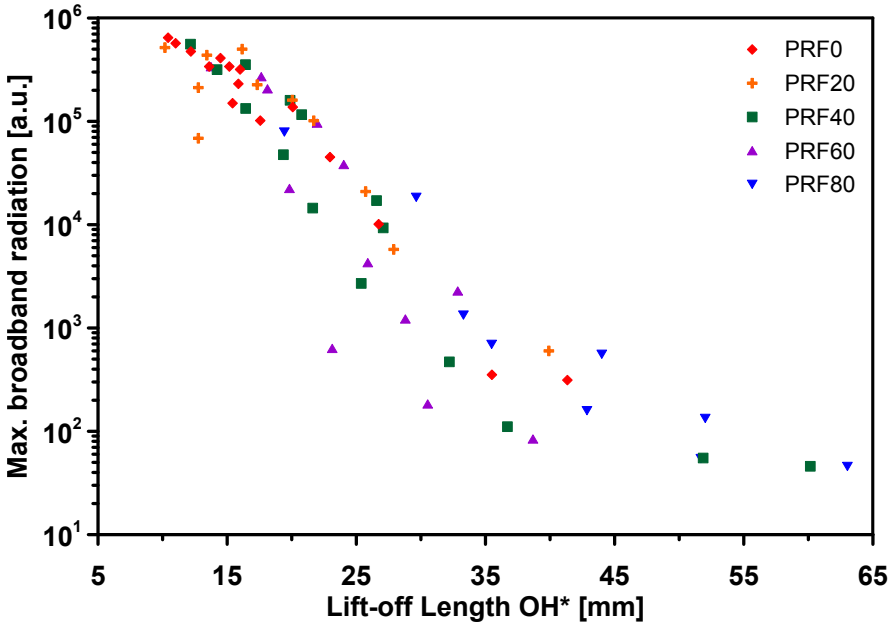

Figure 5.21. *Lift-off Length and broadband radiation relationship for Primary Reference Fuels under all conditions, time after SOI.*

The effect of the fuel seems to follow the same trend as for the other parameters, where the higher concentration of *iso*-octane causes the mixture to produce less soot and therefore register lower radiation values. This is because the higher octane number values cause the ignition delay to be longer, which for each given operating point is elongating the lift-off length, therefore the equivalence ratio is leaner at the start of combustion. For these reasons, less soot is produced and lower values of broadband radiation are detected. Figures 5.18 to 5.20 also show the effect of the fuel composition under the different conditions. In all cases it is clear that the less sooting conditions are the ones with higher PRFs. Furthermore, the combined effect of oxygen-fuel is also present, as it affects greatly the reactivity of the mixture, as was mentioned earlier. This results are consistent with [54], where the reduction of smoke emissions by using gasoline instead of diesel is comparable to the reduction of soot from *n*-heptane to *iso*-octane.

5.9.1 Relationship between broadband radiation and lift-off length

Another interesting trend that was found is the relationship between the lift-off length and the amount of broadband radiation generated. A previous study [50] has presented a tendency for the lift-off length to be smaller for shorter ignition delay times, as was shown in Section 5.8.1. Additionally, a trend between the ignition delay and the amount of soot generated and luminosity registered was also displayed.

Although, the actual amount of soot was not measured in this study, relationships between the quantity of soot measured and the radiation emitted are known to exist [50];

moreover, another study has reported an interaction between the ignition delay time and soot formation [44]. Figure 5.21 presents the relationship between the LoL and broadband radiation and a clear trend can be seen. As the mixture takes longer to ignite, the spray keeps on penetrating into the chamber, hence leading to longer lift-off lengths. Additionally, as this happens, the mixture is more diluted as the fuel mass fraction decreases while more air is being entrained. This dilution leads to lower combustion temperatures and therefore slows the kinetics of soot formation [55]. This causes a leaner combustion which results in less soot generated due to the large amount of oxygen available for the premixed combustion phase [43, 56]. The exact opposite appears to occur for shorter ignition delay times, the spray has not had enough time to penetrate, so the lift-off lengths are closer to the nozzle tip and because of the richer equivalence ratios, the broadband radiation registered is higher.

5.9.2 Transition to non-sooting diffusion flame

As was mentioned in the analysis of the baseline case (Section 5.5), both broadband radiation and OH* chemiluminescence measure the presence of a flame. This latter value is the best indicative that a combustion is taking place within a spray and is always present, on the other hand, the soot may no be present even if a spray is reacting [45, 57].

Figure 5.22 shows the relationship between the lift-off length (chemiluminescence) and the soot onset length (broadband radiation). For most cases the SOL is longer than the LoL, this is because the OH* radical appears much sooner than the soot due to the chemical reactions taking place in the spray, so it is reasonable for the lift-off length to be shorter. However, there are some cases in which they have very similar values, and sometimes the soot onset length being slightly shorter. This corresponds with the least reactive conditions (low oxygen/temperature/n-heptane) where the amount of soot is so low that the radiation captured by the broadband radiation camera may come from the chemiluminescence of radicals in the visible wavelengths; which is consistent with the results presented in [57] where a large intensity difference was observed. This effect is also easier to see in Figure 5.22 where the values of soot onset length equal or shorter the lift-off length correspond to the cases in which less radiation was detected. Such results evidence the transition to a non-sooting flame [1, 14, 30]. Low reactivity conditions (higher octane number, low oxygen concentration or air temperature) not only increase the ignition delay time and the lift-off length, but also due to the relationship between the LoL and the air entrainment could lead the diffusion flame to be non-sooting.

5.10 Stabilized flame length

As was explained in Section 3.3.3 the length of the flame was measured by means of broadband radiation, but stabilized values are not achieved for all operating conditions due to either spatial or temporal limitations in the acquisition setup as well as the lack of actual radiation under some conditions. Radiation onset occurs after the start of combustion, if the resulting radiation is strong enough to be detected, measured flame penetration will be similar to that of the reacting spray tip penetration. Figure 5.23 shows the evolution of the flame penetration under the oxygen concentration variation.

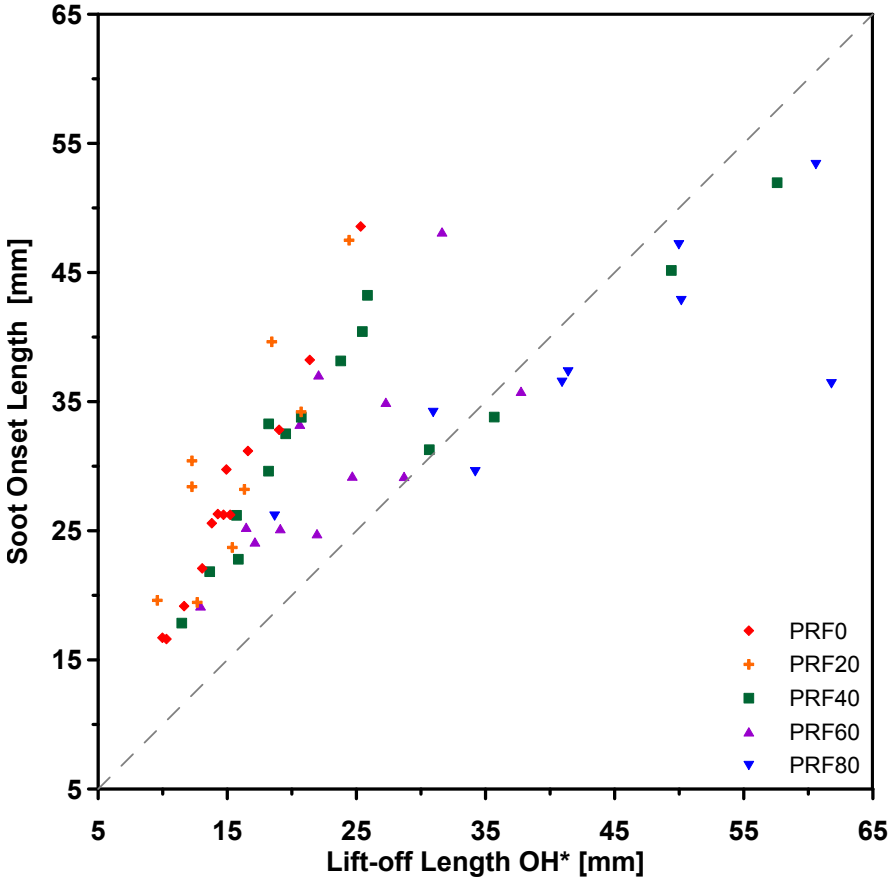

Figure 5.22. *OH* radical LoL and broadband radiation SOL relationship for Primary Reference Fuels under all conditions.*

For all three cases it can be seen that the flame penetrates faster than the corresponding spray tip of the non-reacting reference. Also, and according to what was seen in the study of the spray penetration, the deviation of the flame penetration occurs earlier and more aggressively as the oxygen concentration increases. Finally, the higher concentration of oxygen also causes the flame to stabilize closer to the nozzle. The reason for this behaviour is that the more reactive the air-fuel mixture the closer the stoichiometric surface will be to the injector, resulting in a shorter stabilized flame length.

Figures 5.24 and 5.25 show the stabilized flame length values under oxygen concentration and air temperature variations, respectively. As mentioned earlier, the flame length does not stabilize within the time and space limits of the present study for all conditions, so only a few cases are being shown. Figure 5.24 shows that the injection pressure does not have an effect on the flame length, as opposed to the lift-off length, which became longer as the pressure was increased. There are some differences seen in Figure 5.24 but no clear trend is evident and they can be attributed to experimental dispersion. On the other hand, the higher oxygen concentration causes the flame to stabilize closer to the nozzle tip as the local equivalence ratio increases due to the increase in oxygen; this trend can be seen for all the blends shown. On a different way, the trend

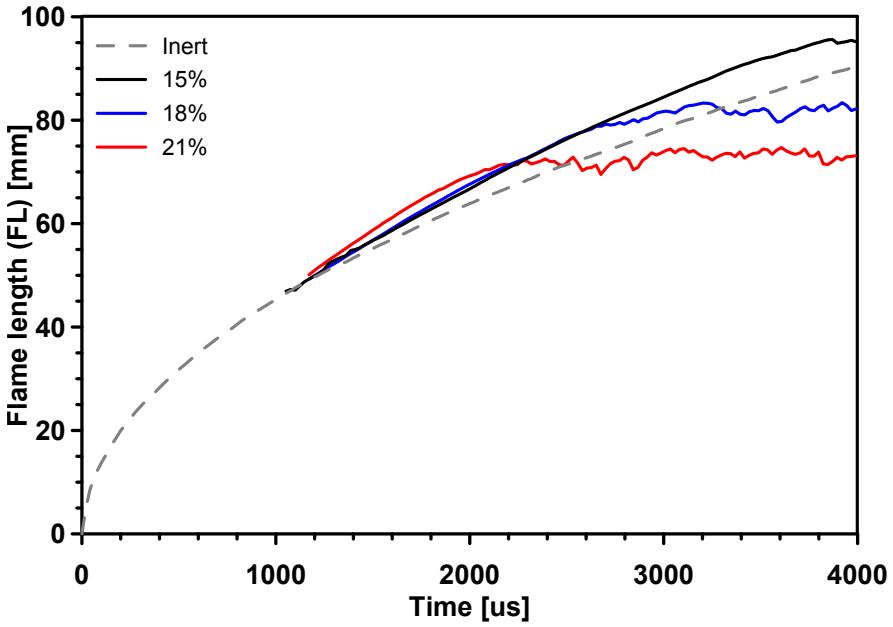

Figure 5.23. *Flame length comparison for PRF0 under oxygen concentration variation at 900 K and 150 MPa, time after SOI.*

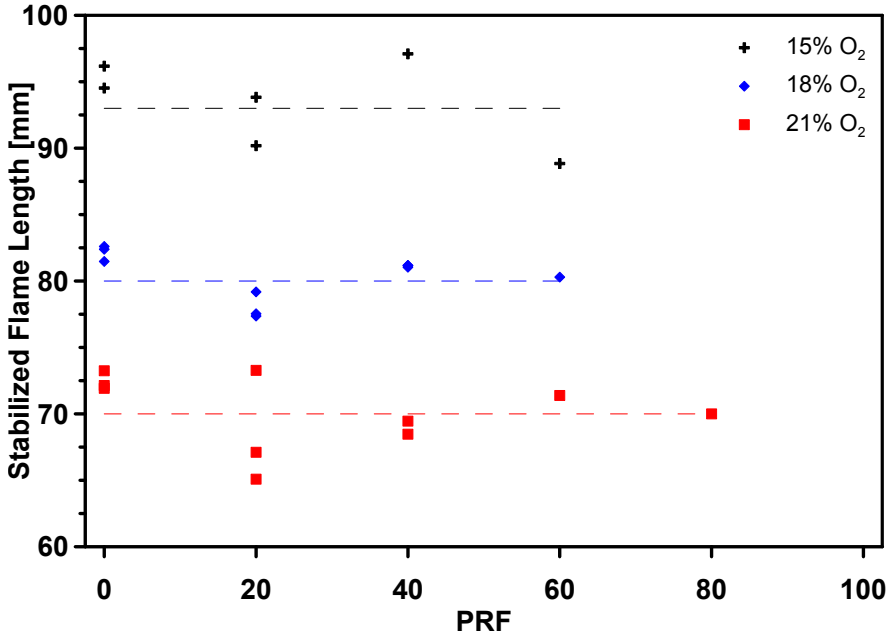

Figure 5.24. *Stabilized flame length comparison for Primary Reference Fuels under oxygen concentration variation, at 900 K and all injection pressures. Dashed lines represent average values over different fuels.*

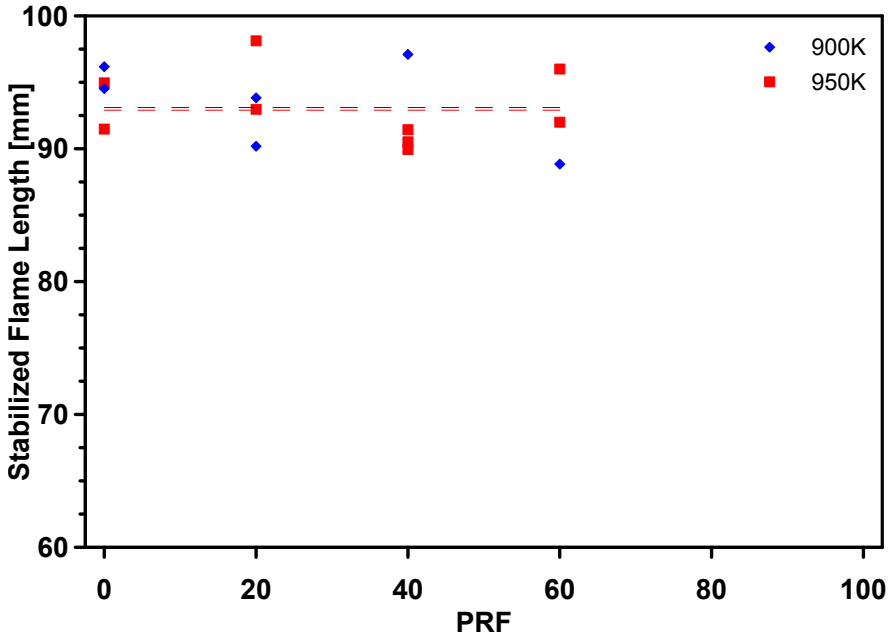

Figure 5.25. *Stabilized flame length comparison for Primary Reference Fuels under air temperature variation, at 15 $\%O_2$ and all injection pressures. Dashed lines represent average values over different fuels.*

of the flame length under temperature changes is not clear. Although the stabilized length of the flame seems to remain fairly constant for the two temperatures shown in Figure 5.25, the combined effect of air temperature and injection pressure is very erratic. However, this is due to experimental dispersion and also because the flame length values are too close to the window limit. Additionally, from Figures 5.24 and 5.25 it can be also appreciated that the fuel reactivity does not have a strong effect on the stabilized flame, this could be due to the fact that the flame is defined by a stoichiometric surface and not the reactivity of the mixture (ie. octane number), and in this study the stoichiometric equivalence ratios between *n*-heptane and *iso*-octane are similar to each other (i.e. 0.0455 and 0.0456, respectively under Spray A nominal conditions).

As was explained in the previous paragraph the increased reactivity of the mixtures caused the reactive core of the spray to be closer to the nozzle. So the position and size of the reactive core of the spray is affected by the conditions, being the lift-off length more sensitive to this changes than the flame length. Higher octane numbers cause longer lift-off lengths while leaving the flame length unaffected. On the other hand, the increment of the oxygen concentration brings both, the lift-off length and flame length, closer to the nozzle, while the higher air temperature causes this behaviour only on the lift-off length. It is worth mentioning that the lift-off length and the flame length have different stabilization mechanisms, as the former is related to the reactivity and autoignition of the mixture, while the latter is more dependant of the mixture; therefore, the differences shown among the lift-off length and the flame length are acceptable. Although Figure 5.23

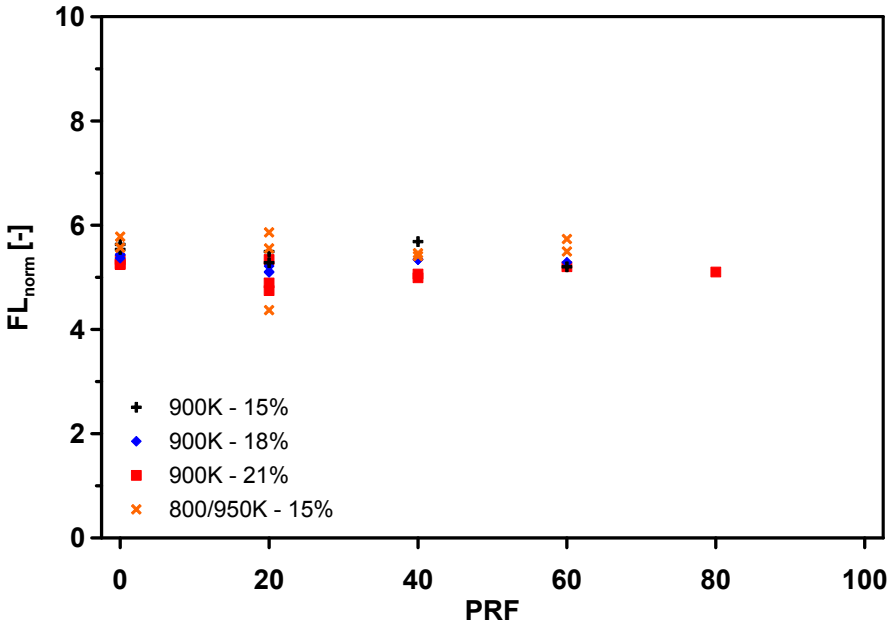

Figure 5.26. *Normalized flame length (FL_{norm}) versus fuel composition at ambient temperature and oxygen concentration variations.*

does not show a temperature variation, Figure 5.26 shows that the effect of temperature is negligible on the stabilized flame length.

5.10.1 Scaling law for stabilized flame length

Stabilized flame length measurements under diesel engine conditions are rarely available in the literature, mainly due to the length, which is usually larger than most optical accesses, and the time needed for stabilization, which is quite long in terms of engine scales. Comparable results to the ones shown here are those reported in [58], which use long-exposure OH* chemiluminescence images to quantify the stabilized flame length for different nozzle diameters. To compare the present results with those measurements, the obtained flame lengths have been normalized for the different experimental conditions according to the following scaling law based on a momentum-controlled diffusion flame description:

$$FL_{norm} = FL \cdot \frac{z_{st}}{d_{eq} \cdot \sqrt{\frac{\rho_a}{\rho_{st,r}}}}$$

where $d_{eq} = d_0 \cdot \sqrt{\frac{\rho_f}{\rho_a}}$ is the equivalent diameter, which was already used for normalization of the penetration under inert conditions, z_{st} is the stoichiometric mixture fraction, and $\sqrt{\frac{\rho_a}{\rho_{st,r}}}$ is a term that

Table 5.6. *Summary of trends per parameter. (*Shift in Combustion timing).*

Parameter	Sr	τ	LoL	FL	BR
$\uparrow P_{inj}$	$\uparrow$	$\approx$	$\uparrow$	$\approx$	$\downarrow$
$\uparrow T_a$	$\uparrow^*$	$\downarrow$	$\downarrow$	$\approx$	$\uparrow$
$\uparrow O_2$	$\uparrow^*$	$\downarrow$	$\downarrow$	$\downarrow$	$\uparrow$
$\uparrow ON$	$\downarrow^*$	$\uparrow$	$\uparrow$	$\approx$	$\downarrow$

accounts for entrainment reduction due to the combustion-induced density decrease, where $\rho_{st,r}$ is the stoichiometric mixture density under reacting conditions.

This term has been demonstrated to justify entrainment decrease under atmospheric pressure gas flames [59]. Figure 5.26 presents the results of the normalized flame length (FL_{norm}), which shows the values to be in the range of $4-6$ for most operating conditions, in agreement with those from [58]. Therefore, it confirms that the stabilization of the diffusion flame is controlled by mixing arguments, and not by fuel reactivity. A similar scaling law for atmospheric gaseous flames was presented as a Ph.D. thesis [60], where the term $\sqrt{\frac{\rho_a}{\rho_{st,r}}}$ was also applied.

5.11 Recapitulation and Synthesis

A summary of the effects on the auto-ignition and combustion processes is presented in Table 5.6. The following trends have been found:

- A rise in injection pressure will result in a higher spray momentum, thus causing it to penetrate faster into the chamber. As a result, an earlier formation of ignitable mixtures can also be expected, which may explain the slightly shorter ignition delay times. Due to higher local velocities, it causes the lift-off length to be longer; however, the stabilized flame length does not seem to be affected [52]. This longer lift-off length creates leaner mixtures at the flame base and therefore less soot is formed.

- The ambient temperature and oxygen concentration have a very similar impact on the spray processes. They have no apparent effect on spray penetration during the inert spray evolution, but they do have an effect on the reacting spray development. As the temperature rises or oxygen concentration increases, the reactivity of the mixture increases dramatically, so the fuel will start to burn earlier and closer to the nozzle, resulting in shorter ignition delay times and lift-off lengths. Where they have different effects regarding the stabilized flame length, as a higher oxygen concentration will results in shorter lengths while the temperature appears not to have an effect on the stabilized flame for the parametric variation done. The former parameter affected directly the stoichiometric equivalence ratio, which was then reflected on the flame length. On the other hand, the air temperature affects the combustion temperature and therefore the local density which in turn would

affect the flame length too; however, the temperature variation for the results presented may have been too small to cause an effect on the density and therefore the flame length. Finally, the shorter ignition delay times will cause the start of the acceleration phase to start sooner and its slope to be more pronounced, therefore resulting in longer penetrations.

Increasing the octane number of the mixture has a completely opposite effect on the combustion behaviour in comparison to augmenting the quantity of oxygen or temperature in the air. As *iso*-octane is less reactive than *n*-heptane, increasing its concentration will only cause the mixture to start to burn later and further away from the injector tip. Even though *iso*-octane has a slightly higher sooting tendency than *n*-heptane, the increase in lift-off causes much leaner local equivalence ratios at the flame base, resulting in lower soot formation and a concurrent decrease in broadband radiation intensity. Moreover, the stabilized flame length was shown not to be affected much by the fuel composition. Finally, two trends were defined regarding the octane number of the blend. On one hand, for the lower half of the octane scale (PRF0-20-40) the reactivity of the mixture (lift-off lengths and ignition delay times) seemed to be diminished linearly with the fuel proportion. On the other hand, in the upper half (PRF60-80-100) a non-linear trend was found for all the parameters measured.

A scaling law for the stabilized flame length based on momentum-controlled considerations has been validated for those conditions where such stabilization occurs. This scaling law agrees with similar results in the literature for the blends presented in this chapter.

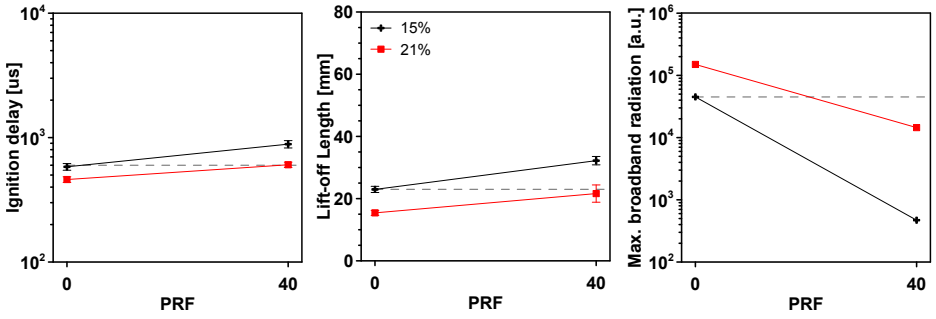

Figure 5.27. *Analysis of fuel composition oxygen concentration variation. Summary of results previously shown.*

As a small discussion on the applicability of the present results for engine performance studies, a comparison will be made to extend the conclusions of the present study to an engine running on diesel alone and a mixture of gasoline-diesel under different oxygen concentrations in order to simulate two levels of EGR. For that purpose, ignition delay and lift-off results for PRF0 with 15 % of oxygen and PRF40 with 21 % of oxygen will be compared. They could be taken as representative of a diesel engine running with pure diesel and an EGR level of 30 % for a high load case, or with a diesel-gasoline blend and no EGR. Taking a look at Figure 5.27 it can be seen that both cases have an ignition delay time of 600 μs. Additionally, it can be seen that PRF0 and PRF40 have approximately the

same lift-off length, 23 mm and 22 mm. This would mean a similar combustion timing for both fuels, which is always interesting in terms of engine calibration. Furthermore, due to the higher oxygen amount in ambient air, the local equivalence ratio at the lift-off for the diesel-gasoline mixture (PRF40) would be much leaner (0.83 *vs* 1.03), which should result in lower soot formation within the flame, and therefore lower exhaust particulates. This can be observed as for PRF0 the broadband radiation is around 45000 $a.u.$ while for 21 % of oxygen it is less than 20000 $a.u.$. This could mean that adding gasoline to the blend and reducing the EGR would result in a spray with almost identical ignition characteristics (τ & LoL), but with much lower soot produced than in the case of pure Diesel with EGR. The aforementioned comparison agrees with general trends presented in recent studies using primary reference fuels and similar strategies to reduce emissions while maintaining engine performance [35, 37, 51, 54, 61–68]. Nevertheless, further research on this topic is needed, to confirm the previous conclusion.

Bibliography

[1] Pickett L.M., Genzale C.L., Bruneaux G., Malbec L.M., Hermant L., Christiansen C. and Schramm J. "Comparison of diesel spray combustion in different high-temperature, high-pressure facilities.". *SAE International Journal of Engines*, Vol. 3(2) n^o 2010-01-2106, pp. 156–181, 2010.

[2] *National Institute of Standards and Technology (NIST) Chemistry WebBook*. http://webbook.nist.gov/chemistry/.

[3] *Engine Combustion Network*. http://www.sandia.gov/ecn.

[4] Benajes J., Payri R., Bardi M. and Martí-Aldaraví P. "Experimental characterization of diesel ignition and lift-off length using a single-hole ECN injector". *Applied Thermal Engineering*, Vol. 58, pp. 554–563, 2013.

[5] Payri R., García-Oliver J.M., Bardi M. and Manin J. "Fuel temperature influence on diesel sprays in inert and reacting conditions". *Applied Thermal Engineering*, Vol. 35, pp. 185–195, 2012.

[6] Siebers D.L. "Liquid-phase fuel penetration in diesel sprays". *SAE Technical Paper*, n^o 980809, 1998.

[7] Siebers D.L. "Scaling liquid-phase fuel penetration in diesel sprays based on mixing-limited vaporization". *SAE Technical Paper*, n^o 1999-01-0528, 1999.

[8] Pastor J.V., García-Oliver J.M., Pastor J.M. and Vera-Tudela W. "One-dimensional diesel spray modeling of multicomponent fuels". *Atomization and Sprays*, Vol. 25(2), pp. 485–517, 2015.

[9] Higgins B., Mueller C. and Siebers D. "Measurements of fuel effects on liquid-phase penetration in DI sprays". *SAE Technical Paper*, n^o 1999-01-0519, 1999.

[10] Malbec L.M., Egúsquiza J., Bruneaux G. and Meijer M. "Characterization of a set of ECN Spray A injectors: Nozzle to nozzle variations and effect of spray characteristics". *SAE International Journal of Engines*, Vol. 6(3) n^o 2013-24-0037, pp. 1642–1660, 2013.

[11] Payri R., Salvador F.J., Gimeno J. and Zapata L.D. "Diesel nozzle geometry influence on spray liquid-phase fuel penetration in evaporative conditions". *Fuel*, Vol. 87(7), pp. 1165–1176, 2008.

[12] Morrison R.T. and Boyd R.N. *Química Orgánica*. Pearson Educación, 1998.

[13] Kook S. and Pickett L.M. "Liquid length and vapor penetration of conventional, Fischer-Tropsch, coal-derived, and surrogate fuel sprays at high-temperature and high-pressure ambient conditions". *Fuel*, Vol. 93, pp. 539–548, 2012.

[14] Pickett L.M., Kook. S. and Williams T. "Visualization of diesel spray penetration, cool-flame, ignition, high-temperature combustion, and soot formation using high-speed imaging". *SAE International Journal of Engines*, Vol. 2(1) n^o 2009-01-0658, pp. 439–459, 2009.

[15] Skeen S.A., Manin J. and Pickett L.M. "Simultaneous formaldehyde PLIF and high-speed schlieren imaging for ignition visualization in high-pressure spray flames". *Proceedings of the Combustion Institute*, Vol. 35(3), pp. 3167–3174, 2015.

[16] Dec J.E. "A conceptual model of DI diesel combustion based on laser-sheet imaging". *SAE Technical Paper*, n^o 970873, 1997.

[17] Desantes J.M., Pastor J.V., García-Oliver J.M. and Briceño F.J. "An experimental analysis on the evolution of the transient tip penetration in reacting diesel sprays". *Combustion and Flame*, Vol. 161(8), pp. 2137–2150, 2014.

[18] Paryi R., García-Oliver J.M., Xuan T. and Bardi M. "A study on diesel spray tip penetration and radial expansion under reacting conditions". *Applied Thermal Engineering*, Vol. 90, pp. 619–629, 2015.

[19] Skeen S., Manin J., Pickett L., Dalen K. and Ivarsson A. "Quantitative spatially resolved measurements of total radiation in high-pressure spray flames". *SAE Technical Paper*, n^o 2014-01-1252, 2015.

[20] Pastor J.V., Payri R., García-Oliver J.M. and Briceño F. "Schlieren methodology for the analysis of transient diesel flame evolution". *SAE International Journal of Engines*, Vol. 6(3) n^o 2013-24-0041, pp. 1661–1676, 2013.

[21] Möller S., Dutzler G.K., Priesching P., Pastor J.V. and Micó C. "Multi-Component Modeling of Diesel Fuel for Injection and Combustion Simulation". *SAE Technical Paper*, n^o 2013-24-0007, 2013.

[22] Payri R., García A., Domenech V., Durrett R. and Plazas A.H. "An experimental study of gasoline effects on injection rate, momentum flux and spray characteristics using a common rail diesel injection system". *Fuel*, Vol. 97, pp. 390–399, 2012.

[23] Verhoeven D., Vanhemelryck J.L. and Baritaud T. "Macroscopic and ignition characteristics of high-pressure sprays of single-component fuels". *SAE Technical Paper*, n^o 981069, 1998.

[24] Wang X., Kuti Z. HuaZ. Huang.A., Zhang W. and Nishida K. "An experimental investigation on spray, ignition and combustion characteristics of biodiesels". *Proceedings of the Combustion Institute*, Vol. 33(2), pp. 2071–2077, 2011.

[25] Kobori S., Kamimoto T. and Kosaka H. "Ignition, combustion and emissions in a DI diesel engines equipped with a micro-hole nozzle". *SAE Technical Paper*, n^o 960321, 1996.

[26] Ramírez-Hernández J. *Combustion studies for high speed direct injection diesel engines under low temperature cold start conditions.* Doctoral Thesis, Universitat Politècnica de València, 2012.

[27] Idicheria C.A. and Pickett L.M. "Effect of EGR on diesel premixed-burn equivalence ratio". *Proceedings of the Combustion Institute*, Vol. 31, pp. 2931–2938, 2007.

[28] Pickett L.M. and Siebers D.L. "Fuel effects on soot processes of fuel jets at DI diesel conditions". *SAE Technical Paper*, n^o 2003-01-3080, 2003.

[29] Vandersickel A., Hartmann M., Vogel K., Wright Y.M., Fikri M., Starke R., Schulz C. and Boulouchos K. "The autoignition of practical fuels at HCCI conditions: High-pressure shock tube experiments and phenomenological modeling". *Fuel*, Vol. 93, pp. 492–501, 2012.

[30] Pickett L.M., Siebers D.L. and Idicheria C.A. "Relationship between ignition processes and the lift-off length of diesel fuel jets". *SAE Technical Paper*, n^o 2005-01-3843, 2005.

[31] Ito T., Ueda M., Matsumoto T., Kitamura. T., Senda J. and Fujimoto H. "Effects of ambient gas conditions on ignition and combustion process of oxygenated fuel sprays". *SAE Technical Paper*, n^o 2003-01-1790, 2003.

[32] Jung Y., Manin J., Skeen S. and Pickett L. "Measurement of liquid and vapour penetration of diesel sprays with a variation in spreading angle". *SAE Technical Paper*, n^o 2015-01-0946, 2015.

[33] Pastor J.V., García-Oliver J.M., Pastor J.M. and Ramírez-Hernández J.G. "Ignition and combustion development for high speed direct injection diesel engines under low temperature cold start conditions". *Fuel*, Vol. 90(4), pp. 1556–1566, 2011.

[34] Hartmann M., Gushterova I., Fikri M., Schulz C. and Schießl R. "Auto-ignition of toluene-doped n-heptane and iso-octane/air mixtures: High-pressure shock-tube experiments and kinetics modeling". *Combustion and Flame*, Vol. 158, pp. 172–178, 2011.

[35] Reitz R.D. "High-Efficiency Fuel Reactivity Controlled Compression Ignition (RCCI) Combustion". In *16th Directions in Engine-Efficiency and Emissions Research (DEER) Conference, Detroit, MI.* Engine Research Center, University of Wisconsin-Madison, August 2010.

[36] Heywood J. *Internal Combustion Engine Fundamentals.* McGraw-Hill Education, 1988.

[37] Hildingsson L., Kalghatgi G., Tait N., Johansson B. and Harrison A. "Fuel Octane Effects in the Partially Premixed Combustion Regime in Compression Ignition Engines". *SAE Technical Paper*, n^o 2009-01-2648, 2009.

[38] Flynn P.F., Durrett R.P., Hunter G.L., zur Loye A.O., Akinyemi O.C., Dec J.E. and Westbrook C.K. "Diesel combustion: An intengrated view combining laser diagnostics, chemical kinetics, and empirical validation". *SAE Technical Paper*, n^o 1999-01-0509, 1999.

[39] Zhang J., Niu S., Zhang Y., Tang C., Jiang X., Hu E. and Huang Z. "Experimental and modeling study of the auto-ignition of n-heptane/n-butanol mixtures". *Combustion and Flame*, Vol. 160, pp. 31–39, 2013.

[40] Peters N. *Turbulent Combustion.* Cambridge University Press, 2000.

[41] Yates A., Viljoen C. and Swarts S. "Understanding the relation between cetane number and combustion bomb ignition delay measurements". *SAE Technical Paper*, n^o 2004-01-2017, 2004.

[42] Pickett L.M. "Low flame temperature limits for mixing-controlled diesel combustion". *Proceedings of the Combustion Institute*, Vol. 30, pp. 2727–2735, 2005.

[43] Siebers D. and Higgins B. "Flame lift-off on direct-injection diesel sprays under quiescent conditions". *SAE Technical Paper*, n^o 2001-01-0530, 2001.

[44] Payri F., Pastor J.V., Nerva J.G. and García-Oliver J. "Lift-off length and KL extinction measurements of biodiesel and Fischer-Tropsch fuels under quasi-steady diesel engine conditions". *SAE International Journal of Engines*, Vol. 4(2) n^o 2011-24-0037, pp. 2278–2297, 2011.

[45] Higgins B. and Siebers D. "Measurement of the Flame Lift-Off Location on DI Diesel Sprays Using OH Chemiluminescence". *SAE Technical Paper*, n^o 2001-01-0918, 2001.

[46] Persson H., Andersson Ö. and Egnell R. "Fuel effects on flame lift-off under diesel conditions". *Combustion and Flame*, Vol. 158, pp. 91–97, 2011.

[47] van Lipzig J.P.J., Nilsson E.J.K., de Goey L.P.H. and Konnov A.A. "Laminar burning velocities of n-heptane, iso-octane, ethanol and their binary and tertiary mixtures". *Fuel*, Vol. 90, pp. 2773–2781, 2011.

[48] Nerva J.G. *An assessment of fuel physical and chemical properties in the combustion of a Diesel spray.* Doctoral Thesis, Universitat Politècnica de València, 2013.

[49] Pastor J.V., Payri R., García-Oliver J.M. and Nerva J.G. "Schlieren measurements of the ECN-Spray A penetration under inert and reacting conditions". *SAE Technical Paper*, n^o 2012-01-0456, 2012.

[50] Donkerbroek A.J., Boot M.D., Luijten C.C.M., Dam N.J. and ter Meulen J.J. "Flame lift-off length and soot production of oxygenated fuels in relation with ignition delay in a DI heavy-duty diesel engine". *Combustion and Flame*, Vol. 158, pp. 525–538, 2011.

[51] Kunte S., Bertola A., Obrecht P. and Boulouchos K. "Temporal soot evolution and diesel engine combustion: influence of fuel composition, injection parameters, and exhaust gas recirculation". *International Journal of Engine Research*, Vol. 7, pp. 459–470, 2006.

[52] Siebers D.L. and Pickett L.M. "Injection pressure and orifice diameter effects on soot in DI diesel fuel jets". In *Proceedings of the Thiesel 2002 Conference on Thermo- and Fluid Dynamic Processes in Diesel Engines*, pp. 109–132, 2002.

[53] Kim M. and Yoon Y. "Flame residence time and strain rate in turbulent hydrogen non-premixed jet fflame with coaxial air". *Proceedings of the Combustion Institute*, Vol. 31, pp. 1609–1616, 2007.

[54] Kalghatgi G.T., Gurubaran R. Kumara, Davenport A., Harrison A.J., Hardalupas Y. and Taylor A.M.K.P. "Some advantages and challenges of running a Euro IV, V6 diesel engine on a gasoline fuel". *Fuel*, Vol. 108, pp. 197–207, 2013.

[55] Idicheria C.A. and Pickett L.M. "Ignition, soot formation, and end-of-combustion ttransient in diesel combustion under high-EGR conditions". *International Journal of Engine Research*, Vol. 12, pp. 376–392, 2011.

[56] Siebers D., Higgins B. and Pickett L. "Flame Lift-off on direct-injection diesel fuel jets: Oxygen concentration effects". *SAE Technical Paper*, n^o 2002-01-0890, 2002.

[57] Dec J.E. and Espey C. "Ignition and early soot formation in a DI diesel engine using multiple 2-D imaging diagnostics". *SAE Technical Paper*, n^o 950456, 1995.

[58] Pickett L.M. and Siebers D.L. "Orifice diameter effects on diesel fuel jet flame". *Journal of Engineering for Gas Turbines and Power*, Vol. 127(1), pp. 187–196, 2005.

[59] Han D. and Mungal M.G. "Direct measurement of entrainment in reacting/nonreacting turbulent jets". *Combustion and Flame*, Vol. 124(3), pp. 370–386, 2001.

[60] García J.M. *Aportaciones al estudio del proceso de combustión turbulenta de chorros en motores diesel de inyección directa*. Doctoral Thesis, Universitat Politècnica de València, 2004.

[61] Lü X.C., Chen W., Hou Y.C. and Huang Z. "Study on the ignition, combustion and emissions of a HCCI combustion engines fueled with primary reference fuels". *SAE Technical Paper*, n^o 2005-01-0155, 2005.

[62] Manente V. *Gasoline Partially Premixed Combustion - An advanced internal combustion engine concept aimed to high efficiency, low emissions and low acoustic noise in the whole load range*. Doctoral Thesis, Lund Institute of Technology, 2010.

[63] Yao M., Zhang B., Zheng Z., Cheng Z. and Xing Y. "Experimental study on the effects of EGR and octane number of PRF fuel on combustion and emission characeristics of HCCI engines". *SAE Technical Paper*, n^o 2005-01-0174, 2005.

[64] Hanson R., Splitter D. and Reitz R.D. "Operating a heavy-duty direct-injection compression-ignition engine with gasoline for low emissions". *SAE Technical Paper*, n^o 2009-01-1442, 2009.

[65] Bessonette P., Schleyer C., Duffy K., Hardy W. and Liechty M.P. "Effects of Fuel Property Changes on Heavy-Duty HCCI Combustion". *SAE Technical Paper*, n^o 2007-01-0191, 2007.

[66] Kalghatgi G., Risberg P. and Ångström H.E. "Advantages of Fuels with High Resistance to Auto-ignition in Late-injection, Low-temperature, Compression Ignition Combustion". *SAE Technical Paper*, n^o 2006-01-3385, 2006.

[67] Kalghatgi G., Risberg P. and Ångström H.E. "Partially Pre-Mixed Auto-Ignition of Gasoline to Attain Low Smoke and Low NOx at High Load in a Compression Ignition Engines and Comparison with a Diesel Fuel". *SAE Technical Paper*, n^o 2007-01-0006, 2007.

[68] Reitz R.D., R.Hanson, Splitter D. and Kokjohn S. "High-Efficiency, Ultra-Low Emission Combustion in a Heavy-Duty Engine via Fuel Reactivity Control". In *15th Diesel Engine-Efficiency and Emissions Research (DEER) Conference, Dearborn, MI*. Engine Research Center, University of Wisconsin-Madison, August 2009.

Chapter 6

Conclusions and future work

Contents

6.1 Introduction

In this closing chapter, a look back into Chapter 1 will be done to check what has been added in Chapters 4 and 5 and if the main goal of this thesis has been fulfilled. Furthermore, the results obtained and analysis done will be linked to the motivation of the study to see how this work of research contributes to them. Since the evaporation and combustion of the fuel spray are of paramount importance in an engine, the objectives were to study each of these processes separately. Additionally, given the complexity of conventional fuels employed in commercial engines, selected blends of known composition and properties were used in order to aid this study and to have less uncertainties. Finally, some suggestions for future works of research will be presented.

6.2 Conclusions

As mentioned in the motivation of the study, two research directions were identified: One being the use of bio-fuels and the other being gasoline-diesel blends. Given the objectives defined to study the fuel spray, the second route was thought to make more sense for the analysis needed. A wide range of fuels under various contour conditions have been tested in order to understand the effect of the physical and chemical properties on the different spray processes. Moreover, to be able to isolate the mixing and evaporation from the combined effects that are the product of the heat released and reactions taking place during the combustion, tests have been performed also under inert conditions. As was mentioned in the approach to be taken, fuel blends of single-components were used in order to have control over the composition and properties and be able to quantify the parameters measured with more precision than by using conventional fuels. Therefore, the upcoming sections will present the conclusions drawn from the results shown in Chapters 4 and 5 separating inert from reactive conditions.

6.2.1 Mixing and evaporation under inert conditions

In this section the conclusions regarding the mixing and evaporation of the spray will be presented divided in two groups, general effects of the contour conditions and the specific effects of the fuel properties.

General effects

A higher injection pressure resulted in longer penetrations of the vapour phase but equal-to-shorter ones of the stabilized liquid phase. The higher exit velocity made the fuel travel faster into the chamber, which would result in longer penetrations of both phases. However, it also caused the fuel to evaporate faster due to slightly better mixing, thus compensating each other and resulting in little changes in the liquid length. On the other hand, a hotter environment proved to have no effect on the vapour penetration, since the air entrainment is not altered by changes in the air temperature. However, it did play a fundamental role on the liquid length as the entrained air was hotter and more enthalpy was transferred from the air to the liquid fuel, resulting in shorter lengths.

Finally, a denser environment caused the penetration of both, liquid and vapour, phases to be shorter. This effect was caused by the over-entrainment of air and the consequentially increased spray angle.

Fuel specific effects

The effect of the fuel properties is of no significant importance on the vapour penetration; however, its effect on the liquid length is a bit more complex than the aforementioned conditions. On one had, if the fuels compared were the same type of chained alkanes (i.e. binary blends), the boiling temperature would be enough to predict a trend. On the other hand, if the fuels were a mixture of various different components (i.e. diesel and surrogate) the trends may be predicted by analysing the distillation curves. But, if the fuels were alkanes of different chain type (i.e. primary reference fuels), in order to predict a trend the boiling temperature and chain type would have to be taken into account.

The study with a real fuel and a surrogate showed that a similar temperature range in the distillation curves proved to be important for liquid length and evaporation estimation. Nevertheless, the physical properties were found to be less sensitive on evaporation-favourable conditions, such as high temperature (881 K) or pressure (7.26 MPa). Moreover, a single component fuel with similar vaporization enthalpy proved to be an adequate surrogate for a real fuel in evaporation properties and liquid penetration values. This was confirmed via experiments and a computational 1D model, as it was demonstrated that the cumulative liquid and vapour fractions were almost identical for the six-component surrogate and *n*-hexadecane alone. The spray temperature was also the same, which further proved that the heat absorption and evaporation enthalpy of both fuels was very similar. It is worth mentioning that this similarity was because the model calculates the temperature based on the enthalpy balance and liquid-vapour equilibrium, which is almost identical for both cases.

The study using primary reference fuels further proved the importance of the vaporization enthalpy compared to the density and boiling point. Also, the effect of the molecular structure was found to be of critical importance in the liquid length, as the *iso*-octane while being a denser fuel with a higher boiling temperature than *n*-heptane presented an experimental and modelled shorter stabilized liquid length due to its branched-chained structure and lower vaporization enthalpy. An additional calculation performed with the 1D model showed that if it had been a straight chained alkane as *n*-octane instead, the results would have been as expected by either the boiling temperature of density tendencies. Therefore, such properties should be used only when employing components of the same molecular structure or when no other evaporation-related properties are available as when working with real fuels.

Finally, the modifications done on the 1D spray model proved to yield reliable results which helped quantify parameters that were not measured and also clarify trends that were not evident from the experiments alone. On one hand, the double angle feature was able to predict a tip penetration with a much better fit than with a constant angle; additionally, this modification also allowed the stabilized liquid length to be calculated more precisely. On the other hand, the state relationships with an evaporation model using real components instead of ideal assumption, resulted in the calculation of a dew

curve and energy balances within the whole range of fuel mass fractions along the spray which also helped with the calculation of the liquid length. Finally, the inclusion of multi-component fuels proved to be extremely helpful when modelling the binary blends and specially the six-component surrogate.

6.2.2 Auto-ignition and combustion

In the same way as the previous section, the conclusions regarding auto-ignition and combustion of the spray will be drawn split into general effects of the contour conditions and specific effects of the fuel properties.

General effects

The analysis of the spray evolution and measurement of the different spray parameters under inert and reactive conditions showed four clear stages: First a behaviour similar to the inert spray before de SoC; second the pre-reactions taking place with evident changes in density; third the ignition, radial expansion of the spray and acceleration of the spray tip; and fourth the ending of the acceleration phase and the quasi-steady period.

As was mentioned in the previous chapter, in order to study the effect under reactive conditions the density was kept constant and ambient oxygen concentration and temperature were varied. The effect of the injection pressure has different trends for the parameters quantified. The spray penetrates faster as the exit velocity of the fuel is increased, this causes an slight improvement on the mixing so the ignition delay is reduced. Nevertheless, since the spray is travelling faster, the ignition will take place further away from the nozzle, leading to longer lift-off lengths. This improvement in the mixing and the dilution of the mixture also results in lower equivalence ratios at the instant of ignition and hence, less broadband radiation is registered implying a lower soot volume.

On the other hand, higher ambient temperatures led to shorter ignition delay times with an exponential trend with temperature. Since the mixture ignition was taking place earlier, for constant injection pressures it was closer to the nozzle, also resulting in shorter lift-off lengths. This also led to the reacting penetration deviating from its inert counterpart sooner as the acceleration phase of the S_r/S_i happened earlier, but they all stabilized on the same value regardless of the temperature. Moreover, more luminosity from the broadband radiation was captured as the combustion temperatures were also higher, which leads to think that more soot could be present within the spray surface, as higher temperatures favour the soot formation reactions. The increased concentration of oxygen had no effect on the mixing or air entrainment. However, the higher amount of oxidizer cause the spray to reach the stoichiometric ratios closer to the nozzle, which in turn resulted in shorter lift-off lengths and ignition delay times. In a similar way to the air temperature, this also cause the acceleration phase of the penetration to start sooner and more aggressively because of the higher reactivity of the air-fuel mixture. The effect on the soot generation is uncertain with just radiation images, as a high oxygen concentration would lead to leaner flames but also to higher combustion temperatures, which is why the broadband radiation emitted also increased.

Fuel specific effects

As was already observed in the inert tests, the fuel properties had no effect on the penetration of the vapour phase of the spray. On the other hand and in a similar way to the air temperature or oxygen concentration, the chemical fuel properties affect the reactivity of the mixture. In this particular case, since both pure components were Primary Reference Fuels, their octane numbers were on both ends of the scale and also had very different cetane numbers, being the latter the most important as it is an indicator of the ignition quality of a fuel. Also, and in a similar way to the liquid length, the molecular structure of the fuel was important in determining its propensity to react, as straight-chained alkanes have faster ignition times, while branched-chained ones have slower reactions. Therefore, the higher the percentage of *n*-heptane, the more reactive the blend, leading to smaller ignition delay times, shorter lift-off lengths and more broadband radiation detected. Therefore, the acceleration phase of the S_r/S_i happened earlier and more aggressively. Moreover, the dependency of such parameters was observed to have two very marked trends: On one hand, for the lower half of the octane scale (PRF0-20-40) the reactivity of the mixture (lift-off lengths and ignition delay times) decreases linearly with the fuel proportion, while on the the upper half (PRF60-80-100) a non linear trend can be seen. This trend was very notorious for all quantified variables, implying a dominant fuel on each half of the blend range. Additionally, for some of the conditions tested some blends did not ignite within the time window and field of view of the experimental setup. This led to no values of lift-off length of ignition delay times detected, as well as "reactive" curves identical the inert ones.

The flame length showed no clear trend related to the injection pressure or air temperature, even though the latter was the most influential variable on all the other parameters. This was due to the fact that the flame surface is defined by a sheath of stoichiometric equivalence ratio; therefore, the only ambient parameter capable of altering this was the oxygen concentration. Moreover, the fuel blend should also present a big influence on the flame length, as the stoichiometric equivalence ratio is highly dependent on the composition. Nevertheless, since the fuels studied have a similar composition among them, the equivalence ratio was similar enough not to present any noticeable difference in the flame length. If fuels with very different composition had been used, a trend in the flame length may have been observed. This was clear after the normalization of the variable was done, where all the values were uniform and fell within a certain range regardless of the fuel blend. Furthermore, with the presented scaling law (Section 5.10.1) it can be concluded that the flame stabilization depends on the mixing (d_{eq} term), the fuel stoichiometry (z_{st} term) and the reduction of the air entrainment due temperature increased caused by the combustion ($\sqrt{\frac{\rho_a}{\rho_{st,r}}}$ term); as the only stratification of the flame length witnessed was caused by the oxygen concentration variation.

The comparison of the soot onset length determined by measuring the spray broadband radiation and the lift-off length calculated via OH* chemiluminescence, proved that the best indicator for the combustion was the OH*, as some conditions and fuels presented very little or no soot even though the mixture was reacting. The relationships among the variables studies also showed a clear trend regarding the fuel, as the values corresponding to the blends where *iso*-octane was the dominant component coincided with the values less favourable to ignition. Finally, the combined effects of the ambient conditions and fuel

properties proved to yield "equivalent" conditions in which by changing the fuel reactivity and oxygen concentration, similar ignition delay times and lift-off length values could be obtained while generating less radiation, which could lead to soot reduction.

6.3 Future work

In order to complement the results presented in this research and to carry on with the investigation of the fuel properties on the different spray processes, the following task could be performed:

- The broadband radiation was an indicator of the soot luminosity within the spray; however, it was not an accurate indicator of the soot volume, as some low temperature flames could generate significant amounts of soot while emitting very little radiation. Therefore, the Laser Extinction Method (LEM) could be applied to similar experiments in order to get a precise measurement of the soot volume with different blends. Additionally, the broadband radiation imaging could be replaced with the two-colour method (2C) in order to measure the spray temperature along with the incandescence of soot.

- The test matrices performed contained parametric variations of some properties based on a baseline case. An extended test matrix studying the combined effects of all air temperatures and oxygen concentrations would be useful, as well as a variation of ambient density under reacting conditions.

- A parametric study using binary blends (*n*-decane & *n*-hexadecane) to study the differences in evaporation was presented in Chapter 4. Furthermore, blends of *n*-heptane and *iso*-octane were used to study the ignition and combustion of the spray in Chapter 5. An interesting work would be the study of a spray using blends of fuels that have very different physical and chemical properties, such as *iso*-octane and *n*-hexadecane.

- The discussion of the applicability of the results presented in Chapter 5 presented potential soot reduction while achieving similar combustion characteristic. It would be interesting to tests such fuels under similar conditions in an engine and measure the effects on the emissions and efficiency.

Bibliography

Engine Combustion Network.
http://www.sandia.gov/ecn. (cited on pp. 48, 75, 76, 117, 118, 129, 130, 131, 133, 134, 136)

National Institute of Standards and Technology (NIST) Chemistry WebBook.
http://webbook.nist.gov/chemistry/. (cited on pp. 73, 118)

Wärtsilä Corporation.
http://www.wartsila.com/en/Home. (cited on p. 3)

Arai M., Tabata M., Hiroyasu and Shimizu M.
Disintegrating process and spray characteristics of fuel jet injected by a diesel nozzle.
SAE Technical Paper, n^o 840275, 1984. (cited on p. 16)

Araneo L., Coghe A. and Cossali G.E.
Experimental analysis of structure and characteristics of a diesel spray head vortex.
In *Proceedings of the thirteen ICLASS*, pp. 103–109, 1997. (cited on p. 16)

Arcoumanis C. and Cutter P.A.
Flow and heat transfer characteristics of impinging diesel sprays under cross-flow conditions.
SAE Technical Paper, n^o 950448, 1995. (cited on p. 16)

Arcoumanis C. and Gavaises M.
Linking nozzle flow with spray characteristics in a diesel fuel injection system.
Atomization and Sprays, Vol. 8(3), pp. 307–347, 1998. (cited on p. 16)

Arcoumanis C. and Kamimoto T.
Flow and Combustion in Reciprocating Engines.
Springer-Verlag, 2009. (cited on pp. 16, 20, 24, 28)

Arrègle J.
Análisis de la estructura y dinámica interna de chorros Diesel.
Doctoral Thesis, Universitat Politècnica de València, 1997. (cited on p. 16)

Arrègle J., Pastor J.V. and Ruiz S.
The Influence of injection parameters on diesel spray characteristics.
SAE Technical Paper, n^o 1999-01-0200, 1999. (cited on pp. 19, 86, 96)

Baert R.S.G., Frijters P.J.M., Somers B., Luijten C.C.M. and de Boer W.
Design and Operation of a High Pressure, High Temperature Cell for HD Diesel Spray Diagnostics: Guidelines and Results.
SAE Technical Paper, n^o 2009-01-0649, 2009. (cited on pp. 5, 45)

Bardi M.
Partial needle lift and injection rate shape effect on the formation and combustion of the diesel spray.
Doctoral Thesis, Universitat Politècnica de València, 2014. (cited on pp. 45, 46)

Bardi M., Payri R., Malbec L.M., Bruneaux G., Pickett L.M., Manin J., Bazyn T. and Genzale C.
Engine Combustion Network: Comparison of spray development, vaporization, and combustion in different combustion vessels.
Atomization and Sprays, Vol. 22(10), pp. 807–842, 2012. (cited on pp. 45, 48)

Benajes J., Molina S., García A. and Monsalve-Serrano J.
Effects of direct injection timing and blending ratio on RCCI combustion with different low reactivity fuels.
Energy Conversion and Management, Vol. 99, pp. 193–209, 2015. (cited on p. 33)

Benajes J., Payri R., Bardi M. and Martí-Aldaraví P.
Experimental characterization of diesel ignition and lift-off length using a single-hole ECN injector.
Applied Thermal Engineering, Vol. 58, pp. 554–563, 2013.
(cited on pp. 118, 129, 130, 131, 132, 133, 134, 136)

Bermúdez V., García J.M., Juliá E. and Martínez S.
Engine with Optically Accessible Cylinder Head: A Research Tool for Injection and Combustion Processes.
SAE Technical Paper, n^o 2003-01-1110, 2003. (cited on p. 43)

Bessonette P., Schleyer C., Duffy K., Hardy W. and Liechty M.P.
Effects of Fuel Property Changes on Heavy-Duty HCCI Combustion.
SAE Technical Paper, n^o 2007-01-0191, 2007. (cited on p. 148)

Borée J., Atassi N. and Charnay G.
Measurements and image analysis of the turbulent field in an axisymmetric jet subject to a sudden velocity decrease.
Experimental Thermal and Fluid Science, Vol. 14, pp. 45–51, 1997. (cited on p. 51)

Bower G.R. and Foster D.E.
The effect of split injection on fuel distribution in an engine-fed combustion chamber.
SAE Technical Paper, n^o 930864, 1993. (cited on p. 20)

Browne K.R., Partridge I.M. and Greeves G.
Fuel property effects on fuel/air mixing in an experimental diesel engine.
SAE Technical Paper, n^o 860223, 1986. (cited on p. 21)

Canaan R.E., Dec J.E., Green R.M. and Daly D.T.
The influence of fuel volatility on the liquid-phase fuel penetration in a heavy-duty DI diesel engine.
SAE Technical Paper, n^o 980510, 1998. (cited on pp. 33, 91, 93)

Chikahisa T. and Murayama T.
Theory and experiments on air-entrainment in fuel sprays and their application to interpret diesel combustion processes.
SAE Technical Paper, n^o 950447, 1995. (cited on p. 17)

Cho I.Y., Fujimoto H., Kuniyoshi H., Ha J.Y, Tanabe H. and Sato G.T.
Similarity law of entrainment into diesel spray and steady spray.
SAE Technical Paper, n^o 900447, 1990. (cited on p. 16)

Correas D.
Theoretical and experimental study of isothermal diesel free sprays.
Doctoral Thesis, Universitat Politècnica de València, 1998. (cited on p. 19)

Cossali G.E., Gerla A., Coghe A. and Brunello G.
Effect of gas density and temperature on air entrainment in a transient diesel spray.
SAE Technical Paper, n^o 960862, 1996. (cited on p. 16)

Cossali G.E, L. G. Brunello and Coghe A.
LDV characterization of air entrainment in transient diesel sprays.
SAE Technical Paper, n^o 910178, 1991. (cited on p. 16)

de la Morena J.
Estudio de la influencia de las características del flujo interno en tobera sobre el proceso de inyección diésel en campo próximo.
Doctoral Thesis, Universitat Politècnica de València, 2011. (cited on p. 79)

Dec J.E.
A conceptual model of DI diesel combustion based on laser-sheet imaging.
SAE Technical Paper, n^o 970873, 1997. (cited on pp. 25, 26, 28, 29, 30, 32, 50, 122)

Dec J.E. and Espey C.
Ignition and early soot formation in a DI diesel engine using multiple 2-D imaging diagnostics.
SAE Technical Paper, n^o 950456, 1995. (cited on p. 141)

Dec J.E. and Espey C.
Chemiluminescence imaging of autoignition in a DI diesel engine.
SAE Technical Paper, n^o 982685, 1998. (cited on p. 23)

Desantes J., Benajes J., García A. and Monsalve-Serrano J.
The role of the in-cylinder gas temperature and oxygen concentration over low load reactivity controlled compression ignition combustion efficiency.
Energy, Vol. 78, pp. 854–868, 2014. (cited on p. 33)

Desantes J.M., López J.J., García J.M. and Pastor J.M.
Evaporative diesel spray modeling.
Atomization and Sprays, Vol. 17, pp. 193–231, 2007. (cited on pp. 56, 59)

Desantes J.M., Pastor J.V., García-Oliver J.M. and Briceño F.J.
An experimental analysis on the evolution of the transient tip penetration in reacting diesel sprays.
Combustion and Flame, Vol. 161(8), pp. 2137–2150, 2014. (cited on pp. 122, 124, 125, 128)

Desantes J.M., Pastor J.V., García-Oliver J.M. and Pastor J.M.
A 1D model for the description of mixing-controlled reacting diesel sprays.
Combustion and Flame, Vol. 156, pp. 234–249, 2009. (cited on p. 51)

Desantes J.M., Pastor J.V., Payri R. and Pastor J.M.
Experimental Characterization of Internal Nozzle Flow and Diesel Spray Behavior. Part II. Evaporative Conditions.
Atomization and Sprays, Vol. 15, pp. 517–543, 2005. (cited on p. 22)

Desantes J.M., Payri R., Salvador F.J. and Gil A.
Development and validation of a theoretical model for diesel spray penetration.
Fuel, Vol. 85, pp. 910–917, 2006. (cited on pp. 81, 96)

Donkerbroek A.J., Boot M.D., Luijten C.C.M., Dam N.J. and ter Meulen J.J.
Flame lift-off length and soot production of oxygenated fuels in relation with ignition delay in a DI heavy-duty diesel engine.
Combustion and Flame, Vol. 158, pp. 525–538, 2011. (cited on pp. 33, 135, 140)

Elliott J. R. and Lira C.T.
Introductory Chemical Engineering Thermodynamics.
Prentice Hall International Series in the Physical and Chemical Engineering Sciences. Prentice Hall, 2nd edition, 2012. (cited on p. 59)

Espey C. and Dec J.E.
The effect of TDC temperature and density on the liquid-phase fuel penetration in a DI diesel engine.
SAE Technical Paper, n^o 952456, 1995. (cited on pp. 20, 21, 81, 86, 100)

Faeth G.M.
Evaporation and combustion of sprays.
Progress in Energy and Combustion Science, Vol. 9, pp. 1–76, 1983. (cited on p. 5)

Flynn P.F., Durrett R.P., Hunter G.L., zur Loye A.O., Akinyemi O.C., Dec J.E. and Westbrook C.K.
Diesel combustion: An intengrated view combining laser diagnostics, chemical kinetics, and empirical validation.
SAE Technical Paper, n^o 1999-01-0509, 1999. (cited on pp. 31, 32, 132)

Galle J., Defruyt S., de Maele C. Van, Rodriguez R. Piloto, Denon Q., Verliefde A. and Verhelst S.
Experimental investigation concerning the influence of fuel type and properties on the injection and atomization of liquid biofuels in an optical combustion chamber.
Biomass and Bioenergy, Vol. 57, pp. 215–228, 2013. (cited on pp. 33, 81, 86, 93, 96)

García J.M.
Aportaciones al estudio del proceso de combustión turbulenta de chorros en motores diesel de inyección directa.
Doctoral Thesis, Universitat Politècnica de València, 2004. (cited on pp. 16, 22, 23, 43, 146)

García-Sánchez F., Eliosa-Jiménez G., Silva-Oliver G. and García-Flores B. E.
Vapor-Liquid equilibrium data for the Nitrogen + n-Decane system from (344 to 563) K and at pressures up to 50 Mpa.
Journal of Chemical & Engineering Data, Vol. 54, pp. 1560–1568, 2009. (cited on pp. 59, 60)

García-Sánchez F., Eliosa-Jiménez G., Silva-Oliver G. and Vázquez-Román R.
Vapor-Liquid Equilibria of Nitrogen-Hydrocarbon Systems Using the PC-SAFT Equation of State.
Fluid Phase Equilibria, Vol. 217, pp. 241–253, 2004. (cited on pp. 59, 60)

Gaydon A.G.
The Spectroscopy of Flames.
Chapman and Hall, 1974. (cited on p. 49)

Gimeno J.
Desarrollo y aplicación de la medida del flujo de cantidad de movimiento de un chorro diesel.
Doctoral Thesis, Universitat Politècnica de València, 2008. (cited on p. 79)

González C.
Estudio de la influencia de la geometría de la tobera de inyección en la combustión y emisión de contaminantes de un motor diesel.
Doctoral Thesis, Universitat Politècnica de València, 2005. (cited on p. 22)

Gülder Ö.L.
Views on the structure of transient diesel sprays.
Atomization and Sprays, Vol. 10(3-5), pp. 355–386, 2000. (cited on p. 16)

Han D. and Mungal M.G.
Direct measurement of entrainment in reacting/nonreacting turbulent jets.
Combustion and Flame, Vol. 124(3), pp. 370–386, 2001. (cited on pp. 17, 146)

Han W.Q. and Yao C.D.
Research on high cetane and hig octane number fuels and the mechanism for their common oxidation and auto-ignition.
Fuel, Vol. 150, pp. 29–40, 2015. (cited on p. 34)

Hanson R., Kokjohn S., Splitter D. and Reitz R.
An experimental investigation of fuel reactivity controlled PCCI combustion in a heavy-duty engine.
SAE Technical Paper, n^o 2010-01-0864, 2010. (cited on p. 33)

Hanson R., Splitter D. and Reitz R.D.
Operating a heavy-duty direct-injection compression-ignition engine with gasoline for low emissions.
SAE Technical Paper, n^o 2009-01-1442, 2009. (cited on pp. 4, 148)

Hartmann M., Gushterova I., Fikri M., Schulz C. and Schießl R.
Auto-ignition of toluene-doped n-heptane and iso-octane/air mixtures: High-pressure shock-tube experiments and kinetics modeling.
Combustion and Flame, Vol. 158, pp. 172–178, 2011. (cited on p. 132)

Heywood J.
Internal Combustion Engine Fundamentals.
McGraw-Hill Education, 1988. (cited on pp. 13, 14, 16, 20, 21, 23, 24, 25, 132)

Higgins B., Mueller C. and Siebers D.
Measurements of fuel effects on liquid-phase penetration in DI sprays.
SAE Technical Paper, n^o 1999-01-0519, 1999. (cited on pp. 21, 33, 81, 86, 91, 93, 100, 119)

Higgins B. and Siebers D.
Measurement of the Flame Lift-Off Location on DI Diesel Sprays Using OH Chemiluminescence.
SAE Technical Paper, n^o 2001-01-0918, 2001. (cited on pp. 5, 25, 49, 50, 134, 141)

Higgins B., Siebers D. and Aradi A.
Diesel-spray ignition and premixed-burn behavior.
SAE Technical Paper, n^o 2000-01-0940, 2000. (cited on p. 23)

Hildingsson L., Kalghatgi G., Tait N., Johansson B. and Harrison A.
Fuel Octane Effects in the Partially Premixed Combustion Regime in Compression Ignition Engines.
SAE Technical Paper, n^o 2009-01-2648, 2009. (cited on pp. 4, 132, 148)

Hiroyasu H. and Arai M.
Structures of fuel sprays in diesel engines.
SAE Technical Paper, n^o 900475, 1990. (cited on pp. 16, 17, 18, 19, 20, 34)

Hiroyasu H. and Kadota T.
Fuel droplet distribution in diesel combustion chamber.
SAE Technical Paper, n^o 740715, 1974. (cited on p. 16)

Hodges J.T., Baritaud T.A. and Heinze T.A.
Planar liquid and gas fuel and droplet size visualization in a DI diesel engine.
SAE Technical Paper, n^o 910726, 1991. (cited on pp. 16, 20)

Huh K.Y., Lee E. and Koo J.
Diesel spray atomization model considering nozzle exit turbulence conditions.
Atomization and Sprays, Vol. 8(4), pp. 453–469, 1998. (cited on p. 16)

Idicheria C.A. and Pickett L.M.
Effect of EGR on diesel premixed-burn equivalence ratio.
Proceedings of the Combustion Institute, Vol. 31, pp. 2931–2938, 2007. (cited on pp. 130, 132)

Idicheria C.A. and Pickett L.M.
Ignition, soot formation, and end-of-combustion ttransient in diesel combustion under high-EGR conditions.
International Journal of Engine Research, Vol. 12, pp. 376–392, 2011. (cited on p. 141)

Ito T., Ueda M., Matsumoto T., Kitamura. T., Senda J. and Fujimoto H.
Effects of ambient gas conditions on ignition and combustion process of oxygenated fuel sprays.
SAE Technical Paper, n^o 2003-01-1790, 2003. (cited on pp. 33, 130, 132)

Jung Y., Manin J., Skeen S. and Pickett L.
Measurement of liquid and vapour penetration of diesel sprays with a variation in spreading angle.
SAE Technical Paper, n^o 2015-01-0946, 2015. (cited on pp. 86, 130)

Kalghatgi G., Risberg P. and Ångström H.E.
Advantages of Fuels with High Resistance to Auto-ignition in Late-injection, Low-temperature, Compression Ignition Combustion.
SAE Technical Paper, n^o 2006-01-3385, 2006. (cited on pp. 4, 148)

Kalghatgi G., Risberg P. and Ångström H.E.
Partially Pre-Mixed Auto-Ignition of Gasoline to Attain Low Smoke and Low NOx at High Load in a Compression Ignition Engines and Comparison with a Diesel Fuel.
SAE Technical Paper, n^o 2007-01-0006, 2007. (cited on p. 148)

Kalghatgi G.T., Gurubaran R. Kumara, Davenport A., Harrison A.J., Hardalupas Y. and Taylor A.M.K.P.
Some advantages and challenges of running a Euro IV, V6 diesel engine on a gasoline fuel.
Fuel, Vol. 108, pp. 197–207, 2013. (cited on pp. 4, 33, 140, 148)

Kamimoto T., Yokota H. and Kobayashi H.
Effect of high pressure injection on soot formation processes in a rapid compression machine to simulate diesel flames.
SAE Technical Paper, n^o 871610, 1987. (cited on pp. 21, 22)

Kamimoto T., Yokota H. and Kobayashi H.
A new technique for the measurement of sauter mean diameter of droplets in unsteady dense sprays.
SAE Technical Paper, n^o 890316, 1989. (cited on p. 16)

Kim M. and Yoon Y.
Flame residence time and strain rate in turbulent hydrogen non-premixed jet fflame with coaxial air.
Proceedings of the Combustion Institute, Vol. 31, pp. 1609–1616, 2007. (cited on p. 138)

Kim T. and Ghandhi J.B.
Characterization of evaporating diesel sprays using exciplex laser-induced fluorescence measurements.
Atomization and Sprays, Vol. 13, pp. 535–559, 2003. (cited on p. 5)

Kitamura T., Ito T., Senda J. and Fujimoto H.
Mechanism of smokeless diesel combustion with oxygenated fuels based on the dependence of the equivalence ratio and temperature on soot particle formation.
International Journal of Engine Research, Vol. 3(4), pp. 223–248, 2002. (cited on p. 28)

Knox B.W., Genzale C.L., Pickett L.M., García-Oliver J.M. and Vera-Tudela W.
Combustion recession after end of injection in diesel sprays.
SAE International Journal of Engines, Vol. 8(2) n^o 2015-01-0797, 2015. (cited on pp. 6, 34)

Kobori S., Kamimoto T. and Kosaka H.
Ignition, combustion and emissions in a DI diesel engines equipped with a micro-hole nozzle.
SAE Technical Paper, n^o 960321, 1996. (cited on pp. 26, 129)

Kook S. and Pickett L.M.
Liquid length and vapor penetration of conventional, Fischer-Tropsch, coal-derived, and surrogate fuel sprays at high-temperature and high-pressure ambient conditions.
Fuel, Vol. 93, pp. 539–548, 2012. (cited on pp. 19, 20, 21, 33, 81, 86, 91, 93, 120, 128)

Kosaka H., Nishigaki T., Kamimoto T., Sano T., Matsutani A. and Harada S.
Simultaneous 2-D imaging of OH radicals and soot in a diesel flame by laser sheet techniques.
SAE Technical Paper, n^o 960834, 1996. (cited on pp. 26, 50)

Kunte S., Bertola A., Obrecht P. and Boulouchos K.
Temporal soot evolution and diesel engine combustion: influence of fuel composition, injection parameters, and exhaust gas recirculation.
International Journal of Engine Research, Vol. 7, pp. 459–470, 2006. (cited on pp. 138, 148)

Kuti O.A., Zhu J., Nishida K., Wang X. and Huang Z.
Characterization of spray and combustion processes of biodiesel fuel injected by diesel engine common rail system.
Fuel, Vol. 104, pp. 838–846, 2013. (cited on pp. 86, 100)

Lefebvre A.H.
Atomization and Sprays.
Hemisphere Publishing Corporation, 1989. (cited on pp. 15, 16)

López J.J.
Estudio teórico-experimental del chorro libre diesel no evaporativo y de su interacción con el movimiento del aire.
Doctoral Thesis, Universitat Politècnica de València, 2003. (cited on p. 16)

López J.J., García-Oliver J.M., García A. and Domenech V.
Gasoline effects on spray characteristics, mixing and auto-ignition processes in a CI engine under partially premixed combustion conditions.
Applied Thermal Engineering, Vol. 70(1), pp. 996–1006, 2014. (cited on pp. 34, 81, 86, 96, 100)

Lü X.C., Chen W., Hou Y.C. and Huang Z.
Study on the ignition, combustion and emissions of a HCCI combustion engines fueled with primary reference fuels.
SAE Technical Paper, n^o 2005-01-0155, 2005. (cited on pp. 34, 148)

Luijten C.C.M. and Kurvers C.
Real gas effects in mixing-limited diesel spray vaporization models.
Atomization and Sprays, Vol. 20(7), pp. 595–609, 2010. (cited on pp. 56, 59)

Machrafi H., Cavadia S. and Gilbert P.
An experimental and numerical analysis of the HCCI aiuto-ignition process of primary reference fuels, toluene reference fuels and diesel fuels in an engine, varying the engine parameters.
Fuel Processing Technology, Vol. 89, pp. 1007–1016, 2008. (cited on p. 34)

Malbec L.M., Egúsquiza J., Bruneaux G. and Meijer M.
Characterization of a set of ECN Spray A injectors: Nozzle to nozzle variations and effect of spray characteristics.
SAE International Journal of Engines, Vol. 6(3) n^o 2013-24-0037, pp. 1642–1660, 2013.
(cited on pp. 21, 86, 100, 119, 130, 134, 135)

Manente V.
Gasoline Partially Premixed Combustion - An advanced internal combustion engine concept aimed to high efficiency, low emissions and low acoustic noise in the whole load range.
Doctoral Thesis, Lund Institute of Technology, 2010. (cited on pp. 4, 148)

Manente V., Tunestål P. and Johansson B.
Half Load Partially Premixed Combustion, PPC, with High Octane Number Fuels. Gasoline and Ethanol Compared with Diesel.
In *Symposium on International Automotive Technology (SIAT), Pune, India.* The Automotive Research Association of India, Research Institution of the Automotive Industry, January 2009. (cited on p. 4)

Manin J.
Analysis of mixing processes in liquid and vaporized diesel sprays through LIF and Rayleigh scattering measurements.
Doctoral Thesis, Universitat Politècnica de València, 2011. (cited on pp. 81, 86, 96, 100)

Martínez S.
Desarrollo de una instalación experimental para el estudio de chorros diesel evaporados en atmósfera inerte y reactiva.
Doctoral Thesis, Universitat Politècnica de València, 2003. (cited on pp. 21, 22, 43)

Möller S., Dutzler G.K., Priesching P., Pastor J.V. and Micó C.
Multi-Component Modeling of Diesel Fuel for Injection and Combustion Simulation.
SAE Technical Paper, n^o 2013-24-0007, 2013. (cited on p. 128)

Morrison R.T. and Boyd R.N.
Química Orgánica.
Pearson Educación, 1998. (cited on p. 120)

Mueller C.J. and Martin G.C.
Effects of oxygenated compounds on combustion and soot evolution in a DI diesel engines: Broadband natural luminosity imaging.
SAE Technical Paper, n^o 2002-01-1631, 2002. (cited on p. 33)

Naber J. and Siebers D.L.
Effects of gas density and vaporization on penetration and dispersion of diesel sprays.
SAE Technical Paper, n^o 960034, 1996. (cited on pp. 16, 17, 19, 25, 48, 81, 96)

Nerva J.G.
An assessment of fuel physical and chemical properties in the combustion of a Diesel spray.
Doctoral Thesis, Universitat Politècnica de València, 2013.
(cited on pp. 4, 33, 43, 47, 86, 100, 102, 135, 137)

Obokata T., Hashimoto T. and Takahashi H.
LDA analysis of diesel spray and entrainment air flow.
In *Comodia international symposium*, pp. 231–236, 1990. (cited on p. 16)

Oefelein J., Dahms R. and Lacaze G.
Detailed modeling and simulation of high-pressure fuel injection processes in diesel engines.
SAE International Journal of Engines, Vol. 5(3) n^o 2012-01-1258, pp. 1410–1419, 2012.
(cited on p. 56)

Paryi R., García-Oliver J.M., Xuan T. and Bardi M.
A study on diesel spray tip penetration and radial expansion under reacting conditions.
Applied Thermal Engineering, Vol. 90, pp. 619–629, 2015. (cited on pp. 122, 124)

Pastor J.V., Arrègle J., García J.M. and Zapata L.D.
Segmentation of diesel spray images with log-likelihood ratio test algorithm for non-Gaussian distributions.
Applied Optics, Vol. 46(6), pp. 888–899, 2007. (cited on p. 47)

Pastor J.V., Arrègle J. and Palomares A.
Diesel spray image segmentation with a likelihood ratio test.
Applied Optics, Vol. 40(17), pp. 2876–2885, 2001. (cited on p. 47)

Pastor J.V., García-Oliver J.M., López J.J. and Vera-Tudela W.
An experimental study of the effects of fuel properties on reactive spray evolution using Primary Reference Fuels.
Fuel, Vol. 163, pp. 260–270, 2016. (cited on p. 6)

Pastor J.V., García-Oliver J.M., Nerva J.G. and Giménez B.
Fuel effect on the liquid-phase penetration of an evaporating spray under transient diesel-like conditions.
Fuel, Vol. 90(11), pp. 3369–3381, 2011. (cited on pp. 33, 81, 86, 100)

Pastor J.V., García-Oliver J.M., Novella R. and Vera-Tudela W.
Investigation on ignition and combustion characteristics of primary reference fuels under diesel engine conditions.
In *Der Arbeitsprozess des Verbrennungsmotors*, pp. 378–393. Institut für Verbrennungskraftmaschinen und Thermodynamik, Technische Universität Graz, September 2013. (cited on pp. 6, 34)

Pastor J.V., García-Oliver J.M., Pastor J.M. and Ramírez-Hernández J.G.
Ignition and combustion development for high speed direct injection diesel engines under low temperature cold start conditions.
Fuel, Vol. 90(4), pp. 1556–1566, 2011. (cited on p. 132)

Pastor J.V., García-Oliver J.M., Pastor J.M. and Vera-Tudela W.
One-dimensional diesel spray modeling of multicomponent fuels.
Atomization and Sprays, Vol. 25(2), pp. 485–517, 2015. (cited on pp. 6, 33, 51, 79, 119)

Pastor J.V., López J.J., García J.M. and Pastor J.M.
A 1D model for the description of mixing-controlled inert diesel sprays.
Fuel, Vol. 87, pp. 2871–2885, 2008. (cited on pp. 51, 56, 59)

Pastor J.V., Payri R., García-Oliver J.M. and Briceño F.
Schlieren methodology for the analysis of transient diesel flame evolution.
SAE International Journal of Engines, Vol. 6(3) n^o 2013-24-0041, pp. 1661–1676, 2013.
(cited on pp. 48, 128, 134)

Pastor J.V., Payri R., García-Oliver J.M. and Nerva J.G.
Schlieren measurements of the ECN-Spray A penetration under inert and reacting conditions.
SAE Technical Paper, n^o 2012-01-0456, 2012. (cited on pp. 48, 135, 137)

Payri F., Pastor J.V., Nerva J.G. and García-Oliver J.
Lift-off length and KL extinction measurements of biodiesel and Fischer-Tropsch fuels under quasi-steady diesel engine conditions.
SAE International Journal of Engines, Vol. 4(2) n^o 2011-24-0037, pp. 2278–2297, 2011.
(cited on pp. 33, 132, 134, 135, 137, 141)

Payri R., García A., Domenech V., Durrett R. and Plazas A.H.
An experimental study of gasoline effects on injection rate, momentum flux and spray characteristics using a common rail diesel injection system.
Fuel, Vol. 97, pp. 390–399, 2012. (cited on pp. 33, 86, 93, 128)

Payri R., García-Oliver J.M., Bardi M. and Manin J.
Fuel temperature influence on diesel sprays in inert and reacting conditions.
Applied Thermal Engineering, Vol. 35, pp. 185–195, 2012.
(cited on pp. 21, 45, 80, 81, 86, 100, 119, 129, 132, 134)

Payri. R., Gimeno J., Bardi M. and Plazas A.
Study liquid length penetration results obtained with a direct acting piezo electric injector.
Applied Energy, Vol. 106, pp. 152–162, 2013. (cited on pp. 21, 22, 81, 86, 100)

Payri R., Salvador F.J., Gimeno J. and Zapata L.D.
Diesel nozzle geometry influence on spray liquid-phase fuel penetration in evaporative conditions.
Fuel, Vol. 87(7), pp. 1165–1176, 2008. (cited on pp. 100, 119)

Peng D. and Robinson D. B.
A New Two-Constant Equation of State.
Industrial Engineering Chemistry Fundamentals, Vol. 15 (1), pp. 59–64, 1976. (cited on p. 65)

Persson H., Andersson Ö. and Egnell R.
Fuel effects on flame lift-off under diesel conditions.
Combustion and Flame, Vol. 158, pp. 91–97, 2011. (cited on pp. 34, 134)

Peters N.
Turbulent Combustion.
Cambridge University Press, 2000. (cited on pp. 25, 132)

Pickett L., Manin J., Kastengren A. and Powell C.
Comparison of near-field structure and growth of a diesel spray using light-based optical microscopy and x-ray radiagraphy.
SAE International Journal of Engines, Vol. 7(2), pp. 1044–1053, 2014. (cited on p. 16)

Pickett L.M.
Low flame temperature limits for mixing-controlled diesel combustion.
Proceedings of the Combustion Institute, Vol. 30, pp. 2727–2735, 2005. (cited on p. 132)

Pickett L.M., Genzale C.L., Bruneaux G., Malbec L.M., Hermant L., Christiansen C. and Schramm J.
Comparison of diesel spray combustion in different high-temperature, high-pressure facilities.
SAE International Journal of Engines, Vol. 3(2) n^o 2010-01-2106, pp. 156–181, 2010.
(cited on pp. 48, 76, 115, 141)

Pickett L.M., Kook. S. and Williams T.
Visualization of diesel spray penetration, cool-flame, ignition, high-temperature combustion, and soot formation using high-speed imaging.
SAE International Journal of Engines, Vol. 2(1) n^o 2009-01-0658, pp. 439–459, 2009.
(cited on pp. 48, 121, 141)

Pickett L.M., Manin J., Genzale C.L., Siebers D.L., Musculus M.P.B. and Idicheria C.A.
Relationship between diesel fuel spray vapor penetration/dispersion and local fuel mixture fraction.
SAE International Journal of Engines, Vol. 4(1) n^o 2011-01-0686, pp. 764–799, 2011.
(cited on pp. 48, 81, 86, 96)

Pickett L.M., Manin J., Payri R., Bardi M. and Gimeno J.
Transient rate of injection effects on spray development.
SAE Technical Paper, n^o 2013-24-0001, 2013. (cited on pp. 19, 79)

Pickett L.M. and Siebers D.L.
Fuel effects on soot processes of fuel jets at DI diesel conditions.
SAE Technical Paper, n^o 2003-01-3080, 2003. (cited on pp. 130, 132, 134, 135, 137)

Pickett L.M. and Siebers D.L.
Orifice diameter effects on diesel fuel jet flame.
Journal of Engineering for Gas Turbines and Power, Vol. 127(1), pp. 187–196, 2005.
(cited on pp. 145, 146)

Pickett L.M., Siebers D.L. and Idicheria C.A.
Relationship between ignition processes and the lift-off length of diesel fuel jets.
SAE Technical Paper, n^o 2005-01-3843, 2005. (cited on pp. 26, 33, 130, 132, 134, 135, 141)

Qiu L., Wang Y., Jiao Q., Wang H. and Reitz R.D.
Development of a thermodynamically consistent, robust and efficient phase equilibrium solver and its validations.
Fuel, Vol. 115, pp. 1–16, 2014. (cited on p. 56)

Qiu L., Wang Y., Wang H., Jiao Q. and Reitz R.D.
Simulating Condensation in a Supercritical Gas Jet.
In *25th Annual Conference on Liquid Atomization and Spray Systems*. ILASS Americas, May 2013. (cited on p. 56)

Ramírez-Hernández J.
Combustion studies for high speed direct injection diesel engines under low temperature cold start conditions.
Doctoral Thesis, Universitat Politècnica de València, 2012. (cited on p. 130)

Reid R. C., Prausnitz J. M. and Poling B. E.
The properties of gases and liquids.
McGraw-Hill, fourth edition, 1998. (cited on p. 59)

Reitz R.D.
High-Efficiency Fuel Reactivity Controlled Compression Ignition (RCCI) Combustion.
In *16th Directions in Engine-Efficiency and Emissions Research (DEER) Conference, Detroit, MI*. Engine Research Center, University of Wisconsin-Madison, August 2010. (cited on pp. 4, 132, 148)

Reitz R.D. and Bracco F.V.
On the dependence of spray angle and other spray parameters on nozzle design and operating conditions.
SAE Technical Paper, n^o 790494, 1979. (cited on p. 19)

Reitz R.D. and Bracco F.V.
Mechanism of atomization of a liquid jet.
Physics of Fluids, Vol. 25(10), pp. 1730–1742, 1982. (cited on p. 16)

Reitz R.D., R.Hanson, Splitter D. and Kokjohn S.
High-Efficiency, Ultra-Low Emission Combustion in a Heavy-Duty Engine via Fuel Reactivity Control.
In *15th Diesel Engine-Efficiency and Emissions Research (DEER) Conference, Dearborn, MI*. Engine Research Center, University of Wisconsin-Madison, August 2009. (cited on pp. 4, 148)

Ricou F.P. and Spalding D.B.
Measurements of entrainment by axisymetrical turbulent jets.
Journal of Fluid Mechanics, Vol. 11, pp. 21–32, 1961. (cited on p. 16)

Sebastian H.M., Slmnick J.J., Lin H.M. and Chao K.C.
Vapor-Liquid Equilibrium in Binary Mixtures of Carbon Dioxide + n-Decane and Carbon Dioxide + n-Hexadecane.
Journal of Chemical & Engineering Data, Vol. 25, pp. 138–140, 1980. (cited on pp. 59, 60)

Settles G.S.
Schlieren and Shadowgraph Techniques: Visualizing Phenomena in Transparent Media.
Springer-Verlag, Berlin, Germany, 2001. (cited on pp. 5, 48)

Siebers D. and Higgins B.
Flame lift-off on direct-injection diesel sprays under quiescent conditions.
SAE Technical Paper, n^o 2001-01-0530, 2001. (cited on pp. 25, 26, 27, 78, 132, 134, 141)

Siebers D., Higgins B. and Pickett L.
Flame Lift-off on direct-injection diesel fuel jets: Oxygen concentration effects.
SAE Technical Paper, n^o 2002-01-0890, 2002. (cited on pp. 25, 26, 78, 141)

Siebers D.L.
Liquid-phase fuel penetration in diesel sprays.
SAE Technical Paper, n^o 980809, 1998. (cited on pp. 16, 20, 21, 22, 33, 81, 86, 91, 93, 100, 119)

Siebers D.L.
Scaling liquid-phase fuel penetration in diesel sprays based on mixing-limited vaporization.
SAE Technical Paper, n^o 1999-01-0528, 1999.
(cited on pp. 16, 20, 21, 22, 33, 59, 78, 81, 86, 91, 93, 98, 100, 119)

Siebers D.L. and Pickett L.M.
Injection pressure and orifice diameter effects on soot in DI diesel fuel jets.
In *Proceedings of the Thiesel 2002 Conference on Thermo- and Fluid Dynamic Processes in Diesel Engines*, pp. 109–132, 2002. (cited on pp. 138, 146)

Skeen S., Manin J., Pickett L., Dalen K. and Ivarsson A.
Quantitative spatially resolved measurements of total radiation in high-pressure spray flames.
SAE Technical Paper, n^o 2014-01-1252, 2015. (cited on p. 125)

Skeen S.A., Manin J. and Pickett L.M.
Simultaneous formaldehyde PLIF and high-speed schlieren imaging for ignition visualization in high-pressure spray flames.
Proceedings of the Combustion Institute, Vol. 35(3), pp. 3167–3174, 2015. (cited on p. 121)

Som S., Ramirez A.I., Longman D.E. and Aggarwal S.K.
Effect of nozzle orifice geometry on spray, combustion, and emission characteristics under diesel engine conditions.
Fuel, Vol. 90(3), pp. 1267–1276, 2011. (cited on pp. 16, 86, 100)

Taylor C.F.
The Internal-Combustion Engine in Theory and Practice.
MIT Press, 1985. (cited on pp. 22, 23, 24, 25)

Tinaut F.V., Melgar A. and Giménez B.
A model of atomization of a transient evaporative spray.
SAE Technical Paper, n^o 1999-01-0913, 1999. (cited on p. 15)

Tindal M.J., Williams T.J. and Harcombe A.T.
Fuel spray formation in an experimental swirl chamber.
SAE Technical Paper, n^o 870451, 1987. (cited on p. 19)

van Lipzig J.P.J., Nilsson E.J.K., de Goey L.P.H. and Konnov A.A.
Laminar burning velocities of n-heptane, iso-octane, ethanol and their binary and tertiary mixtures.
Fuel, Vol. 90, pp. 2773–2781, 2011. (cited on p. 135)

Vandersickel A., Hartmann M., Vogel K., Wright Y.M., Fikri M., Starke R., Schulz C. and Boulouchos K.
The autoignition of practical fuels at HCCI conditions: High-pressure shock tube experiments and phenomenological modeling.
Fuel, Vol. 93, pp. 492–501, 2012. (cited on p. 130)

Verhoeven D., Vanhemelryck J.L. and Baritaud T.
Macroscopic and ignition characteristics of high-pressure sprays of single-component fuels.
SAE Technical Paper, n^o 981069, 1998. (cited on pp. 21, 22, 129)

Wan Y. and Peters N.
Scaling of spray penetration with evaporation.
Atomization and Sprays, Vol. 9(2), pp. 111–132, 1999. (cited on p. 19)

Wang X., Kuti Z. HuaZ. Huang.A., Zhang W. and Nishida K.
An experimental investigation on spray, ignition and combustion characteristics of biodiesels.
Proceedings of the Combustion Institute, Vol. 33(2), pp. 2071–2077, 2011.
(cited on pp. 86, 100, 129, 132)

Won Y.H., Kamimoto T., Kobayashi H. and Kosaka H.
2-D visualization in unsteady spray flame by means of laser sheet scattering technique.
SAE Technical Paper, n^o 910223, 1991. (cited on p. 28)

Won Y.H., Kamimoto T. and Kosaka H.
A study on soot formation in unsteady spray flames via 2-D soot imaging.
SAE Technical Paper, n^o 920114, 1992. (cited on p. 28)

Xionq Q., Inaba K., Ogawa H. and Shibata G.
Influence of fuel properties on opoperation range and thermal efficiency of premixed diesel combustion.
SAE International Journal of Fuels and Lubricants, Vol. 6(3) n^o 2013-32-9054, pp. 1005–1013, 2013.
(cited on p. 34)

Yao M., Zhang B., Zheng Z., Cheng Z. and Xing Y.
Experimental study on the effects of EGR and octane number of PRF fuel on combustion and emission characeristics of HCCI engines.
SAE Technical Paper, n^o 2005-01-0174, 2005. (cited on p. 148)

Yates A., Viljoen C. and Swarts S.
Understanding the relation between cetane number and combustion bomb ignition delay measurements.
SAE Technical Paper, n^o 2004-01-2017, 2004. (cited on pp. 132, 135)

Yeh C.N., Kamimoto T., Korobi S. and Kosaka H.
2-D imaging of fuel vapor concentration in a diesel spray via excuplex-based Fluorescence technique.
SAE Technical Paper, n^o 932652, 1993. (cited on p. 22)

Yokota H., Kamimoto T., Kosaka H. and Tsujimura K.
Fast burning and reduced soot formation via ultra-high pressure diesel fuel injection.
SAE Technical Paper, n^o 910225, 1991. (cited on p. 26)

Zhang J., Niu S., Zhang Y., Tang C., Jiang X., Hu E. and Huang Z.
Experimental and modeling study of the auto-ignition of n-heptane/n-butanol mixtures.
Combustion and Flame, Vol. 160, pp. 31–39, 2013. (cited on p. 132)

Zhang L. and Kong S.C.
High-pressure vaporization modeling of multi-component petroleum-biofuel mixtures under engine conditions.
Combustion and Flame, Vol. 158, pp. 1705–1717, 2011. (cited on p. 56)